Pelagic marine ecosystem responses to late Pleistocene climate change

Matthew Andrew Sutton

St Anne's College

University of Oxford

A thesis submitted for the degree of

Doctor of Philosophy

Michaelmas 2024

Table of contents

List of tables

List of figures

Acknowledgements

The number of people who have supported me in this project over the past five years is too great mention in the limited space I have available. Nonetheless, I would like to acknowledge those whose contribution was truly invaluable.

Firstly, I want to thank my inspiring, compassionate, and unflappable supervisors, Erin Saupe and Tracy Aze. I cannot overstate how reassuring their personal and professional mentorship has been to me. The rare combination of empathy and scientific rigour that they both possess in abundance has guided me through difficult times and helped to turn me into a both a better scientist and a better person.

I am indebted to many people who gave substantial time and energy to this project despite not being official supervisors. Elizabeth Sibert's infectious enthusiasm inspired me to explore the world of ichthyoliths, and she was an infinite source of wisdom on all things fish teeth. Savannah Worne kindly hosted me for multiple trips to the British Geological Survey and Loughborough University labs, and I'm particularly grateful to her continued support, even when results didn't go as planned. I am hugely grateful to Alba González-Lanchas for helping me salvage an aspect of my project that had proven particularly challenging. I am thankful to Jane Barling for kindly spending many hours in the Earth Sciences clean labs guiding me through the art of rock digestion.

Completing this project exposed me to the importance of those who facilitate scientific research. I am particularly thankful to Owen Green and Steve Wyatt from the Department of Earth Sciences, without whom this work would have been impossible. Similarly, Jack Lacey at BGS and Camille Godbillot at CEREGE both lent me their expertise during unfamiliar lab work, helping to make this work possible. Victoria Forth, whose energy in running the Doctoral Training Partnership never ceases to amaze me, was a huge help in navigating the administrative side of postgraduate life.

This work was supported by a scholarship from the Natural Environment Research Council (NE/S007474/1). Several domestic and international visits for conferences and data collection were supported by travel grants from St Anne's College. I am also thankful to the International Ocean Discovery Program for providing the sample material from which all data in this thesis was derived.

Completing this work would have been impossible without the unconditional support of my friends and family. Within Oxford Earth Sciences I am particularly thankful for the joyous company of Ana Pagu, Ben Johnson, Dan Gittins, and Odysseus Archontikis. I was fulfilled and grounded by the friendship of so many others both inside and outside of the University over the past five years.

Whilst my parents never fully understood exactly why I spent half a decade of my life sieving mud; it is to them that I owe my love of learning and my belief in the spiritually enriching power of education.

Sarah has been my muse, my counsellor, my confidant, and my champion through everything. Not a single day passed over the past five years when she did not offer me unconditional love, support, and inspiration. She has been my partner through this in every meaning of the word, and her belief in me means more than words can convey.

Abstract of the thesis

Pelagic marine ecosystems occupy the most expansive habitat on the Earth and influence global climate through the organic carbon pump. In this thesis I tested for changes in North Atlantic primary, fish, and export production using two sediment cores – subpolar ODP Hole 982B and midlatitude IODP Hole U1313A – during late Pleistocene glacial-interglacial cycles in the past 200 kyrs. I hypothesised that there were causative changes in ecosystem production at different trophic levels driven by climate change, including long-term oceanographic and water temperature changes.

Coccolithophores are an ecologically important clade of eukaryotic phytoplankton in the modern pelagic ocean. I reconstructed the accumulation rate and demography of coccoliths and found significantly higher subpolar coccolith accumulation during interglacial intervals relative to glacial intervals. This was likely due to the importance of North Atlantic Transitional Waters (NATW) in sustaining warm and relatively eutrophic conditions favourable to coccolithophore proliferation during interglacial intervals. In contrast, there was no significant glacial-interglacial change in coccolith accumulation or taxonomy at the midlatitude site, which I attribute to the persistent presence of NATW.

Excess barium (Ba_{XS}), a proxy for organic carbon export, increased rapidly in the subpolar North Atlantic during the past two deglaciations. In the midlatitude ocean, Ba_{XS} was strongly correlated with glaciogenic and aeolian detrital input proxies. High latitude export may have been limited by enhanced glacial stratification, but basin-scale export was likely enhanced by allogenic nutrient-driven increases in the midlatitude ocean, which coincided with greater continental aridity and ice rafting. These findings imply that the midlatitude North Atlantic could have been a hitherto unrecognised region of enhanced biogenic carbon sequestration during past glacial intervals, contributing to the drawdown of atmospheric carbon dioxide.

Ichthyoliths, microfossil fish remains, record the abundance and composition of mesopelagic fish fauna. Interglacial ichthyolith accumulation rate (IAR) was higher than glacial IAR at both sites but showed little relationship to proxy reconstructions of primary production. This suggests that mesopelagic fish production was strongly influenced by temperature-induced changes in trophic transfer efficiency on multi-millennium timescales. If this trend was sustained, mesopelagic fish abundances could respond positively to long-term future ocean warming, contrary to what is predicted by most marine ecosystem models. IODP Site U1313 had by far the highest mean IAR of any site where IAR has been constructed to-date. This result suggests either that the midlatitude Pleistocene North Atlantic was far more productive for mesopelagic fishes than these other pelagic locations, or that the IAR proxy imperfectly captures fish productivity in this setting. This work highlights the Pleistocene North Atlantic as a promising region for future ichthyolith research.

Linear regressions of the three productivity proxies suggest that coccolithophore production was positively related to organic carbon export in the midlatitude North Atlantic during the Last Interglacial and during glacial intervals in the subpolar ocean, indicating the importance of coccolith biomass to export in oligotrophic conditions.

Future anthropogenic climate change will cause substantial changes to ocean ecosystems. The late Pleistocene provides examples of ecosystem responses to major oceanographic perturbations in the recent geological past, which may prove useful analogues for near-future change.

This thesis evidences the utility of palaeontological and geochemical approaches to reconstructing biological responses to past climate change. Glacial-interglacial climates were marked by distinct changes in coccolithophore, fish, and export production in the North Atlantic. Coccolithophore production responded most strongly to changes in the position of NATW, export production was strongly influenced by allogenic nutrient inputs, and mesopelagic fish production showed a positive relationship with ocean temperature. Whilst these methods have limitations, such as capturing only a fraction of total production, they can provide an empirical means of informing future climate change scenarios.

Chapter 1: A review of North Atlantic core sample sites, late Pleistocene climate, and ocean productivity

Abstract

The pelagic marine environment is the single largest habitat on Earth. Changes in the strength of the organic carbon pump, driven by concomitant changes in diverse pelagic marine ecosystems, may have contributed to glacial-interglacial climate cycles during the Pleistocene by altering atmospheric carbon dioxide concentrations. Quantification of changes in pelagic primary, fish, and export production in the recent geological past through the use of established proxies holds potential to inform possible future ecosystem responses to anthropogenic climate change. The North Atlantic is a suitable region to investigate such changes due to the relatively high abundance of existing Pleistocene climatic and biological records. I will use subpolar ODP Site 982 and midlatitude IODP Site U1313 in this thesis, as both cores possess existing high-resolution age models and record substantial changes in oceanographic configuration, sea surface temperature, and allogenic inputs over the past 200 kyrs.

Chapter contents

1.1. Introduction

Pelagic ecosystems occupy more than 50% of the Earth's surface area and play a crucial role in regulating global climate (Siegel *et al.*, 2014; Boyd *et al.*, 2019; Nowicki, DeVries and Siegel, 2022) and sustaining biodiversity (Ryther, 1969; Angel, 1993; Hannisdal and Peters, 2011). Anthropogenic climate change is expected to have multifaceted impacts on pelagic environments through, for example, ocean warming (Doney *et al.*, 2020; Tittensor *et al.*, 2021) and stratification (Fu, Randerson and Moore, 2016; Li *et al.*, 2020). However, detailed understanding of how contemporary and future climate change may affect these biological communities is still lacking.

Deep marine sediments provide a relatively high-resolution record of past climate change and the impact of these changes on pelagic ecosystems. Earth's history is punctuated by episodes of rapid environmental change that affected marine ecosystems, notably mass extinction events (Raup and Sepkoski, 1982; Bond and Wignall, 2014), Oceanic Anoxic Events (Jenkyns, 1980; Robinson *et al.*, 2017), and cyclical orbital-driven climate cycles (Emiliani, 1955; Lisiecki and Raymo, 2005). Records from these events provide quantitative information on biological activity that can inform future ecosystem response under different anthropogenic climate change pathways (Burke *et al.*, 2018).

In this thesis I will use two North Atlantic sediment cores: ODP Site 982 (Shipboard Scientific Party, 1996), and IODP Site U1313 (Expedition 306 Scientists, 2006), to examine how past climate change impacted pelagic ecosystems by producing high-resolution records of coccolithophore, export (using excess barium), and fish productivity over the last 200 ka. I selected this interval due to its potential similarity to near-future climate states, and hence its possible use as an analogue for the changes expected in the coming decades (Burke *et al.*, 2018). Phytoplankton, such as coccolithophores, dominate total primary production in the pelagic ocean and phytoplankton productivity imposes a bottom-up control on the productivity of higher trophic levels via trophic transfer (Chassot *et al.*, 2010; Stock *et al.*, 2017). Notably, primary production imposes constraints on mesopelagic fishes (Gjøsaeter and Kawaguchi K., 1980; Anderson *et al.*, 2019), the most abundant vertebrates on the planet (Irigoien *et al.*, 2014). Fishes are important both as a food source for humans (FAO, 2020) and as a component of the biological carbon pump through diel vertical migration (DVM) (Davison *et al.*, 2013). Climatically induced changes in pelagic primary and export productivity have the potential to impact both fish production (Chassot *et al.*, 2010; Britten and Sibert, 2020) and vertical carbon transport (Bolton *et al.*, 2011; Fu, Randerson and Moore, 2016).

I processed sediments from these two cores for ichthyoliths (fish teeth and shark scales) to measure ichthyolith accumulate rates (IAR) (Sibert *et al.*, 2017) and to assess changes in fish production prior, during, and after the Last Interglacial (MIS 5). Simultaneously, I processed the same samples to generate new datasets for coccolithophore demographics and abundance using a combination of automated and manual counting (Flores and Sierro, 1997; Beaufort and Dollfus, 2004); and excess barium using whole rock digestion and inductively coupled plasma mass spectrometry (Schoepfer *et al.*, 2015; Liguori, De Almeida and de Rezende, 2016). This study is the first to investigate ichthyolith and phytoplankton abundances from the same marine sediment samples to test for concomitant responses in primary producers and fish during an interval of major environmental change. This data synthesis enables a greater understanding of the baseline response of pelagic marine ecosystems to climatic perturbations that is independent of other anthropogenic impacts such as pollution and overfishing. This research will supplement and expanding existing predictions for future ecosystems (Henson *et al.*, 2021; Tittensor *et al.*, 2021) using empirical measurements.

This thesis will address the following questions:

- Are there causative changes in North Atlantic primary production, export production, and fish production in response to climate on glacial-interglacial timescales?
- Do distinct plankton communities occupy the North Atlantic during glacial and interglacial intervals?
- Do changes in export productivity reflect synchronous changes in the overlying pelagic plankton and fish communities?
- Can we resolve positive trophic connections between plankton and fish using the microfossil record?

This thesis contains six chapters investigating and synthesing different components of pelagic productivity. **Chapter One** (this chapter) provides the bibliographic foundation of all subsequent chapters. It introduces Pleistocene climate change; the sediment cores used through this work and their ages models; and discusses the different types of productivity and how we reconstruct these in deep time using the geological record. **Chapter Two** presents coccolith accumulation rate and demographic data, using this as a proxy for coccolithophore primary production. **Chapter Three** presents data on excess barium (Ba_{XS}) and its use in reconstructing export productivity over the past 200 kyr. **Chapter Four** concerns change in the productivity of North Atlantic fishes before, during, and after Marine Isotope Stage (MIS) 5, reconstructed using IAR. **Chapter Five** uses linear regressions of the datasets generated in the three previous chapters to investigate relationships between primary, fish, and export production. **Chapter Six** concludes the thesis by recapitulating the findings of earlier chapters and summarising the reconstructed changes in phytoplankton, fishes, and the carbon cycle. It discusses the relevance of these findings to understanding future anthropogenic climate change as well as suggesting future work.

1.2. Background

1.2.1. Pleistocene Climate

My thesis uses samples from the past 200 kyr, encompassing part of the Pleistocene, 2580–11.7 ka (Cohen *et al.*, 2013), and the Holocene, 11.7 ka–present. I chose to focus on this interval for numerous reasons, including: its value as a case study for relatively rapid climate change during glacial-interglacial transitions (also called terminations); the widespread availability of sediment from the late Pleistocene; and the similarity of Pleistocene and contemporary marine fauna and flora, providing strong potential for comparison with near-future changes.

The Pleistocene is a geological epoch characterised by the final closure of the Isthmus of Panama, long-term global cooling (Lisiecki and Raymo, 2005), and the presence of permanent Northern Hemisphere ice sheets (Gibbard, Head and Walker, 2010). The epoch is characterised by long-term cooling, with higher frequency, orbitally-forced cycles between cold glacial and warm interglacial climate states (Lisiecki and Raymo, 2005). These cycles were first characterised based on oxygen isotope measurements in foraminifera-bound carbonate by Emiliani (1955) and are now defined via the LR04 global benthic oxygen isotope stack (Figure 1.1) by Lisiecki & Raymo (2005) into Marine Isotope Stages (MISs), sometimes referred to as Oxygen Isotope Stages (OISs). The benthic oxygen isotope curve reflects changes in global deepwater temperature and ice volume (Elderfield *et al.*, 2012). It allows the Pleistocene to be divided into odd-numbered interglacial intervals, except for MIS 3 (Railsback *et al.*, 2015), and even-numbered glacial MISs. There is significant variation in duration, mean temperature, and global ice volume between and within interglacial stages, but they are broadly characterised by elevated global mean ocean and land surface temperature and lower mean ice volume than glacial stages (Tzedakis *et al.*, 2009).

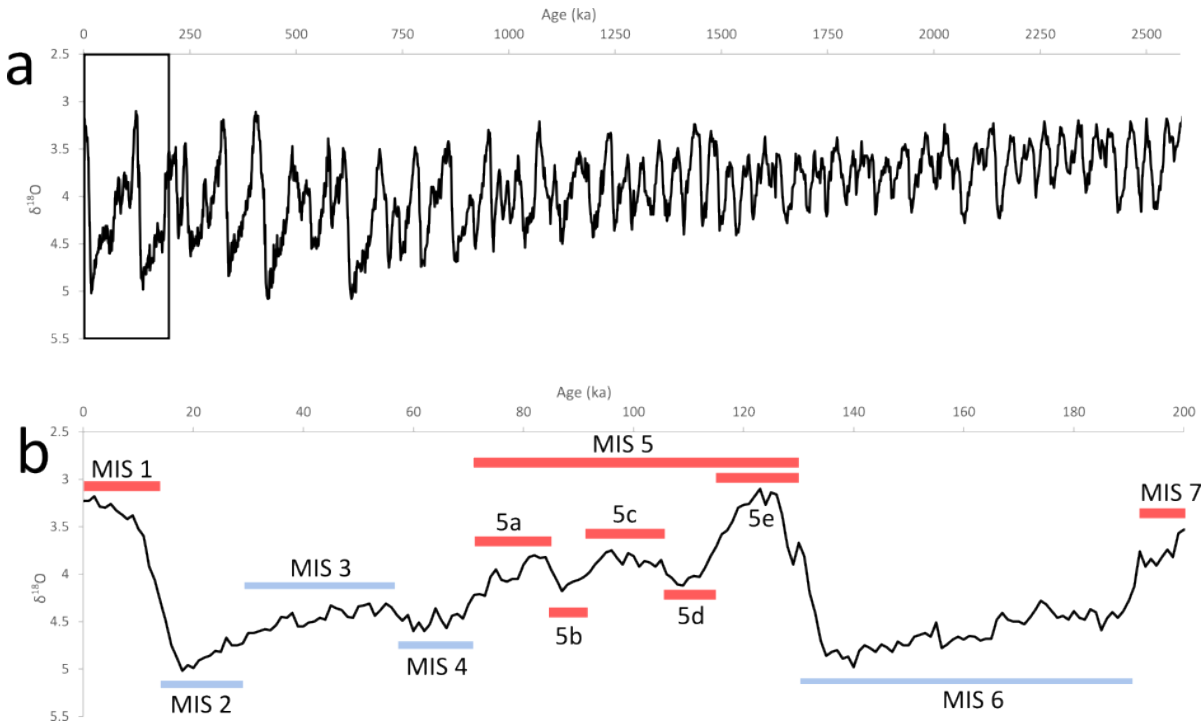

Figure 1.1 – The LR04 benthic oxygen isotope stack for (a) the Pleistocene and Holocene, the box on the left highlights the past 200 kyr; and (b) shows LR04 data for the past 200 kyr with Marine Isotope Stages labelled. Red and blue bars indicate glacial-interglacial definitions used in this thesis. Modified from Lisiecki and Raymo (2005).

This thesis concentrates on the last 200 ka (Figure 1.1b), which spans MIS 1-7. Table 1.1 provides date ranges and names used in this thesis. The Last Interglacial (LIG) here refers to the entirety of MIS 5, which differs from the narrower definition used by some studies to refer exclusively to the peak interglacial conditions during the MIS 5e substage (e.g. Shackleton, 1969). Last Glacial Period (LGP) refers to all of MIS 2, 3, and 4. MIS 3 was initially characterised as an interglacial climate, but numerous studies have demonstrated that this interval is more comparable to adjacent glacial states (Railsback *et al.*, 2015).

Table 1.1 – MIS boundary dates from the LR04 stack (Lisiecki and Raymo, 2005) and equivalent terms used in this thesis.

Marine Isotope Stage/s (MIS)	Interval (ka)	Equivalent term
1	0-14	Holocene
2-4	14-71	Last Glacial Period (LGP)
5	71-130	Last Interglacial (LIG)
6	130-191	Penultimate Glacial Period (PGP)
7	191-243	N/A

1.2.2. North Atlantic Oceanography

Pleistocene climatic change in the North Atlantic is probably more comprehensively studied than any other region of the globe. The North Atlantic Current (NAC) is an extension of a western boundary current that transports warm, saline water from tropical latitudes into the northeastern North Atlantic, strongly influencing local conditions between 40° and 60° latitude (Krauss, 1986; Rossby, 1996). It can also be considered as an 'upper limb' of the Atlantic Meridional Overturning Circulation (AMOC), which

is defined by the density-driven subduction of cold, saline water masses at high latitude – North Atlantic Deep Water (NADW) and Antarctic Bottom Water (AABW) – and the stratification and lateral transportation of these water masses at depth in the Atlantic (Talley *et al.*, 2011).

Much contemporary research is focussed on near-future changes in NAC and AMOC strength because of how these systems influence on the regional climate of North Atlantic landmasses (e.g. McCarthy et al., 2020; Ditlevsen and Ditlevsen, 2023; Westen, Kliphuis and Dijkstra, 2024). Potential volatility in AMOC strength is understood through proxy and model reconstructions of Pleistocene oceanography. During the Last Glacial Maximum (LGM), the Subarctic Front and NAC were located around 20° further south than in the present day (Ruddiman and McIntyre, 1976; Eynaud *et al.*, 2009; Waelbroeck *et al.*, 2009), leading to decreases in temperature in northwestern Europe sufficient to enable the growth and expansion of major ice sheets (Bekaert *et al.*, 2023), reduced delivery of saline water to high latitudes, and curtailing AMOC strength (Schmidt, Vautravers and Spero, 2006; Menviel *et al.*, 2020; Pöppelmeier, Scheen, *et al.*, 2021). AMOC strength variation has been observed both between glacial and interglacial states (Ruddiman and McIntyre, 1976; Adkins *et al.*, 1997; Alonso-Garcia, Sierro and Flores, 2011; Guihou *et al.*, 2011; Hennissen *et al.*, 2014; Holmes *et al.*, 2022), and on millennial timescales within glacial intervals (Heinrich, 1988; Schmidt, Vautravers and Spero, 2006; Stein et al., 2009; Dokken et al., 2013; Naafs et al., 2013).

During the LGP, the North Atlantic underwent major, millennial-scale changes in local climatic and oceanographic state (Bond *et al.*, 1992, 1993; Broecker *et al.*, 1992; Dansgaard *et al.*, 1993; Henry *et al.*, 2016). Dansgaard-Oeschger (DO) cycles are a prominent example of millenail-scale variabilitiy. They were first recognised via major, antiphased oscillations in the $\delta^{18}O$ record of the Greenland and Antarctic ice sheets (Dansgaard *et al.*, 1993). The Northern Hemisphere underwent cold stadial phases followed by sub-centennial timescale transitions into warm interstadial phases. In Greenland, the magnitude of local temperature change was between 5–16.5°C (Kindler *et al.*, 2014). In the marine realm, some stadials of DO cycles coincide with Heinrich Events, which are sedimentary horizons dominated by ice-rafted debris (IRD) (Heinrich, 1988; Bond *et al.*, 1992; Broecker *et al.*, 1992). At least six Heinrich Events occurred during the LGP, and IRD deposition reached as far south as 40°N, including the midlatitude IODP Site U1313 that is used in this thesis (Bond *et al.*, 1992; Hemming, 2004; Expedition 306 Scientists, 2006; Naafs *et al.*, 2013).

Glacial-interglacial changes in turnover and community diversity have been elucidated in several clades, including ostracods (Didié and Bauch, 2000; Yasuhara *et al.*, 2008), coccolithophores (González-Lanchas *et al.*, 2020; Trotta *et al.*, 2022), diatoms (Nair *et al.*, 2015; Phillips and Harwood, 2017) and foraminifera (Kandiano, 2002; Portilho-Ramos *et al.*, 2017). However, the biotic response of other marine groups, notably fishes, to high-frequency Pleistocene climate change remains poorly constrained. Few studies have attempted to investigate responses between trophic levels using the pelagic fossil record. This thesis focuses on the LIG due to its potential as an analogue for low-to-intermediate severity near-future climate states (Burke *et al.*, 2018) with the goal of elucidating biotic response to these environmental perturbations in the pelagic realm.

1.2.3. Sites & Age Models

Within the North Atlantic, I selected two sediment cores for generating productivity datasets: ODP Hole 982B and IODP Hole U1313A. Both sites are from the pelagic ocean and record continuous sedimentation over the full temporal span of my research, enabling high-resolution records to be produced. ODP Hole 982B is situated at a latitude of 57°N, compared to 41°N for IODP Hole U1313A.

In the present day, these latitudes are located within North Atlantic Transitional Waters (NATW). NATW is defined by the influence of the NAC, which migrates significantly on glacial-interglacial timescales (Dansgaard *et al.*, 1993; Henry *et al.*, 2016; Bolton *et al.*, 2018). Using multiple sites across different latitudes permits an improved perspective of how biotic response varied across the ocean basin, and whether ecological and climatic changes are strongly correlated.

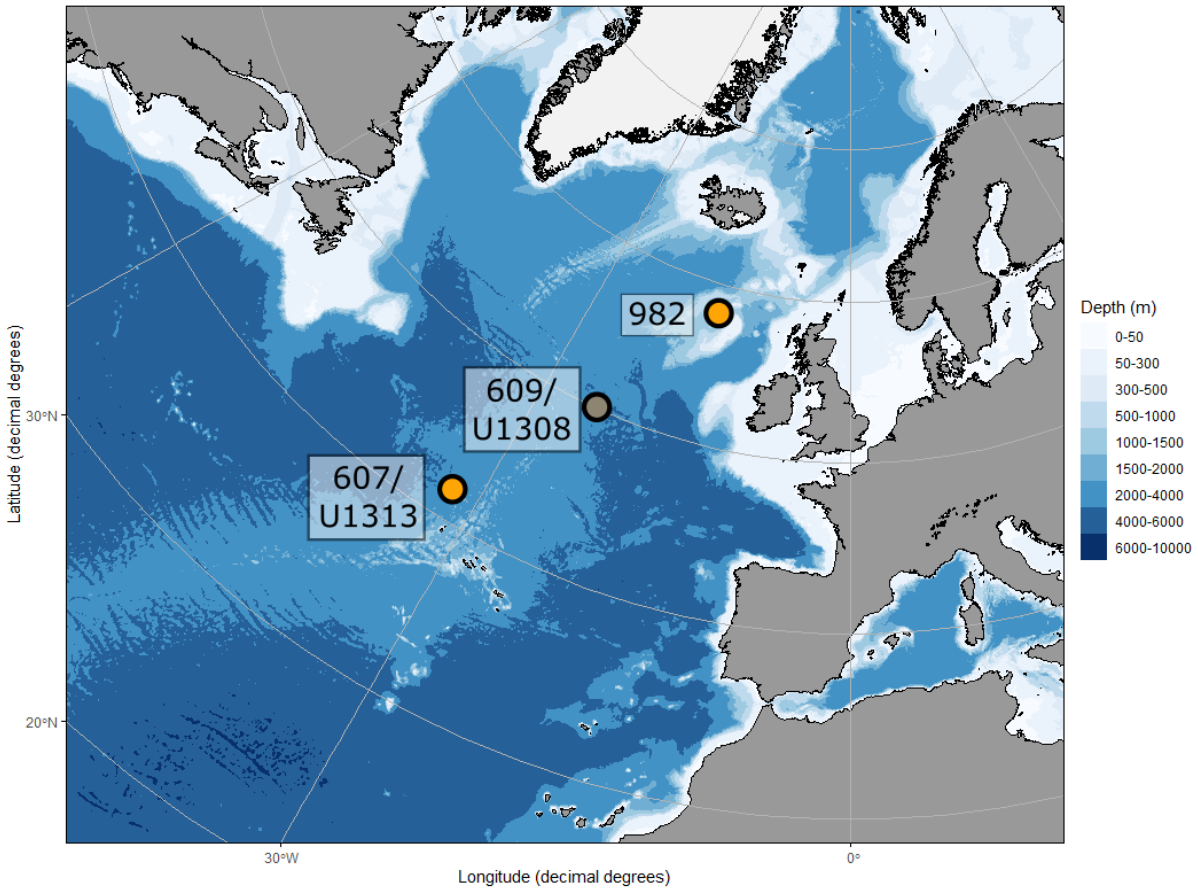

Figure 1.2 – Bathymetric map of the North Atlantic with Sites ODP 982, IODP 1308 (which supports the Site IODP U1313 age model), and IODP U1313 plotted. Made using ggOceanMaps in ggplot2 (Wickham, 2016; NOAA National Centers for Environmental Information, 2022; Vihtakari, 2023).

ODP Hole 982B

ODP Site 982 forms part of Leg 162 of the Ocean Drilling Project (ODP). Four holes (A, B, C and D) were drilled by Advanced Piston Coring (APC) in the Hatton-Rockall Basin between the Hatton and Rockall banks and approximately equidistant between Iceland and Ireland (Shipboard Scientific Party, 1996). The samples used in this study derive from hole 982B, whilst most of the secondary data used for age models and comparisons derive from Hole 982A. Both holes have complete recovery throughout the interval of interest for this study. The International Ocean Discovery Program (IODP) and its predecessor organisations correlate between cores by matching a core-specific 'metres below sea floor' (mbsf) onto a site-wide 'metres composite depth' (mcd) scale, enabling direct comparison between adjacent cores. For the top 6 sections (0-7.5 mcd) of 982A and the top 4 sections of 982B (0-5.38 mcd), mbsf and mcd are equal (Shipboard Scientific Party, 1996). This depth includes all of the past 200 kyr at this site (Herbert *et al.*, 2016) and negates the need to adjust reported mcd and mbsf when comparing published results from 982A with my data from 982B.

Table 1.2 – Latitude-longitude and depth data for ODP Holes 982A and 982B. Depth is given in metres below rig floor (mbrf), which differs from mbsf.

ODP Hole	Latitude	Longitude	Seafloor depth (mbrf)
982A	57°30.992'N	15°52.001'W	1146.3
982B	57°31.002'N	15°51.993'W	1145.0

The age model for ODP Site 982 is derived from the orbitally-tuned LR04 benthic oxygen isotope record (Lisiecki and Raymo, 2005), which was generated based on the benthic foraminifera *Cibicidoides spp.* $\delta^{18}O$ record of (Venz *et al.*, 1999). The LR04 age model was further refined by Herbert et al. (2016) using the Bayesian age model program "Bacon" (Blaauw and Christen, 2011). This recalibration has only a minor impact on the age model for ODP Site 982 (shown in Figure 1.3) but is preferable due to the greater constraint permitted in quantifying errors in both age and sedimentation rate (Figure 1.4) for the site. I use a linear interpolation of the Herbert et al. (2016) age model as the basis of dating samples from ODP Site 982 throughout this thesis.

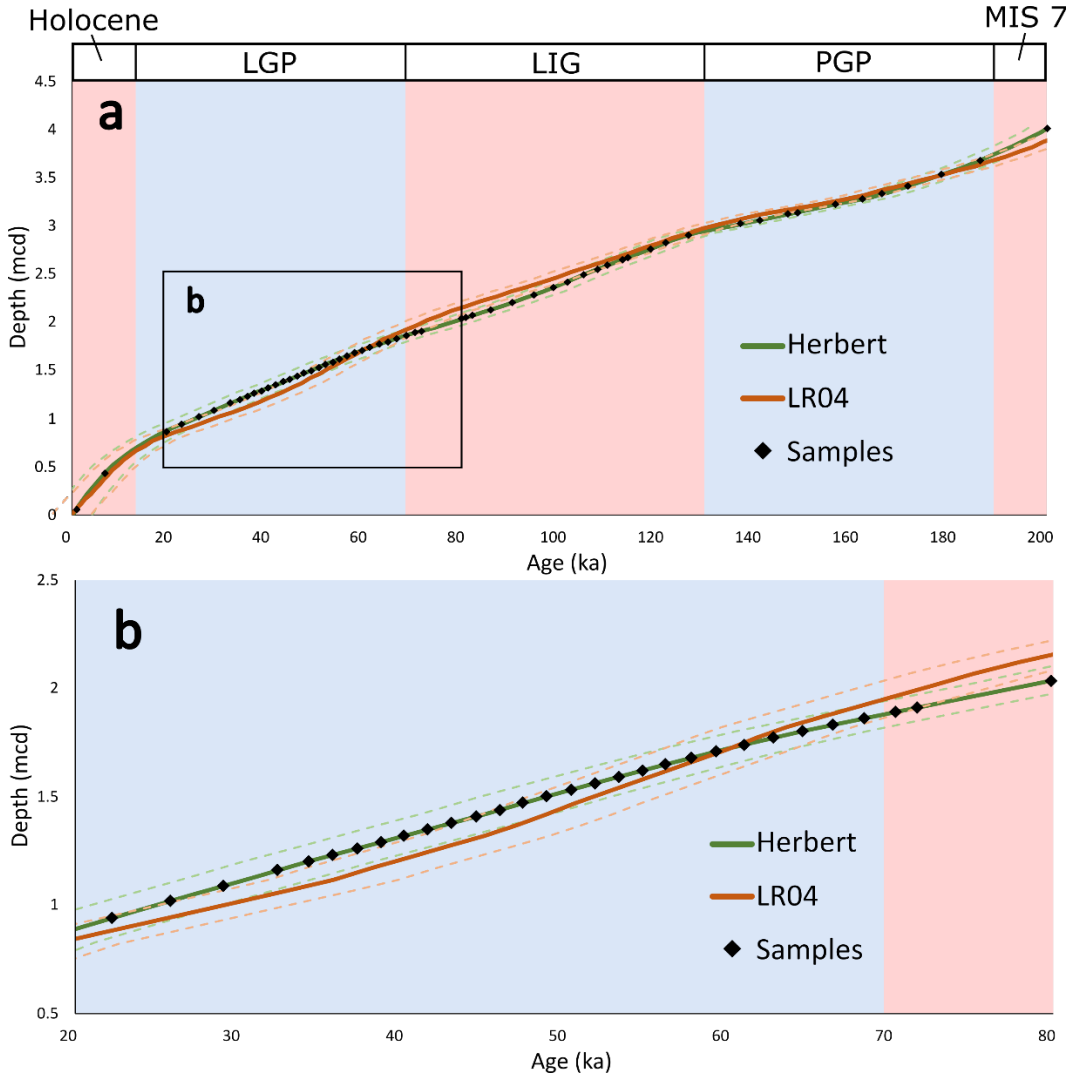

Figure 1.3 – Graphical comparison between two age models for ODP Site 982: Lisiecki and Raymo (2005) and Herbert et al. (2016). Top panel (a) shows full 200 kyr span of samples used in this thesis. Bottom panel (b) shows enlarged version of the 20-80 ka interval, where my sampling is at highest resolution. Black diamonds indicate depths of my samples on the Herbert et al. (2016) model. Dashed lines show age estimate error and background colours show the span of glacial (blue) and interglacial (red) intervals.

Although ODP Site 982 has a well-resolved age model with nearly continuous sedimentation over the last 200 ka, several potential issues merit further discussion. This site is located 131 km west-southwest of Rockall Island, the sole (<1km^2) Holocene subaerial exposure of the Rockall Bank (Hitchen, 2004). Eustatic sea level fall during glacial intervals significantly expanded this subaerial exposure, which may have contributed to variable and generally increased non-IRD detrital input to ODP Site 982 (Shipboard Scientific Party, 1996). Significant and variable detrital (non-pelagic) sediment contributions during glacial times have the potential to complicate our age model by diluting sediment. However, Heinrich events provide temporally discrete ties within glacial intervals that may partly offset these issues.

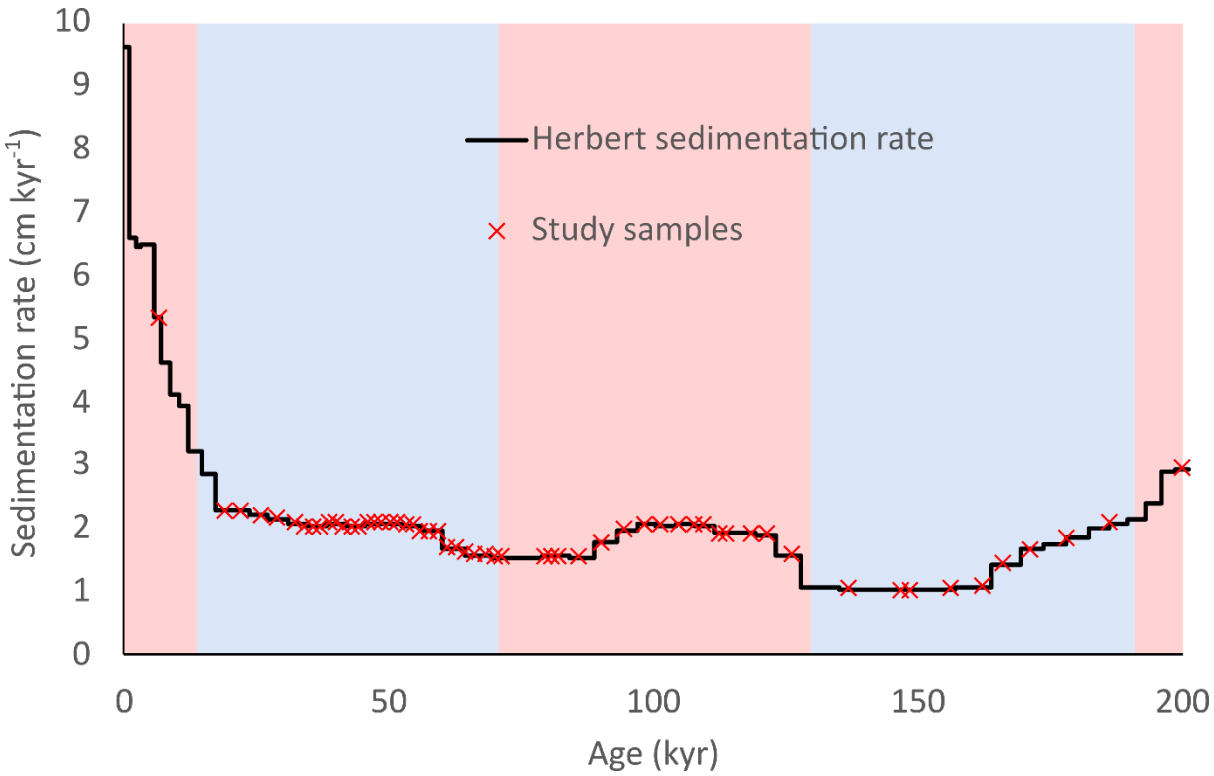

Figure 1.4 – Sedimentation rate over the past 200 kyrs at ODP Site 982, as reconstructed by Hertbert *et al*. (2016), with samples used in this study shown by red crosses. Background blue and red colours indicate glacial and interglacial intervals, respectively.

Relevant existing records for ODP Site 982 are described below and summarised in Figure 1.5.

Deepwater temperature and ice volume

Benthic oxygen isotope ratios ($\delta^{18}O$) derived from foraminifera tests record changes in deep water temperature, which is conserved within water masses and globally conservative (but not uniform), and ice volume (Shackleton, 1987). Venz et al. (1999) produced a benthic $\delta^{18}O$ record for ODP Site 982 from *Cibicidoides spp.*, which also forms part of the global LR04 stack (Lisiecki and Raymo, 2005). This record shows similar temporal trends to LR04, with glacial-interglacial changes of ~2‰ and minimum values corresponding to the strongest interglacial conditions in the Holocene and early LIG (Venz *et al.*, 1999).

Sediment composition

Calcium carbonate ($CaCO_3$) is the major sedimentary constituent of ODP Site 982 sediment throughout the past 200 kyr. Peak %$CaCO_3$ of 80-90% occur during the LIG and Holocene (Baumann and Huber,

1999; Venz *et al.*, 1999). There is a strong correlation between $\%CaCO_3$ and coccolith abundance, but no significant relationship between planktic foraminifera abundance and $\%CaCO_3$ (Baumann and Huber, 1999). Minimum sedimentary $\%CaCO_3$ occurs during glacial intervals due to dilution of sediment by detrital input, primarily from IRD (Ruddiman, 1977; Baumann and Huber, 1999).

IRD is elevated during glacial intervals relative to interglacial intervals in the high-resolution (mean interval of 2.5 kyr) dataset of Venz et al. (1999), in broad agreement with another, lower resolution dataset (Baumann and Huber, 1999). Mean IRD exceeds 2.5% in both the LGP (2.51%) and PGP (2.92%) and is lower in the Holocene (1.05%) and LIG (2.11%), although the latter is skewed by a single IRD peak at Termination II (26.2%). If this datapoint is omitted, mean IRD during the LIG (1.02%) is lower than that of the Holocene. Strong IRD peaks are seen during Terminations II and III, with a more subdued peak during Termination I (Venz *et al.*, 1999). Heinrich events are not seen in the IRD record of ODP Site 982, as the invasion of cold northern waters pushed the IRD-belt to the south of the Rockall Plateau during glacial intervals (Ruddiman *et al.*, 1989).

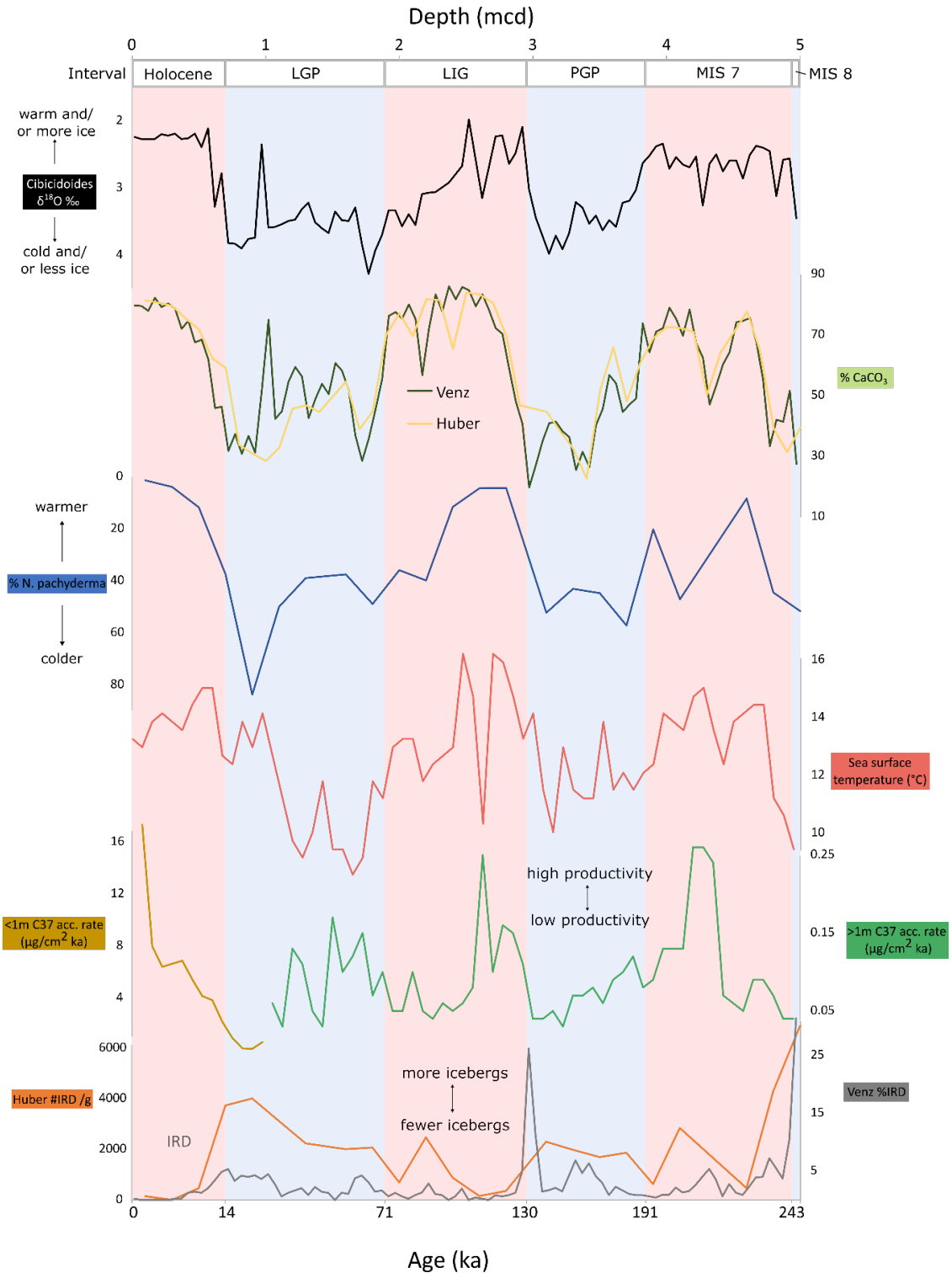

Figure 1.5 - Compilation of relevant existing datasets for the top 5 metres composite depth (mcd) for ODP Site 982, with glacial-interglacial boundaries shown. From top to bottom: Benthic foraminifera (Cibicidoides spp.) $\delta^{18}O$, a proxy for global ice volume and temperature (Venz *et al.*, 1999); %$CaCO_3$ in samples (Baumann and Huber, 1999; Venz *et al.*, 1999); % *N. pachyderma* in planktic foraminifera assemblages (Baumann and Huber, 1999); $U^{K'}_{37}$-derived SST estimates (Lawrence *et al.*, 2009; Herbert *et al.*, 2016); C37-alkenone accumulation rate (Bolton *et al.*, 2011); and ice-rafted debris (IRD) (Baumann and Huber, 1999; Venz *et al.*, 1999). Note that the x-axis is linearly scaled by depth and therefore the bottom age axis is non-linear.

Sea surface temperature

Lawrence et al. (2009) produced a sea surface temperature (SST) record for ODP Site 982 using the C37 alkenone unsaturation index ($U^{K'}_{37}$) (Rosell-Melé *et al.*, 1995). The $U^{K'}_{37}$ proxy uses the relative abundance of di- and tri-unsaturated ketones, which are produced by some species of haptophyte algae. Lawrence et al. (2009) found that mean SST during the LIG was 13.6°C, similar to that of the Holocene (13.9°C), and significantly greater than that of the LGP (11.1°C) and the PGP (12.0°C). The maximum SST of 16.2°C occurred during the LIG at 104 ka and 115 ka. Rapid cooling occurred early in the LGP, with a minimum SST of 8.6°C recorded at 56 ka. $U^{K'}_{37}$ SST reconstructions may be impacted by non-temperature effects, including: allochthonous deposition due to transport by ocean currents (Ohkouchi *et al.*, 2002), bias towards representing summer conditions if this is when alkenone-producing haptophytes are most productive (Conte *et al.*, 2006; Herfort *et al.*, 2006); and the recording of non-SST values when alkenone-producing haptophytes occupy a photic zone that extends beneath the mixed layer (Prahl, Mix and Sparrow, 2006).

Further evidence for glacial-interglacial cooling and warming at ODP Site 982 comes from the planktic foraminifera species *Neogloboquadrina pachyderma*. *N. pachyderma* dominates planktic foraminifera assemblages in polar waters of the present day and late Quaternary and so its abundance is used as a proxy for the presence of cold water masses (Westgård *et al.*, 2023). It is absent or near-absent in the planktic foraminifera microfossil record of ODP Site 982 throughout warmest intervals of the LIG and Holocene (Baumann and Huber, 1999; Lawrence *et al.*, 2009) and has higher average abundances during the LGP and PGP (Baumann and Huber, 1999). This strongly suggests the southward movement of the polar front and the incursion of cold water masses during glacial intervals and the northward retreat of those water masses during interglacial intervals.

A notable discrepancy between the two water temperature proxies outlined above occurs during the late LIG, where *N. pachyderma* peaks at 83.7% of the planktic foraminiferal assemblage (Baumann and Huber, 1999) at ~20 ka, approximately coincident with the Last Glacial Maximum (LGM), but the $U_{37}^{K'}$ record suggests SST comparable to the late Holocene (Lawrence *et al.*, 2009). Other datasets strongly suggest that the mid-latitude North Atlantic experienced full-glacial conditions around the time of the LGM (e.g. Waelbroeck et al., 2009; Naafs et al., 2012; Annan and Hargreaves, 2013), so it is likely that the $U^{K'}_{37}$ record for this interval may be impacted by one of the biases discussed previously.

Productivity

The only published export productivity proxy data for ODP Site 982 was generated by Bolton et al. (2011). They use C37 alkenone accumulation rates to reconstruct export by alkenone-producing haptophyte algae (Volkman *et al.*, 1980, 1995; Bolton *et al.*, 2011; Raja and Rosell-Melé, 2021). A striking feature of this record is the increase in C_{37} accumulation rates by five orders of magnitude from the LGM to late Holocene that dwarfs earlier interglacial peaks. This could potentially reflect the strong preservation of alkenones within young sediments, rather than a dramatic increase in haptophyte productivity in the Holocene. Another, much smaller, peak in C37 accumulation rate occurs during MIS 7, followed by a gradual decline and nadir in the late PGP and then a relatively rapid fivefold increase into the early LIG (Bolton *et al.*, 2011). This suggests a strong increase in the productivity of haptophyte algae following Termination II. Accumulation rates from the late LIG to the middle of the LGP show no clear relationship to other environmental proxies.

IODP Hole U1313A

IODP Site U1313 was drilled during IODP Expedition 306 and is a reoccupation of Deep Sea Drilling Project (DSDP) Site 607. The seafloor at this site is found at just over 3400m, making it significantly

deeper than ODP Site 982. IODP Site U1313 sits approximately 390 km northwest of the Azores on the western side of the Mid Atlantic Ridge (Expedition 306 Scientists, 2006). This thesis uses samples from U1313A, which was one of four cores (A, B, C and D) drilled using the APC system in March 2005 (Expedition 306 Scientists, 2006).

Table 1.3 – Latitude-longitude and depth data for IODP Holes U1313A and U1313B (Expedition 306 Scientists, 2006) and IODP Holes U1308C and U1308E (Expedition 303 Scientists, 2006), included because of their use in generating the age model for IODP Site U1313 (Naafs *et al.*, 2013). Depth is given in metres below rig floor (mbrf).

IODP Hole	Latitude	Longitude	Seafloor depth (mbrf)
U1313A	41°0.0679'N	32°57.4386'W	3423.3
U1313B	41°0.0818'N	32°57.4380'W	3424.6
U1308C	49°52.6838'N	24°14.2867'W	3872.7
U1308E	49°52.6998'N	24°14.2866'W	3882.3

This thesis uses a linear interpolation of the IODP Site U1313 age model generated by Naafs et al. (2013). This age model was generated by correlating the XRF profiles of U1313B and another mid-latitude Atlantic core, IODP Site U1308 (a reoccupation of DSDP Site 609) (Expedition 303 Scientists, 2006). IODP Site U1308 is dated (Hodell *et al.*, 2008) by correlating benthic foraminifera (*C. wuellerstorfi* and *C. kullenbergi*) $\delta^{18}O$ with the LR04 stack (Lisiecki and Raymo, 2005) and the MD95-2042 core (Shackleton *et al.*, 2004), supplemented by ^{14}C dating for the youngest core section (Bond *et al.*, 1993). Naafs et al. (2013) produced Si/Sr and Ca/Sr profiles for U1313B using XRF, which were then tuned to U1308 using the Match 2.0 software (Lisiecki and Lisiecki, 2002). These elements are most temporally informative during the LGP and other glacial intervals due to the distinct composition of IRD peaks during Heinrich events in the LGP and Heinrich-like events in earlier glacial intervals (Hodell *et al.*, 2008; Naafs *et al.*, 2013; Naafs, Hefter and Stein, 2013). I use the IODP mcd scale to correlate the age of U1313B, for which the XRF profile was generated, with U1313A, from which my samples are sourced.

Stein et al. (2009) produced an alternative age model for 0 - 11 mcd of U1313 by correlating lightness, $\%CaCO_3$ and benthic $\delta^{18}O$ data between U1313B and Site DSDP 607 (the previous occupation of this same site), which is absolutely dated using benthic oxygen isotopes as part of the original LR04 stack (Lisiecki and Raymo, 2005). This age model is relatively high resolution in their study interval of 320-640 ka, but comparatively low resolution for younger periods. Furthermore, it is likely to prove particularly unreliable in the 6.33-10.02 mcd span (~140-240 ka), as there are no samples in this age range. For these reasons, I instead use the Naafs et al. (2013) age model.

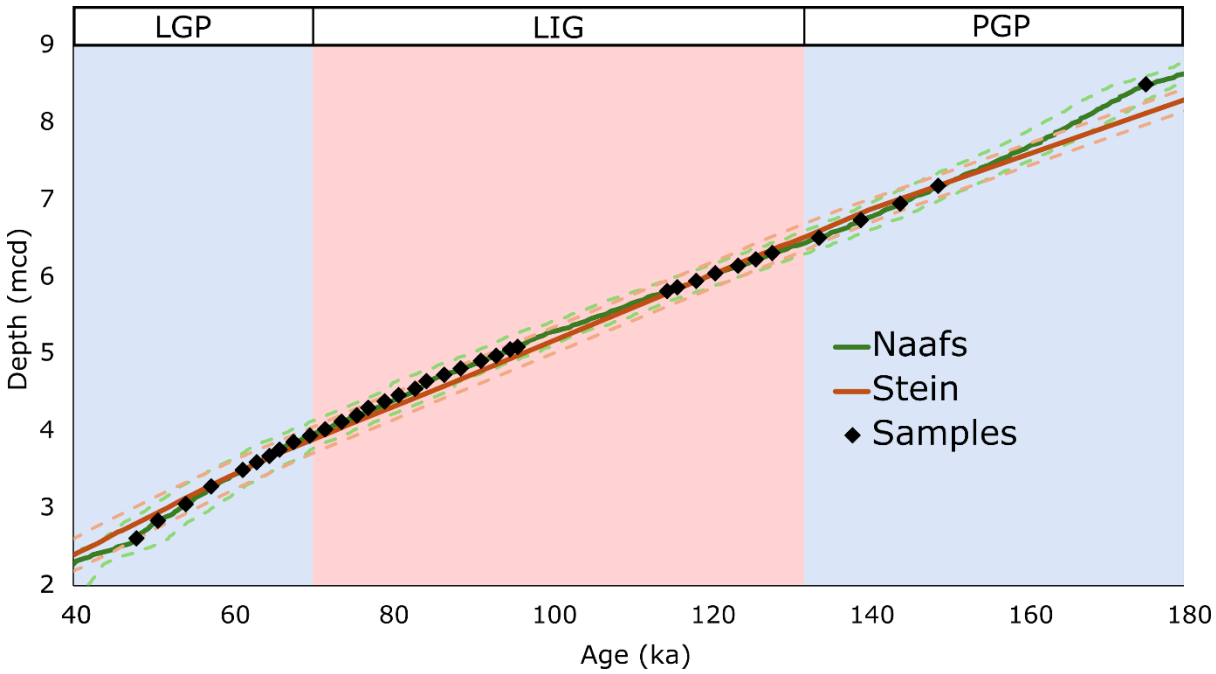

Figure 1.6 – Graphical comparison of the age-depth models of Naafs et al. (2013) and Stein et al. (2009) for 40-180 ka, which fully spans sampled intervals used in this thesis. Dashed lines show estimated error in age reconstruction for Naafs et al. (2013) (green) and Stein et al. (2009) (red). Black diamonds show the position of my samples on the Naafs et al. (2013) model. Background colours indicate whether the interval is interglacial (red) or glacial (blue), with interval names shown at the top.

In a linear interpolation of my sample depths, the maximum temporal offset between the Naafs et al. (2013) and Stein et al. (2009) age models in the last 140 ka is 3.6 ka, which is less than the 4 ka estimated error in the LR04 stack age. At greater ages the maximum offset for any IODP Site U1313 sample is 10.4 ka (a PGP sample), which is not unexpected due to the sample gap mentioned above. The age-depth reconstructions of these two models and impact on my sample age reconstructions are shown in Figure 1.6. Reconstructed sedimentation rate for IODP Site U1313 is shown in Figure 1.7.

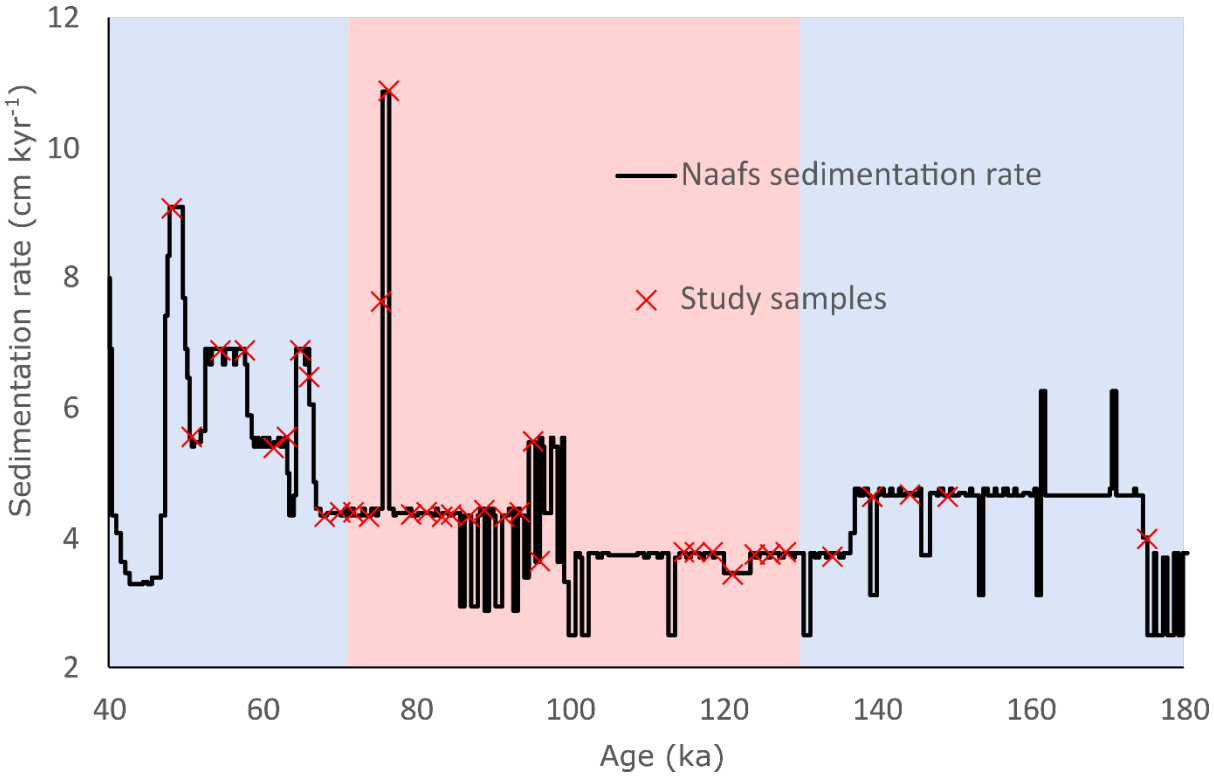

Figure 1.7 - Sedimentation rate at IODP Site U1313 between 40 and 180 kyrs, re, as reconstructed by Naafs *et al*. (2013), with samples used in this study shown by red crosses. Background blue and red colours indicate glacial and interglacial intervals, respectively.

Relevant existing records for IODP Site U1313 are described below and summarised in Figure 1.8.

Sea surface temperature and ice volume

Smith et al. (2013) produced a $\delta^{18}O$ record for the planktic foraminifera *Globigerina bulloides*, which inhabits the mixed layer in subpolar-to-midlatitude regions in the present day (Ottens, 1991; Sahoo *et al.*, 2022). This record shows a similar trend and magnitude of change to the benthic LR04 stack (Lisiecki and Raymo, 2005), with minima of 0-1‰ during the LIG and Holocene and maxima of 2-3‰ during the PGP and LGP. High $\delta^{18}O$ values reflect low temperatures, high global ice volume, and possibly freshening due to iceberg meltwater input during glacial intervals (Smith *et al.*, 2013).

Peaks in the relative abundance of *N. pachyderma* of up to 18% are coincident with highest $\delta^{18}O$ values during the LGP (Smith *et al.*, 2013) and therefore likely reflect cold intervals in the mid-latitude North Atlantic. In contrast, mean % *N. pachyderma* during the LIG is only 0.85% (Smith *et al.*, 2013), demonstrating the persistence of temperate-to-subtropical conditions throughout MIS 5.

High resolution $U^{k'}_{37}$-derived SST data for IODP Site U1313 shows high temperatures persisting throughout the early-to-mid LIG and Holocene, with maximum values of 18.8°C and 18.6°C, respectively (Naafs *et al.*, 2012), similar to the current annual mean surface temperature of 18.3°C (Locarnini *et al.*, 2013). Minimum SSTs occur during the earliest part of the LGP (11.9°C at 62.0 ka) and around the time of the LGM (11.2°C at 19.7 ka) (Naafs *et al.*, 2012). A lower resolution record covering the same interval shows very strong correlation (Stein *et al.*, 2009).

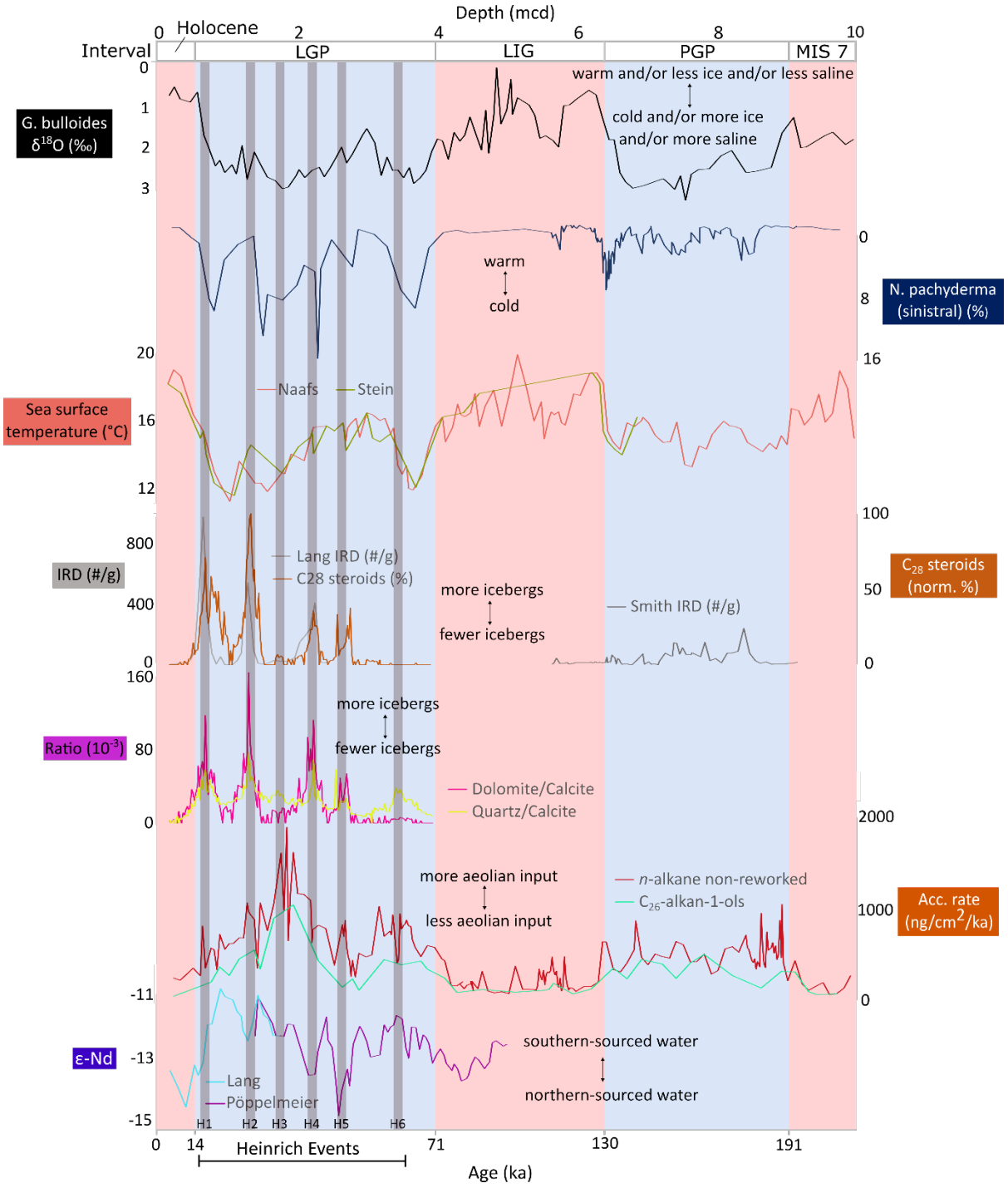

Figure 1.8 - Compilation of relevant existing datasets for the top 10 mcd at IODP Site U1313, with glacial-interglacial boundaries shown. From top to bottom: % *N. pachyderma* in total planktic foraminifera assemblage (Smith *et al.*, 2013); $U^{K}37'$-reconstructed sea surface temperature (Stein *et al.*, 2009; Naafs *et al.*, 2013); *G. bulloides* $\delta^{18}O$ (Smith *et al.*, 2013); IRD counts (Smith *et al.*, 2013; Lang *et al.*, 2016) and C_{28}-steroid normalised % (Naafs *et al.*, 2013); dolomite:calcite and quartz:calcite ratios (Naafs *et al.*, 2013); n-alkane non-reworked and C_{26}-alkan-1-ols accumulation rate (Naafs *et al.*, 2012); ε-Nd (Lang *et al.*, 2016; Pöppelmeier, Gutjahr, *et al.*, 2021). Approximate ages of LGP Heinrich events are shown by dark vertical bars. Note that the x-axis is scaled by mcd, shown at the top, and therefore the bottom age axis is not linearly scaled.

Allogenic inputs

Naafs et al. (2012) reconstructed aeolian inputs to IODP Site U1313 using the flux of two forms of higher plant leaf wax: *n*-alkanl-1-ols and *n*-alkanes. These lipids are carried from continental settings by wind and are a proxy for wind-blown dust, which can be important in relieving nutrient limitation in pelagic environments (Martin, 1990; Martínez-García *et al.*, 2014; Browning and Moore, 2023). Naafs et al. (2013)found that aeolian inputs were strongly elevated during the LGP and PGP relative to the LIG and Holocene, which they attributed to enhanced aridity and glaciogenic dust formation being delivered to the North Atlantic from North America by westerly winds (Naafs *et al.*, 2012).

Heinrich Events are evident in the IRD record of Site U1313, located close to the southern margin of the 'IRD belt' for the LGP (Ruddiman *et al.*, 1989). Raw IRD counts, geochemical proxies, and sedimentological data enable all six Heinrich Events of the past 70 ka to be resolved (Naafs, Hefter and Stein, 2013; Smith *et al.*, 2013; Lang *et al.*, 2016). The relative abundances of quartz and dolomite during Heinrich events evidence that Heinrich Event 3 (H3) and H6 were dominated by European or Greenland-sourced IRD, whilst H1, H2, H4, and H5 show a strong dolomite signal that is typical for IRD originating in the Hudson Strait (Hodell *et al.*, 2008; Naafs *et al.*, 2013). Lower IRD peaks from Heinrich-like events are also evident during the PGP (Smith *et al.*, 2013).

Ocean circulation

The more southerly location of IODP Site U1313 relative to ODP Site 982 makes it well-suited to studies of changing benthic water masses during glacial-interglacial cycles. In the present day, North Atlantic deep water (NADW) dominates this portion of the basin due to subduction of cold, dense water masses in the north (Lang *et al.*, 2016). Several studies have attempted to reconstruct the relative past contributions of NADW and Antarctic bottom water (AABW) in this region in the geological past (Lang *et al.*, 2016; Pöppelmeier, Gutjahr, *et al.*, 2021). Limited NADW formation, and overall weaker AMOC during glacial episodes, is suggested by the neodymium isotope record, which indicates a predominantly AABW source during the LGP, followed by an abrupt switch to a NADW source at the start of the Holocene (Lang *et al.*, 2016; Pöppelmeier, Gutjahr, *et al.*, 2021).

1.3. Primary production

Using sediments from ODP Hole 982B and IODP Hole U1313A, this thesis aims to quantify the magnitude and direction of changes in North Atlantic productivity during glacial-interglacial cycles of the late Pleistocene. Primary production is the foundation of all ecosystems as well as one of the primary mechanisms for removing carbon dioxide from the atmosphere, hence altering global climate. Long-term reductions in marine primary production could impose bottom-up energetic constraints on higher trophic levels, such as fishes (Chassot *et al.*, 2010).

Primary production is the synthesis of organic compounds from inorganic sources by autotrophic organisms and is the prerequisite of all trophic interactions in every ecosystem on the planet. Primary production results in the fixation of marine carbon as biomass, lowering the saturation of inorganic carbon in the shallow ocean and hence enabling the transfer of carbon dioxide from the atmosphere into the ocean (Falkowski, Barber and Smetacek, 1998). Export production also plays an important role in moderating global climate by transporting carbon-rich organic matter from the surface to deep ocean, where it can be isolated from the atmosphere for hundreds or thousands of years (Passow and Carlson, 2012; Iversen, 2023).

Slightly under half of all global primary production is marine in origin (Field *et al.*, 1998), although marine biomass comprises less than 1% of the global total (Ciais *et al.*, 2013). The lability of marine biomass occurs because oceanic primary producers mostly consist of phytoplankton, which typically have a lifespan of only a few days, in contrast to months or years for terrestrial plants (Marba, Duarte and Agusti, 2007).

Photoautotrophy fixes over two orders of magnitude more carbon than chemoautotrophy (Field *et al.*, 1998; Middelburg, 2011), making photosynthesis by far the dominant form of primary production in the modern biosphere. At the broadest level, photosynthesis involves the conversion of carbon dioxide and water into sugars using energy from sunlight. This process fixes inorganic carbon into organic compounds and releases molecular oxygen, which is summarised in the following (simplified) reaction (Sigman and Hain, 2012):

$$CO_2(aq) + H_2O \rightarrow CH_2O + O_2$$

Photosynthesis consists of light-dependent and light-independent reactions. Both occur within discrete areas of chloroplasts—organelles found in photoautotrophic eukaryotes (Nelson and Ben-Shem, 2004). These processes originated in photosynthetic cyanobacteria, some of which were later incorporated into eukaryotic cells through endosymbiosis (Archibald, 2015).

Light-dependent reactions produce two key molecules: nicotinamide adenine dinucleotide phosphate (NADPH) and adenosine triphosphate (ATP). Both molecules form through electron transfer chains in the light-absorbing structures (photosystems) of cells. NADPH is a reduced electron carrier molecule and ATP is an energy storage molecule generated as protons travel across hydrogen gradients (Nelson and Ben-Shem, 2004). Photoautotrophs synthesise atmospheric carbon dioxide into sugars via the (light-independent) Calvin Cycle. ATP and NADPH are the fuel for this process.

Photosystems are made of layers of light-harvesting photosynthetic pigments, including cholorophyll-*a* and cholorophyll-*b*. The unique reflectance properties of chlorophyll-*a* allow its detection by satellite-based remote sensing (Gitelson and Merzlyak, 1996; Porcar-Castell *et al.*, 2014). In the marine realm, chlorophyll-*a* concentration, mixed layer depth, temperature, and other local variables, are used to calculate estimates of primary production (Gitelson and Merzlyak, 1996; Porcar-Castell *et al.*, 2014; NASA Goddard Space Flight Center, Ocean Ecology Laboratory and Ocean Biology Processing Group, 2022).

Light is rapidly attenuated in the shallow ocean by organic particles, inorganic particles, and water molecules. Incident light is only strong enough to drive the photosynthetic reaction in the shallow portion of the upper ocean called the euphotic zone, where photosynthetically active radiation remains >1% of the level found at the surface (Sigman and Hain, 2012). Euphotic depth can vary substantially both by region and season and depends on the concentration of attenuating particles in the water column. In oligotrophic gyres, the mean euphotic depth may be as great 150 m, whereas euphotic depth in turbid, eutrophic coastal waters can be shallower than 10 m (Siegel *et al.*, 2014).

Equatorial latitudes experience high levels of insolation throughout the year, and therefore photoautotroph growth is not primarily limited by light availability, but by nutrient availability. In contrast, higher latitudes undergo seasonal light limitation during the winter, impacting both the timing and magnitude of productivity. Throughout high-latitude winter, low light levels support significantly reduced photosynthetic activity compared to spring, summer, and autumn (Sigman and Hain, 2012)**.** Light levels increase into spring, but remain a limiting factor until summer, when productivity once again becomes nutrient limited (Mitchell *et al.*, 1991; Joy-Warren *et al.*, 2019), as shown in Figure 1.9.

a

b

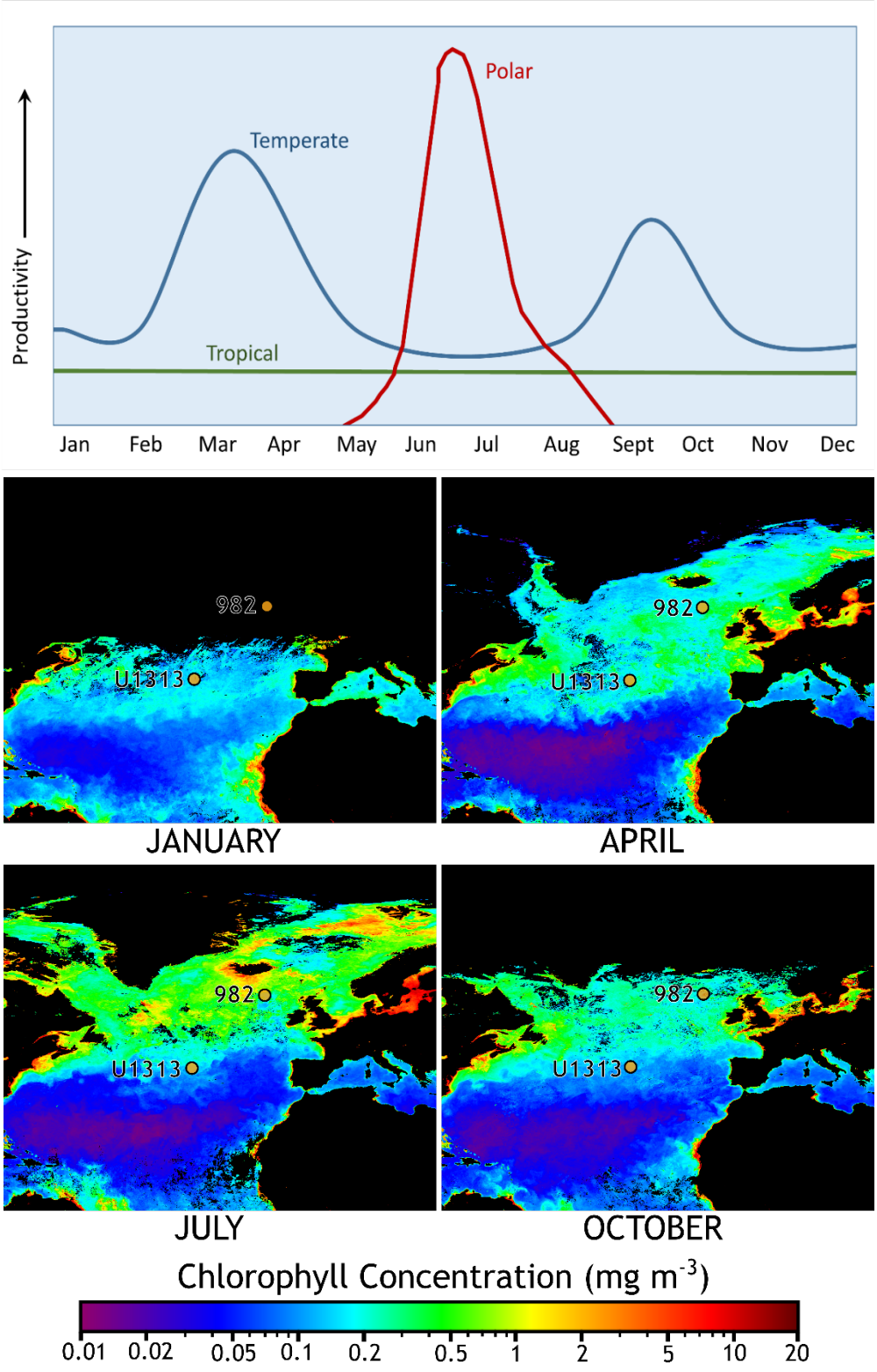

Figure 1.9 – Aqueous primary productivity over a year. (a) Relative magnitude of productivity in three Northern Hemisphere regions, reproduced from Webb (2021). (b) Mean daily chlorophyll-a concentration in the North Atlantic during four 4 months in 2023, measured by the Aqua-MODIS instrument with ODP Site 982 and IODP Site U1313 labelled, adapted from NASA Goddard Space Flight Center, Ocean Ecology Laboratory and Ocean Biology Processing Group (2022). Note that the absence of data at high latitudes during winter is due to insufficient light reaching the instrument.

Oceanic photosynthesis depends on the availability of nutrients—any molecule utilised by an organism for some biological purpose. Nutrients are divisible into two major categories: macronutrients (phosphate and nitrate) and micronutrients. Eutrophic regions are defined by relatively high levels of nutrient input and primary production, whilst oligotrophic areas are characterised by little nutrient input and low productivity. The average chemistry of photosynthesis in the marine environment, accounting for nutrients, can be represented by the following equation, reproduced from Paytan and McLaughlin (2007):

$$106CO_2 + 16HNO_3 + H_3PO_4 + 122H_2O + trace\ elements\ and\ vitamins \rightarrow C_{106}H_{263}O_{110}N_{16}P + 138O_2$$

Coastal waters and upwelling zones are often eutrophic due to allochthonous nutrient input via fluvial, aeolian, and tidal processes, as well as the recirculation of deep, nutrient-rich water masses to the euphotic zone. Anthropogenic nutrients can also dominate total input in densely populated areas (Hale *et al.*, 2015; Zhou *et al.*, 2020), potentially triggering phytoplankton blooms, hypoxia, and mass mortality events (Diaz and Rosenberg, 1995). In oligotrophic areas, such as the subtropical North Atlantic, the resupply of nutrients to the euphotic zone by mixing is weak due to strong vertical stratification. These regions are therefore typically macronutrient limited, primarily by nitrate and secondarily by phosphate (Moore *et al.*, 2013; Browning and Moore, 2023). Open ocean gyres, sometimes termed 'ocean deserts', are characterised by low nutrient input, high recycling rates and low primary production. Despite occupying the majority of the ocean by surface area, oligotrophic gyres sustain a lower fish biomass than the more spatially limited eutrophic areas (Bianchi *et al.*, 2021). IODP Site U1313 is close to the boundary of the subtropical and subpolar gyres and shows subtropical-to-temperate-style patterns in primary production, with peaks during the spring and summer. Being on the boundary of these distinct oceanographic systems, this site is particularly sensitive to oceanographic reorganisation during Pleistocene glacial-interglacial cycles (Ruddiman and McIntyre, 1976; Heinrich, 1988; Bolton *et al.*, 2018; Guerreiro *et al.*, 2023). Stronger vertical mixing, and hence elevated mean annual primary production, is likely to have coincided with the southward migration of the Subarctic Front during glacial times (Bolton *et al.*, 2018).

In subpolar gyres such as the high-latitude North Atlantic, productivity is light-limited during the winter. Nutrients are resupplied via strong vertical mixing and the mixed layer is seasonally resupplied with nutrients, spurring blooms from spring into autumn (Webb, 2021). At ODP Site 982, contemporary primary production increases in spring and peaks in midsummer (Figure 1.9), reflecting the position of this site on the boundary of the temperate and polar ocean (Sutton *et al.*, 2017). During glacial intervals in the Pleistocene, it is likely that the southward migration of the Subarctic Front led to more polar-type productivity patterns at this site, with stronger stratification and a more pronounced summer productivity peak (Bolton *et al.*, 2011; Guerreiro *et al.*, 2023).

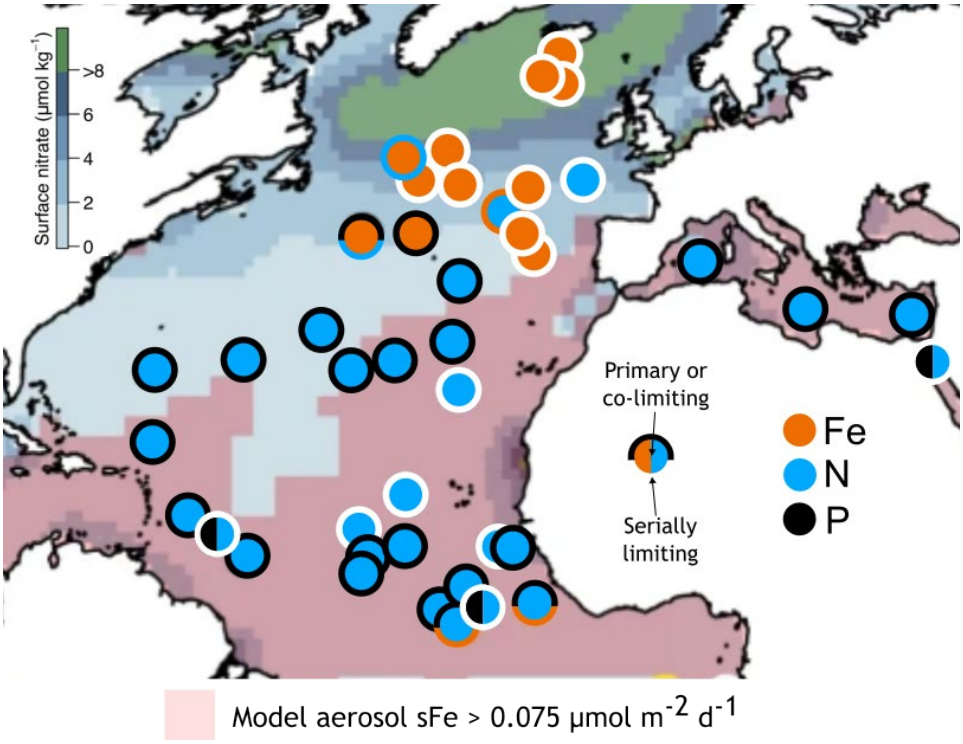

Figure 1.10 – Map of North Atlantic nutrient limitation, modified from Browning and Moore (2023). Background gradient shows surface nitrate concentration in µmol kg^{-1} and regions where modelled bioavailable aeolian Fe deposition exceeds 0.075 µmol m^{-2} d^{-1} (Chien *et al.*, 2016). Circles show experimental observations of primary nutrient limitation or co-limitation (inner circle), or secondary limitation and/or co-limitation (outer ring). Limiting nutrients are shown on the right key and white outer circles indicate that no serially limiting nutrient was identified.

1.4. Export production

Primary production fuels food chains and plays a role in controlling global climate. However, as the shallow ocean and atmosphere are in equilibrium on timescales of around one year, any changes in the saturation state of carbon are quickly communicated between the two reservoirs (Zeebe and Wolf-Gladrow, 2001). Longer-term sequestration of atmospheric carbon into the ocean requires that carbon to be exported from the shallow ocean. This exported carbon can remain isolated from the atmosphere for hundreds of years (Passow and Carlson, 2012; Iversen, 2023) and provides a food source for deep sea consumers. During Pleistocene glacial intervals, stronger export production may have contributed to a substantial lowering of atmospheric carbon dioxide concentrations (Martin, 1990; Passow and Carlson, 2012; Yu *et al.*, 2019).

Most organic carbon produced through photosynthesis is rapidly consumed and returned to inorganic forms in the surface ocean via heterotroph respiration and bacterial degradation (Eppley and Peterson, 1979). Export production is the quantity of organic carbon that escapes recycling in the shallow ocean and is physically transported beneath a defined depth horizon. The precise depth used varies significantly, including: the bottom of the photic zone (Nowicki, DeVries and Siegel, 2022), 150 m (Davison *et al.*, 2013; Guidi *et al.*, 2016), the base of the mesopelagic layer (~1000 m) (Henson, Sanders and Madsen, 2012), 2000 m depth (Tréguer *et al.*, 2018), and 3000 m depth (Lampitt *et al.*, 2010). Characterising relationships between primary and export production requires regional and ecosystem-specific approaches (Passow and Carlson, 2012) due to strong spatio-temporal differences in vertical

ocean structure (Sigman and Hain, 2012; Fu, Randerson and Moore, 2016)**,** allochthonous nutrient inputs (Browning and Moore, 2023) and ecosystem structure (Jin. *et al.*, 2006; Guidi *et al.*, 2009, 2016; Iversen, 2023).

The rate of organic matter degradation varies substantially with depth in the ocean. In pelagic environments, grazing by small zooplankton rapidly remineralises organic matter in the euphotic zone, whilst the much slower process of microbial degradation tends to dominate in the lower portion of the mesopelagic later (Guidi *et al.*, 2009; Henson, Sanders and Madsen, 2012). Below 1000 m, in the bathypelagic, there is only scarce remineralisation of sinking organic matter by heterotroph activity. Material crossing this horizon is sometimes considered as the 'sequestration flux', denoting that the carbon here will be isolated from the atmosphere for >100 years (Passow and Carlson, 2012).

Carbon is exported from the surface ocean via two primary mechanisms: the solubility pump and the biological carbon pump. These two mechanisms act to produce a gradient from low to high dissolved inorganic carbon (DIC) with depth (Roy-Barman and Jeandel, 2016).

The solubility pump describes the dissolution and downwelling of dissolved inorganic carbon (DIC) along isopycnal gradients at high latitudes. Bicarbonate (HCO_3) is the dominant DIC species in the modern ocean, with smaller amounts of aqueous carbon dioxide (CO_2) and carbonate ($CaCO_3$) also present. The reaction of atmospheric carbon dioxide to form bicarbonate is shown below, modified from Roy-Barman and Jeandel (2016):

$$CO_2(g) \rightarrow CO_2(aq) + H_2O \rightarrow H_2CO_2 \rightarrow H^+ + HCO_3$$

Downwelling of DIC-rich water masses primarily occurs in the Southern Ocean and North Atlantic, as part of the meridional overturning circulation (MOC). Around 10% of the vertical marine DIC gradient is attributable this mechanism (Boyd *et al.*, 2019).

The remaining 90% of the vertical DIC gradient is caused by the biological pump (also called the organic carbon pump), which is the biologically-mediated transport of particulate organic carbon (POC) from the euphotic zone to the ocean interior via gravitational settling, diel vertical migration (DVM) of zooplankton and fishes, and vertical mixing (Davison *et al.*, 2013; Omand *et al.*, 2015; Archibald, Siegel and Doney, 2019; Kelly *et al.*, 2019; Iversen, 2023).

Phytoplankton in the euphotic zone consume DIC and nutrients to form biomass (organic matter). This generation of POC reduces the saturation of DIC, adjusting ocean-atmosphere equilibrium and stimulating the transfer of atmospheric carbon dioxide into the ocean. A simplified version of this process is shown below, modified from Sigman and Hain (2012):

$$DIC + nutrients + H_2O \rightarrow POC + O_2$$

A data-constrained ensemble numerical model estimated mean global carbon export from the euphotic zone and found that, of all carbon exported from the euphotic zone, 60% consisted of faecal pellets (Nowicki, DeVries and Siegel, 2022; Figure 1.11). In the North Atlantic, faecal pellet production is most significant at low latitudes, whilst the relative importance of aggregate export, the mixing pump, and DVM all tend to increase with latitude (Nowicki, DeVries and Siegel, 2022). It should be noted that this model only simulated zooplankton DVM and excluded fish, therefore likely underestimating the total contribution of DVM to carbon export globally (Davison *et al.*, 2013; Anderson *et al.*, 2019).

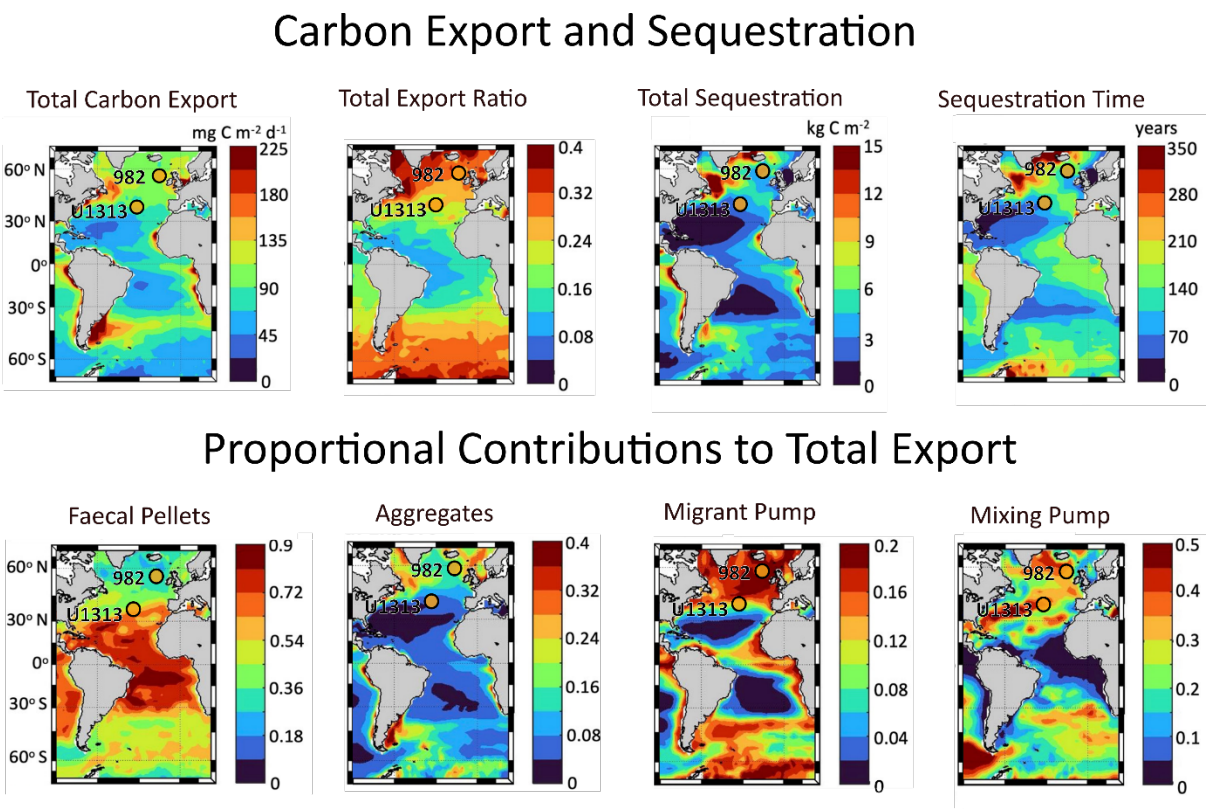

Figure 1.11 – Summary figures from a model simulation study of annual export production in the global ocean, modified from Nowicki, DeVries and Siegel (2022) and showing only the Atlantic Basin. The top four panels show export and sequestration summaries for total carbon exported from the euphotic zone; export ratio (annual export production divided by primary production); total carbon inventory stored under steady state conditions; and how long sequestered carbon remains in the ocean. The bottom four panels show the proportional contribution to total export of: zooplankton faecal pellets; biological aggregates sinking from the euphotic zone; active transport of carbon by zooplankton migration; and physical mixing through mechanisms such as subduction and mixed layer detrainment. Locations of ODP Site 982 and IODP Site U1313 are shown.

Ecology is important in understanding export. Guidi et al. (2009) found that more than two thirds of mass flux variance for large particles reaching 1 km depth in the global ocean could be explained by the size structure of the overlying phytoplankton community and its chlorophyll *a* mass. A more recent community genetics approach found that, in the oligotrophic ocean, a handful of viral, prokaryotic, and eukaryotic lineages alone could explain most variation in carbon export (Guidi *et al.*, 2016). The association of specific viral phages (such as those of the cyanobacteria *Synechococcus*) with a strengthened biological pump was discovered in the past decade (Guidi *et al.*, 2016; Breitbart *et al.*, 2018; Laber *et al.*, 2018), and is likely to be an area of substantial interest for researchers in the near future.

Broecker (1982) was the first to suggest that changes in the strength of the biological pump could explain glacial-interglacial atmospheric CO_2 concentrations during the Pleistocene. Martin (1990) suggested that this strengthened biological pump could have arisen from increased iron flux into the ocean during glacial intervals. Iron is the primary limiting nutrient across broad areas of the Southern, Pacific, and North Atlantic Oceans in the present day (Moore *et al.*, 2013; Browning and Moore, 2023). These areas are often termed 'high-nutrient, low chlorophyll' (HNLC) regions. Ship studies have shown that the artificial addition of iron can significantly enhance both primary production (Boyd *et al.*, 2007; Yoon *et al.*, 2018) and export production (Smetacek *et al.*, 2012) in HNLC areas. Glacial climates were

more arid than interglacial intervals, and evidence from sediment cores suggests that enhanced iron flux from wind-born dust coincided with episodes of greater export production (Loveley *et al.*, 2017), although the link between the two remains controversial (Costa *et al.*, 2016; Jacobel *et al.*, 2019).

In stratified, oligotrophic environments such as the subtropical North Atlantic, non-mineralising picophytoplankton, such as the cyanobacteria *Prochlorochoccus*, tend to dominate primary production (Olson *et al.*, 1990; Bolaños *et al.*, 2020; Haëntjens *et al.*, 2022). This results in the prevalence of long, inefficient food webs (Armengol *et al.*, 2019) and negligible direct sinking of particulate organic carbon. Consequently, the stratified subtropics have the lowest export ratio (net primary production divided by export production) any oceanic realm (Nowicki, DeVries and Siegel, 2022).

In the subpolar gyre, seasonal mixing promotes greater nutrient inputs to the euphotic zone (de Boyer Montégut *et al.*, 2004), allowing seasonal blooms of larger, eukaryotic phytoplankton such as diatoms and coccolithophores (Barcelos e Ramos *et al.*, 2017; Haëntjens *et al.*, 2022). These large phytoplankton have higher sinking rates than picophytoplankton and sustain shorter, more efficient food webs (Armengol *et al.*, 2019). These ecological factors result in a higher export ratio in the subpolar gyre than the subtropical gyre in the present day (Nowicki, DeVries and Siegel, 2022).

1.5. Phytoplankton

Phytoplankton are photosynthesising organisms with highly diverse cladistic associations and distinct evolutionary histories. They are broadly divisible into two groups: the eukaryotic algae and prokaryotic bacteria. Spatial and temporal heterogeneity in phytoplankton biomass is a ubiquitous feature of the global ocean. Ocean food web shape and structure is defined by the abundance, composition, and trophic relationships of phytoplankton autotrophs at their base (e.g. Chassot et al., 2010; Marañón, 2015; Armengol et al., 2019). Phytoplankton productivity and ecosystem structure influence the global carbon cycle through the biological pump, as previously discussed. Physical and biogeochemical environmental variables such as light availability, nutrient supply, and the vertical structure of the water column, also strongly impact phytoplankton dynamics (Moore *et al.*, 2013; Joy-Warren *et al.*, 2019).

In the modern ocean, phytoplankton are central in modulating the Earth's climate through the biological carbon pump. Variations in the strength of this pump on millennial timescales can contribute to significant changes in atmospheric carbon dioxide concentration, notably during glacial-interglacial cycles of the Pleistocene (Sigman and Boyle, 2000; Sigman, Hain and Haug, 2010; Martínez-García *et al.*, 2014; Yu *et al.*, 2019). In the absence of phytoplankton, Earth's current atmospheric CO_2 levels would be around 150 to 200 ppmV higher (Falkowski *et al.*, 2000).

Bacterial picophytoplankton can efficiently scavenge scarce nutrients in oligotrophic environments and hence tend to dominate primary production in subtropical ocean gyres (Olson *et al.*, 1990; Raven, 1998; Guidi *et al.*, 2016), including contributing more than 80% of total primary production in the oligotrophic Atlantic Ocean (Tilstone *et al.*, 2017).

Micro- and nanophytoplankton, which include all eukaryotic phytoplankton, are most abundant in eutrophic environments, such as upwelling zones, coastal regions, and high latitudes. Diatoms are the most globally abundant eukaryotic phytoplankton in the modern ocean (Benoiston *et al.*, 2017; Edwards *et al.*, 2022). Diatoms possess silica frustules with a relatively high direct sinking potential (Smetacek *et al.*, 2012; Abrantes *et al.*, 2016; Tréguer *et al.*, 2018) and can dominate primary

production, plankton biomass, and export in polar waters such as the high latitude North Atlantic (Edwards *et al.*, 2022).

Coccolithophores are calcified eukaryotic nanophytoplankton in the phylum *Haptophyta* (Young *et al.*, 2003). Alongside other non-calcifying haptophytes, coccolithophores contribute up to 20% of total primary production in the tropical-to-subtropical Atlantic, episodically rising as high as 40% during blooms in the temperate and polar Atlantic (Poulton *et al.*, 2006, 2007, 2013).

This thesis investigates the productivity of North Atlantic coccolithophores using the pelagic microfossil record. Coccolithophores are one of the few extant plankton groups whose palaeoecology can be studied in detail using the geological record due to high preservation potential in seafloor sediment above the carbonate compensation depth (CCD), the depth horizon beneath which calcite undersaturation in seawater leads to its dissolution from seafloor sediment (Woosley, 2016). Coccolith preservation in the North Atlantic is good, and the CCD is positioned significantly below the depth of surface sediment for both cores used in this study (Shipboard Scientific Party, 1996; Expedition 306 Scientists, 2006). This thesis uses the accumulation rate of coccoliths in seafloor sediment as a proxy for the productivity of this group (Flores and Sierro, 1997) and simultaneously assessed changes in the demography of coccolithophore assemblages, illuminating changes in water column properties such as temperature and stratification (e.g. Baumann et al., 2005; Marino et al., 2014; González-Lanchas et al., 2020).

1.6. Fishes

Alongside changes in primary and export production, this thesis investigates fish ecology in the North Atlantic during an interval of significant environmental change using the microfossil record.

Fishes are the most species-rich and numerically abundant vertebrate group on the planet (Nelson, Grande and Wilson, 2016). They are also the dominant consumers in intermediate and upper trophic levels in marine ecosystems. Over 90% of extant fish species are actinopterygians, or ray-finned fishes (Nelson, Grande and Wilson, 2016), whose diversity emerged during the 'Second Age of Fishes' in the late Cretaceous and early Cenozoic (Friedman, 2010; Near *et al.*, 2012; Alfaro and Faircloth, 2018).

The majority of fish biomass in the global ocean consists of small (<20cm) actinopterygian fishes in the mesopelagic ocean (200-1000m) (Gjøsaeter and Kawaguchi K., 1980; Kaiser, 2011; Dornan *et al.*, 2022). It is therefore also highly likely that mesopelagic fishes dominate the open ocean piscine microfossil record. Ecologically, mesopelagic fishes act as an intermediate trophic step between mesozooplankton and larger pelagic fishes (Gjøsaeter and Kawaguchi K., 1980). They are often taxonomically and numerically dominated by the family *Myctophidae*, the lanternfishes (Gjøsaeter and Kawaguchi K., 1980; Catul, Gauns and Karuppasamy, 2011; Schwarzhans and Carnevale, 2021). *Benthosema glaciale* (the glacier lanternfish) is the most abundant pelagic North Atlantic fish species and mainly feeds on the copepod *Calanus finmarchicus* (Hudson *et al.*, 2014; Knutsen *et al.*, 2023). A 2004 ship survey found that distinct myctophid fish communities were present north and south of the North Atlantic Subarctic Front (Sutton *et al.*, 2008; Hudson *et al.*, 2014; Kenchington *et al.*, 2017), which is a feature that also divides IODP Site U1313 and ODP Site 982 in the present day.

Whilst they are not directly harvested or consumed by humans, mesopelagic fishes retain an anthropocentric significance as a food source for large pelagic groups such as swordfishes, dolphins, whales, and tuna (Pusineri *et al.*, 2008; Pereira *et al.*, 2011). In recent years there has also been increasing interest in the potential harvesting of hitherto unexploited mesopelagic faunas for

aquaculture feed and direct consumption by humans, including in the North Atlantic (Heino *et al.*, 2011; Grimaldo *et al.*, 2020). The exploration of mesopelagic fishes as a food source is motivated by human dietary and economic reliance on fisheries, which supply 17% of all animal protein humanity consumes and have an economic value exceeding $360 billion USD (FAO, 2020).

Mesopelagic fishes undertake a DVM, whereby they rise into the euphotic zone at night to feed on zooplankton or large phytoplankton and migrate to deeper waters in daylight as a mechanism to avoid light-dependent predation (Anderson *et al.*, 2019; Kelly *et al.*, 2019). DVM is of central importance in the biological carbon pump as a significant mechanism for transporting organically bound carbon to depth, where it is released via respiration and the excretion of faecal pellets (Davison *et al.*, 2013; Irigoien *et al.*, 2014; Nowicki, DeVries and Siegel, 2022). A global LIDAR-based study (inclusive of zooplankton as well as fishes) found that the absolute biomass of vertically migrating animals is greatest in productive waters such as those found in temperate and polar waters, but that these faunas constitute a greater proportion of total biomass in the less productive subtropics (Behrenfeld *et al.*, 2019). Hence, DVM by mesopelagic fishes may contribute most significantly to total export production at locations with similar oceanographic characteristics as IODP Site U1313.

Mesopelagic fishes typically occupy depths of 200-1000 m (Kaiser, 2011) and can be detected by acoustic reflection surveys (e.g. Gjøsaeter and Kawaguchi K., 1980; Kaartvedt, Staby and Aksnes, 2012; Clavel-Henry et al., 2020; Dornan et al., 2022). Accurate estimates of mesopelagic fish biomass are extremely challenging due to limitations of acoustic measurements, fish escape (Kaartvedt, Staby and Aksnes, 2012), fish avoidance in net-based surveys (Pauly *et al.*, 2021), and poorly constrained models (Clavel-Henry *et al.*, 2020). Global mass estimates are in the range 1-16 Gtonnes (Irigoien *et al.*, 2014; Anderson *et al.*, 2019; Proud *et al.*, 2019; Pauly *et al.*, 2021). Even the lowest estimates would imply that the mesopelagic ocean is by far the most productive global habitat for vertebrates (Irigoien *et al.*, 2014; Nelson, Grande and Wilson, 2016). Mesopelagic fish biomass also demonstrates a strong correlation with local primary productivity in tropical open-ocean environments (Irigoien *et al.*, 2014), though a more recent survey resolved no significant relationship between primary production and non-gelatinous mesopelagic micronekton biomass in the high-latitude North Atlantic (Klevjer *et al.*, 2020).

Work over the past decade has utilised the marine microfossil record of fish teeth and chondrichthyan dermal denticles, collectively termed ‘ichthyoliths’, to investigate the connections between fish ecology and environmental change in the geological past (Sibert, Hull and Norris, 2014; Sibert and Norris, 2015; Sibert *et al.*, 2018; Werner, 2019; Britten and Sibert, 2020; Sibert and Rubin, 2021). Ichthyoliths are composed of calcium phosphate and have high preservation potential in a wide range of seafloor sediments (Doyle and Riedel, 1979), from which they can be isolated using standardised, sediment-specific methods (Sibert *et al.*, 2017). Mid-to-low latitude pelagic North Atlantic sediments are usually composed of coccolith or foraminifera carbonate ooze (Dutkiewicz *et al.*, 2015), necessitating the dissolution of the carbonate fraction using acetic acid prior to ichthyolith extraction (Sibert *et al.*, 2017).

Relative changes in ichthyolith accumulation rate (IAR) through time are a tool for reconstructing changes in the abundance of fishes in the overlying water column. For example, IAR was used to demonstrate heterogeneity in the response of fishes to the K-Pg boundary event in the Tethys Sea and Pacific Ocean (Sibert, Hull and Norris, 2014) and the diversification of pelagic ray-finned fishes in the earliest Palaeogene (Sibert and Norris, 2015).

The body fossil record of fishes is extremely limited, and it is practically impossible to acquire macrofossil specimens from the open ocean seafloor, making ichthyoliths the only viable means of understanding fish ecology, abundance, and diversity in Earth's largest habitat.

In this thesis I generate new IAR records to investigate changes in the abundance and diversity of pelagic North Atlantic fishes during the late Pleistocene. This thesis presents the highest-ever resolution pelagic ichthyolith research; it is also the first to look at Pleistocene glacial-interglacial cycles; and the first to directly compares the phytoplankton and fish microfossil records using the same sample material.

1.7. Geochemical productivity proxies

Estimating primary production on geological timescales, as opposed to the present day, presents substantial challenges. The oldest direct measurements of plankton productivity come from the continuous plankton recorder, almost a century ago (Reid *et al.*, 2003), and most direct measurements of productivity extend back no more than a few decades (Lombard *et al.*, 2019). Older reconstructions depend on the use of proxy measurements. Dozens of different productivity proxies exist, though their application typically depends on certain criteria being met. No proxy is universally applicable across all climatic and ecological regimes and even under optimal conditions, palaeoproductivity reconstructions are imperfectly comparable to extant data from in-situ measurements and remote sensing.

Proxies exist for estimating relative changes in primary, export, and clade-specific productivity in the geological past. These are usually derived from geochemical analysis of deep-sea sediments (e.g. McManus et al., 1998; Jin. et al., 2006; Schoepfer et al., 2015; Raja and Rosell-Melé, 2021) or the accumulation of microfossils (e.g. Flores and Sierro, 1997; Warnock and Scherer, 2014; Britten and Sibert, 2020).

In this thesis, I generate new palaeoproductivity datasets of excess barium accumulation rate ($Ba_{XS}AR$), calcareous nannofossil accumulation rate (NAR), and IAR. I also make use of existing alkenone mass accumulation rate (MAR) datasets.

Barite ($BaSO_4$) hosts barium and, in seafloor sediments, barite can be biogenic, detrital, or hydrothermal in origin. Biogenic barite forms within microenvironments in sinking organic matter (McManus *et al.*, 1998; Gingele *et al.*, 1999; Ganeshram *et al.*, 2003), and can be used as a proxy for export production on geological timescales (Schoepfer *et al.*, 2015; Bridgestock *et al.*, 2019). In this thesis I use excess (non-detrital) barium as an export production proxy because of its high reliability as an export proxy in open-ocean regions with low detrital inputs (Paytan and Griffith, 2007), and because barite preservation potential is high in oxygenated sediment porewaters where the reduction of sulphate by bacteria is minimal (McManus *et al.*, 1998; Schoepfer *et al.*, 2015; Nagakura *et al.*, 2022). Detrital inputs are generally low in the pelagic North Atlantic during the late Pleistocene (Eagle *et al.*, 2003), although detrital barium sourced from iceberg rafting and wind-blown dust does need to be accounted for when calculating excess barium (Eagle *et al.*, 2003; Schoepfer *et al.*, 2015). For the two cores used in this study, sulphate depletion in the upper 5-10 m of sediment is minimal (Shipboard Scientific Party, 1996; Expedition 306 Scientists, 2006) and hence no significant dissolution and remobilisation of barite has occurred since deposition.

Other geochemical palaeoproductivity proxies, such as total organic carbon and organic phosphorous, have much lower burial efficiencies (<10% vs 30-50% for barite) in oxic seafloor environments

(Dymond, Suess and Lyle, 1992; Paytan and Griffith, 2007; Schoepfer *et al.*, 2015), and hence were not utilised in this research.

C_{37} alkenones are di- and tri-unsaturated methyl ketones that are produced by haptophyte algae, notably *Gephyrocapsa* coccolithophores (Volkman *et al.*, 1980, 1995), and have high preservation potential in a variety of seafloor sediments (Farrimond, Eglinton and Brassell, 1986; Bolton *et al.*, 2010; Raja and Rosell-Melé, 2021). The accumulation rate of C_{37} alkenones in surface sediment shows a strong correlation with sea surface chlorophyll-*a* (Raja and Rosell-Melé, 2021), demonstrating its potential utility as a proxy for phytoplankton biomass and productivity in the geological past. However, Marino et al. (2022) found that NAR and C_{37} alkenone accumulation rate were decoupled in the Mediterranean during the Pleistocene, suggesting instead that C_{37} alkenone accumulation rate reflects the past abundance only of alkenone-producing species within the genus *Gephyrocapsa*. Conversely, Bolton et al. (2010) found strong agreement between NAR and C_{37} alkenone accumulation rate during the late Pliocene in the equatorial Atlantic and Pacific.

1.8. Conclusion

Marine ecosystems both strongly influence and are influenced by Earth's climate, particularly during the glacial-interglacial cycles of the Pleistocene. The quantification of how these ecosystems changed in the geological past can inform future projections of their response to ongoing and future anthropogenic climate change. The deep marine geological record provides the only direct means of quantifying these changes, and this thesis will combine numerous existing methodologies for reconstructing biological productivity to provide a novel overview of how pelagic North Atlantic ecosystems responded to environmental perturbations during the past 200 kyr.

References

Abrantes, F. *et al.* (2016) 'Diatoms Si uptake capacity drives carbon export in coastal upwelling systems', *Biogeosciences*, 13(14), pp. 4099–4109. Available at: https://doi.org/10.5194/bg-13-4099-2016.

Adkins, J.F. *et al.* (1997) 'Variability of the North Atlantic thermohaline circulation during the last interglacial period', *Nature 1997 390:6656*, 390(6656), pp. 154–156. Available at: https://doi.org/10.1038/36540.

Alfaro, M.E. and Faircloth, B.C. (2018) 'Explosive diversification of marine fishes at the Cretaceous–Palaeogene boundary', *Nature Ecology & Evolution* [Preprint]. Available at: https://doi.org/10.1038/s41559-018-0494-6.

Alonso-Garcia, M., Sierro, F.J. and Flores, J.A. (2011) 'Arctic front shifts in the subpolar North Atlantic during the Mid-Pleistocene (800–400 ka) and their implications for ocean circulation', *Palaeogeography, Palaeoclimatology, Palaeoecology*, 311(3–4), pp. 268–280. Available at: https://doi.org/10.1016/J.PALAEO.2011.09.004.

Anderson, T.R. *et al.* (2019) 'Quantifying carbon fluxes from primary production to mesopelagic fish using a simple food web model', *ICES Journal of Marine Science*, 76(3), pp. 690–701. Available at: https://doi.org/10.1093/ICESJMS/FSX234.

Angel, M. V. (1993) 'Biodiversity of the Pelagic Ocean', *Conservation Biology*, 7(4), pp. 760–772. Available at: https://doi.org/10.1046/j.1523-1739.1993.740760.x.

Annan, J.D. and Hargreaves, J.C. (2013) 'A new global reconstruction of temperature changes at the Last Glacial Maximum', *Climate of the Past*, 9(1), pp. 367–376. Available at: https://doi.org/10.5194/cp-9-367-2013.

Archibald, J.M. (2015) 'Endosymbiosis and Eukaryotic Cell Evolution', *Current Biology*, 25(19), pp. R911–R921. Available at: https://doi.org/10.1016/j.cub.2015.07.055.

Archibald, K.M., Siegel, D.A. and Doney, S.C. (2019) 'Modeling the Impact of Zooplankton Diel Vertical Migration on the Carbon Export Flux of the Biological Pump', *Global Biogeochemical Cycles*, 33(2), pp. 181–199. Available at: https://doi.org/10.1029/2018GB005983.

Armengol, L. *et al.* (2019) 'Planktonic food web structure and trophic transfer efficiency along a productivity gradient in the tropical and subtropical Atlantic Ocean', *Scientific Reports*, 9(1), pp. 1–19. Available at: https://doi.org/10.1038/s41598-019-38507-9.

Barcelos e Ramos, J. *et al.* (2017) 'Nutrient-specific responses of a phytoplankton community: a case study of the North Atlantic Gyre, Azores', *Journal of Plankton Research*, 39(4), pp. 744–761. Available at: https://doi.org/10.1093/plankt/fbx025.

Bassis, J.N., Petersen, S. V. and Mac Cathles, L. (2017) 'Heinrich events triggered by ocean forcing and modulated by isostatic adjustment', *Nature 2017 542:7641*, 542(7641), pp. 332–334. Available at: https://doi.org/10.1038/nature21069.

Baumann, K.-H. *et al.* (2005) 'The significance of extant coccolithophores as indicators of ocean water masses, surface water temperature, and palaeoproductivity: a review', *Paläontologische Zeitschrift 2005 79:1*, 79(1), pp. 93–112. Available at: https://doi.org/10.1007/BF03021756.

Baumann, K.-H. and Huber, R. (1999) 'Sea-surface gradients between the North Atlantic and the Norwegian Sea during the last 3.1 m.y.: comparison of Sites 982 and 985', in *Proceedings of the Ocean Drilling Program, 162 Scientific Results*. Ocean Drilling Program, pp. 179–190. Available at: https://doi.org/10.2973/odp.proc.sr.162.014.1999.

Beaufort, L. and Dollfus, D. (2004) 'Automatic recognition of coccoliths by dynamical neural networks', *Marine Micropaleontology*, 51(1–2), pp. 57–73. Available at: https://doi.org/10.1016/j.marmicro.2003.09.003.

Behrenfeld, M.J. *et al.* (2019) 'Global satellite-observed daily vertical migrations of ocean animals', *Nature 2019 576:7786*, 576(7786), pp. 257–261. Available at: https://doi.org/10.1038/s41586-019-1796-9.

Bekaert, D. V. *et al.* (2023) 'Last glacial maximum cooling of 9 °C in continental Europe from a 40 kyr-long noble gas paleothermometry record', *Quaternary Science Reviews*, 310, p. 108123. Available at: https://doi.org/10.1016/J.QUASCIREV.2023.108123.

Benoiston, A.S. *et al.* (2017) 'The evolution of diatoms and their biogeochemical functions', *Philosophical Transactions of the Royal Society B: Biological Sciences*, 372(1728). Available at: https://doi.org/10.1098/rstb.2016.0397.

Bianchi, D. *et al.* (2021) 'Estimating global biomass and biogeochemical cycling of marine fish with and without fishing', *Science Advances*, 7(41). Available at: https://doi.org/10.1126/SCIADV.ABD7554/SUPPL_FILE/SCIADV.ABD7554_DATA_FILE_S1.ZIP.

Blaauw, M. and Christen, J.A. (2011) 'Flexible paleoclimate age-depth models using an autoregressive gamma process', *Bayesian Analysis*, 6(3), pp. 457–474. Available at: https://doi.org/10.1214/11-BA618.

Bolaños, L.M. *et al.* (2020) 'Small phytoplankton dominate western North Atlantic biomass', *The ISME Journal*, 14(7), pp. 1663–1674. Available at: https://doi.org/10.1038/S41396-020-0636-0.

Bolton, C.T. *et al.* (2010) 'Glacial–interglacial productivity changes recorded by alkenones and microfossils in late Pliocene eastern equatorial Pacific and Atlantic upwelling zones', *Earth and Planetary Science Letters*, 295(3–4), pp. 401–411. Available at: https://doi.org/10.1016/j.epsl.2010.04.014.

Bolton, C.T. *et al.* (2011) 'Biotic and geochemical evidence for a global latitudinal shift in ocean biogeochemistry and export productivity during the late Pliocene', *Earth and Planetary Science Letters*, 308(1–2), pp. 200–210. Available at: https://doi.org/10.1016/j.epsl.2011.05.046.

Bolton, C.T. *et al.* (2018) 'North Atlantic Midlatitude Surface-Circulation Changes Through the Plio-Pleistocene Intensification of Northern Hemisphere Glaciation', *Paleoceanography and Paleoclimatology*, 33(11), pp. 1186–1205. Available at: https://doi.org/10.1029/2018PA003412.

Bond, D.P.G. and Wignall, P.B. (2014) 'Large igneous provinces and mass extinctions: An update', in *Volcanism, Impacts, and Mass Extinctions: Causes and Effects*. Geological Society of America, pp. 29–55. Available at: https://doi.org/10.1130/2014.2505(02).

Bond, G. *et al.* (1992) 'Evidence for massive discharges of icebergs into the North Atlantic ocean during the last glacial period', *Nature 1992 360:6401*, 360(6401), pp. 245–249. Available at: https://doi.org/10.1038/360245a0.

Bond, G. *et al.* (1993) 'Correlations between climate records from North Atlantic sediments and Greenland ice', *Nature 1993 365:6442*, 365(6442), pp. 143–147. Available at: https://doi.org/10.1038/365143a0.

Boyd, P.W. *et al.* (2007) 'Mesoscale iron enrichment experiments 1993-2005: Synthesis and future directions', *Science*, 315(5812), pp. 612–617. Available at: https://doi.org/10.1126/science.1131669.

Boyd, P.W. *et al.* (2019) 'Multi-faceted particle pumps drive carbon sequestration in the ocean', *Nature*, 568(7752), pp. 327–335. Available at: https://doi.org/10.1038/s41586-019-1098-2.

de Boyer Montégut, C. *et al.* (2004) 'Mixed layer depth over the global ocean: An examination of profile data and a profile-based climatology', *Journal of Geophysical Research: Oceans*, 109(C12), pp. 1–20. Available at: https://doi.org/10.1029/2004JC002378.

Breitbart, M. *et al.* (2018) 'Phage puppet masters of the marine microbial realm', *Nature Microbiology*, 3(7), pp. 754–766. Available at: https://doi.org/10.1038/s41564-018-0166-y.

Bridgestock, L. *et al.* (2019) 'Increased export production during recovery from the Paleocene–Eocene thermal maximum constrained by sedimentary Ba isotopes', *Earth and Planetary Science Letters*, 510, pp. 53–63. Available at: https://doi.org/10.1016/j.epsl.2018.12.036.

Britten, G.L. and Sibert, E.C. (2020) 'Enhanced fish production during a period of extreme global warmth', *Nature Communications*, 11(1), p. 5636. Available at: https://doi.org/10.1038/s41467-020-19462-w.

Broecker, W. *et al.* (1992) 'Origin of the northern Atlantic's Heinrich events', *Climate Dynamics*, 6(3–4), pp. 265–273. Available at: https://doi.org/10.1007/BF00193540/METRICS.

Broecker, W.S. (1982) 'Glacial to interglacial changes in ocean chemistry', *Progress in Oceanography*, 11(2), pp. 151–197. Available at: https://doi.org/10.1016/0079-6611(82)90007-6.

Browning, T.J. and Moore, C.M. (2023) 'Global analysis of ocean phytoplankton nutrient limitation reveals high prevalence of co-limitation', *Nature Communications 2023 14:1*, 14(1), pp. 1–12. Available at: https://doi.org/10.1038/s41467-023-40774-0.

Burke, K.D. *et al.* (2018) 'Pliocene and Eocene provide best analogs for near-future climates', *Proceedings of the National Academy of Sciences of the United States of America*, 115(52), pp. 13288–13293. Available at: https://doi.org/10.1073/pnas.1809600115.

Catul, V., Gauns, M. and Karuppasamy, P.K. (2011) 'A review on mesopelagic fishes belonging to family Myctophidae', *Reviews in Fish Biology and Fisheries*, 21(3), pp. 339–354. Available at: https://doi.org/10.1007/S11160-010-9176-4/FIGURES/9.

Chassot, E. *et al.* (2010) 'Global marine primary production constrains fisheries catches', *Ecology Letters*, 13(4), pp. 495–505. Available at: https://doi.org/10.1111/j.1461-0248.2010.01443.x.

Chien, C. Te *et al.* (2016) 'Effects of African dust deposition on phytoplankton in the western tropical Atlantic Ocean off Barbados', *Global Biogeochemical Cycles*, 30(5), pp. 716–734. Available at: https://doi.org/10.1002/2015GB005334.

Ciais, P. *et al.* (2013) 'Carbon and Other Biogeochemical Cycles', in Intergovernmental Panel on Climate Change (ed.) *Climate Change 2013 - The Physical Science Basis*. Cambridge: Cambridge University Press, pp. 465–570. Available at: https://doi.org/10.1017/CBO9781107415324.015.

Clavel-Henry, M. *et al.* (2020) 'Spatial Distribution and Abundance of Mesopelagic Fish Biomass in the Mediterranean Sea', *Frontiers in Marine Science*, 7, p. 573986. Available at: https://doi.org/10.3389/FMARS.2020.573986/BIBTEX.

Cohen, K.M. *et al.* (2013) 'The ICS International Chronostratigraphic Chart', *Episodes*, 36(3), pp. 199–204.

Conte, M.H. *et al.* (2006) 'Global temperature calibration of the alkenone unsaturation index (U 37k) in surface waters and comparison with surface sediments', *Geochemistry, Geophysics, Geosystems*, 7(2). Available at: https://doi.org/10.1029/2005GC001054.

Costa, K.M. *et al.* (2016) 'No iron fertilization in the equatorial Pacific Ocean during the last ice age', *Nature*, 529(7587), pp. 519–522. Available at: https://doi.org/10.1038/nature16453.

Dansgaard, W. *et al.* (1993) 'Evidence for general instability of past climate from a 250-kyr ice-core record', *Nature 1993 364:6434*, 364(6434), pp. 218–220. Available at: https://doi.org/10.1038/364218a0.

Davison, P.C. *et al.* (2013) 'Carbon export mediated by mesopelagic fishes in the northeast Pacific Ocean', *Progress in Oceanography*, 116, pp. 14–30. Available at: https://doi.org/10.1016/J.POCEAN.2013.05.013.

Diaz, R.J. and Rosenberg, R. (1995) 'Marine benthic hypoxia: a review of its ecological effects and the behavioural responses of benthic macrofauna', in *Oceanography and Marine Biology: an annual review. Vol. 33*. University College London Press, pp. 245–303.

Didié, C. and Bauch, H.A. (2000) 'Species composition and glacial–interglacial variations in the ostracode fauna of the northeast Atlantic during the past 200,000 years', *Marine Micropaleontology*, 40(1–2), pp. 105–129. Available at: https://doi.org/10.1016/S0377-8398(00)00034-7.

Ditlevsen, P. and Ditlevsen, S. (2023) 'Warning of a forthcoming collapse of the Atlantic meridional overturning circulation', *Nature Communications 2023 14:1*, 14(1), pp. 1–12. Available at: https://doi.org/10.1038/s41467-023-39810-w.

Dokken, T.M. *et al.* (2013) 'Dansgaard-Oeschger cycles: Interactions between ocean and sea ice intrinsic to the Nordic seas', *Paleoceanography*, 28(3), pp. 491–502. Available at: https://doi.org/10.1002/PALO.20042.

Doney, S.C. *et al.* (2020) 'The impacts of ocean acidification on marine ecosystems and reliant human communities', *Annual Review of Environment and Resources*, 45(Volume 45, 2020), pp. 83–112. Available at: https://doi.org/10.1146/ANNUREV-ENVIRON-012320-083019/CITE/REFWORKS.

Dornan, T. *et al.* (2022) 'Large mesopelagic fish biomass in the Southern Ocean resolved by acoustic properties', *Proceedings of the Royal Society B: Biological Sciences*, 289(1967). Available at: https://doi.org/10.1098/rspb.2021.1781.

Doyle, P.S. and Riedel, W.R. (1979) *Ichthyoliths: present status of taxonomy and stratigraphy of microscopic fish skeletal debris*. University of California at San Diego.

Dutkiewicz, A. *et al.* (2015) 'Census of seafloor sediments in the world's ocean', *Geology*, 43(9), pp. 795–798. Available at: https://doi.org/10.1130/G36883.1.

Dymond, J., Suess, E. and Lyle, M. (1992) 'Barium in Deep-Sea Sediment: A Geochemical Proxy for Paleoproductivity', *Paleoceanography*, 7(2), pp. 163–181. Available at: https://doi.org/10.1029/92PA00181.

Eagle, M. *et al.* (2003) 'A comparison between excess barium and barite as indicators of carbon export', *Paleoceanography*, 18(1). Available at: https://doi.org/10.1029/2002PA000793.

Edwards, M. *et al.* (2022) 'Climate variability and multi-decadal diatom abundance in the Northeast Atlantic', *Communications Earth & Environment 2022 3:1*, 3(1), pp. 1–8. Available at: https://doi.org/10.1038/s43247-022-00492-9.

Elderfield, H. *et al.* (2012) 'Evolution of ocean temperature and ice volume through the mid-Pleistocene climate transition', *Science*, 337(6095), pp. 704–709. Available at: https://doi.org/10.1126/SCIENCE.1221294/SUPPL_FILE/ELDERFIELD_SM.PDF.

Emanuele, D. *et al.* (2015) 'Sea-surface dynamics and palaeoenvironmental changes in the North Atlantic Ocean (IODP Site U1313) during Marine Isotope Stage 19 inferred from coccolithophore assemblages', *Palaeogeography, Palaeoclimatology, Palaeoecology*, 430, pp. 104–117. Available at: https://doi.org/10.1016/j.palaeo.2015.04.014.

Emiliani, C. (1955) 'Pleistocene Temperatures', *The Journal of Geology*, 63(6), pp. 538–578. Available at: https://doi.org/10.1086/626295.

Eppley, R.W. and Peterson, B.J. (1979) 'Particulate organic matter flux and planktonic new production in the deep ocean', *Nature 1979 282:5740*, 282(5740), pp. 677–680. Available at: https://doi.org/10.1038/282677a0.

Expedition 303 Scientists (2006) 'Site U1308', in *Proceedings of the IODP, 303/306*. Integrated Ocean Drilling Program. Available at: https://doi.org/10.2204/iodp.proc.303306.108.2006.

Expedition 306 Scientists (2006) 'Site U1313', in *Proceedings of the IODP, 303/306*. Integrated Ocean Drilling Program. Available at: https://doi.org/10.2204/iodp.proc.303306.112.2006.

Eynaud, F. *et al.* (2009) 'Position of the Polar Front along the western Iberian margin during key cold episodes of the last 45 ka', *Geochemistry, Geophysics, Geosystems*, 10(7). Available at: https://doi.org/10.1029/2009GC002398.

Falkowski, P. *et al.* (2000) 'The global carbon cycle: a test of our knowledge of earth as a system.', *Science (New York, N.Y.)*, 290(5490), pp. 291–6. Available at: https://doi.org/10.1126/science.290.5490.291.

Falkowski, P.G., Barber, R.T. and Smetacek, V. (1998) 'Biogeochemical controls and feedbacks on ocean primary production', *Science*, 281(5374), pp. 200–206. Available at: https://doi.org/10.1126/SCIENCE.281.5374.200/ASSET/8DA24923-585D-4624-B7D5-1D2D74007006/ASSETS/GRAPHIC/SE298667504A.JPEG.

FAO (2020) *The State of World Fisheries and Aquaculture*, *Fisheries Oceanography*. Available at: https://doi.org/10.1111/fog.12466.

Farrimond, P., Eglinton, G. and Brassell, S.C. (1986) 'Alkenones in Cretaceous black shales, Blake-Bahama Basin, western North Atlantic', *Organic Geochemistry*, 10(4–6), pp. 897–903. Available at: https://doi.org/10.1016/S0146-6380(86)80027-4.

Field, C.B. *et al.* (1998) 'Primary production of the biosphere: Integrating terrestrial and oceanic components', *Science*, 281(5374), pp. 237–240. Available at: https://doi.org/10.1126/science.281.5374.237.

Flores, J.A. and Sierro, F.J. (1997) 'Revised Technique for Calculation of Calcareous Nannofossil Accumulation Rates', *Micropaleontology*, 43(3), p. 321. Available at: https://doi.org/10.2307/1485832.

Friedman, M. (2010) 'Explosive morphological diversification of spiny-finned teleost fishes in the aftermath of the end-Cretaceous extinction', *Proceedings of the Royal Society B: Biological Sciences*, 277(1688), pp. 1675–1683. Available at: https://doi.org/10.1098/rspb.2009.2177.

Fu, W., Randerson, J.T. and Moore, J.K. (2016) 'Climate change impacts on net primary production (NPP) and export production (EP) regulated by increasing stratification and phytoplankton community structure in the CMIP5 models', *Biogeosciences*, 13(18), pp. 5151–5170. Available at: https://doi.org/10.5194/bg-13-5151-2016.

Ganeshram, R.S. *et al.* (2003) 'An experimental investigation of barite formation in seawater', *Geochimica et Cosmochimica Acta*, 67(14), pp. 2599–2605. Available at: https://doi.org/10.1016/S0016-7037(03)00164-9.

Gibbard, P.L., Head, M.J. and Walker, M.J.C. (2010) 'Formal ratification of the Quaternary System/Period and the Pleistocene Series/Epoch with a base at 2.58 Ma', *Journal of Quaternary Science*, 25(2), pp. 96–102. Available at: https://doi.org/10.1002/jqs.1338.

Gingele, F.X. *et al.* (1999) 'Biogenic Barium as a Proxy for Paleoproductivity: Methods and Limitations of Application', *Use of Proxies in Paleoceanography*, pp. 345–364. Available at: https://doi.org/10.1007/978-3-642-58646-0_13.

Gitelson, A.A. and Merzlyak, M.N. (1996) 'Signature Analysis of Leaf Reflectance Spectra: Algorithm Development for Remote Sensing of Chlorophyll', *Journal of Plant Physiology*, 148(3–4), pp. 494–500. Available at: https://doi.org/10.1016/S0176-1617(96)80284-7.

Gjøsaeter, J. and Kawaguchi K. (1980) *A review of the world resources of mesopelagic fish*. Rome.

González-Lanchas, A. *et al.* (2020) 'A new perspective of the Alboran Upwelling System reconstruction during the Marine Isotope Stage 11: A high-resolution coccolithophore record', *Quaternary Science Reviews*, 245, p. 106520. Available at: https://doi.org/10.1016/J.QUASCIREV.2020.106520.

Grimaldo, E. *et al.* (2020) 'Investigating the potential for a commercial fishery in the Northeast Atlantic utilizing mesopelagic species', *ICES Journal of Marine Science*, 77(7–8), pp. 2541–2556. Available at: https://doi.org/10.1093/ICESJMS/FSAA114.

Guerreiro, C. V. *et al.* (2023) 'Response of coccolithophore communities to oceanographic and atmospheric processes across the North- and Equatorial Atlantic', *Frontiers in Marine Science*, 10, p. 1119488. Available at: https://doi.org/10.3389/FMARS.2023.1119488/BIBTEX.

Guidi, L. *et al.* (2009) 'Effects of phytoplankton community on production, size, and export of large aggregates: A world-ocean analysis', *Limnology and Oceanography*, 54(6), pp. 1951–1963. Available at: https://doi.org/10.4319/lo.2009.54.6.1951.

Guidi, L. *et al.* (2016) 'Plankton networks driving carbon export in the oligotrophic ocean', *Nature*, 532(7600), pp. 465–470. Available at: https://doi.org/10.1038/nature16942.

Guihou, A. *et al.* (2011) 'Enhanced Atlantic Meridional Overturning Circulation supports the Last Glacial Inception', *Quaternary Science Reviews*, 30(13–14), pp. 1576–1582. Available at: https://doi.org/10.1016/J.QUASCIREV.2011.03.017.

Haëntjens, N. *et al.* (2022) 'Phytoplankton size distributions in the western North Atlantic and their seasonal variability', *Limnology and Oceanography*, 67(8), pp. 1865–1878. Available at: https://doi.org/10.1002/LNO.12172.

Hale, R.L. *et al.* (2015) 'Nitrogen and phosphorus fluxes from watersheds of the northeast U.S. from 1930 to 2000: Role of anthropogenic nutrient inputs, infrastructure, and runoff', *Global Biogeochemical Cycles*, 29(3), pp. 341–356. Available at: https://doi.org/10.1002/2014GB004909.

Hannisdal, B. and Peters, S.E. (2011) 'Phanerozoic earth system evolution and marine biodiversity', *Science*, 334(6059), pp. 1121–1124. Available at: https://doi.org/10.1126/science.1210695.

Heino, M. *et al.* (2011) 'Catchability of pelagic trawls for sampling deep-living nekton in the mid-North Atlantic', *ICES Journal of Marine Science*, 68(2), pp. 377–389. Available at: https://doi.org/10.1093/ICESJMS/FSQ089.

Heinrich, H. (1988) 'Origin and consequences of cyclic ice rafting in the Northeast Atlantic Ocean during the past 130,000 years', *Quaternary Research*, 29(2), pp. 142–152. Available at: https://doi.org/10.1016/0033-5894(88)90057-9.

Hemming, S.R. (2004) 'Heinrich events: Massive late Pleistocene detritus layers of the North Atlantic and their global climate imprint', *Reviews of Geophysics*, 42(1), p. 1005. Available at: https://doi.org/10.1029/2003RG000128.

Hennissen, J.A.I. *et al.* (2014) 'Palynological evidence for a southward shift of the North Atlantic Current at ~2.6 Ma during the intensification of late Cenozoic Northern Hemisphere glaciation', *Paleoceanography*, 29(6), pp. 564–580. Available at: https://doi.org/10.1002/2013PA002543.

Henry, L.G. *et al.* (2016) 'North Atlantic ocean circulation and abrupt climate change during the last glaciation', *Science*, 353(6298), pp. 470–474. Available at: https://doi.org/10.1126/SCIENCE.AAF5529/SUPPL_FILE/PAPV2.PDF.

Henson, S.A. *et al.* (2021) 'Future phytoplankton diversity in a changing climate', *Nature Communications 2021 12:1*, 12(1), pp. 1–8. Available at: https://doi.org/10.1038/s41467-021-25699-w.

Henson, S.A., Sanders, R. and Madsen, E. (2012) 'Global patterns in efficiency of particulate organic carbon export and transfer to the deep ocean', *Global Biogeochemical Cycles*, 26(1), p. n/a-n/a. Available at: https://doi.org/10.1029/2011GB004099.

Herbert, T.D. *et al.* (2016) 'Late Miocene global cooling and the rise of modern ecosystems', *Nature Geoscience*, 9(11), pp. 843–847. Available at: https://doi.org/10.1038/ngeo2813.

Herfort, L. *et al.* (2006) 'Application of the TEX86 temperature proxy to the southern North Sea', *Organic Geochemistry*, 37(12), pp. 1715–1726. Available at: https://doi.org/10.1016/J.ORGGEOCHEM.2006.07.021.

Hitchen, K. (2004) 'The geology of the UK Hatton-Rockall margin', *Marine and Petroleum Geology*, 21(8), pp. 993–1012. Available at: https://doi.org/10.1016/J.MARPETGEO.2004.05.004.

Hodell, D.A. *et al.* (2008) 'Onset of "Hudson Strait" Heinrich events in the eastern North Atlantic at the end of the middle Pleistocene transition (~640 ka)?', *Paleoceanography*, 23(4). Available at: https://doi.org/10.1029/2008PA001591.

Holmes, D.E. *et al.* (2022) 'Reorganization of Atlantic Waters at sub-polar latitudes linked to deep-water overflow in both glacial and interglacial climate states', 18, pp. 989–1009. Available at: https://doi.org/10.5194/cp-18-989-2022.

Hudson, J.M. *et al.* (2014) 'Myctophid feeding ecology and carbon transport along the northern Mid-Atlantic Ridge', *Deep Sea Research Part I: Oceanographic Research Papers*, 93, pp. 104–116. Available at: https://doi.org/10.1016/j.dsr.2014.07.002.

Irigoien, X. *et al.* (2014) 'Large mesopelagic fishes biomass and trophic efficiency in the open ocean', *Nature Communications 2014 5:1*, 5(1), pp. 1–10. Available at: https://doi.org/10.1038/ncomms4271.

Iversen, M.H. (2023) 'Carbon Export in the Ocean: A Biologist's Perspective', *Annual Review of Marine Science*, 15(Volume 15, 2023), pp. 357–381. Available at: https://doi.org/10.1146/ANNUREV-MARINE-032122-035153/CITE/REFWORKS.

Jacobel, A.W. *et al.* (2019) 'No evidence for equatorial Pacific dust fertilization', *Nature Geoscience*, 12(3), pp. 154–155. Available at: https://doi.org/10.1038/s41561-019-0304-z.

Jenkyns, H.C. (1980) 'Cretaceous anoxic events: from continents to oceans', *Journal of the Geological Society*, 137(2), pp. 171–188. Available at: https://doi.org/10.1144/gsjgs.137.2.0171.

Jin., X. *et al.* (2006) 'Diagnosing the contributions of phytoplankton functional groups to the production and export of particulate organic carbon, CaCO3, and opal from global nutrient and alkalinity

distributions', *Global Biogeochemical Cycles*, 20(2), pp. 1–17. Available at: https://doi.org/10.1029/2005GB002532.

Joy-Warren, H.L. *et al.* (2019) 'Light Is the Primary Driver of Early Season Phytoplankton Production Along the Western Antarctic Peninsula', *Journal of Geophysical Research: Oceans*, 124(11), pp. 7375–7399. Available at: https://doi.org/10.1029/2019JC015295.

Kaartvedt, S., Staby, A. and Aksnes, D.L. (2012) 'Efficient trawl avoidance by mesopelagic fishes causes large underestimation of their biomass', *Marine Ecology Progress Series*, 456, pp. 1–6. Available at: https://doi.org/10.3354/MEPS09785.

Kaiser, M.J. (2011) *Marine Ecology: Processes, Systems and Impacts*. Oxford University Press. Available at: https://doi.org/10.1017/S0376892906253244.

Kandiano, E.S. (2002) 'IMPLICATIONS OF PLANKTIC FORAMINIFERAL SIZE FRACTIONS FOR THE GLACIAL-INTERGLACIAL PALEOCEANOGRAPHY OF THE POLAR NORTH ATLANTIC', *The Journal of Foraminiferal Research*, 32(3), pp. 245–251. Available at: https://doi.org/10.2113/32.3.245.

Kelly, T.B. *et al.* (2019) 'The Importance of Mesozooplankton Diel Vertical Migration for Sustaining a Mesopelagic Food Web', *Frontiers in Marine Science*, 6. Available at: https://doi.org/10.3389/fmars.2019.00508.

Kenchington, E.L. *et al.* (2017) 'Barcoding Atlantic Canada's mesopelagic and upper bathypelagic marine fishes', *PLOS ONE*, 12(9), p. e0185173. Available at: https://doi.org/10.1371/JOURNAL.PONE.0185173.

Kindler, P. *et al.* (2014) 'Climate of the Past Temperature reconstruction from 10 to 120 kyr b2k from the NGRIP ice core', 10, pp. 887–902. Available at: https://doi.org/10.5194/cp-10-887-2014.

Klevjer, T. *et al.* (2020) 'Micronekton biomass distribution, improved estimates across four north Atlantic basins', *Deep Sea Research Part II: Topical Studies in Oceanography*, 180, p. 104691. Available at: https://doi.org/10.1016/J.DSR2.2019.104691.

Knutsen, T. *et al.* (2023) 'Feeding ecology of Benthosema glaciale across the North Atlantic', *Frontiers in Marine Science*, 10, p. 1086607. Available at: https://doi.org/10.3389/FMARS.2023.1086607/BIBTEX.

Krauss, W. (1986) 'The North Atlantic Current', *Journal of Geophysical Research: Oceans*, 91(C4), pp. 5061–5074. Available at: https://doi.org/10.1029/JC091IC04P05061.

Laber, C.P. *et al.* (2018) 'Coccolithovirus facilitation of carbon export in the North Atlantic', *Nature Microbiology*, 3(5), pp. 537–547. Available at: https://doi.org/10.1038/s41564-018-0128-4.

Lampitt, R.S. *et al.* (2010) 'Long-term variability of downward particle flux in the deep northeast Atlantic: Causes and trends', *Deep Sea Research Part II: Topical Studies in Oceanography*, 57(15), pp. 1346–1361. Available at: https://doi.org/10.1016/j.dsr2.2010.01.011.

Lang, D.C. *et al.* (2016) 'Incursions of southern-sourced water into the deep North Atlantic during late Pliocene glacial intensification', *Nature Geoscience*, 9(5), pp. 375–379. Available at: https://doi.org/10.1038/ngeo2688.

Lawrence, K.T. *et al.* (2009) 'High-amplitude variations in North Atlantic sea surface temperature during the early Pliocene warm period', *Paleoceanography*, 24(2), p. n/a-n/a. Available at: https://doi.org/10.1029/2008PA001669.

Li, G. *et al.* (2020) 'Increasing ocean stratification over the past half-century', *Nature Climate Change 2020 10:12*, 10(12), pp. 1116–1123. Available at: https://doi.org/10.1038/s41558-020-00918-2.

Liguori, B.T.P., De Almeida, M.G. and de Rezende, C.E. (2016) 'Barium and its importance as an indicator of (Paleo)productivity', *Anais da Academia Brasileira de Ciencias*, 88(4), pp. 2093–2103. Available at: https://doi.org/10.1590/0001-3765201620140592.

Lisiecki, L.E. and Lisiecki, P.A. (2002) 'Application of dynamic programming to the correlation of paleoclimate records', *Paleoceanography*, 17(4), pp. 1–1. Available at: https://doi.org/10.1029/2001PA000733.

Lisiecki, L.E. and Raymo, M.E. (2005) 'A Pliocene-Pleistocene stack of 57 globally distributed benthic δ 18O records', *Paleoceanography*, 20(1), pp. 1–17. Available at: https://doi.org/10.1029/2004PA001071.

Locarnini, R.A. *et al.* (2013) 'World ocean atlas 2013. Volume 1, Temperature'. Available at: https://doi.org/10.7289/V55X26VD.

Lombard, F. *et al.* (2019) 'Globally Consistent Quantitative Observations of Planktonic Ecosystems', *Frontiers in Marine Science*, 6(MAR). Available at: https://doi.org/10.3389/fmars.2019.00196.

Loveley, M.R. *et al.* (2017) 'Millennial-scale iron fertilization of the eastern equatorial Pacific over the past 100,000 years', *Nature Geoscience*, 10(10), pp. 760–764. Available at: https://doi.org/10.1038/ngeo3024.

Marañón, E. (2015) 'Cell Size as a Key Determinant of Phytoplankton Metabolism and Community Structure', *Annual Review of Marine Science*, 7(1), pp. 241–264. Available at: https://doi.org/10.1146/annurev-marine-010814-015955.

Marba, N., Duarte, C.M. and Agusti, S. (2007) 'Allometric scaling of plant life history', *Proceedings of the National Academy of Sciences*, 104(40), pp. 15777–15780. Available at: https://doi.org/10.1073/pnas.0703476104.

Marino, M. *et al.* (2014) 'Coccolithophores as proxy of seawater changes at orbital-to-millennial scale during middle Pleistocene Marine Isotope Stages 14-9 in North Atlantic core MD01-2446', *Paleoceanography*, 29(6), pp. 518–532. Available at: https://doi.org/10.1002/2013PA002574.

Marino, M. *et al.* (2022) 'Paleoproductivity proxies and alkenone precursors in the Western Mediterranean during the Early-Middle Pleistocene transition', *Palaeogeography, Palaeoclimatology, Palaeoecology*, 601, p. 111104. Available at: https://doi.org/10.1016/J.PALAEO.2022.111104.

Martin, J.H. (1990) 'Glacial-interglacial CO 2 change: The Iron Hypothesis', *Paleoceanography*, 5(1), pp. 1–13. Available at: https://doi.org/10.1029/PA005i001p00001.

Martínez-García, A. *et al.* (2014) 'Iron Fertilization of the Subantarctic Ocean During the Last Ice Age', *Science*, 343(6177), pp. 1347–1350. Available at: https://doi.org/10.1126/science.1246848.

McCarthy, G.D. *et al.* (2020) 'Sustainable Observations of the AMOC: Methodology and Technology', *Reviews of Geophysics*, 58(1), p. e2019RG000654. Available at: https://doi.org/10.1029/2019RG000654.

McManus, J. *et al.* (1998) 'Geochemistry of barium in marine sediments: Implications for its use as a paleoproxy', *Geochimica et Cosmochimica Acta*, 62(21–22), pp. 3453–3473. Available at: https://doi.org/10.1016/s0016-7037(98)00248-8.

Menviel, L.C. *et al.* (2020) 'An ice–climate oscillatory framework for Dansgaard–Oeschger cycles', *Nature Reviews Earth & Environment 2020 1:12*, 1(12), pp. 677–693. Available at: https://doi.org/10.1038/s43017-020-00106-y.

Middelburg, J.J. (2011) 'Chemoautotrophy in the ocean', *Geophysical Research Letters*, 38(24). Available at: https://doi.org/10.1029/2011GL049725.

Mitchell, B.G. *et al.* (1991) 'Light limitation of phytoplankton biomass and macronutrient utilization in the Southern Ocean', *Limnology and Oceanography*, 36(8), pp. 1662–1677. Available at: https://doi.org/10.4319/lo.1991.36.8.1662.

Moore, C.M. *et al.* (2013) 'Processes and patterns of oceanic nutrient limitation', *Nature Geoscience*, 6(9), pp. 701–710. Available at: https://doi.org/10.1038/ngeo1765.

Naafs, B.D.A. *et al.* (2012) 'Strengthening of North American dust sources during the late Pliocene (2.7 Ma)', *Earth and Planetary Science Letters*, 317–318, pp. 8–19. Available at: https://doi.org/10.1016/j.epsl.2011.11.026.

Naafs, B.D.A. *et al.* (2013) 'Warming of surface waters in the mid-latitude North Atlantic during Heinrich events', *Paleoceanography*, 28(1), pp. 153–163. Available at: https://doi.org/10.1029/2012PA002354.

Naafs, B.D.A., Hefter, J. and Stein, R. (2013) 'Millennial-scale ice rafting events and Hudson Strait Heinrich(-like) Events during the late Pliocene and Pleistocene: a review', *Quaternary Science Reviews*, 80, pp. 1–28. Available at: https://doi.org/10.1016/J.QUASCIREV.2013.08.014.

Nagakura, T. *et al.* (2022) 'Biological Sulfate Reduction in Deep Subseafloor Sediment of Guaymas Basin', *Frontiers in Microbiology*, 13, p. 845250. Available at: https://doi.org/10.3389/FMICB.2022.845250/BIBTEX.

Nair, A. *et al.* (2015) 'Glacial-interglacial variability in diatom abundance and valve size: Implications for Southern Ocean paleoceanography', *Paleoceanography*, 30(10), pp. 1245–1260. Available at: https://doi.org/10.1002/2014PA002680.

NASA Goddard Space Flight Center, Ocean Ecology Laboratory and Ocean Biology Processing Group (2022) *Moderate-resolution Imaging Spectroradiometer (MODIS) Chlorophyll concentration*.

Near, T.J. *et al.* (2012) 'Resolution of ray-finned fish phylogeny and timing of diversification', *Proceedings of the National Academy of Sciences of the United States of America*, 109(34), pp. 13698–13703. Available at: https://doi.org/10.1073/PNAS.1206625109/SUPPL_FILE/ST02.DOC.

Nelson, J.S., Grande, T.C. and Wilson, M.V.H. (2016) *Fishes of the World*. 5th edn. John Wiley & Sons.

Nelson, N. and Ben-Shem, A. (2004) 'The complex architecture of oxygenic photosynthesis', *Nature Reviews Molecular Cell Biology*, 5(12), pp. 971–982. Available at: https://doi.org/10.1038/nrm1525.

NOAA National Centers for Environmental Information (2022) 'NOAA National Centers for Environmental Information. 2022: ETOPO 2022 15 Arc-Second Global Relief Model.' Available at: https://www.ncei.noaa.gov/products/etopo-global-relief-model (Accessed: 4 August 2023).

Nowicki, M., DeVries, T. and Siegel, D.A. (2022) 'Quantifying the Carbon Export and Sequestration Pathways of the Ocean's Biological Carbon Pump', *Global Biogeochemical Cycles*, 36(3). Available at: https://doi.org/10.1029/2021GB007083.

Ohkouchi, N. *et al.* (2002) 'Spatial and temporal offsets between proxy records in a sediment drift', *Science*, 298(5596), pp. 1224–1227. Available at: https://doi.org/10.1126/SCIENCE.1075287/ASSET/E90D6457-9A22-44BE-82C7-1A559E102D7F/ASSETS/GRAPHIC/SE4421016002.JPEG.

Olson, R.J. *et al.* (1990) 'Spatial and temporal distributions of prochlorophyte picoplankton in the North Atlantic Ocean', *Deep Sea Research Part A. Oceanographic Research Papers*, 37(6), pp. 1033–1051. Available at: https://doi.org/10.1016/0198-0149(90)90109-9.

Omand, M.M. *et al.* (2015) 'Eddy-driven subduction exports particulate organic carbon from the spring bloom', *Science*, 348(6231), pp. 222–225. Available at: https://doi.org/10.1126/science.1260062.

Ottens, J.J. (1991) 'Planktic foraminifera as North Atlantic water mass indicators', *Oceanologica Acta* , 14(2), pp. 123–140.

Passow, U. and Carlson, C. (2012) 'The biological pump in a high CO2 world', *Marine Ecology Progress Series*, 470(2), pp. 249–271. Available at: https://doi.org/10.3354/meps09985.

Pauly, D. *et al.* (2021) 'The biology of mesopelagic fishes and their catches (1950– 2018) by commercial and experimental fisheries', *Journal of Marine Science and Engineering*, 9(10), p. 1057. Available at: https://doi.org/10.3390/JMSE9101057/S1.

Paytan, A. and Griffith, E.M. (2007) 'Marine barite: Recorder of variations in ocean export productivity', *Deep Sea Research Part II: Topical Studies in Oceanography*, 54(5–7), pp. 687–705. Available at: https://doi.org/10.1016/j.dsr2.2007.01.007.

Paytan, A. and McLaughlin, K. (2007) 'The Oceanic Phosphorus Cycle', *Chemical Reviews*, 107(2), pp. 563–576. Available at: https://doi.org/10.1021/cr0503613.

Pereira, J.N. *et al.* (2011) 'Diet of mid-Atlantic Sowerby's beaked whales Mesoplondon bidens', *Deep Sea Research Part I: Oceanographic Research Papers*, 58(11), pp. 1084–1090. Available at: https://doi.org/10.1016/J.DSR.2011.08.004.

Phillips, M.P. and Harwood, D.M. (2017) 'Marine diatom assemblage variation across Pleistocene glacial-interglacial transitions from Integrated Ocean Drilling Program Site C9001, Northwest Pacific', *Palaeogeography, Palaeoclimatology, Palaeoecology*, 483, pp. 172–187. Available at: https://doi.org/10.1016/J.PALAEO.2016.07.040.

Pöppelmeier, F., Scheen, J., *et al.* (2021) 'Simulated stability of the Atlantic Meridional Overturning Circulation during the Last Glacial Maximum', *Climate of the Past*, 17(2), pp. 615–632. Available at: https://doi.org/10.5194/CP-17-615-2021.

Pöppelmeier, F., Gutjahr, M., *et al.* (2021) 'Stable Atlantic Deep Water Mass Sourcing on Glacial-Interglacial Timescales', *Geophysical Research Letters*, 48(15), pp. 1–10. Available at: https://doi.org/10.1029/2021GL092722.

Porcar-Castell, A. *et al.* (2014) 'Linking chlorophyll a fluorescence to photosynthesis for remote sensing applications: mechanisms and challenges', *Journal of Experimental Botany*, 65(15), pp. 4065–4095. Available at: https://doi.org/10.1093/jxb/eru191.

Portilho-Ramos, R.C. *et al.* (2017) 'Coupling of equatorial Atlantic surface stratification to glacial shifts in the tropical rainbelt', *Scientific Reports 2017 7:1*, 7(1), pp. 1–8. Available at: https://doi.org/10.1038/s41598-017-01629-z.

Poulton, A.J. *et al.* (2006) 'Phytoplankton mineralization in the tropical and subtropical Atlantic Ocean', *Global Biogeochemical Cycles*, 20(4). Available at: https://doi.org/10.1029/2006GB002712.

Poulton, A.J. *et al.* (2007) 'Relating coccolithophore calcification rates to phytoplankton community dynamics: Regional differences and implications for carbon export', *Deep Sea Research Part II: Topical Studies in Oceanography*, 54(5–7), pp. 538–557. Available at: https://doi.org/10.1016/J.DSR2.2006.12.003.

Poulton, A.J. *et al.* (2013) 'The 2008 Emiliania huxleyi bloom along the Patagonian Shelf: Ecology, biogeochemistry, and cellular calcification', *Global Biogeochemical Cycles*, 27(4), pp. 1023–1033. Available at: https://doi.org/10.1002/2013GB004641.

Prahl, F.G., Mix, A.C. and Sparrow, M.A. (2006) 'Alkenone paleothermometry: Biological lessons from marine sediment records off western South America', *Geochimica et Cosmochimica Acta*, 70(1), pp. 101–117. Available at: https://doi.org/10.1016/J.GCA.2005.08.023.

Proud, R. *et al.* (2019) 'From siphonophores to deep scattering layers: uncertainty ranges for the estimation of global mesopelagic fish biomass', *ICES Journal of Marine Science*, 76(3), pp. 718–733. Available at: https://doi.org/10.1093/ICESJMS/FSY037.

Pusineri, C. *et al.* (2008) 'Feeding niche segregation among the Northeast Atlantic community of oceanic top predators', *Marine Ecology Progress Series*, 361, pp. 21–34. Available at: https://doi.org/10.3354/meps07318.

Railsback, L.B. *et al.* (2015) 'An optimized scheme of lettered marine isotope substages for the last 1.0 million years, and the climatostratigraphic nature of isotope stages and substages', *Quaternary Science Reviews*, 111, pp. 94–106. Available at: https://doi.org/10.1016/j.quascirev.2015.01.012.

Raja, M. and Rosell-Melé, A. (2021) 'Appraisal of sedimentary alkenones for the quantitative reconstruction of phytoplankton biomass', *Proceedings of the National Academy of Sciences*, 118(2). Available at: https://doi.org/10.1073/PNAS.2014787118.

Raup, D.M. and Sepkoski, J.J. (1982) 'Mass Extinctions in the Marine Fossil Record', *Science*, 215(4539), pp. 1501–1504.

Raven, J.A. (1998) 'The twelfth Tansley Lecture. Small is beautiful: The picophytoplankton', *Functional Ecology*, 12(4), pp. 503–513. Available at: https://doi.org/10.1046/j.1365-2435.1998.00233.x.

Reid, P.C. *et al.* (2003) 'The Continuous Plankton Recorder: concepts and history, from Plankton Indicator to undulating recorders', *Progress in Oceanography*, 58(2–4), pp. 117–173. Available at: https://doi.org/10.1016/j.pocean.2003.08.002.

Robinson, S.A. *et al.* (2017) 'State of the Science: Mesozoic climates and oceans - a tribute to Hugh Jenkyns and Helmut Weisser', *Sedimentology*, 64(1), pp. 1–15.

Rosell-Melé, A. *et al.* (1995) 'Atlantic core-top calibration of the U37K index as a sea-surface palaeotemperature indicator', *Geochimica et Cosmochimica Acta*, 59(15), pp. 3099–3107. Available at: https://doi.org/10.1016/0016-7037(95)00199-A.

Rossby, T. (1996) 'The North Atlantic Current and surrounding waters: At the crossroads', *Reviews of Geophysics*, 34(4), pp. 463–481. Available at: https://doi.org/10.1029/96RG02214.

Roy-Barman, M. and Jeandel, C. (2016) 'CO2 Exchanges between the Ocean and the Atmosphere', in *Marine Geochemistry*. Oxford University Press, pp. 235–264. Available at: https://doi.org/10.1093/acprof:oso/9780198787495.003.0008.

Ruddiman, W.F. (1977) 'Late Quaternary deposition of ice-rafted sand in the subpolar North Atlantic (lat 40° to 65°N)', *Geological Society of America Bulletin*, 88(12), p. 1813. Available at: https://doi.org/10.1130/0016-7606(1977)88<1813:LQDOIS>2.0.CO;2.

Ruddiman, W.F. *et al.* (1989) 'Pleistocene evolution: Northern hemisphere ice sheets and North Atlantic Ocean', *Paleoceanography*, 4(4), pp. 353–412. Available at: https://doi.org/10.1029/PA004I004P00353.

Ruddiman, W.F. and McIntyre, A. (1976) 'Northeast Atlantic Paleoclimatic Changes over the Past 600,000 Years', *Memoir of the Geological Society of America*, 145, pp. 111–146. Available at: https://doi.org/10.1130/MEM145-P111.

Ryther, J.H. (1969) 'Photosynthesis and Fish Production in the Sea: The production of organic matter and its conversion to higher forms of life vary throughout the world ocean', *Science*, 166(3901), pp. 72–76. Available at: https://www.science.org.

Sahoo, N. *et al.* (2022) 'Planktic Foraminiferal Assemblages in Surface Sediments From the Subpolar North Atlantic Ocean', *Frontiers in Marine Science*, 8, p. 781675. Available at: https://doi.org/10.3389/FMARS.2021.781675/BIBTEX.

Schmidt, M.W., Vautravers, M.J. and Spero, H.J. (2006) 'Rapid subtropical North Atlantic salinity oscillations across Dansgaard–Oeschger cycles', *Nature 2006 443:7111*, 443(7111), pp. 561–564. Available at: https://doi.org/10.1038/nature05121.

Schoepfer, S.D. *et al.* (2015) 'Total organic carbon, organic phosphorus, and biogenic barium fluxes as proxies for paleomarine productivity', *Earth-Science Reviews*, 149, pp. 23–52. Available at: https://doi.org/10.1016/j.earscirev.2014.08.017.

Schwarzhans, W. and Carnevale, G. (2021) 'The rise to dominance of lanternfishes (Teleostei: Myctophidae) in the oceanic ecosystems: a paleontological perspective', *Paleobiology*, 47(3), pp. 446–463. Available at: https://doi.org/10.1017/pab.2021.2.

Shackleton, N.J. (1969) 'The last interglacial in the marine and terrestrial records', *Proceedings of the Royal Society of London. Series B. Biological Sciences*, 174(1034), pp. 135–154. Available at: https://doi.org/10.1098/rspb.1969.0085.

Shackleton, N.J. (1987) 'OXYGEN ISOTOPES, ICE VOLUME AND SEA LEVEL', *Quaternary Science Reviews*, 6, pp. 183–90.

Shackleton, N.J. *et al.* (2004) 'Absolute calibration of the Greenland time scale: implications for Antarctic time scales and for Δ14C', *Quaternary Science Reviews*, 23(14–15), pp. 1513–1522. Available at: https://doi.org/10.1016/J.QUASCIREV.2004.03.006.

Shipboard Scientific Party (1996) 'Site 982', in *Proceedings of the Ocean Drilling Program, 162 Initial Reports*. Ocean Drilling Program, pp. 91–138. Available at: https://doi.org/10.2973/odp.proc.ir.162.104.1996.

Sibert, E. *et al.* (2018) 'Two pulses of morphological diversification in Pacific pelagic fishes following the Cretaceous-Palaeogene mass extinction', *Proceedings of the Royal Society B: Biological Sciences*, 285(1888). Available at: https://doi.org/10.1098/RSPB.2018.1194.

Sibert, E.C. *et al.* (2017) 'Methods for isolation and quantification of microfossil fish teeth and elasmobranch dermal denticles (Ichthyoliths) from marine sediments', *Palaeontologia Electronica*, 20(1), pp. 1–14. Available at: https://doi.org/10.26879/677.

Sibert, E.C., Hull, P.M. and Norris, R.D. (2014) 'Resilience of Pacific pelagic fish across the Cretaceous/Palaeogene mass extinction', *Nature Geoscience*, 7(9), pp. 667–670. Available at: https://doi.org/10.1038/ngeo2227.

Sibert, E.C. and Norris, R.D. (2015) 'New age of fishes initiated by the Cretaceous-Paleogene mass extinction', *Proceedings of the National Academy of Sciences of the United States of America*, 112(28), pp. 8537–8542. Available at: https://doi.org/10.1073/PNAS.1504985112/-/DCSUPPLEMENTAL/PNAS.201504985SI.PDF.

Sibert, E.C. and Rubin, L.D. (2021) 'An early Miocene extinction in pelagic sharks', *Science*, 372(6546), pp. 1105–1107. Available at: https://doi.org/10.1126/science.aaz3549.

Siegel, D.A. *et al.* (2014) 'Global assessment of ocean carbon export by combining satellite observations and food-web models', *Global Biogeochemical Cycles*, 28(3), pp. 181–196. Available at: https://doi.org/10.1002/2013GB004743.

Sigman, D.M. and Boyle, E.A. (2000) 'Glacial/interglacial variations in atmospheric carbon dioxide', *Nature*, 407(6806), pp. 859–869. Available at: https://doi.org/10.1038/35038000.

Sigman, D.M. and Hain, M.P. (2012) 'The Biological Productivity of the Ocean', *Nature Education*, 3(6), pp. 1–16.

Sigman, D.M., Hain, M.P. and Haug, G.H. (2010) 'The polar ocean and glacial cycles in atmospheric CO2 concentration', *Nature*, 466(7302), pp. 47–55. Available at: https://doi.org/10.1038/nature09149.

Smetacek, V. *et al.* (2012) 'Deep carbon export from a Southern Ocean iron-fertilized diatom bloom', *Nature*, 487(7407), pp. 313–319. Available at: https://doi.org/10.1038/nature11229.

Smith, M.E. *et al.* (2013) 'Data report: oxygen isotopes and foraminifer abundance record for the last glacial-interglacial cycle and marine isotope Stage 6 at IODP Site U1313', in, pp. 1–11. Available at: https://doi.org/10.2204/iodp.proc.303306.216.2013.

Stein, R. *et al.* (2009) 'Variability of surface water characteristics and Heinrich-like events in the Pleistocene midlatitude North Atlantic Ocean: Biomarker and XRD records from IODP Site U1313 (MIS 16-9)', *Paleoceanography*, 24(2), p. n/a-n/a. Available at: https://doi.org/10.1029/2008PA001639.

Stock, C.A. *et al.* (2017) 'Reconciling fisheries catch and ocean productivity', *Proceedings of the National Academy of Sciences of the United States of America*, 114(8), pp. E1441–E1449. Available at: https://doi.org/10.1073/PNAS.1610238114/-/DCSUPPLEMENTAL/PNAS.201610238SI.PDF.

Sutton, T.T. *et al.* (2008) 'Vertical structure, biomass and topographic association of deep-pelagic fishes in relation to a mid-ocean ridge system', *Deep Sea Research Part II: Topical Studies in Oceanography*, 55(1–2), pp. 161–184. Available at: https://doi.org/10.1016/J.DSR2.2007.09.013.

Sutton, T.T. *et al.* (2017) 'A global biogeographic classification of the mesopelagic zone', *Deep Sea Research Part I: Oceanographic Research Papers*, 126, pp. 85–102. Available at: https://doi.org/10.1016/J.DSR.2017.05.006.

Talley, L.D. *et al.* (2011) 'Atlantic Ocean', *Descriptive Physical Oceanography*, pp. 245–301. Available at: https://doi.org/10.1016/B978-0-7506-4552-2.10009-5.

Tilstone, G.H. *et al.* (2017) 'Micro-phytoplankton photosynthesis, primary production and potential export production in the Atlantic Ocean', *Progress in Oceanography*, 158, pp. 109–129. Available at: https://doi.org/10.1016/J.POCEAN.2017.01.006.

Tittensor, D.P. *et al.* (2021) 'Next-generation ensemble projections reveal higher climate risks for marine ecosystems', *Nature Climate Change 2021 11:11*, 11(11), pp. 973–981. Available at: https://doi.org/10.1038/s41558-021-01173-9.

Tréguer, P. *et al.* (2018) 'Influence of diatom diversity on the ocean biological carbon pump', *Nature Geoscience*, 11(1), pp. 27–37. Available at: https://doi.org/10.1038/s41561-017-0028-x.

Trotta, S. *et al.* (2022) 'Early Pleistocene calcareous nannofossil assemblages from the Gulf of Cadiz reveal glacial-interglacial and millennial-scale variability', *Palaeogeography, Palaeoclimatology, Palaeoecology*, 608, p. 111304. Available at: https://doi.org/10.1016/J.PALAEO.2022.111304.

Tzedakis, P.C. *et al.* (2009) 'Interglacial diversity', *Nature Geoscience*, 2(11), pp. 751–755. Available at: https://doi.org/10.1038/ngeo660.

Venz, K.A. *et al.* (1999) 'A 1.0 Myr Record of Glacial North Atlantic Intermediate Water Variability from ODP Site 982 in the Northeast Atlantic', *Paleoceanography*, 14(1), pp. 42–52. Available at: https://doi.org/10.1029/1998PA900013.

Vihtakari, M. (2023) 'ggOceanMaps: Plot Data on Oceanographic Maps using "ggplot2"'. Available at: https://mikkovihtakari.github.io/ggOceanMaps/ (Accessed: 4 August 2023).

Volkman, J.K. *et al.* (1980) 'Long-chain alkenes and alkenones in the marine coccolithophorid Emiliania huxleyi', *Phytochemistry*, 19(12), pp. 2619–2622. Available at: https://doi.org/10.1016/S0031-9422(00)83930-8.

Volkman, J.K. *et al.* (1995) 'Alkenones in Gephyrocapsa oceanica: Implications for studies of paleoclimate', *Geochimica et Cosmochimica Acta*, 59(3), pp. 513–520. Available at: https://doi.org/10.1016/0016-7037(95)00325-T.

Waelbroeck, C. *et al.* (2009) 'Constraints on the magnitude and patterns of ocean cooling at the Last Glacial Maximum', *Nature Geoscience 2009 2:2*, 2(2), pp. 127–132. Available at: https://doi.org/10.1038/ngeo411.

Warnock, J.P. and Scherer, R.P. (2014) 'A revised method for determining the absolute abundance of diatoms', *Journal of Paleolimnology*, 53(1), pp. 157–163. Available at: https://doi.org/10.1007/s10933-014-9808-0.

Webb, P. (2021) 'Patterns of Primary Production', in *Introduction to Oceanography*. Roger Williams University. Available at: https://rwu.pressbooks.pub/webboceanography/chapter/7-4-patterns-of-primary-production/.

Werner, L.K. (2019) *A Pleistocene record of global fish production and implications for sustainability of polar fisheries*. Masters Thesis. University of California San Diego. Available at: https://escholarship.org/uc/item/41w8n1cw#main (Accessed: 19 September 2024).

Westen, R.M. van, Kliphuis, M. and Dijkstra, H.A. (2024) 'Physics-based early warning signal shows that AMOC is on tipping course', *Science Advances*, 10(6), p. 1189. Available at: https://doi.org/10.1126/SCIADV.ADK1189.

Westgård, A. *et al.* (2023) 'Large-scale culturing of Neogloboquadrina pachyderma, its growth in, and tolerance of, variable environmental conditions', *Journal of Plankton Research*, 45(5), pp. 732–745. Available at: https://doi.org/10.1093/PLANKT/FBAD034.

Wickham, H. (2016) 'ggplot2: Elegant Graphics for Data Analysis'. Springer-Verlag New York. Available at: http://ggplot2.tidyverse.org (Accessed: 4 August 2023).

Woosley, R.J. (2016) 'Carbonate Compensation Depth', in W.M. White (ed.) *Encyclopedia of Geochemistry*, pp. 1–2. Available at: https://doi.org/10.1007/978-3-319-39193-9_85-1.

Yasuhara, M. *et al.* (2008) 'Abrupt climate change and collapse of deep-sea ecosystems', *Proceedings of the National Academy of Sciences of the United States of America*, 105(5), pp. 1556–1560. Available at: https://doi.org/10.1073/PNAS.0705486105/SUPPL_FILE/05486FIG4.PDF.

Yoon, J.-E. *et al.* (2018) 'Reviews and syntheses: Ocean iron fertilization experiments – past, present, and future looking to a future Korean Iron Fertilization Experiment in the Southern Ocean (KIFES) project', *Biogeosciences*, 15(19), pp. 5847–5889. Available at: https://doi.org/10.5194/bg-15-5847-2018.

Young, J.R. *et al.* (2003) 'A guide to extant coccolithophore taxonomy.', *Journal of Nannoplankton Research*, S1, pp. 1–132. Available at: https://doi.org/10.58998/jnr2297.

Yu, J. *et al.* (2019) 'More efficient North Atlantic carbon pump during the Last Glacial Maximum', *Nature Communications*, 10(1), p. 2170. Available at: https://doi.org/10.1038/s41467-019-10028-z.

Zeebe, R.E. and Wolf-Gladrow, D. (2001) 'CO2 in Seawater: Equilibrium, Kinetics, Isotopes', in D. Halpern (ed.) *CO2 in Seawater: Equilibrium, Kinetics, Isotopes*. 1st edn. Elsevier, pp. 1–84. Available at: https://books.google.co.uk/books?hl=en&lr=&id=g3j3Zn4kEscC&oi=fnd&pg=PA1&dq=+Zeebe,+R%3B+Wolf-Gladrow,+D+(2001).+CO2+in+seawater:+Equilibrium,+Kinetics,+Isotopes&ots=ldSrO_wmyO&sig=a_xGLA55teOrq08qQ1ikaDAEqQg&redir_esc=y#v=onepage&q=Zeebe%2C%20R%3B%20Wolf-Gladrow%2C%20D%20(2001).%20CO2%20in%20seawater%3A%20Equilibrium%2C%20Kinetics%2C%20Isotopes&f=false (Accessed: 23 July 2024).

Zhou, Yun *et al.* (2020) 'Eutrophication control strategies for highly anthropogenic influenced coastal waters', *Science of the Total Environment*, 705, p. 135760. Available at: https://doi.org/10.1016/j.scitotenv.2019.135760.

Chapter 2: Coccolithophore abundance and demographic changes in the North Atlantic over the past 200 kyr

Abstract

Coccolithophores are ubiquitous unicellular phytoplankton that are widespread in the pelagic ocean. Using nannofossil abundances from two North Atlantic sediment cores, I reconstruct the productivity of coccolithophores over the past 200 kyr. Automated counting methods were generally unreliable, as their outputs were found not to match manual and SEM approaches, and so most data was instead generated using established manual methods. I found a significant increase in productivity during the Last Interglacial (LIG) relative to glacial intervals in the subpolar North Atlantic, whilst no significant change occurred in the subtropical North Atlantic. *Gephyrocapsa* spp. coccoliths dominate assemblages at both sites throughout glacial intervals and interglacial intervals. These patterns can be attributed to the southward migration of North Atlantic Transitional Waters (NATW) during glacial intervals. This migration caused a substantial cooling of the northerly site, and the loss of optimal conditions for coccolithophores. The subtropical site remained within the influence of the North Atlantic Current system throughout glacial and interglacial conditions, as shown by the latitudinal extent of ice-rafted debris (IRD), meaning no systematic change in productivity.

Chapter contents

2.1. Introduction

In this chapter, I record changes in the productivity of North Atlantic coccolithophores over the past 200 kyr and, through comparison to past work and existing records, estimate which climatic and oceanographic changes exerted the greatest influence on these autotrophs. All primary data generated and analysed in this chapter derive from two North Atlantic sediment cores, ODP Hole 982B and IODP Hole U1313A, which are described in detail in Chapter 1.

Coccolithophores are unicellular eukaryotic phytoplankton belonging to class Prymnesiophyceae in phylum Haptophyta (Young *et al.*, 2003). Through calcification, coccolithophores intracellularly produce coccoliths, which surround the cell to form a coccosphere. The microfossil record of coccolithophores extends back to the late Triassic, and coccoliths are the major sedimentary component of widespread Jurassic and Cretaceous chalk formations (Stanley, Ries and Hardie, 2005; Jordan, 2009). In the Quaternary, including the modern, coccolithophores and foraminifera produce the majority of carbonate that reaches seafloor sediments (Sprengel *et al.*, 2002; Broecker and Clark, 2009; Dutkiewicz *et al.*, 2015). As an abundant, calcareous group, they play an important role in both the biological carbon pump and the carbonate pump, with a high potential to influence air-sea carbon dioxide exchange and hence global climate (Rost and Riebesell, 2004; Laber *et al.*, 2018). There are approximately 200 known extant species of coccolithophore in the modern ocean (Young *et al.*, 2003), although only around 30 species comprise more than 5% of the total population in any biogeographic region of the Atlantic (Poulton *et al.*, 2017).

Marañón et al. (2001) found that coccolithophores and other non-calcifying haptophytes comprise around 10-20% of total standing Atlantic chlorophyll *a* biomass during spring and autumn below 50° latitude. Coccolithophores contribute up to 20% of total phytoplankton primary production in the tropical-to-subtropical Atlantic (Poulton *et al.*, 2006, 2007), though this figure may episodically be as great as 40% during blooming events in temperate-to-polar latitudes (Broerse *et al.*, 2000; Poulton *et al.*, 2007, 2013; Rousseaux and Gregg, 2013).

Picophytoplankton do most of the primary production in the pelagic Atlantic Ocean (Marañón *et al.*, 2001; Tilstone *et al.*, 2017; Bolaños *et al.*, 2020), although coccolithophores tend to be the dominant eukaryotic phytoplankton in the oligotrophic open ocean (Rousseaux and Gregg, 2013; Hagino and Young, 2015). Coccolithophores, which are usually nanophytoplankton (Jordan, 2009; Young, Bown and Lees, 2022), have greater potential than picophytoplankton to produce aggregates through direct sinking of coccoliths (Broerse *et al.*, 2000; Schmidt *et al.*, 2014; Laber *et al.*, 2018), or compaction and release of faecal pellets by heterotroph consumers (e.g. zooplankton and fishes) (Turner, 2002; Davison *et al.*, 2013; Li *et al.*, 2024). Hence coccolithophores have a disproportionate significance in exporting carbon from the euphotic zone of ocean gyres, relative to their abundance.

Coccolithophore community assemblages are sensitive to biogeochemical conditions including stratification, salinity, and temperature (Baumann *et al.*, 2005; Marino *et al.*, 2014; Gibbs *et al.*, 2016). This sensitivity, alongside their high preservation potential in marine sediments, means coccolithophores have great utility in reconstructing environmental conditions through time. In the Atlantic, there is greater inter-seasonal variability in coccolithophore assemblages in the temperate ocean than the warm, stratified subtropics (Poulton *et al.*, 2017).

Studying coccolithophore biology in the geological past relies on the study of coccoliths, which are commonly preserved in seafloor sediment where it exists above the carbonate compensation depth (Woosley, 2016; Sosdian, Rosenthal and Toggweiler, 2018). Coccoliths have historically been classified

through a morphospecies concept (Young *et al.*, 2003), though more recent genetic studies have highlighted that some common morphospecies, such as *Gephyrocapsa huxleyi* (formerly *Emiliania huxleyi*) are in fact multiple biological species (Bendif *et al.*, 2019; Filatov *et al.*, 2021). Geological studies necessarily rely on the morphospecies concept. Observations of niche tolerances in extant coccolithophores can inform hypotheses of environmental change using the geological record; more specifically, where coccolith preservation in the seafloor sediment reflects the diversity of the overlying coccolithophore assemblage, it is possible to use the relative abundance of certain coccolith taxa to reconstruct changes in palaeoceanography, such as eutrophication, migration of oceanographic fronts, and temperature (e.g. Baumann et al., 2005; Jordan, 2009; Marino et al., 2014; Hernández-Almeida et al., 2019; González-Lanchas et al., 2020; Guerreiro et al., 2023; Argenio et al., 2024).

There is strong latitudinal oceanographic zonation within the modern North Atlantic. IODP Site U1313 is found within North Atlantic Transitional Waters (NATW) that separate the subtropical gyre (south of the Subtropical Front) from the North Atlantic Current (NAC) and Subarctic Front (Krauss, 1986; Fratantoni, 2001). IODP Site U1313 is influenced by anticyclonic eddies related to the Azores Current, episodically triggering downwelling and limiting primary production, though the winter mixed layer is deeper and primary productivity is significantly higher here compared to the subtropical region to the south of the Azores Current (AzC) (Mouriño-Carballido and Neuer, 2008; Schwab *et al.*, 2012). ODP Site 982 is directly influenced by the NAC and is proximal to the Subarctic Front and associated subpolar waters (Krauss, 1986; Shipboard Scientific Party, 1996). A deep winter mixed layer and strong, NAC-induced vertical mixing leads to higher annual net primary productivity here relative to IODP Site U1313 (Schwab *et al.*, 2012; Emanuele *et al.*, 2015). The oceanographic context of the North Atlantic is shown in Figure 2.1.

During glacial intervals of the Pleistocene, it is likely that contemporary oceanographic patterns were broadly similar to those of the present day, but that the Subarctic Front was significantly displaced to the south, greatly expanding the influence of cold waters in the North Atlantic and shifting the NAC, and associated productivity bands, southwards (McIntyre, Ruddiman and Jantzen, 1972; Villanueva *et al.*, 2001; Schwab *et al.*, 2012).

Additionally, stronger allogenic nutrient inputs from wind-blown dust may have enhanced productivity and impacted the relative dominance of phytoplankton in the North Atlantic during past glacial intervals (Prospero, 1996; Naafs *et al.*, 2012; Chien *et al.*, 2016; Williams *et al.*, 2016; Bolton *et al.*, 2018).

A study of an Atlantic site close to the Iberian Margin at a similar latitude to U1313 found elevated coccolithophore abundances and the prevalence of warm water taxa during mid-Pleistocene interglacial intervals (MIS 9, 11 and 13) relative to the glacial intervals (MIS 10, 12 and 14), which they attribute to more oligotrophic conditions favouring high coccolithophore productivity (Marino *et al.*, 2014). Further research on nearby sites (shown in Figure 2.1) suggests deeper mixing and elevated diatom productivity and organic carbon flux during cold intervals of the Last Glacial Period (LGP) and LIG (Lebreiro *et al.*, 1997; Nave *et al.*, 2010), highlighting the potential decoupling of coccolithophore productivity and overall net primary productivity in the open ocean North Atlantic.

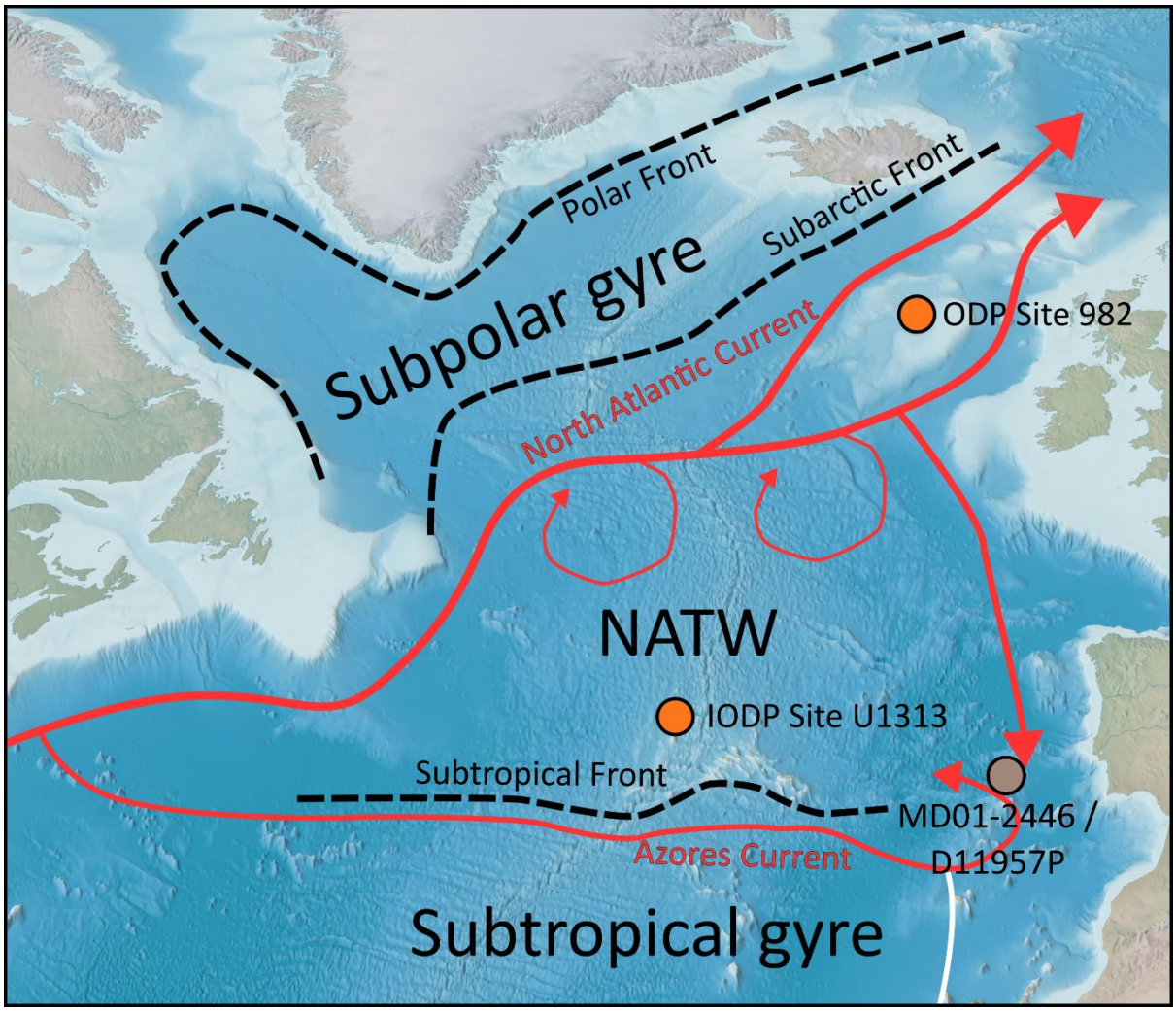

Figure 2.1 – Summary of modern North Atlantic surface oceanography and its influence on ODP Site 982 and IODP Site U1313. The location of cores MD01-2446 (Nave *et al.*, 2010) and D11957P (Lebreiro *et al.*, 1997) are included for reference. Red arrows show major branches of the North Atlantic Current. NATW is North Atlantic Transitional Waters. Figure modified from Argenio et al. (2024).

As coccolith-producing Haptophyte algae represent only a fraction of total primary productivity (Gasol, Del Giorgio and Duarte, 1997; Rousseaux and Gregg, 2013; Lombard *et al.*, 2019) and coccolith accumulation rate could vary independently of whole-ecosystem production, it would be challenging to extrapolate total primary production from coccolith accumulation rates alone. Most coccolithophore species are adapted to warm, stable oligotrophic environments, with few specialist species favouring eutrophic conditions (Baumann *et al.*, 2005). Local shifts from cool eutrophic to warm oligotrophic conditions during glacial-interglacial transitions could result in coccolithophores replacing diatoms as the dominant eukaryotic phytoplankton group, which may be reflected in the sedimentary record (Behrenfeld, 2014; Phillips and Harwood, 2017; Nissen *et al.*, 2018; Wang, Zeng and Feng, 2024). A more nuanced reconstruction of past environment change can be derived by looking at coccolith abundance alongside other variables such as the relative abundance of coccolith taxa (e.g. Schwab et al., 2012; Marino et al., 2014; Emanuele et al., 2015; González-Lanchas et al.,

2020; Argenio et al., 2024) and independent geochemical indicators of ecosystem productivity (e.g. Bolton et al., 2010; Schoepfer et al., 2015; Raja and Rosell-Melé, 2021; Marino et al., 2022).

In addition to reconstructing coccolithophore productivity as described in this chapter, during this project I attempted to reconstruct North Atlantic diatom production using an established settling chamber method (Warnock and Scherer, 2014). However, I found only single-digit numbers of diatom frustules present in samples from either sediment core, and so did not pursue this work further. It is likely that most biogenic silica exported from the surface of the North Atlantic during the Pleistocene was redissolved either in the water column or surface sediment, and so did not enter the sedimentary record (Nelson *et al.*, 1995; Tréguer and De La Rocha, 2013).

In this chapter, I aim to reconstruct the productivity of coccolithophores in the North Atlantic during the past 200 kyr using coccolith accumulation rates and the relative abundance of coccolith taxa in two deep sea sediment cores. I will test the following hypotheses:

- Coccolithophore abundance and demography was a function of environmental variables, such as temperature and vertical stratification, during the late Quaternary.
- Total coccolithophore abundance was higher in the subpolar Atlantic during the LIG relative to the LGP and Penultimate Glacial Period (PGP) due to the persistence of warm waters and stronger vertical mixing during the LIG.
- The relative abundance of eutrophic coccolith taxa increased during the LGP in the mid-latitude North Atlantic due to stronger allogenic nutrient inputs from enhanced vertical mixing (due to the southward migration of the North Atlantic Current) and higher aeolian dust inputs.

2.2. Methods

2.2.1. SYRACO

Coccolith abundance data were generated using the automated 'SYstème de Reconnaissance Automatique de COccolithes' (SYRACO; Beaufort and Dollfus, 2004; Barbarin, Beaufort and Moron, 2014) to obtain estimates of coccolithophore productivity over the past 200 kyr. Initial data were generated for 54 samples (29 from IODP Site U1313 and 25 from ODP Site 982) in the Micropalaeontological Preparation Laboratory at CEREGE (Centre Européen de Recherche et d'Enseignement de Géosciences de l'Environnement), Aix-en-Provence, in May and June 2022.

To prepare slides for analysis, I used a random settling method, described below, modified from Beaufort (1991) and Flores and Sierro (1997). A homogenised sample of approximately 1 mg dry sediment for each sample was diluted into 100 ml tap water, agitated, and ultrasonicated for around 30 seconds to break up aggregates. An additional 100 mL tap water was added and the solution stirred. Using a pipette, 1 ml of the diluted sample was transferred from the middle of the beaker into a 3D-printed settling chamber. A 12 mm x 12 mm square coverslip was placed into the settling chamber, where it remained on a platform at water level. Two 1 ml aliquots of diluted sample were added into the chamber. The chamber was left for a minimum of four hours to fully settle.

Each settling chamber was slowly drained to avoid remobilising any material. Once drained, the coverslips were dried in an oven at 50°C for 1-2 hours. The dried coverslips were mounted onto slides by applying Norland Optical Adhesive 74, which was then set by exposure to UV light for 30 seconds. Excess glue was removed using a sharp tool and slides were cleaned with a weak soap solution before

imaging. Each slide contains eight coverslips, so that eight samples could be analysed under the microscope without manually replacing them on the stage.

A second coverslip was prepared for some samples (n=5) when specific issues occurred during initial slide preparation. Issues included: skewed placement of a coverslip; coverslips tilting in the settling chamber resulting in uneven settling; and coverslips becoming chipped when removed from the chamber.

A Leica DM6000 automated polarising microscope was used to capture 150 field of view (FOV) images (125 µm by 125 µm) per coverslip. These images were analysed using SYRACO (Beaufort and Dollfus, 2004; Barbarin, Beaufort and Moron, 2014), an artificial neural network-based software that identifies nannoliths and categorises them into morphogroups based on a large training dataset of coccoliths accumulated over the past 20 years (Barbarin, Beaufort and Moron, 2014).

SYRACO tallies nannoliths across every FOV. I used these nannolith counts to calculate nannolith concentration, N (nannoliths g^{-1}), using the formula below, modified from Flores and Sierro (1997):

$$N = n * W^2 * V * w^{-2} * g^{-1} * v^{-1} \qquad \text{(Equation 2.1)}$$

where *n* is total number of nannofossils counted, *W* is width of square settling chamber (2 mm), *V* is water volume added to dry sediment (200 mL), *w* is FOV width used in SYRACO images (125 µm), *g* is dry sediment weight, and *v* is volume of mixture settled onto coverslip (2 mL). Note that modifications have been made from the original formula due to the use of square coverslips and FOVs, rather than the circular ones in the original method.

To account for the potential influence of sedimentation rate and sediment density, I calculated the nannolith accumulation rate (NAR) using the following equation, modified from Flores & Sierro (1997):

$$NAR = N * \rho * S \qquad \text{(Equation 2.2)}$$

Where NAR is nannofossil accumulation rate (coccoliths cm^{-2} kyr^{-1}), ρ is sediment dry bulk density (g cm^{-3}), and *S* is linear sedimentation rate (cm kyr^{-1}). I determined the density of samples using a linear interpolation of discrete dry density values published in the initial reports for IODP Site U1313 (Expedition 306 Scientists, 2006) and ODP Site 982 (Shipboard Scientific Party, 1996). Sample sedimentation rates were calculated using the age models described in Chapter 1.

The methodological standard deviation of the settling method is estimated to be in the range of 2-5% of the total nannolith concentration (Beaufort, 1991; Flores and Sierro, 1997). This error is also likely to apply to this dataset.

In order to compare NAR outputs to broader trends in carbonate sedimentation, I also generated a carbonate mass accumulation rate (MAR) for ODP Site 928 using the equation below:

$$MAR = CaCO_3 * \rho * S \quad \text{(Equation 2.3)}$$

Using $\%CaCO_3$ (g/g) values generated by Venz et al. (1999) and interpolated ρ and *S* values as described for Equation 2.2, above. MAR has unit g cm^{-2} kyr^{-1}.

2.2.2. SYRACO Reliability

Significant discrepancies between the expected and SYRACO-determined coccolith morphogroup counts and proportions led to further investigations for these samples. Analysis of SYRACO morphogroup outputs revealed that 30.9% of specimens in ODP Hole 982B and 24.5% of specimens in IODP Hole U1313A were allocated into groups that had become extinct prior to the past 200 kyr. Of the extinct morphogroup counts, 50.1% were *Reiculofenestra haqii* (last known occurrence ~3.9 Ma) and 49.4% *Gephyrocapsa caribbeanica* (last known occurrence ~0.21 Ma; Young, Bown and Lees, 2022). As no significant sediment remobilisation has been noted for either ODP Site 982 (Shipboard Scientific Party, 1996) or IODP Site U1313 (Expedition 306 Scientists, 2006), and *R. haqii* has last occurrence over 3 Ma earlier than the older sediment used in this research, it is unlikely that these coccoliths have been sourced from reworked sediment. Both *R. haqii* and *G. caribbeanica* are morphologically similar to other reticulofenestrid coccoliths (Young, Bown and Lees, 2022), and are therefore more likely to represent other *Gephyrocapsa* coccoliths that were misidentified by SYRACO.

A further 14.2% and 37.2% of total coccoliths in ODP Hole 982B and IODP Hole U1313A, respectively, were classified as *Florisphaera profunda*. High abundances of this sub-photic zone taxon are environmentally significant as an indicator of oligotrophy (Beaufort et al., 1997; Hernández-Almeida et al., 2019). In 11 of the 59 total samples across both cores, SYRACO calculated that *F. profunda* nannoliths composed a majority of the total assemblage. This is an unexpectedly high value for the mid-to-high latitude Atlantic (Hernández-Almeida *et al.*, 2019), and therefore prompted further investigation.

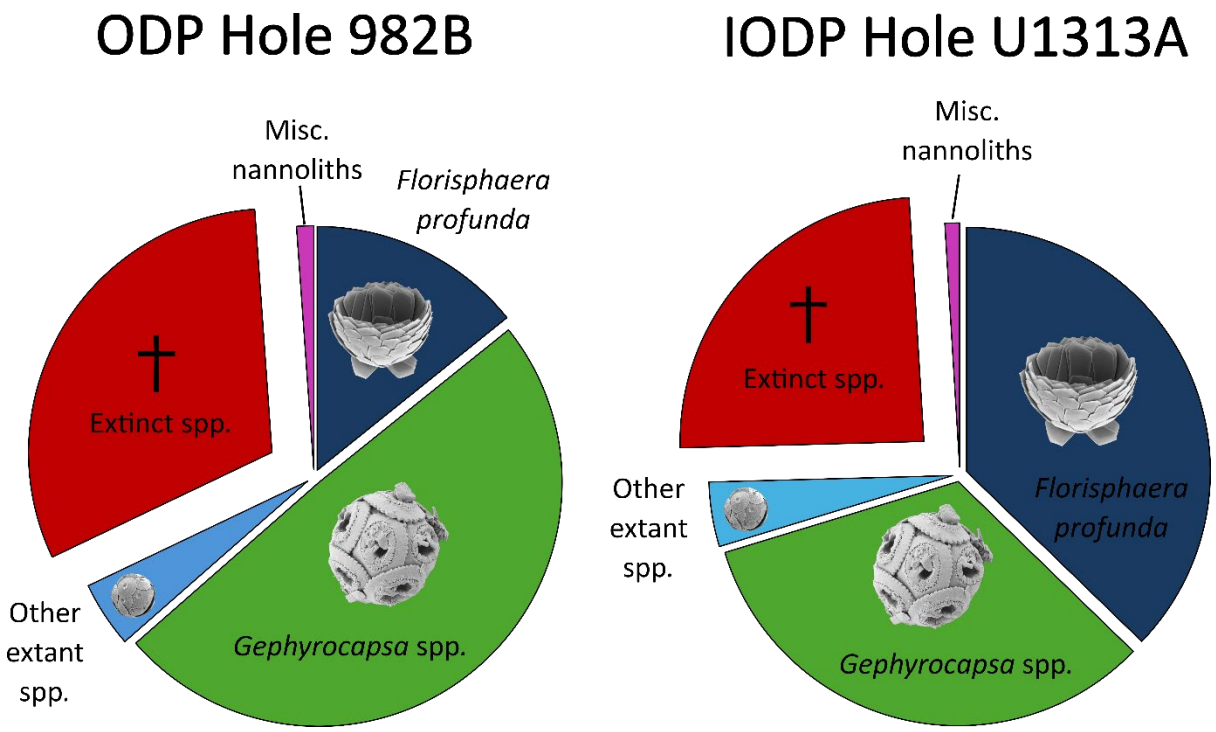

Figure 2.2 – Grouped proportions of SYRACO-identified nannoliths tallied across all samples for ODP Hole 982B (n=69812) and IODP Site U1313 (n=186826). *Florisphaera profunda* and *Coccolithus pelagicus* ('Other extant spp.') images are modified from Nannotax 3 database (Young, Bown and Lees, 2022).

Therefore, to test the reliability of SYRACO nannolith morphogroup identification, I investigated nine samples using a scanning electron microscope (SEM) (listed in Table 3.A1). Stubs were prepared using the method of Flores and Sierro (1997). SEM analyses were conducted at the Sir William Dunn School of Pathology, University of Oxford, using a Zeiss Sigma 300 after the application of a gold-paladium coating using a Quorum Q150R ES multi-coating unit. Visual inspection of random FOVs (n=5–10 per sample) were used to approximate the proportions of coccolith morphospecies and compare these with the SYRACO morphogroup data, with greatest emphasis on whether the total proportion of *F. profunda* in assemblages were consistent with SYRACO outputs.

Visual inspection by SEM confirmed misidentification in the SYRACO outputs. In all analysed slides, *Gephyrocapsa* spp. was the dominant morphogroup, rather than *F. profunda*. The images shown in Figure 2.2 show random FOVs that were broadly representative of the overall assemblage in each sample. SYRACO identified these two samples as having the highest percentage of *F. profunda* in their respective cores, with values of 95.5% in U1313A_26 and 75.5% in 982B_N8. However, in both cases, *Gephyrocapsa* spp. compose the majority of the assemblage and small, fragmented nannoliths that may belong to *F. profunda* or other morphogroups (such as *Calcidiscus leptoporus*) are a smaller component of the total assemblage.

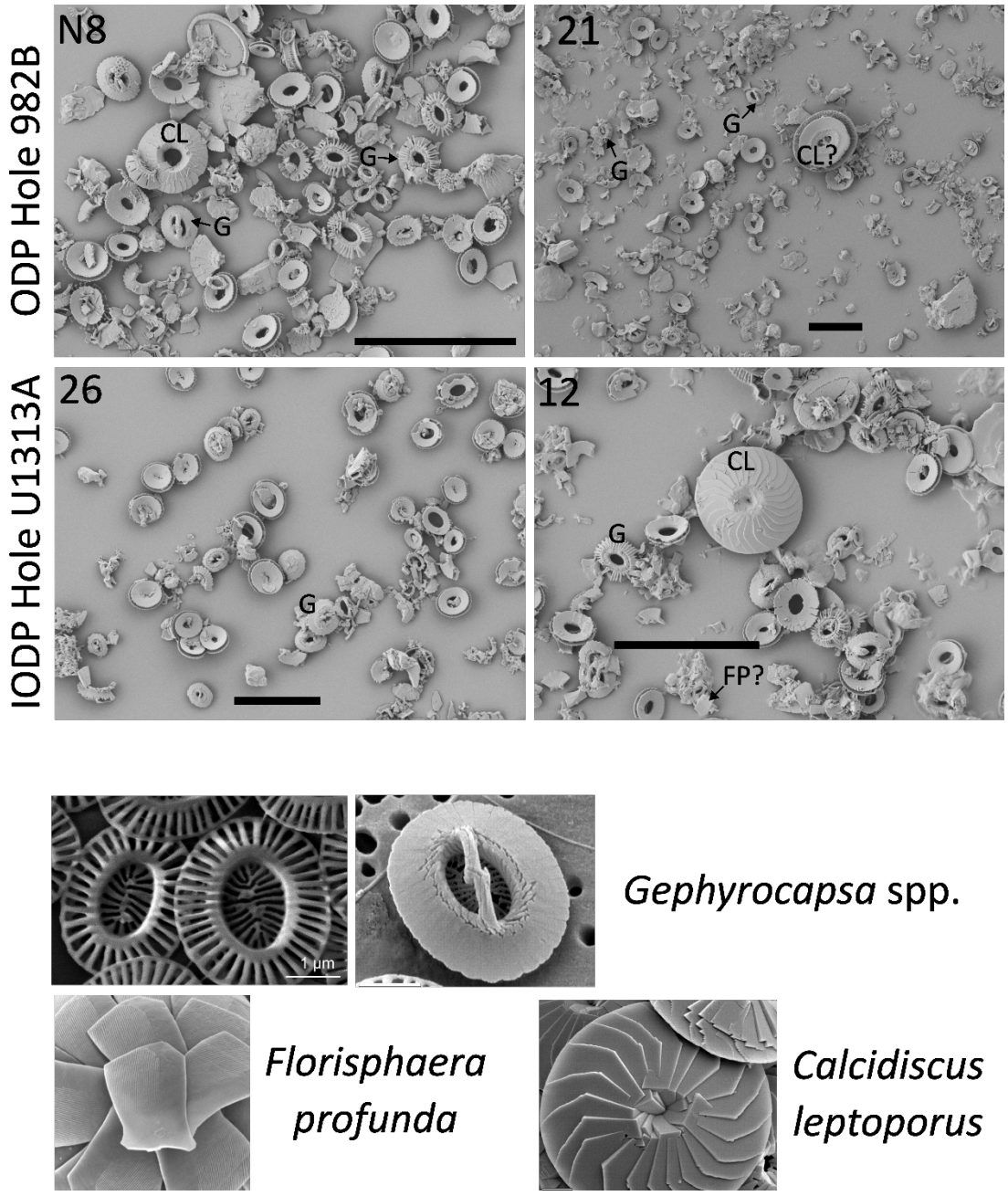

Figure 2.3 – SEM images of four samples, showing broadly representative assemblages for each case. Top two images are from ODP Hole 982B and bottom two images are IODP Hole U1313A. The top left number of each image shows sample number and horizontal black bar represents 10 µm. Bottom key shows example *Gephyrocapsa* spp. (G), *Florisphaera profunda* (FP), and *Calcidiscus leptoporus* (CL) leptoporus, examples of which are labelled in each SEM image. There are no clear examples of *F. profunda*, but a possible coccolith is indicated for IODP Hole U1313A sample 12 (bottom right). Key coccolith images are reproduced from the Nannotax database (Young, Bown and Lees, 2022).

As SEM analyses demonstrated the unreliability of SYRACO data for coccolith demographics, I further checked the reliability of SYRACO coccolith abundance (N) data by comparing them to manually determined abundances. I produced new coccolith abundance data using the method of Flores & Sierro (1997) using the same slides prepared previously for SYRACO. All counting was performed on a Zeiss AXIO Scope.A1 compound petrographic microscope at the Oxford University Museum of Natural

History. For each sample, I tallied all nannoliths in randomly selected FOV (4≤n≤19) until reaching a cumulative total of at least 400 nannoliths. To generate values for nannolith abundance, I used a modified version of Equation 2.1 due to the use of a circular FOV, as opposed to the square FOVs used in SYRACO:

$$N = n * W^2 * V * \pi r^{-2} * g^{-1} * v^{-1} \qquad \text{(Equation 2.4)}$$

where *r* is FOV radius.

NAR values were then calculated as previously, using Equation 2.2.

As well as calculating NAR, I tallied the total number of nannoliths in seven different morphogroups: *Gephyrocapsa* spp., *Coccolithus pelagicus* subsp. *pelagicus* (large), *Coccolithus pelagicus* subsp. braarudii (small), *Syracosphaera* spp., *Helicosphaera* spp., *Calcidiscus leptoporus*, and 'Other'. For the six defined taxonomic groups, the identity of the specimen was confirmed by reference to the Nannotax 3 online database (Young, Bown and Lees, 2022). These seven coccolith morphogroups were chosen based on the abundances observed in SEM and preliminary inspection in transmitted light, as well as their potential value as proxies for environmental conditions and preservation (Baumann *et al.*, 2005; Narciso, Cachão and De Abreu, 2006; Jordan, 2009; Duncan *et al.*, 2016; Poulton *et al.*, 2017; Prista, Narciso and Cachao, 2020).

Small grey fragments that could not be confidentially allocated to any specific morphogroup and were not conclusively coccoliths or coccolith fragments were also counted but were not included in the 400 minimum total nannolith threshold.

2.2.3. Manual counting comparisons

Initially, I recounted the number of nannoliths in a randomly selected subset of 30% of total settled slides for both cores. By doing this, I was able to assess whether there were significant differences between SYRACO-derived and manually-counted abundances and therefore whether a full recount was necessary. At ODP Hole 982B, there was good agreement (n=8; R^2=0.782) between the count data derived from SYRACO and manual counts (Figure 2.4), and thus no further counting was needed and SYRACO data were used to generate NAR estimates.

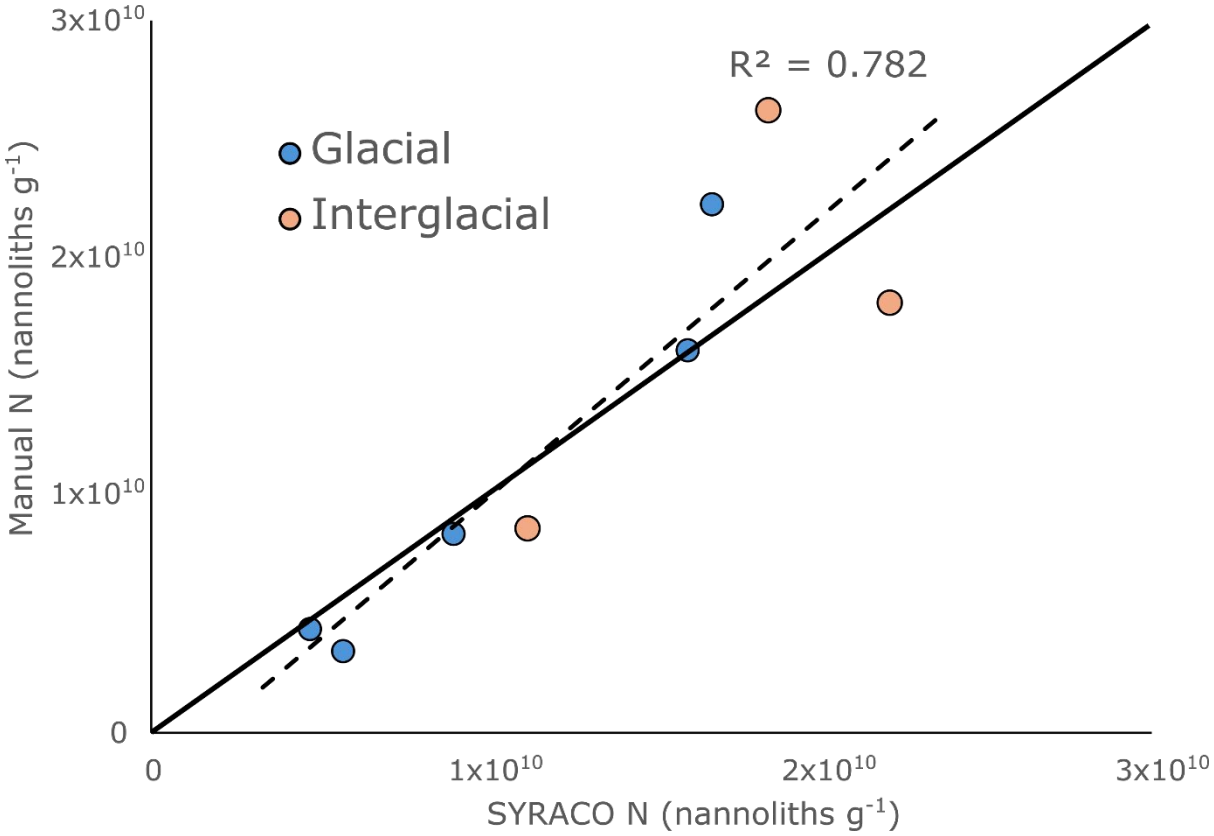

Figure 2.4 – Plot of SYRACO-derived nannolith concentration compared to the concentration calculated from manual counting for ODP Hole 982B. Solid black line shows the hypothetical regression slope where both values are equal. Dashed black line shows the actual slope (R^2=0.782). Blue and red infilling represents sample position in glacial and interglacial times, respectively.

For IODP Hole U1313A, initial count data proved inconclusive (n=9; R^2=0.188), and so I manually recounted all samples. In this full comparison, there was poor agreement between nannolith concentration values derived from the two methods (R^2=0.026), shown graphically in Figure 2.5. Hence, I use manual count nannolith concentration data for all samples (n=28**)** in subsequent analyses for IODP Hole U1313A, rather than the original SYRACO concentration values.

SYRACO overestimated the total number of nannoliths in IODP Hole U1313A samples in 20 out of 28 samples**,** relative to manual counts. This poor agreement likely results from the misidentification of nannoliths as *F. profunda* by SYRACO. It appears likely that fragmented and dark nannoliths were misidentified as *F. profunda* by SYRACO, and manual observations suggest that these dark or fragmented nannoliths were more abundant in Site IODP U1313A than Site ODP 982B.

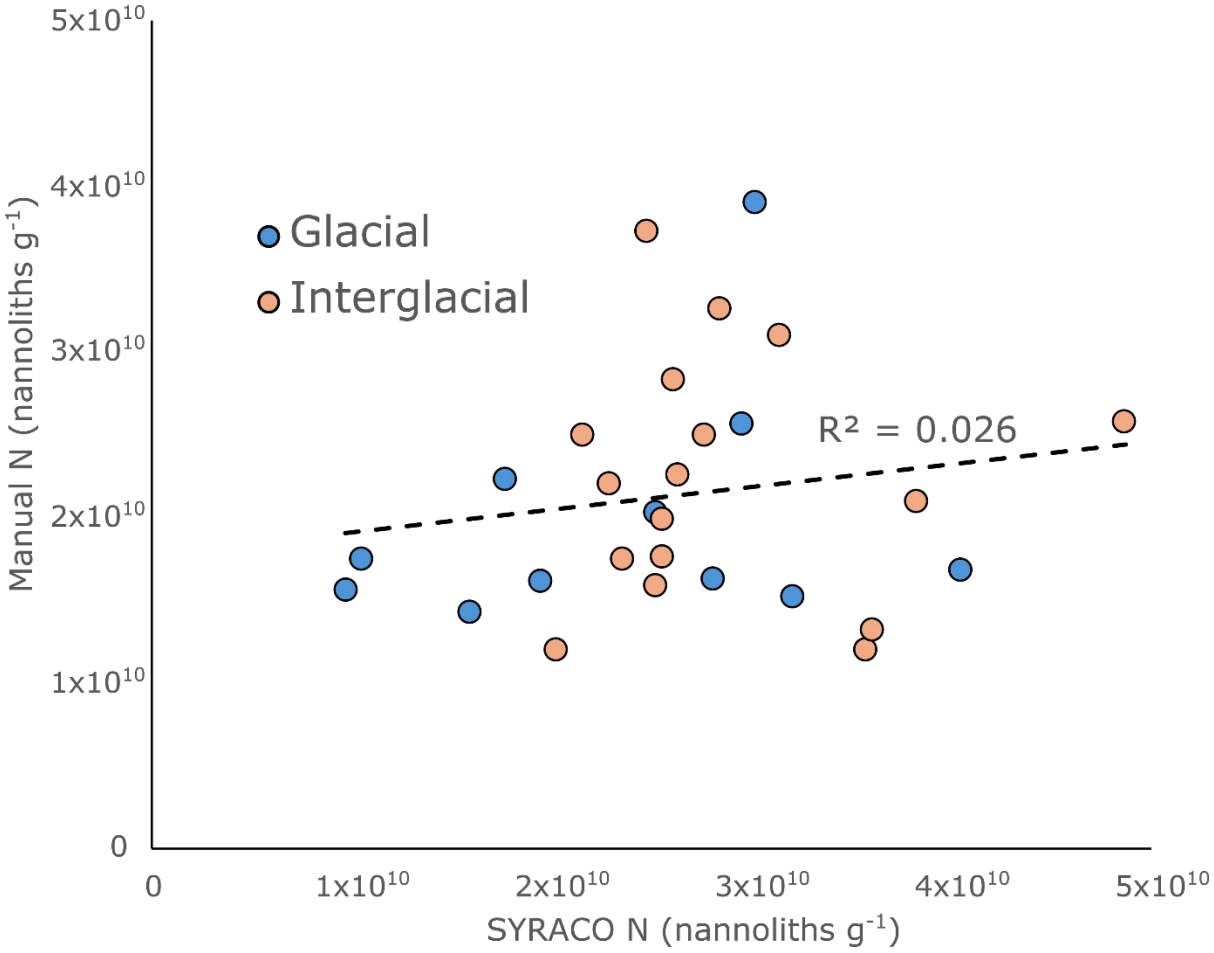

Figure 2.5 – Plot of SYRACO-derived nannolith concentration compared to the concentration calculated from manual counting for IODP Hole U1313A. Solid black line shows the hypothetical regression slope where both values are equal. Dashed black line shows the actual slope (R^2=0.0262). Blue and red infilling represents sample position in glacial and interglacial times, respectively.

2.2.4. Nannolith preservation

Different coccolithophore taxa produce nannoliths of varying robustness and preservation potential. More delicate nannoliths may be more prone to dissolution, which could result in nannolith concentration estimates (and hence NAR) being a signal of preservation rather than productivity. To assess whether the original coccolith assemblage has been significantly altered after deposition by corrosive seafloor conditions, I used a modified version of the '*Calcidiscus leptoporus-Emiliania huxleyi* dissolution index' (CEX; Dittert et al., 1999). This metric compares the relative proportions of the delicate, dissolution-prone coccoliths of *Gephyrocapsa huxleyi*, formerly known as *Emiliania huxleyi* (Bendif et al., 2019; Filatov et al., 2021), against the robust, strongly calcified and dissolution-resistant coccoliths of *C. leptoporus*. In dissolution-prone waters, *C. leptoporus* should be enriched relative to the other taxa, hence resulting in lower CEX values. Due to uncertainty in distinguishing the nannoliths of *G. huxleyi* from other morphospecies within the genus *Gephyrocapsa* in transmitted light microscopy, I combine all *Gephyrocapsa* spp. for a modified version of CEX below:

$$CEX = \frac{Gephyrocapsa\ spp.(\%)}{Gephyrocapsa\ spp.(\%) + Calcidiscus\ leptoporus\ (\%)} \qquad \text{(Equation 2.5)}$$

2.2.5. Statistical tests

I conducted all statistical tests using R version 4.4. I tested for significant differences between the mean NAR values in glacial and interglacial intervals using two-tailed Mann-Whitney U Tests (Mann and Whitney, 1947), as the data were nonparametric.

2.3. Results

2.3.1. CEX

Mean CEX values are 0.981 for ODP Hole 982B and 0.965 for IODP Site U1313. Maximum CEX values for both sites occur in the late LIG and early LGP (90–60 ka) and minimum values occur at 119 ka and 95 ka at Sites ODP 982B and IODP U1313A, respectively.

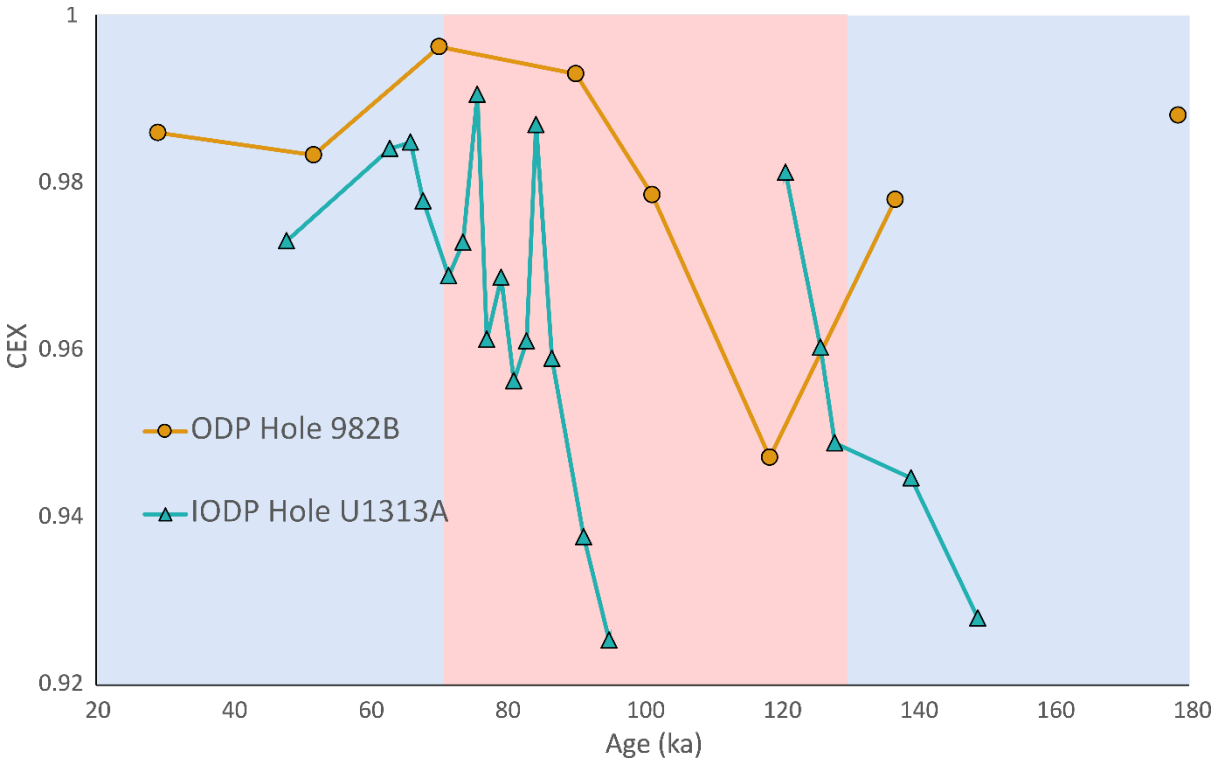

Figure 2.6 - CEX values over time for ODP Hole 982B (orange circles) and IODP Hole U1313A (blue triangles). Background colours indicate the span of the LGP (14–71 ka), LIG (71–130 ka), and PGP (130–191 ka). Where the gap between adjacent samples exceeds 20 kyr, no connecting line is shown.

2.3.2. N, NAR, and MAR

ODP Site 982 (SYRACO)

At ODP Hole 982B, the range of values for N is 3.35×10^{9}–2.39×10^{10} nannoliths g^{-1}, with a mean value of 1.24×10^{10} nannoliths g^{-1}. The four highest values all occur during the LIG, and the lowest value occurs late in the LGP at 19 ka, with the next three lowest values in the PGP at 137–166 ka.

NAR values range from 7.42×10^{9}–1.30×10^{11} nannoliths cm^{-2} kyr^{-1}, with a mean of 3.93×10^{10} nannoliths cm^{-2} kyr^{-1}. The first and second highest NAR values occur in the youngest (7 ka) and oldest (200 ka) samples, respectively, which are elevated relative to the N values primarily due to the relatively high sedimentation rates at this site during the Holocene and MIS 7.

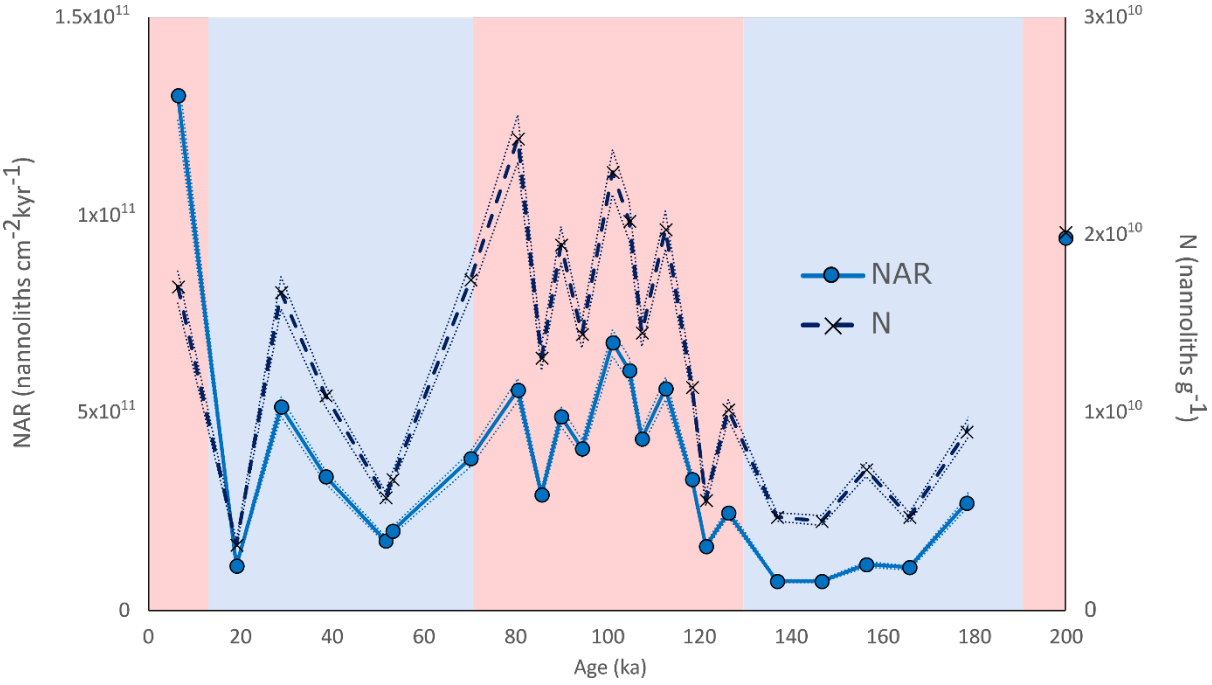

Figure 2.7 – Plot of N (dashed line, black crosses) and NAR (solid line, blue circles) over time for all samples at ODP Hole 982B. Red and blue backgrounds indicate the span of interglacial and glacial intervals, respectively. Dotted lies show upper and lower bounds based on possible range of sedimentation rate and dry bulk density. Where the gap between adjacent samples exceeds 20 kyr (oldest two samples only), no connecting line is shown.

A MWU test suggested significant differences between NAR during interglacial intervals (n=13) compared to glacial intervals (n=11) (U=19, p=0.003). NAR was, on average, higher during interglacial than glacial intervals over the past 200 kyr (Figure 2.8).

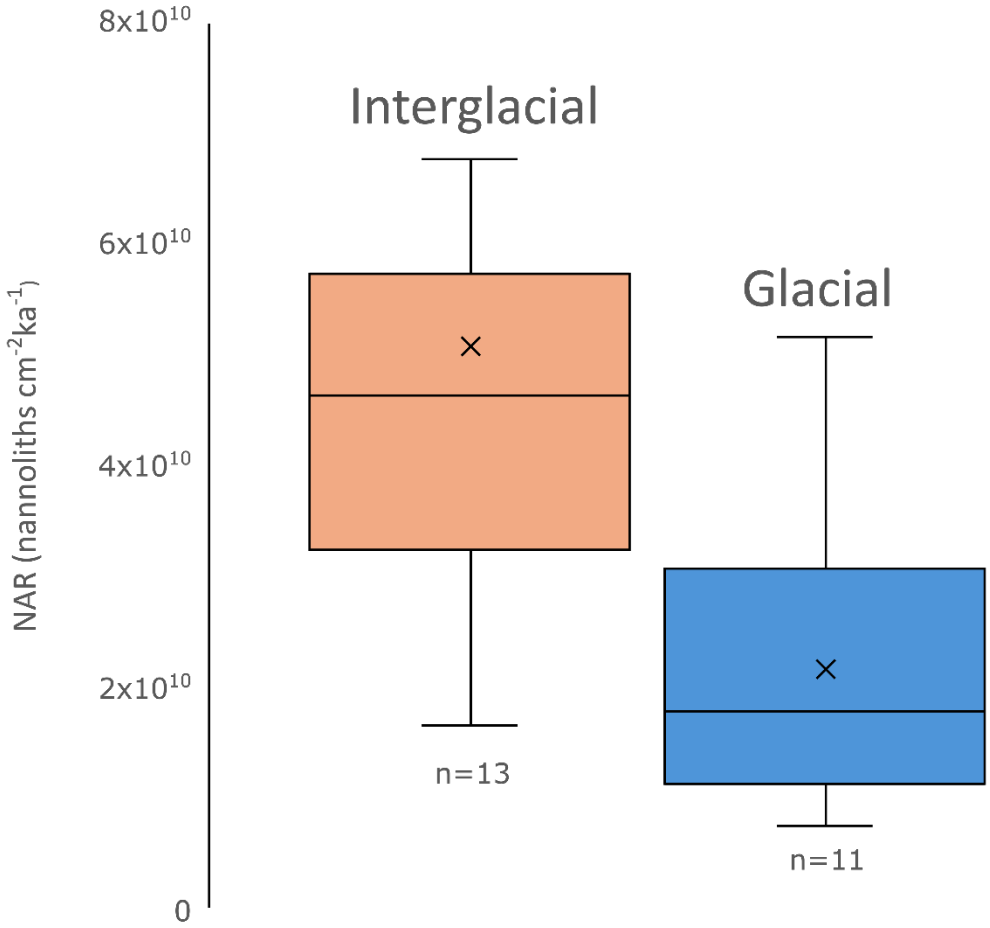

Figure 2.8 – Box plot of NAR values for samples from interglacial (left) and glacial (right) intervals at ODP Hole 982B. The horizontal line within each box indicates the mean of all values and the black crosses show the median value.

Carbonate MAR at ODP Site 982 varied between 32.2 – 596 g cm-2 kyr-1. The highest values were present during the Holocene, and carbonate MAR was generally higher during interglacial intervals relate to glacial intervals (Figure 2.9). There is strong covariation between carbonate MAR and NAR.

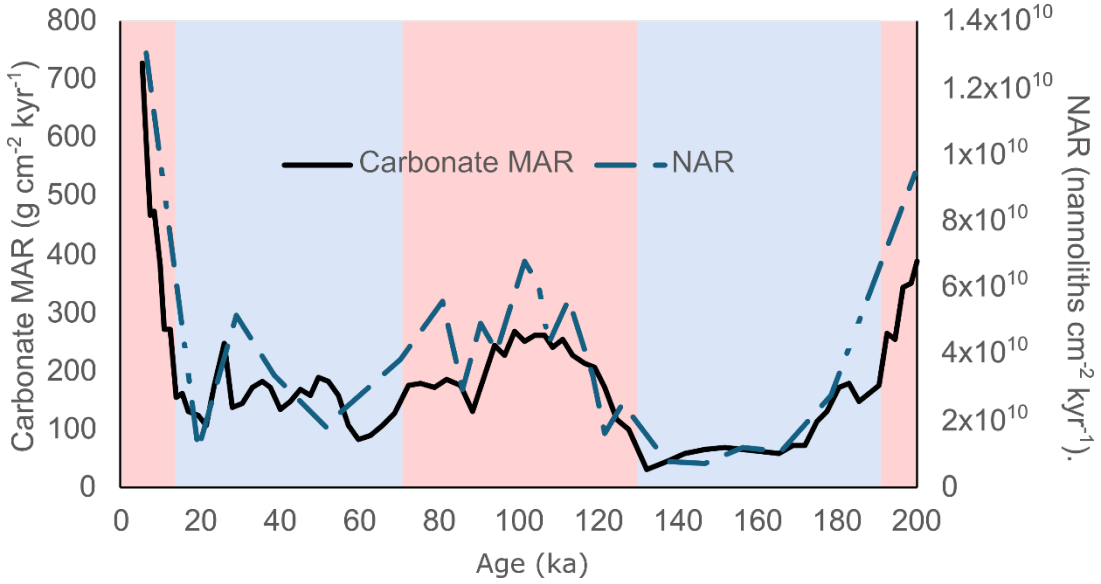

Figure 2.9 – Comparison of carbonate MAR (solid black line) and NAR (dashed blue line) for ODP Hole 982B. Background colours indicate glacial (blue) and interglacial (red) intervals, respectively.

IODP Site U1313 (Manual)

For the manual counts from IODP Hole U1313A, values for N range from 1.19×10^{10} –3.91×10^{10} nannoliths g^{-1}. The mean N value of 2.14×10^{10} nannoliths g^{-1} is 73% higher than the mean for ODP Hole 982B. The highest nannolith counts occur at 134 ka and 118 ka, whilst the three lowest values are found during the late LIG at 95, 83 and 74 ka.

NAR values are between 7.77×10^{10} and 3.56×10^{11} nannoliths cm^{-2} kyr^{-1}. The mean NAR value of 1.50×10^{11} nannoliths cm^{-2} kyr^{-1} is almost four times greater than mean NAR at ODP Hole 982B. The greater discrepancy between N and NAR for IODP Hole U1313A relative to ODP Hole 982B is due to the significantly greater average sedimentation rate of the former.

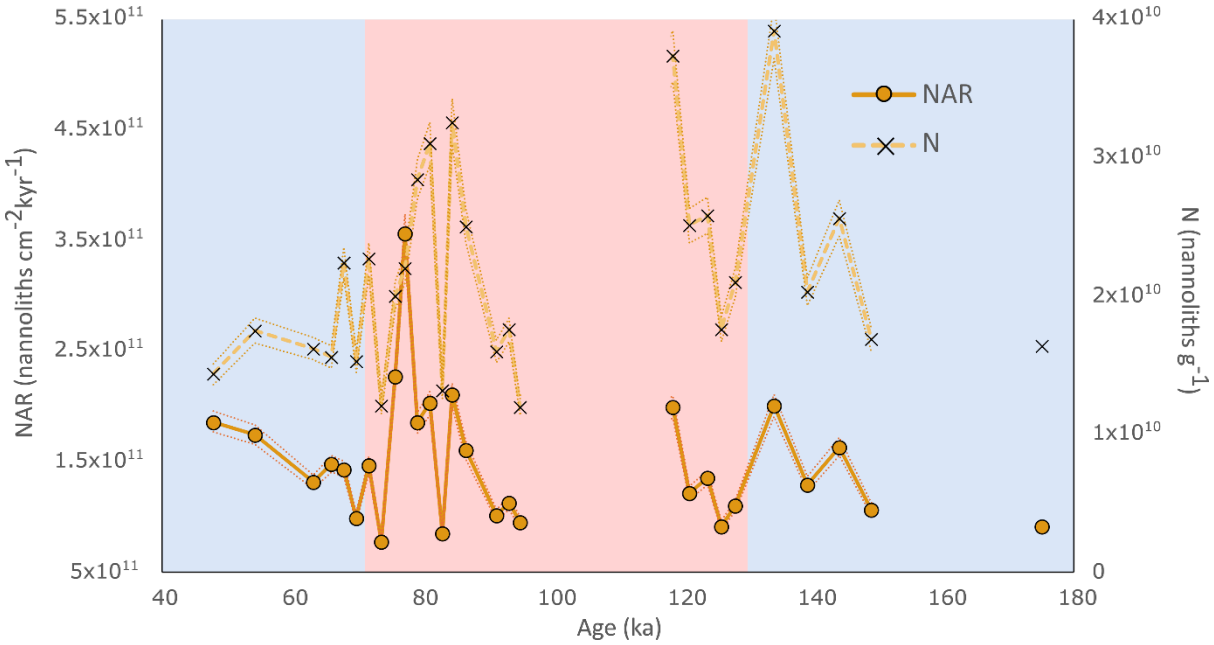

Figure 2.10 – Plot of N (dashed line, black crosses) and NAR (solid line, orange circles) over time for all samples at IODP Hole U1313A. Red and blue backgrounds indicate the span of interglacial and glacial intervals, respectively. Dotted lies show upper and lower bounds based on possible range of sedimentation rate and dry bulk density. Where the gap between adjacent samples exceeds 20 kyr, no connecting line is shown.

Unlike ODP Site 982, there was no significant difference between NAR values during glacial and interglacial intervals at IODP Hole U1313A (U=93, p=1).

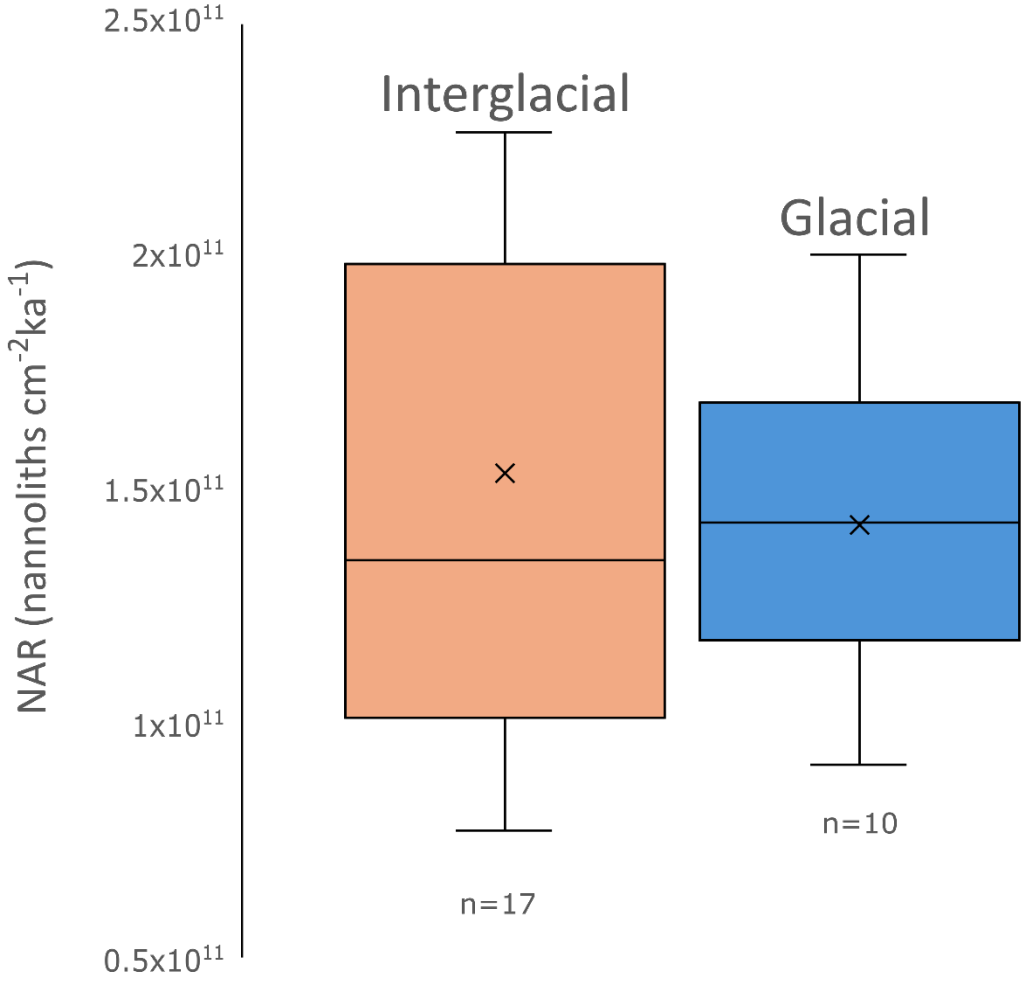

Figure 2.11 – Box plot of NAR values for samples from interglacial (left) and glacial (right) intervals at IODP Hole U1313A. The horizontal line within each box indicates the mean of all values and the black crosses show the median value.

2.3.3. Taxonomy

Gephyrocapsa spp. overwhelmingly dominate all assemblages in IODP Hole U1313A, with abundance ranging from 86.5–97.2% and a mean of 92.2%. *C. leptoporus* is the second most abundant nannolith type, with a mean contribution of 3.5%. Other taxa whose mean abundance exceeds 1% are: *C. pelagicus* subsp*. pelagicus* (1.8%); *C. pelagicus* subsp*. braarudii* (1.1%), and *Syracosphaera* (1.3%).

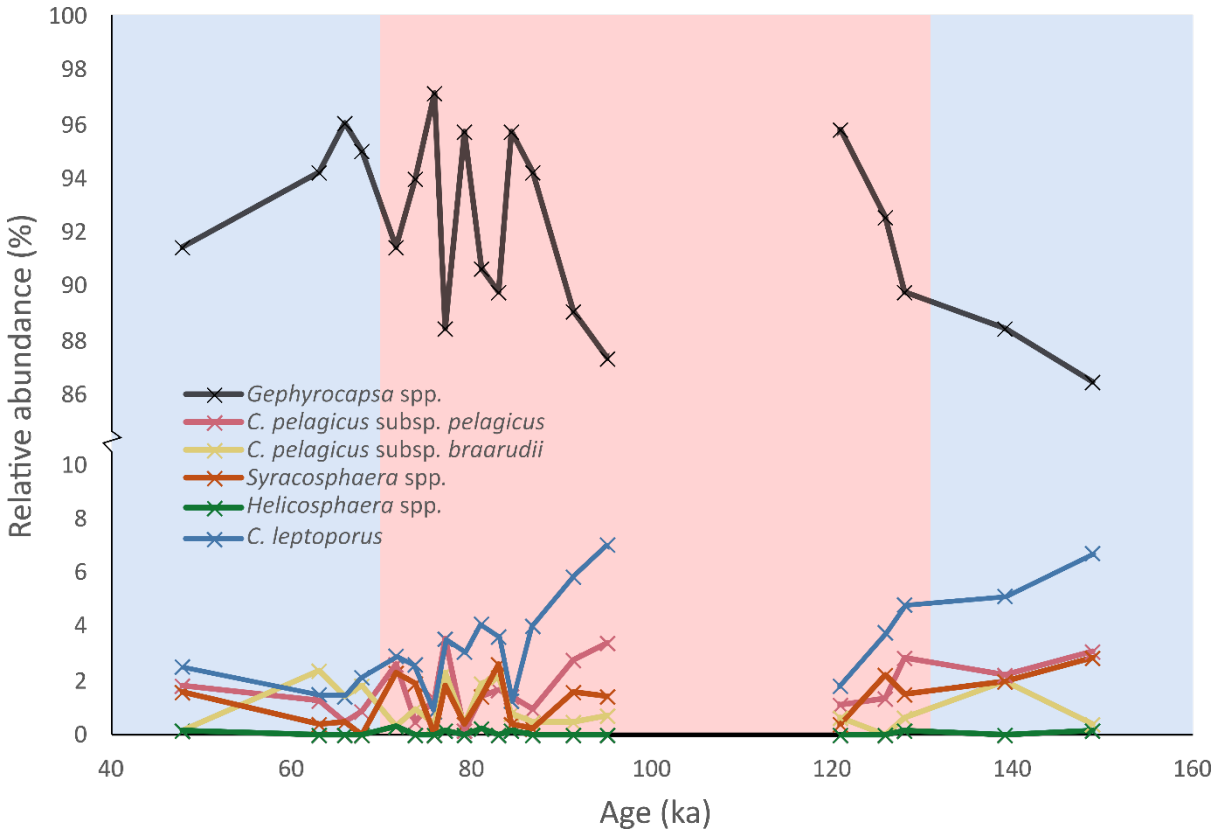

Figure 2.12 – Relative abundances of six coccolith taxa at IODP Hole U1313A between 40–160 ka. Note that the vertical axis is discontinuous due to the high abundance of *Gephyrocapsa* spp.. A 26 kyr gap between adjacent samples at 121–95 ka is not connected. Where the gap between adjacent samples exceeds 20 kyr, no connecting line is shown. Red and blue backgrounds indicate interglacial and glacial intervals, respectively.

Taxonomic data for ODP Hole 982B derive only from the limited set of 8 samples that were manually counted for comparisons to SYRACO, as earlier testing indicates low reliability in SYRACO taxonomy estimates. *Gephyrocapsa* spp. similarly dominate in these samples, ranging from 89.4–98.2% with a mean of 94.3%, marginally higher than in IODP Hole U1313A. Only *C. leptoporus and C.pelagicus* subsp. *pelagicus* have mean abundances greater than 1%, at 1.77% and 1.76%, respectively. Full abundance information for both cores, including taxa with mean relative abundances below 1%, is included in Table 3.A2.

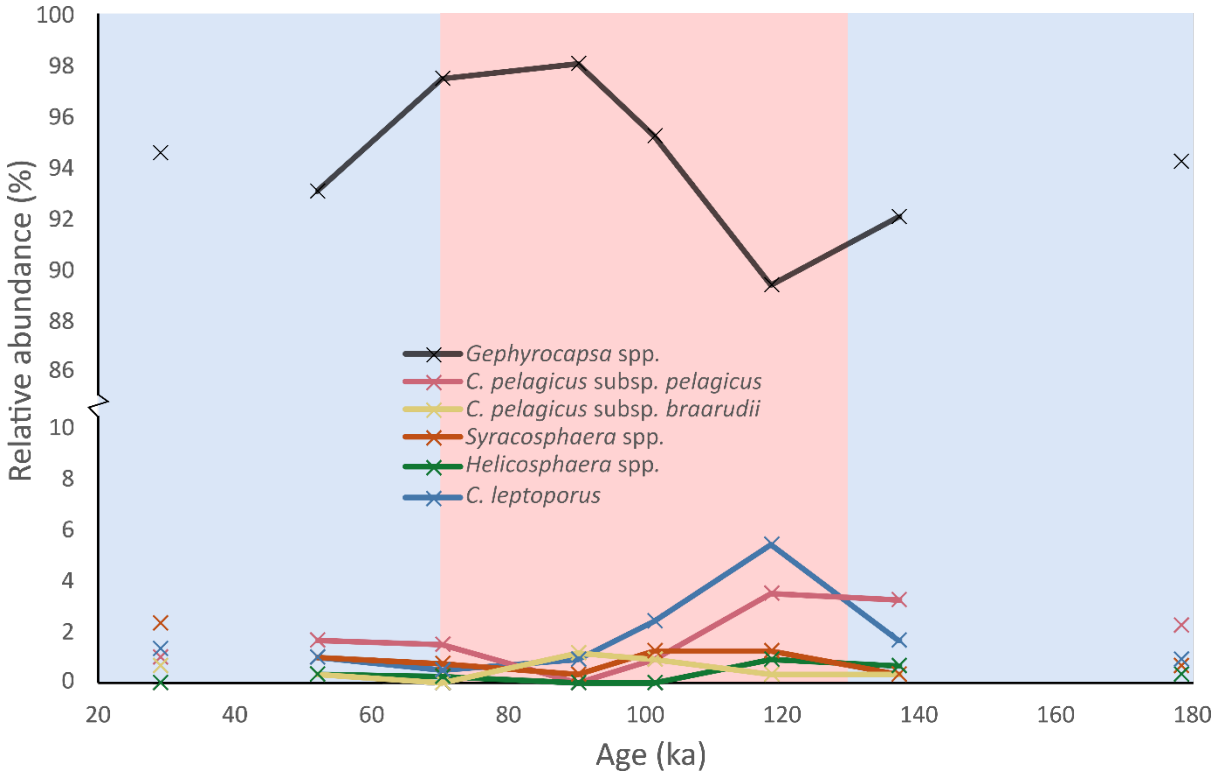

Figure 2.13 – Relative abundances of six coccolith taxa at ODP Hole 982B between 20–180 ka. Note that the vertical axis is discontinuous due to the high abundance of *Gephyrocapsa* spp.. Gaps between adjacent samples that exceed 20 kyr are not shown as connected. Red and blue backgrounds indicate interglacial and glacial intervals, respectively.

2.4. Discussion

All CEX values are comfortably above 0.6, the approximate threshold for deposition below the calcite lysocline (Dittert *et al.*, 1999; Boeckel and Baumann, 2004), indicating that dissolution has had a negligible effect on coccolith preservation at these two North Atlantic sites during the past 200 kyr. Previous work has suggested that an increased northward incursion of corrosive (low-[CO_3^{2-}]) Antarctic Bottom Water (AABW) coincident with the AMOC weakening during glacial intervals may lead to partial dissolution of biogenic calcite in the North Atlantic (Gardner, 1975; Lang *et al.*, 2016; Sosdian, Rosenthal and Toggweiler, 2018). These CEX results suggest that any incursions of AABW did not significantly affect the assemblage composition at either site during the study interval, and that the nannolith assemblages can be interpreted as a palaeoenvironmental proxy as opposed to a record of preservation.

The dominance of *Gephyrocapsa* spp. coccoliths at both sites throughout the LGP, LIG, and PGP is consistent with previous Pleistocene assemblage reconstructions from the North Atlantic (e.g. Schwab et al., 2012; Cavaleiro et al., 2018; Argenio et al., 2024). The higher mean abundance of *Geophyrocapsa* spp. at ODP Site 982 compared to IODP Site U1313 reflects the higher dominance and lower diversity of coccolithophore taxa at high latitudes in the modern North Atlantic (Poulton *et al.*, 2017).

The lack of significant change in coccolith taxonomy is more surprising, given the substantial environmental perturbations associated with glacial-interglacial transitions, such as Termination II at ~130 ka (e.g. Broecker, 1982; Smith et al., 2013; Duncan et al., 2016). Previous studies have demonstrated a temperature association of the large (*C. braarudii*) and small (*C. pelagicus*) *C. pelagicus* subspecies with warm and cool water masses, respectively (Young *et al.*, 2003; Narciso, Cachão and De Abreu, 2006; Hagino and Young, 2015). However, no connection between sea surface temperature and relative abundance of *C. braarudii* is present in this dataset (Figure 2.14). At IODP Hole U1313A, *C. braarudii* has persistently high relative abundance during the coldest part of the early LGP, when summer SST was around 4°C cooler than the late LIG (Stein *et al.*, 2009; Naafs *et al.*, 2013), indicating that its abundance was not primarily controlled by temperature. It therefore seems likely that the relative abundance of *C. pelagicus* subspecies is controlled by other variables, such as vertical mixing and turbidity (Narciso, Cachão and De Abreu, 2006; Prista, Narciso and Cachao, 2020). The small absolute numbers of non-*Gephyrocapsa* taxa in these data, alongside the resolution of samples used in this research (particularly at ODP Site 982), may also limit how meaningfully the patterns of their abundances can be used to describe large-scale environmental change.

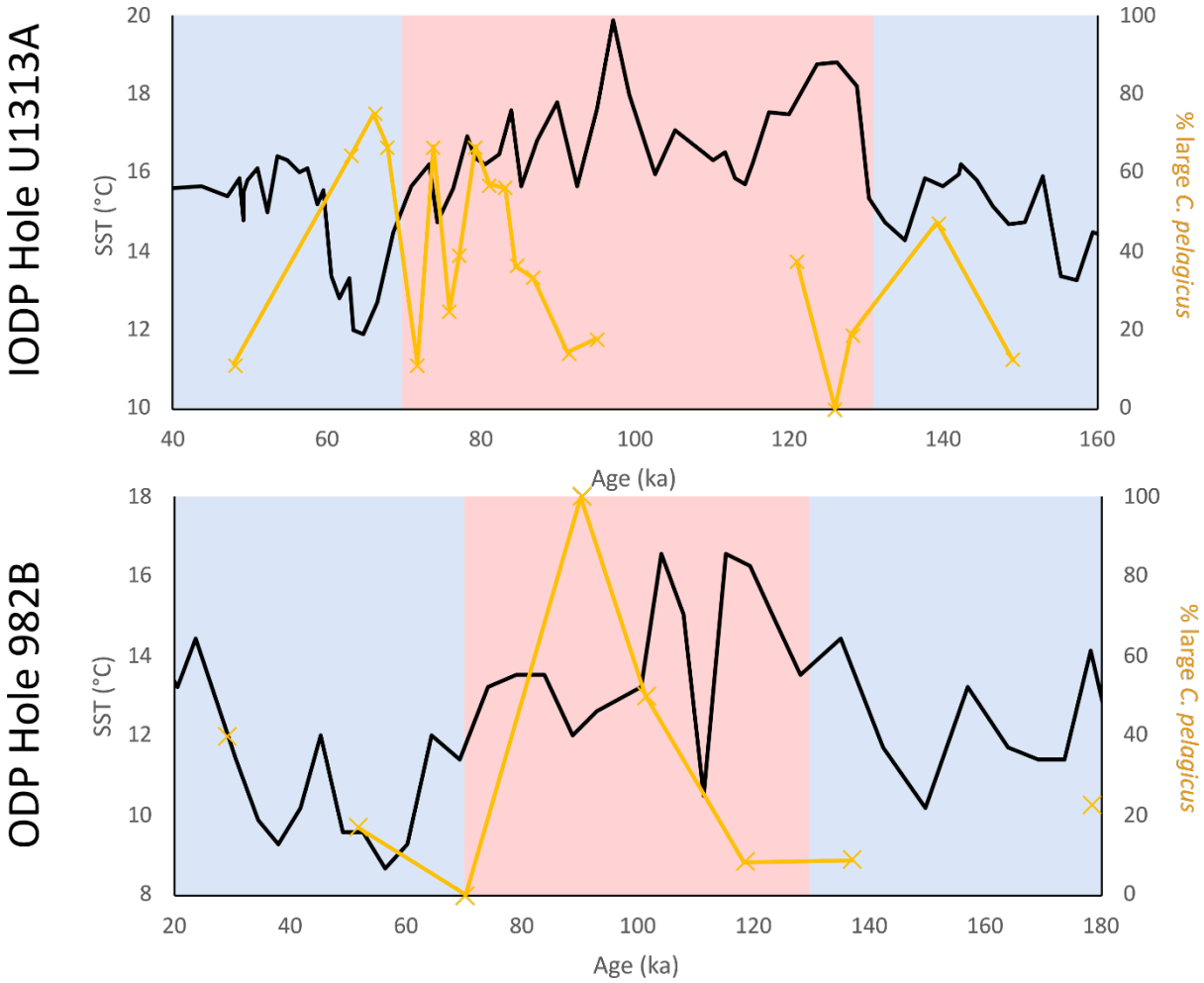

Figure 2.14 – The percentage contribution of *Coccolithus pelagicus* subsp. *braadrudii* to the total *Coccolithus pelagicus* assemblage at IODP Hole U1313A (top) and ODP Hole 982B (bottom). Sea surface temperature (SST) is also shown and derives from Stein *et al*. (2009) and Naafs *et al*. (2013) for the former, and Lawrence *et al*. (2009) and Herbert *et al*. (2016) for the latter. Where the gap between adjacent samples exceeds 20 kyr, no connecting line is shown. Background colour indicates glacial intervals (blue) or interglacial intervals (red).

NAR values are consistently higher at IODP Hole U1313A relative to ODP Hole 982B, suggesting that coccolithophore productivity was significantly greater at the lower latitude site during the late PGP–early LIG and late LIG–early PGP. In the modern pelagic North Atlantic, maximum coccolithophore cell densities (cells per litre of seawater) are higher in the subpolar ocean compared to temperate and subtropical regions (Guerreiro *et al.*, 2023), but intra-annual variability is also much greater due to the dominant role of stratification-controlled bloom events in cooler waters (Behrenfeld *et al.*, 2013; Guerreiro *et al.*, 2023).

Similar patterns are seen in the ODP Site 982 NAR record and the alkenone-derived productivity record of Bolton et al. (2011) for the PGP and early LIG (Figure 2.15). The PGP is characterised by persistent low productivity and the LIG begins with a marked increase into the LIG. However, the alkenone record suggests that productivity returned to low levels by the mid-LIG (~100 ka), whereas the NAR record shows productivity remaining above the PGP mean throughout the whole LIG. The decoupling of nannolith and alkenone concentrations has been noted by other authors (e.g. Marshall et al., 2021) and likely relates to differential productivity between calcifying and non-calcifying alkenone-producing haptophyte algae. The mid-to-late LIG may represent an interval of high coccolithophore productivity, but low productivity from non-calcifying haptophyte algae.

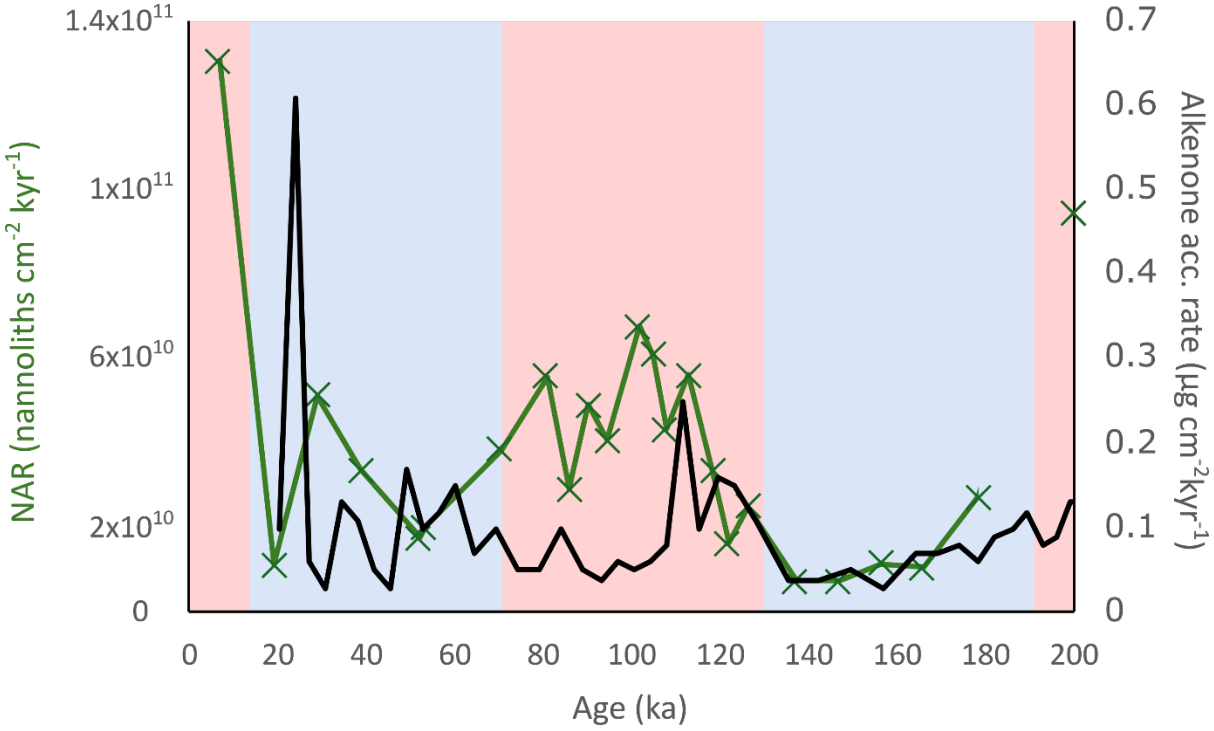

Figure 2.15 – Comparison of NAR (green crosses) and alkenone accumulation rate (black line; Bolton *et al.*, 2011) at ODP Site 982 over the past 200 kyr. Where the gap between adjacent NAR points exceeds 20 kyr (oldest two only), no connecting line is shown. Background colour indicates glacial intervals (blue) or interglacial intervals (red).

A recent study of coccolithophore dynamics at IODP Site U1313 over the past 25 kyr calculated NAR values of 10^{11}–$4x10^{11}$ nannoliths cm^{-2} kyr^{-1} (Argenio *et al.*, 2024), indicating that coccolithophore

productivity was broadly similar at this location after the deposition of the youngest (48 ka) sample in this research.

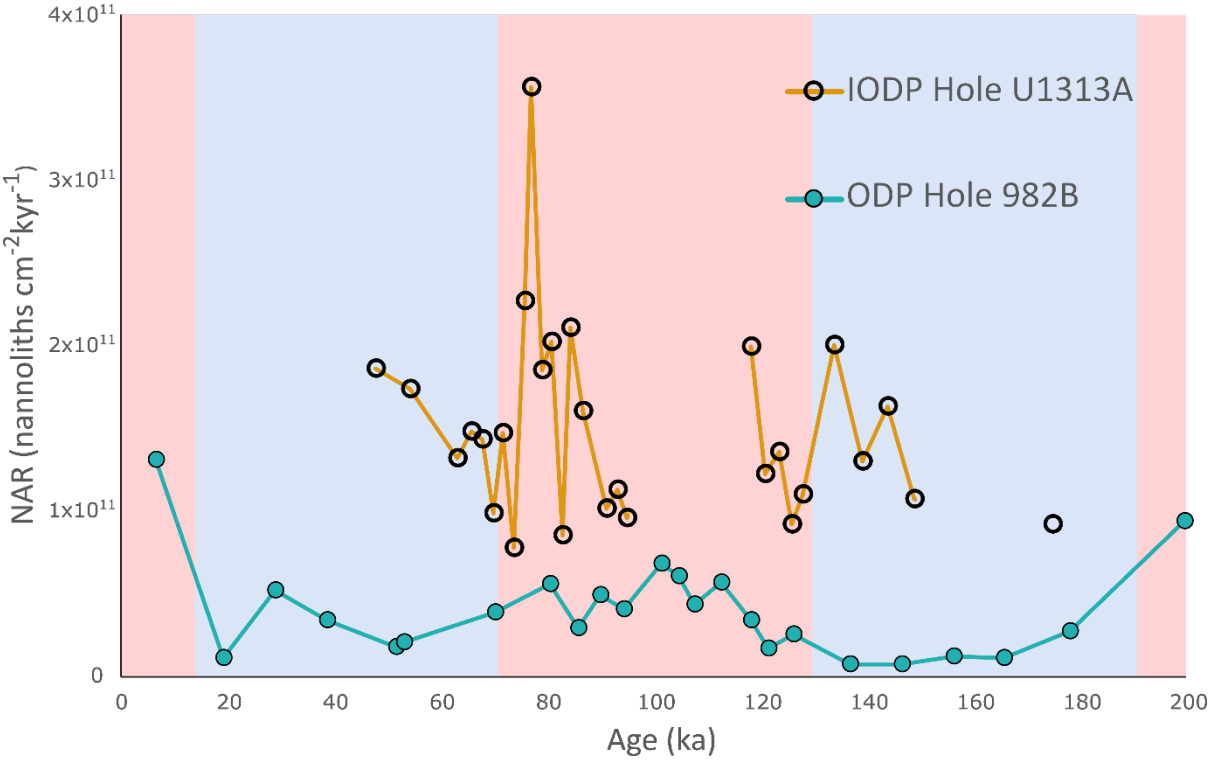

Figure 2.16 – NAR values for all IODP Hole U1313A (orange line, empty black circles) and ODP Hole 982B (blue line and filled circles) samples. Where the gap between samples exceeds 20 kyr, no connecting line is drawn. Background colour indicates glacial intervals (blue) or interglacial intervals (red).

Southward incursions of polar water masses into the North Atlantic basin were a common occurrence during glacial intervals (McIntyre, Ruddiman and Jantzen, 1972; Schwab *et al.*, 2012) and may explain the significant decrease in coccolithophore productivity at ODP Site 982 during the LGP and PGP. Previous studies have indicated the existence of a maximum productivity band in the North Atlantic approximately corresponding with NATW, around 45–55°N in the present day, which migrated southwards during past glacial intervals (Villanueva *et al.*, 2001; Naafs *et al.*, 2010; Cavaleiro *et al.*, 2018). Alkenone-based reconstructions indicate that the summer SST at ODP Site 982 was up to 7°C cooler during glacial intervals relative to the LIG (Lawrence *et al.*, 2009; Herbert *et al.*, 2016) and therefore likely located within the subpolar gyre and away from the NAC. During the peak of glacial phases (notably during Heinrich events), sea ice may have expanded to cover this site during winter, or at least have been proximal to the Rockall Plateau (Naafs *et al.*, 2013; Pedro *et al.*, 2022; Cauquoin *et al.*, 2023). Such low temperatures would have limited coccolithophore abundances, as is the case in the modern Arctic and Southern Oceans (Coello-Camba and Agustí, 2017; Nissen *et al.*, 2018). Furthermore, enhanced vertical mixing and subsequent nutrient resupply may have favoured the proliferation of eutrophic-adapted diatoms at the expense of coccolithophores (Cermeño *et al.*, 2011; Nissen *et al.*, 2018; Wang, Zeng and Feng, 2024).

Decreases in glacial coccolithophore productivity likely contribute to concomitant reduced %$CaCO_3$ in high-latitude Atlantic sediments, which cannot be explained solely by enhanced sediment dilution

(Bacon, 1984). These decreases occur alongside decreased planktonic foraminiferal abundance and diversity at high latitudes during glacial intervals, when foraminifera assemblages become dominated by the cold-water specialist *N. pachyderma* (Baumann and Huber, 1999; Kucera *et al.*, 2005; Jonkers *et al.*, 2024).

In the present-day, IODP Site U1313 lies close to the southern edge of NATW, slightly north of the Subtropical Front and the associated stratified, oligotrophic subtropical gyre. Mean summer SST at this site was lower during the LGP (14.3°C) and PGP (15.1°C) compared to the LIG (16.9°C) (Stein *et al.*, 2009; Naafs *et al.*, 2013). However, in contrast to ODP Site 982, these relatively low summer temperatures were not a permanent feature throughout the LGP and returned to values comparable to the late LIG within 15 kyr of the LIG–LGP transition (Lawrence *et al.*, 2009; Stein *et al.*, 2009; Naafs *et al.*, 2013; Herbert *et al.*, 2016)**.** This suggests that the Subarctic Front was rarely or never located south of IODP Site U1313 during the glacial intervals documented in this study. Furthermore, IODP Site U1313 is located at the southernmost extremity of the 'IRD belt' (Naafs, Hefter and Stein, 2013; Smith *et al.*, 2013; Lang *et al.*, 2016), indicating that whilst it may have been close to the Subpolar Front, it was not wholly inundated by polar waters as icebergs could not survive in locations any further south. The lack of a statistically significant change in NAR (and hence productivity) between glacial intervals and the LIG, as well as the absence of major changes in the demographic composition of preserved coccoliths, suggests that IODP Site U1313 remained influenced by the North Atlantic Current, within the NATW region, throughout the studied interval.

However, this study only considered samples from IODP Hole U1313A within the interval 45–149 ka. The lack of availability of samples younger than 45 ka imposes a significant limitation on characterising the whole LGP, particularly as the late LGP includes the Last Glacial Maximum (LGM). Other studies indicate that the late LGP is characterised by more prolonged intervals of low summer SST than the early LGP (Stein *et al.*, 2009; Naafs *et al.*, 2013) and significantly altered oceanographic conditions. A recent study of late LGP–Holocene coccolithophores from IODP Site U1313 suggests that this site was bathed by subpolar waters during the LGM and that this coincided with elevated coccolithophore productivity, as reconstructed with NAR (Argenio *et al.*, 2024).

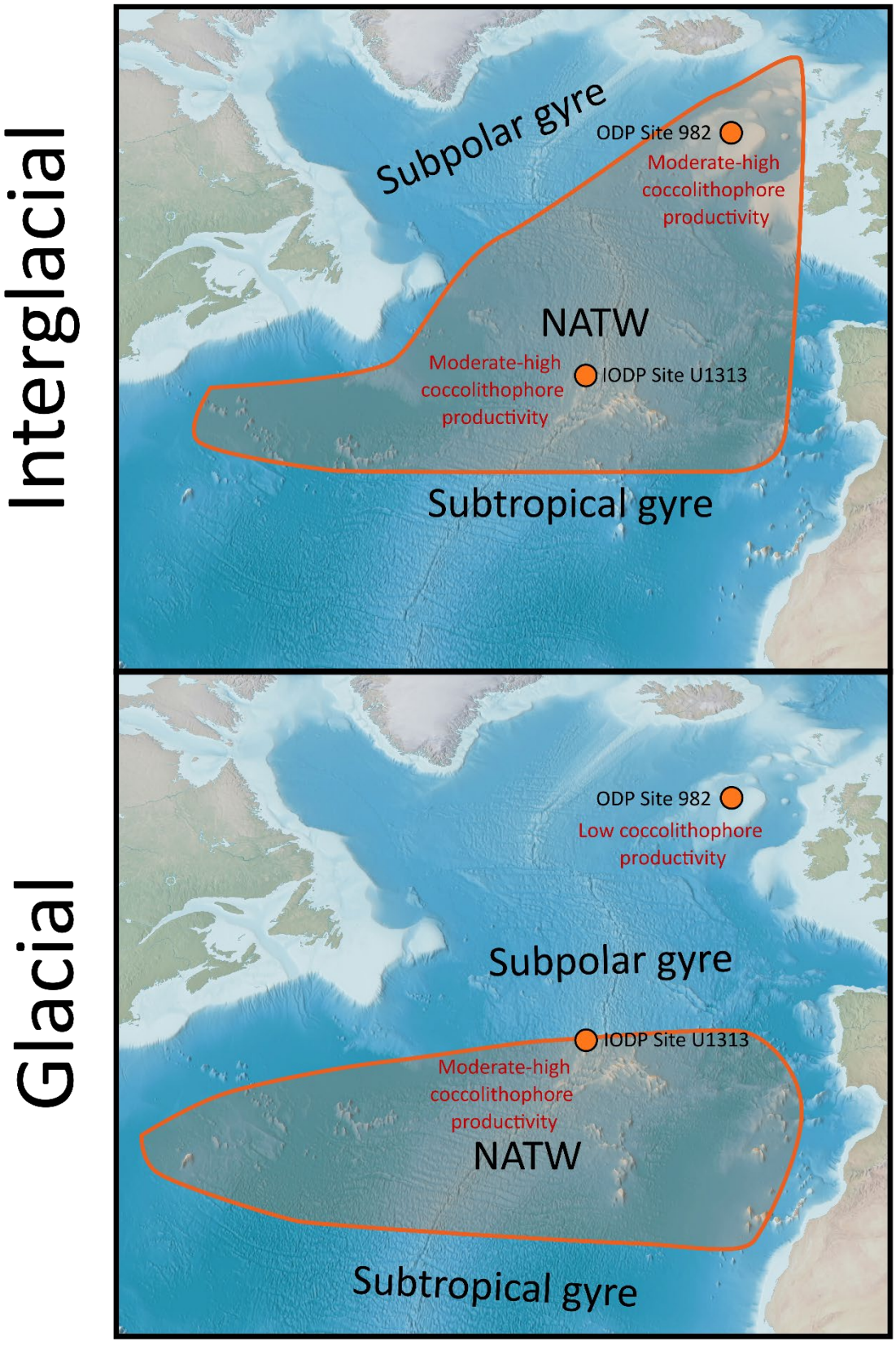

Figure 2.17 – Simplified schematic maps of the approximate migration of the subpolar and subtropical gyres and NATW between interglacial intervals (top; modern and LIG) and glacial intervals (bottom; LGP and PGP) and coccolithophore productivity implied by this work.

2.5. Conclusion

Coccolithophores are significant primary producers in the mid-latitude pelagic ocean and their accumulation rate in sediment can be used to reconstruct their productivity over time. Automated methods for calculating abundances proved unreliable, and so I reconstructed taxonomic and abundance data using a mixture of automated and manual methods. Coccolithophore productivity was significantly higher at the temperate IODP Site U1313 compared to the subpolar ODP Site 982 throughout the past 200 ka, and *Gephyrocapsa* spp. dominated assemblages at both sites. Productivity at ODP Site 982 was higher during the Last Interglacial than adjacent glacial intervals, likely due to a reduction in the relative contribution of coccolithophores to overall primary production in polar water masses. In contrast, productivity at IODP Site U1313 did not change significantly between glacial and interglacial intervals, suggesting that oceanographic conditions did not change drastically between glacial and interglacial intervals in this region of the midlatitude North Atlantic during the studied interval.

Acknowledgements

I am grateful to Luc Beaufort and Camille Godbillot at CEREGE for allowing me to use SYRACO for initial data collection. Enlightening conversations with Jeremy Young, Tom Dunkley-Jones, and Odysseus Archontikis were invaluable in aiding the interpretation of taxonomic outputs. Alba Gonzalez-Lanchas kindly gave up her time to teach me manual settling and counting methods, as well as offering useful advice on the final manuscript.

Appendix

Table 2.A1 – List of samples analysed using SEM and their % *F. profunda* determined by SYRACO.

Core	Sample number	SYRACO % *F. profunda*
982B	20	40.6
982B	21	8.2
982B	39	4.5
982B	N1	7.9
982B	N8	75.6
U1313A	12	24.3
U1313A	26	95.5
U1313A	31	9.1
U1313A	33	66.3

Table 2.A2 – Mean relative abundances of coccolith taxa in both sediment cores. Numbers show relative abundance in %.

	Sediment core	
Taxon name	ODP Hole 982B	IODP Hole U1313A
Gephyrocapsa spp.	94.3	92.2
Coccolithus pelagicus subsp. *braarudii*	1.76	1.77
Coccolithus pelagicus subsp. *pelagicus*	0.549	1.05
Syracosphaera spp.	0.980	1.31
Helicosphaera spp.	0.314	0.0834
Calcidisucs leptoporus spp.	1.77	3.47
Other	0.249	0.104

References

Argenio, C. *et al.* (2024) 'Surface water mass dynamics at IODP Site U1313 through Principal Component Analysis: Evidence from coccolith assemblages in the ~25–7 kyr interval', *Palaeogeography, Palaeoclimatology, Palaeoecology*, 635, p. 111960. Available at: https://doi.org/10.1016/J.PALAEO.2023.111960.

Bacon, M.P. (1984) 'Glacial to interglacial changes in carbonate and clay sedimentation in the Atlantic Ocean estimated from 230Th measurements', *Chemical Geology*, 46(2), pp. 97–111. Available at: https://doi.org/10.1016/0009-2541(84)90183-9.

Barbarin, N., Beaufort, L. and Moron, J.-M. (2014) 'Automatic recognition system of Cenozoic calcareous nannofossils by dynamical neural networks, statistical classification and shape pattern recognition', in *LA RECONNAISSANCE AUTOMATISÉE DES NANNOFOSSILES CALCAIRES DU CÉNOZOÏQUE*. UNIVERSITÉ D'AIX-MARSEILLE, pp. 118–143.

Baumann, K.-H. *et al.* (2005) 'The significance of extant coccolithophores as indicators of ocean water masses, surface water temperature, and palaeoproductivity: a review', *Paläontologische Zeitschrift 2005 79:1*, 79(1), pp. 93–112. Available at: https://doi.org/10.1007/BF03021756.

Baumann, K.-H. and Huber, R. (1999) 'Sea-surface gradients between the North Atlantic and the Norwegian Sea during the last 3.1 m.y.: comparison of Sites 982 and 985', in *Proceedings of the Ocean Drilling Program, 162 Scientific Results*. Ocean Drilling Program, pp. 179–190. Available at: https://doi.org/10.2973/odp.proc.sr.162.014.1999.

Beaufort, L. (1991) 'Adaptation of the random settling method for quantitative studies of calcareous nannofossils', *Micropaleontology*, 37(4), pp. 415–418. Available at: https://doi.org/10.2307/1485914.

Beaufort, L. *et al.* (1997) 'Insolation cycles as a major control of equatorial Indian Ocean primary production', *Science*, 278(5342), pp. 1451–1454. Available at: https://doi.org/10.1126/SCIENCE.278.5342.1451/ASSET/8516FEAD-C31B-4CC0-A1D6-A962642A06FC/ASSETS/GRAPHIC/SE4876016004.JPEG.

Beaufort, L. and Dollfus, D. (2004) 'Automatic recognition of coccoliths by dynamical neural networks', *Marine Micropaleontology*, 51(1–2), pp. 57–73. Available at: https://doi.org/10.1016/j.marmicro.2003.09.003.

Behrenfeld, M.J. *et al.* (2013) 'Annual cycles of ecological disturbance and recovery underlying the subarctic Atlantic spring plankton bloom', *Global Biogeochemical Cycles*, 27(2), pp. 526–540. Available at: https://doi.org/10.1002/gbc.20050.

Behrenfeld, M.J. (2014) 'Climate-mediated dance of the plankton', *Nature Climate Change*, 4(10), pp. 880–887. Available at: https://doi.org/10.1038/nclimate2349.

Bendif, E.M. *et al.* (2019) 'Repeated species radiations in the recent evolution of the key marine phytoplankton lineage Gephyrocapsa', *Nature Communications 2019 10:1*, 10(1), pp. 1–9. Available at: https://doi.org/10.1038/s41467-019-12169-7.

Boeckel, B. and Baumann, K.H. (2004) 'Distribution of coccoliths in surface sediments of the south-eastern South Atlantic Ocean: ecology, preservation and carbonate contribution', *Marine Micropaleontology*, 51(3–4), pp. 301–320. Available at: https://doi.org/10.1016/J.MARMICRO.2004.01.001.

Bolaños, L.M. *et al.* (2020) 'Small phytoplankton dominate western North Atlantic biomass', *The ISME Journal*, 14(7), pp. 1663–1674. Available at: https://doi.org/10.1038/S41396-020-0636-0.

Bolton, C.T. *et al.* (2010) 'Glacial–interglacial productivity changes recorded by alkenones and microfossils in late Pliocene eastern equatorial Pacific and Atlantic upwelling zones', *Earth and Planetary Science Letters*, 295(3–4), pp. 401–411. Available at: https://doi.org/10.1016/j.epsl.2010.04.014.

Bolton, C.T. *et al.* (2011) 'Biotic and geochemical evidence for a global latitudinal shift in ocean biogeochemistry and export productivity during the late Pliocene', *Earth and Planetary Science Letters*, 308(1–2), pp. 200–210. Available at: https://doi.org/10.1016/j.epsl.2011.05.046.

Bolton, C.T. *et al.* (2018) 'North Atlantic Midlatitude Surface-Circulation Changes Through the Plio-Pleistocene Intensification of Northern Hemisphere Glaciation', *Paleoceanography and Paleoclimatology*, 33(11), pp. 1186–1205. Available at: https://doi.org/10.1029/2018PA003412.

Broecker, W. and Clark, E. (2009) 'Ratio of coccolith CaCO3 to foraminifera CaCO3 in late Holocene deep sea sediments', *Paleoceanography*, 24(3). Available at: https://doi.org/10.1029/2009PA001731.

Broecker, W.S. (1982) 'Glacial to interglacial changes in ocean chemistry', *Progress in Oceanography*, 11(2), pp. 151–197. Available at: https://doi.org/10.1016/0079-6611(82)90007-6.

Broerse, A.T.C. *et al.* (2000) 'Coccolithophore export production, species composition, and coccolith-CaCO3 fluxes in the NE Atlantic (34°N21°W and 48°N21°W)', *Deep Sea Research Part II: Topical Studies in Oceanography*, 47(9–11), pp. 1877–1905. Available at: https://doi.org/10.1016/S0967-0645(00)00010-2.

Cauquoin, A. *et al.* (2023) 'Effects of Last Glacial Maximum (LGM) sea surface temperature and sea ice extent on the isotope-temperature slope at polar ice core sites', *Climate of the Past*, 19(6), pp. 1275–1294. Available at: https://doi.org/10.5194/CP-19-1275-2023.

Cavaleiro, C. *et al.* (2018) 'Insolation forcing of coccolithophore productivity in the North Atlantic during the Middle Pleistocene', *Quaternary Science Reviews*, 191, pp. 318–336. Available at: https://doi.org/10.1016/j.quascirev.2018.05.027.

Cermeño, P. *et al.* (2011) 'Competitive dynamics in two species of marine phytoplankton under non-equilibrium conditions', *Marine Ecology Progress Series*, 429, pp. 19–28. Available at: https://doi.org/10.3354/MEPS09088.

Chien, C. Te *et al.* (2016) 'Effects of African dust deposition on phytoplankton in the western tropical Atlantic Ocean off Barbados', *Global Biogeochemical Cycles*, 30(5), pp. 716–734. Available at: https://doi.org/10.1002/2015GB005334.

Coello-Camba, A. and Agustí, S. (2017) 'Thermal thresholds of phytoplankton growth in polar waters and their consequences for a warming polar ocean', *Frontiers in Marine Science*, 4(JUN), p. 224519. Available at: https://doi.org/10.3389/FMARS.2017.00168/BIBTEX.

Davison, P.C. *et al.* (2013) 'Carbon export mediated by mesopelagic fishes in the northeast Pacific Ocean', *Progress in Oceanography*, 116, pp. 14–30. Available at: https://doi.org/10.1016/J.POCEAN.2013.05.013.

Dittert, N. *et al.* (1999) 'Carbonate Dissolution in the Deep-Sea: Methods, Quantification and Paleoceanographic Application', *Use of Proxies in Paleoceanography*, pp. 255–284. Available at: https://doi.org/10.1007/978-3-642-58646-0_10.

Duncan, B. *et al.* (2016) 'Interglacial/glacial changes in coccolith-rich deposition in the SW Pacific Ocean: An analogue for a warmer world?', *Global and Planetary Change*, 144, pp. 252–262. Available at: https://doi.org/10.1016/j.gloplacha.2016.08.001.

Dutkiewicz, A. *et al.* (2015) 'Census of seafloor sediments in the world's ocean', *Geology*, 43(9), pp. 795–798. Available at: https://doi.org/10.1130/G36883.1.

Emanuele, D. *et al.* (2015) 'Sea-surface dynamics and palaeoenvironmental changes in the North Atlantic Ocean (IODP Site U1313) during Marine Isotope Stage 19 inferred from coccolithophore assemblages', *Palaeogeography, Palaeoclimatology, Palaeoecology*, 430, pp. 104–117. Available at: https://doi.org/10.1016/j.palaeo.2015.04.014.

Expedition 306 Scientists (2006) 'Site U1313', in *Proceedings of the IODP, 303/306*. Integrated Ocean Drilling Program. Available at: https://doi.org/10.2204/iodp.proc.303306.112.2006.

Filatov, D.A. *et al.* (2021) 'The mode of speciation during a recent radiation in open-ocean phytoplankton', *Current Biology*, 31(24), pp. 5439-5449.e5. Available at: https://doi.org/10.1016/J.CUB.2021.09.073.

Flores, J.A. and Sierro, F.J. (1997) 'Revised Technique for Calculation of Calcareous Nannofossil Accumulation Rates', *Micropaleontology*, 43(3), p. 321. Available at: https://doi.org/10.2307/1485832.

Fratantoni, D.M. (2001) 'North Atlantic surface circulation during the 1990's observed with satellite-tracked drifters', *Journal of Geophysical Research: Oceans*, 106(C10), pp. 22067–22093. Available at: https://doi.org/10.1029/2000JC000730.

Gardner, J. V. (1975) 'LATE PLEISTOCENE CARBONATE DISSOLUTION CYCLES IN THE EASTERN EQUATORIAL ATLANTIC'.

Gasol, J.M., Del Giorgio, P.A. and Duarte, C.M. (1997) 'Biomass distribution in marine planktonic communities', *Limnology and Oceanography*, 42(6), pp. 1353–1363. Available at: https://doi.org/10.4319/lo.1997.42.6.1353.

Gibbs, S.J. *et al.* (2016) 'Ocean warming, not acidification, controlled coccolithophore response during past greenhouse climate change', *Geology*, 44(1), pp. 59–62. Available at: https://doi.org/10.1130/G37273.1.

González-Lanchas, A. *et al.* (2020) 'A new perspective of the Alboran Upwelling System reconstruction during the Marine Isotope Stage 11: A high-resolution coccolithophore record', *Quaternary Science Reviews*, 245, p. 106520. Available at: https://doi.org/10.1016/J.QUASCIREV.2020.106520.

Guerreiro, C. V. *et al.* (2023) 'Response of coccolithophore communities to oceanographic and atmospheric processes across the North- and Equatorial Atlantic', *Frontiers in Marine Science*, 10, p. 1119488. Available at: https://doi.org/10.3389/FMARS.2023.1119488/BIBTEX.

Hagino, K. and Young, J.R. (2015) 'Biology and paleontology of coccolithophores (Haptophytes)', *Marine Protists: Diversity and Dynamics*, pp. 311–330. Available at: https://doi.org/10.1007/978-4-431-55130-0_12/FIGURES/5.

Herbert, T.D. *et al.* (2016) 'Late Miocene global cooling and the rise of modern ecosystems', *Nature Geoscience*, 9(11), pp. 843–847. Available at: https://doi.org/10.1038/ngeo2813.

Hernández-Almeida, I. *et al.* (2019) 'A dataset of modern and fossil distribution of coccolithophore species Florisphaera profunda in the world's ocean', *Data in Brief*, 22, pp. 826–829. Available at: https://doi.org/10.1016/J.DIB.2018.12.079.

Jonkers, L. *et al.* (2024) 'ForCenS-LGM: a dataset of planktonic foraminifera species assemblage composition for the Last Glacial Maximum', *Scientific Data*, 11(1), p. 361. Available at: https://doi.org/10.1038/s41597-024-03166-7.

Jordan, R.W. (2009) 'Coccolithophores', in *Encyclopedia of Microbiology*. Elsevier, pp. 593–605. Available at: https://doi.org/10.1016/B978-012373944-5.00249-2.

Krauss, W. (1986) 'The North Atlantic Current', *Journal of Geophysical Research: Oceans*, 91(C4), pp. 5061–5074. Available at: https://doi.org/10.1029/JC091IC04P05061.

Kucera, M. *et al.* (2005) 'Reconstruction of sea-surface temperatures from assemblages of planktonic foraminifera: multi-technique approach based on geographically constrained calibration data sets and its application to glacial Atlantic and Pacific Oceans', *Quaternary Science Reviews*, 24(7–9), pp. 951–998. Available at: https://doi.org/10.1016/j.quascirev.2004.07.014.

Laber, C.P. *et al.* (2018) 'Coccolithovirus facilitation of carbon export in the North Atlantic', *Nature Microbiology*, 3(5), pp. 537–547. Available at: https://doi.org/10.1038/s41564-018-0128-4.

Lang, D.C. *et al.* (2016) 'Incursions of southern-sourced water into the deep North Atlantic during late Pliocene glacial intensification', *Nature Geoscience*, 9(5), pp. 375–379. Available at: https://doi.org/10.1038/ngeo2688.

Lawrence, K.T. *et al.* (2009) 'High-amplitude variations in North Atlantic sea surface temperature during the early Pliocene warm period', *Paleoceanography*, 24(2), p. n/a-n/a. Available at: https://doi.org/10.1029/2008PA001669.

Lebreiro, S.M. *et al.* (1997) 'Productivity and paleoceanographic implications on the Tore Seamount (Iberian Margin) during the last 225 kyr: Foraminiferal evidence', *Paleoceanography*, 12(5), pp. 718–727. Available at: https://doi.org/10.1029/97PA01748.

Li, S. *et al.* (2024) 'Multifaceted Contributions of Coccolithophores to Ocean Carbon Export', *Ocean-Land-Atmosphere Research* [Preprint]. Available at: https://doi.org/10.34133/OLAR.0049.

Lombard, F. *et al.* (2019) 'Globally Consistent Quantitative Observations of Planktonic Ecosystems', *Frontiers in Marine Science*, 6(MAR). Available at: https://doi.org/10.3389/fmars.2019.00196.

Mann, H.B. and Whitney, D.R. (1947) 'On a Test of Whether one of Two Random Variables is Stochastically Larger than the Other', *https://doi.org/10.1214/aoms/1177730491*, 18(1), pp. 50–60. Available at: https://doi.org/10.1214/AOMS/1177730491.

Marañón, E. *et al.* (2001) 'Patterns of phytoplankton size structure and productivity in contrasting open-ocean environments', *Marine Ecology Progress Series*, 216, pp. 43–56. Available at: https://doi.org/10.3354/MEPS216043.

Marino, M. *et al.* (2014) 'Coccolithophores as proxy of seawater changes at orbital-to-millennial scale during middle Pleistocene Marine Isotope Stages 14-9 in North Atlantic core MD01-2446', *Paleoceanography*, 29(6), pp. 518–532. Available at: https://doi.org/10.1002/2013PA002574.

Marino, M. *et al.* (2022) 'Paleoproductivity proxies and alkenone precursors in the Western Mediterranean during the Early-Middle Pleistocene transition', *Palaeogeography, Palaeoclimatology, Palaeoecology*, 601, p. 111104. Available at: https://doi.org/10.1016/J.PALAEO.2022.111104.

Marshall, N.R. *et al.* (2021) 'Carbonate dissolution and environmental parameters govern coccolith vs. alkenone abundances in surface sediments from the northwest North Atlantic', *Marine Micropaleontology*, 169, p. 102032. Available at: https://doi.org/10.1016/j.marmicro.2021.102032.

McIntyre, A., Ruddiman, W.F. and Jantzen, R. (1972) 'Southward penetrations of the North Atlantic polar front: faunal and floral evidence of large-scale surface water mass movements over the last 225,000 years', *Deep Sea Research and Oceanographic Abstracts*, 19(1), pp. 61–77. Available at: https://doi.org/10.1016/0011-7471(72)90073-3.

Mouriño-Carballido, B. and Neuer, S. (2008) 'Regional Differences in the Role of Eddy Pumping in the North Atlantic Subtropical Gyre', *Source: Oceanography*, 21(2), pp. 52–61. Available at: https://doi.org/10.2307/24805610.

Naafs, B.D.A. *et al.* (2010) 'Late Pliocene changes in the North Atlantic Current', *Earth and Planetary Science Letters*, 298(3–4), pp. 434–442. Available at: https://doi.org/10.1016/j.epsl.2010.08.023.

Naafs, B.D.A. *et al.* (2012) 'Strengthening of North American dust sources during the late Pliocene (2.7 Ma)', *Earth and Planetary Science Letters*, 317–318, pp. 8–19. Available at: https://doi.org/10.1016/j.epsl.2011.11.026.

Naafs, B.D.A. *et al.* (2013) 'Warming of surface waters in the mid-latitude North Atlantic during Heinrich events', *Paleoceanography*, 28(1), pp. 153–163. Available at: https://doi.org/10.1029/2012PA002354.

Naafs, B.D.A., Hefter, J. and Stein, R. (2013) 'Millennial-scale ice rafting events and Hudson Strait Heinrich(-like) Events during the late Pliocene and Pleistocene: a review', *Quaternary Science Reviews*, 80, pp. 1–28. Available at: https://doi.org/10.1016/J.QUASCIREV.2013.08.014.

Narciso, A., Cachão, M. and De Abreu, L. (2006) 'Coccolithus pelagicus subsp. pelagicus versus Coccolithus pelagicus subsp. braarudii (Coccolithophore, Haptophyta): A proxy for surface subarctic Atlantic waters off Iberia during the last 200 kyr', *Marine Micropaleontology*, 59(1), pp. 15–34. Available at: https://doi.org/10.1016/J.MARMICRO.2005.12.001.

Nave, S. *et al.* (2010) 'Open oceanic productivity changes at mid-latitudes during interglacials and its relation to the Atlantic Meridional Overturning Circulation', *Geophysical Research Abstracts*, 12, pp. 2010–14696.

Nelson, D.M. *et al.* (1995) 'Production and dissolution of biogenic silica in the ocean: Revised global estimates, comparison with regional data and relationship to biogenic sedimentation', *Global Biogeochemical Cycles*, 9(3), pp. 359–372. Available at: https://doi.org/10.1029/95GB01070.

Nissen, C. *et al.* (2018) 'Factors controlling coccolithophore biogeography in the Southern Ocean', *Biogeosciences*, 15(22), pp. 6997–7024. Available at: https://doi.org/10.5194/BG-15-6997-2018.

Pedro, J.B. *et al.* (2022) 'Dansgaard-Oeschger and Heinrich event temperature anomalies in the North Atlantic set by sea ice, frontal position and thermocline structure', *Quaternary Science Reviews*, 289, p. 107599. Available at: https://doi.org/10.1016/J.QUASCIREV.2022.107599.

Phillips, M.P. and Harwood, D.M. (2017) 'Marine diatom assemblage variation across Pleistocene glacial-interglacial transitions from Integrated Ocean Drilling Program Site C9001, Northwest Pacific', *Palaeogeography, Palaeoclimatology, Palaeoecology*, 483, pp. 172–187. Available at: https://doi.org/10.1016/J.PALAEO.2016.07.040.

Poulton, A.J. *et al.* (2006) 'Phytoplankton mineralization in the tropical and subtropical Atlantic Ocean', *Global Biogeochemical Cycles*, 20(4). Available at: https://doi.org/10.1029/2006GB002712.

Poulton, A.J. *et al.* (2007) 'Relating coccolithophore calcification rates to phytoplankton community dynamics: Regional differences and implications for carbon export', *Deep Sea Research Part II: Topical Studies in Oceanography*, 54(5–7), pp. 538–557. Available at: https://doi.org/10.1016/J.DSR2.2006.12.003.

Poulton, A.J. *et al.* (2013) 'The 2008 Emiliania huxleyi bloom along the Patagonian Shelf: Ecology, biogeochemistry, and cellular calcification', *Global Biogeochemical Cycles*, 27(4), pp. 1023–1033. Available at: https://doi.org/10.1002/2013GB004641.

Poulton, A.J. *et al.* (2017) 'Coccolithophore ecology in the tropical and subtropical Atlantic Ocean: New perspectives from the Atlantic meridional transect (AMT) programme', *Progress in Oceanography*, 158, pp. 150–170. Available at: https://doi.org/10.1016/j.pocean.2017.01.003.

Prista, G., Narciso, A. and Cachao, M. (2020) 'Coccolithus pelagicus subsp. braarudii morphological plasticity as a response to variations in the upwelling regime of the west coast of Iberia', *Micropaleontology*, 66(6), pp. 549–571. Available at: https://doi.org/10.47894/mpal.66.6.06.

Prospero, J.M. (1996) 'Saharan Dust Transport Over the North Atlantic Ocean and Mediterranean: An Overview', in, pp. 133–151. Available at: https://doi.org/10.1007/978-94-017-3354-0_13.

Raja, M. and Rosell-Melé, A. (2021) 'Appraisal of sedimentary alkenones for the quantitative reconstruction of phytoplankton biomass', *Proceedings of the National Academy of Sciences*, 118(2). Available at: https://doi.org/10.1073/PNAS.2014787118.

Rost, B. and Riebesell, U. (2004) 'Coccolithophores and the biological pump: responses to environmental changes', *Coccolithophores*, pp. 99–125. Available at: https://doi.org/10.1007/978-3-662-06278-4_5.

Rousseaux, C. and Gregg, W. (2013) 'Interannual Variation in Phytoplankton Primary Production at A Global Scale', *Remote Sensing*, 6(1), pp. 1–19. Available at: https://doi.org/10.3390/rs6010001.

Schmidt, K. *et al.* (2014) 'Not all calcite ballast is created equal: Differing effects of foraminiferan and coccolith calcite on the formation and sinking of aggregates', *Biogeosciences*, 11(1), pp. 135–145. Available at: https://doi.org/10.5194/BG-11-135-2014.

Schoepfer, S.D. *et al.* (2015) 'Total organic carbon, organic phosphorus, and biogenic barium fluxes as proxies for paleomarine productivity', *Earth-Science Reviews*, 149, pp. 23–52. Available at: https://doi.org/10.1016/j.earscirev.2014.08.017.

Schwab, C. *et al.* (2012) 'Coccolithophore paleoproductivity and ecology response to deglacial and Holocene changes in the Azores Current System', *Paleoceanography*, 27(3). Available at: https://doi.org/10.1029/2012PA002281.

Shipboard Scientific Party (1996) 'Site 982', in *Proceedings of the Ocean Drilling Program, 162 Initial Reports*. Ocean Drilling Program, pp. 91–138. Available at: https://doi.org/10.2973/odp.proc.ir.162.104.1996.

Smith, M.E. *et al.* (2013) 'Data report: oxygen isotopes and foraminifer abundance record for the last glacial-interglacial cycle and marine isotope Stage 6 at IODP Site U1313', in, pp. 1–11. Available at: https://doi.org/10.2204/iodp.proc.303306.216.2013.

Sosdian, S.M., Rosenthal, Y. and Toggweiler, J.R. (2018) 'Deep Atlantic Carbonate Ion and CaCO3 Compensation During the Ice Ages', *Paleoceanography and Paleoclimatology*, 33(6), pp. 546–562. Available at: https://doi.org/10.1029/2017PA003312.

Sprengel, C. *et al.* (2002) 'Modern coccolithophore and carbonate sedimentation along a productivity gradient in the Canary Islands region: seasonal export production and surface accumulation rates',

Deep Sea Research Part II: Topical Studies in Oceanography, 49(17), pp. 3577–3598. Available at: https://doi.org/10.1016/S0967-0645(02)00099-1.

Stanley, S.M., Ries, J.B. and Hardie, L.A. (2005) 'Seawater chemistry, coccolithophore population growth, and the origin of Cretaceous chalk', *Geology*, 33(7), p. 593. Available at: https://doi.org/10.1130/G21405.1.

Stein, R. *et al.* (2009) 'Variability of surface water characteristics and Heinrich-like events in the Pleistocene midlatitude North Atlantic Ocean: Biomarker and XRD records from IODP Site U1313 (MIS 16-9)', *Paleoceanography*, 24(2), p. n/a-n/a. Available at: https://doi.org/10.1029/2008PA001639.

Tilstone, G.H. *et al.* (2017) 'Micro-phytoplankton photosynthesis, primary production and potential export production in the Atlantic Ocean', *Progress in Oceanography*, 158, pp. 109–129. Available at: https://doi.org/10.1016/J.POCEAN.2017.01.006.

Tréguer, P.J. and De La Rocha, C.L. (2013) 'The World Ocean Silica Cycle', *Annual Review of Marine Science*, 5(1), pp. 477–501. Available at: https://doi.org/10.1146/annurev-marine-121211-172346.

Turner, J. (2002) 'Zooplankton fecal pellets, marine snow and sinking phytoplankton blooms', *Aquatic Microbial Ecology*, 27(1), pp. 57–102. Available at: https://doi.org/10.3354/ame027057.

Venz, K.A. *et al.* (1999) 'A 1.0 Myr Record of Glacial North Atlantic Intermediate Water Variability from ODP Site 982 in the Northeast Atlantic', *Paleoceanography*, 14(1), pp. 42–52. Available at: https://doi.org/10.1029/1998PA900013.

Villanueva, J. *et al.* (2001) 'A latitudinal productivity band in the Central North Atlantic over the last 270 kyr: An alkelone perspective', *Paleoceanography*, 16(6), pp. 617–626. Available at: https://doi.org/10.1029/2000PA000543.

Wang, J., Zeng, C. and Feng, Y. (2024) 'Meta-analysis reveals responses of coccolithophores and diatoms to warming', *Marine Environmental Research*, 193, p. 106275. Available at: https://doi.org/10.1016/J.MARENVRES.2023.106275.

Warnock, J.P. and Scherer, R.P. (2014) 'A revised method for determining the absolute abundance of diatoms', *Journal of Paleolimnology*, 53(1), pp. 157–163. Available at: https://doi.org/10.1007/s10933-014-9808-0.

Williams, R.H. *et al.* (2016) 'Glacial to Holocene changes in trans-Atlantic Saharan dust transport and dust-climate feedbacks', *Science Advances*, 2(11). Available at: https://doi.org/10.1126/SCIADV.1600445/SUPPL_FILE/1600445_SM.PDF.

Woosley, R.J. (2016) 'Carbonate Compensation Depth', in W.M. White (ed.) *Encyclopedia of Geochemistry*, pp. 1–2. Available at: https://doi.org/10.1007/978-3-319-39193-9_85-1.

Young, J.R. *et al.* (2003) 'A guide to extant coccolithophore taxonomy.', *Journal of Nannoplankton Research*, S1, pp. 1–132. Available at: https://doi.org/10.58998/jnr2297.

Young, J.R., Bown, P.R. and Lees, J.A. (2022) *Nannotax3 website*. Available at: www.mikrotax.org/Nannotax3 (Accessed: 11 March 2024).

Chapter 3: Distinct changes in temperate and subpolar North Atlantic export production triggered by glacial-interglacial climate change over the past 200 ka.

Abstract

Organic carbon export by the biological pump is an important mechanism for transporting carbon from ocean-atmosphere equilibrium into the deep ocean. Changes in the strength of the biological pump have the potential to significantly alter global climate on geological timescales, as well as exerting controls on the nutrient flux to the deep ocean. Excess barium (Ba_{XS}) accumulates in sinking organic matter and can be used as a proxy for past organic carbon export. Using two North Atlantic sediment cores, I use Ba_{XS} to test for changes in export production in the subpolar and temperate ocean regions over the past 200 ka. Allogenic detrital inputs to the North Atlantic from iceberg rafting and aeolian dust were substantially higher during glacial intervals than interglacial intervals. Export production was almost always greater in the temperate than the subpolar North Atlantic, except at the start of the Last Interglacial. In the subpolar ocean, carbon export increased rapidly over the last two glacial-interglacial transitions but remained low throughout the Last and Penultimate Glacial Periods. In contrast, the temperate North Atlantic saw strongest export production during the transition from the Last Interglacial to the Last Glacial Period, coinciding with major increases in aeolian dust flux from North America. Over the past two glacial-interglacial cycles, allogenic nutrient influx played a more quantitatively significant role than changes to ocean stratification and/or ice cover in controlling carbon export, potentially supporting the idea that a stronger biological pump contributed to lowering of atmospheric carbon dioxide concentrations between interglacial intervals and glacial intervals.

Chapter contents

3.1. Introduction

In this chapter I reconstruct the history of late Pleistocene temperate and subpolar carbon export using the barium excess (Ba_{XS}) proxy in North Atlantic sediment cores ODP Hole 982B and IODP Hole U1313A.

Export production is the portion of marine primary production that exits the mixed layer of the ocean and reaches mesopelagic depths (Lampitt *et al.*, 2010; Henson, Sanders and Madsen, 2012; Nowicki, DeVries and Siegel, 2022). Export production is an important component of the carbon cycle, as exported organic carbon is isolated from the atmosphere on the timescale of years-to-centuries (Passow and Carlson, 2012; Iversen, 2023). Changes in global export production therefore have the potential to modify the atmospheric inventory of carbon dioxide and thus impact global climate (Martin, 1990; Martínez-García *et al.*, 2014; Yu *et al.*, 2019) This process was described in Chapter 1.

The biological carbon pump is the primary means of exporting organic carbon from the shallow ocean to depth. It consists of several components, including faecal pellets (Turner, 2002; Frangoulis *et al.*, 2011), organic aggregates (Guidi *et al.*, 2009; Schmidt *et al.*, 2014), and diel vertical migration (DVM; Davison et al., 2013; Archibald, Siegel and Doney, 2019; Saba et al., 2021). The relative importance of different export mechanisms varies substantially in both time and space in the modern global ocean (e.g. Murray et al., 2000; Guidi et al., 2009; Henson, Sanders and Madsen, 2012; Siegel et al., 2014; Fu, Randerson and Moore, 2016; Nowicki, DeVries and Siegel, 2022; Iversen, 2023).

In the North Atlantic, both the quantity and proportion of total primary production that is exported to depth is, on average, highest in the mid-latitudes, intermediate in subpolar regions, and lowest in the subtropics (Henson, Sanders and Madsen, 2012; Siegel *et al.*, 2014; Nowicki, DeVries and Siegel, 2022). Permanent subtropical water column stratification in the subtropics limits the mixing of nutrients into the photic zone and presents a physical barrier to organic particle export (Mouriño-Carballido and Neuer, 2008; Sigman and Hain, 2012; Webb, 2021). In contrast, intermediate and subpolar latitudes are characterised by a seasonally oscillating mixed layer depth allowing the resupply of limiting nutrients to the surface ocean and leading to phytoplankton blooms and coincident increases in organic carbon export (Sigman and Hain, 2012; Webb, 2021). The temperate North Atlantic additionally experiences strong physical mixing due to the action of the North Atlantic Current (NAC), which defines North Atlantic Transitional Waters (NATW), and promotes the downwelling of organic matter (Krauss, 1986; Talley *et al.*, 2011). Productivity in the high-latitude ocean can also be constrained by vertical stratification and seasonal light limitation due to both latitude and sea ice cover (Mitchell *et al.*, 1991; Anderson, Jones and Swift, 2003; Randelhoff and Guthrie, 2016; Joy-Warren *et al.*, 2019).

Productive ocean regions, such as upwelling zones, experience seasonal blooms of large heterotrophic phytoplankton, which support shorter, more efficient food webs, enabling greater export through aggregate sinking and DVM by abundant heterotrophs (Smetacek *et al.*, 2012; Davison *et al.*, 2013; Guidi *et al.*, 2016; Iversen, 2023; Li *et al.*, 2024). Recent studies indicate that high mortality from viral infection of blooming heterotrophic phytoplankton may also play an important role in driving export at high latitudes (Laber *et al.*, 2018; Biggs, Huisman and Brussaard, 2021). Climate-driven changes to ocean structure, as well as varying allogenic nutrient supply, can therefore have significant impacts on phytoplankton size and ecosystem structure, which in turn directly modify export production (Gasol, Del Giorgio and Duarte, 1997; Behrenfeld, 2014; Guidi *et al.*, 2016; Iversen, 2023). Modelling indicates

that export ratios (the proportion of primary production that is exported) is greatest in high-latitude North Atlantic, where sinking aggregates and DVM contribute significantly, whereas faecal pellets are the single most important export mechanism in the subtropics (Nowicki, DeVries and Siegel, 2022).

Pleistocene glacial intervals, such as the Last Glacial Period (LGP) and Penultimate Glacial Period (PGP), are characterised by atmospheric carbon dioxide concentrations up to 100 ppmv lower than interglacial intervals, such as the Last Interglacial (LIG; Petit et al., 1999; Sigman and Boyle, 2000). Furthermore, glacial intervals experience reorganised ocean circulation patterns such as the expansion of cold polar waters to mid-latitudes (Rasmussen *et al.*, 2003; Henry *et al.*, 2016; Pöppelmeier *et al.*, 2021; Holmes *et al.*, 2022) and the expansion of large terrestrial ice sheets in regions such as the North Atlantic (Shackleton, 1987; Bond *et al.*, 1993; Kindler *et al.*, 2014). The character and causes of carbon redistribution between glacial and interglacial climates in the Pleistocene remain enigmatic, but the enhanced efficiency of the biological pump during glacial intervals has the potential to play an important role by transferring additional carbon into the deep ocean reservoir (Martin, 1990; Sigman and Boyle, 2000; Martínez-García *et al.*, 2014; Yu *et al.*, 2019). A great amount of effort has been put into quantifying the potential contribution of aeolian dust, which increased significantly during past glacial intervals, to enhanced primary production through the alleviation of nutrient limitation in high-nutrient low-chlorophyl (HNLC) regions (e.g. Maher et al., 2010; Williams et al., 2016; Jacobel et al., 2019; Koffman et al., 2021; Chen et al., 2023; Zan et al., 2023). Reconstructing the Pleistocene carbon pump can help to test this hypothesis as well as improve our understanding of the response of the biological pump to climatic perturbations, such as the present anthropogenic carbon perturbation.

Past export productivity has been reconstructed using numerous sedimentary proxies, such as total organic carbon (e.g. Kuypers et al., 2002; Algeo et al., 2013), opal (e.g. Pattan et al., 2003), and organic phosphorous (e.g. Schenau, Reichart and De Lange, 2005).Where pelagic sediments are well-oxygenated and sulphate is not depleted, the accumulation rate of barium in the mineral barite, $BaSO_4$, is a robust proxy for export production when detrital inputs are low in both the modern (e.g. Eagle et al., 2003) and geological past (Dymond, Suess and Lyle, 1992; Torfstein, Winckler and Tripati, 2010; Liguori, De Almeida and de Rezende, 2016; Bridgestock *et al.*, 2019). The ocean is undersaturated with respect to barite in normal conditions, but barite can precipitate from solution within supersaturated microenvironments in degrading organic matter aggregates in the mesopelagic ocean (Dymond, Suess and Lyle, 1992; Ganeshram *et al.*, 2003). Modern pelagic North Atlantic bottom waters are relatively well-oxygenated (Talley *et al.*, 2011), and sulphate depletion is minimal in shallow sediments that record the late Pleistocene for both ODP Site 982 (Shipboard Scientific Party, 1996) and IODP Site U1313 (Expedition 306 Scientists, 2006), implying high potential for biogenic barium to be a robust reflection of export production throughout this region (Stern, Dellwig and Waniek, 2017).

Non-biogenic sedimentary barium contributions can derive from detrital (fluvial, aeolian and glacial) and hydrothermal sources (Eagle *et al.*, 2003; Paytan and Griffith, 2007). Reliable reconstruction of export production using the barium proxy is challenging where non-biogenic barium contributions to seafloor sediment are quantitatively dominant over biogenic sources, such as marginal sediments, but can still be possible using barium isotopes (e.g. Bridgestock et al., 2018, 2019). The variable contribution of detrital sources of barium ($Ba_{detrital}$) can be accounted for using a normalisation factor or direct measurement of detrital phases in sediment (e.g. Reitz et al., 2004), whilst the remaining barium fraction is referred to as excess barium (Ba_{XS}). Normalisation requires measurement of other detrital elements that covary with detrital barium in source rocks, such as aluminium or titanium

(Dymond, Suess and Lyle, 1992; Eagle *et al.*, 2003; Reitz *et al.*, 2004; Schoepfer *et al.*, 2015; Liguori, De Almeida and de Rezende, 2016). The two study sites in this thesis were both distal from large landmasses throughout the Pleistocene, meaning the major detrital contributions likely came from ice-rafted debris (IRD) and wind-blown dust (Venz *et al.*, 1999; Naafs *et al.*, 2012, 2013), although increased subaerial exposure of the Rockall Plateau did occur during glacial sea level lowstands, raising the possibility of fluvial inputs from Rockall Island, which is presently around 130 km east of ODP Site 982 and has a total exposure of less than 1000 m^2 (Shipboard Scientific Party, 1996; Hitchen, 2004).

In this chapter I will construct a new Ba_{XS} and $Ba_{XS}AR$ record to test the following hypotheses:

- The zone of highest North Atlantic export production moved southwards during glacial intervals due to the southward migration of the NAC and NATW.
- Glacial-interglacial changes in export production were of a higher magnitude in the subpolar North Atlantic than at mid-latitudes due to stronger oceanographic reconfiguration.
- Detrital sedimentary inputs to both sites were higher during glacial intervals relative to interglacial intervals due to increased ice-rafting and higher dust flux.

3.2. Methods

I digested 43 samples from ODP Hole 982B and 32 samples from IODP Hole U1313A, which were then analysed for determination of Ba and Al concentration by mass spectroscopy. All sample processing took place at the Metal Free Labs at the Department of Earth Sciences, University of Oxford, between December 2022 and April 2023.

Prior to processing, samples were dried in a clean oven at 50°C. I homogenised approximately 2 cm^3 sediment using a mortar and pestle in a positive pressure fume hood. The homogenised sample was then transferred to a clean 20 ml glass vial for storage.

I weighed 50–60 mg of homogenised sample in a Teflon vial on a calibrated scale with a precision of 0.01 mg. Additionally, I weighed 50–60 mg of United States Geological Survey Green River Shale (USGS SGR-1) for use as a standard.

Sample digestions were undertaken using a method modified from Bridgestock et al. (2018), which is outlined below.

I applied 63 µL 28M hydrofluoric acid (HF) and 187µL concentrated 16M nitric acid (HNO_3) to dissolve silicates in the samples. I then added a further 2650 µL 16M HNO_3 for a total solution volume of 3000 µL, including 100 µL Milli-Q (MQ) deionised water that was added immediately after weighing to limit static effects. Visual inspection revealed that dark grainy material remained in some samples after the initial application of HF, which is likely to be undissolved silicates. For these samples, which are detailed in Table 3.1, I added an additional 150 µL HF to dissolve this suspected silicate fraction. Application of additional HF led to the dissolution of the dark material in all cases, supporting the hypothesis that they were undissolved silicate. However, the binary application of different HF volumes across samples has the potential to artificially influence final concentration estimates if aluminosilicate phases are not fully dissolved in samples that didn't receive addition HF treatment. This introduces caveats to interpreting these results, which are considered further in the Appendix. Each sample was then heated without its lid to dryness at 85°C. For the USGS SGR-1 standards, which

were expected to contain significantly more silicate material than most samples, I applied an initial 150 µL HF and 2550 µL HNO_3 for a total sample volume of 3000 µL (including 300 µL MQ added post-weighing).

Table 3.1 – Number of samples from glacial intervals and interglacial intervals that required standard (63 µL) or additional (63 + 150 µL) HF to achieve total dissolution of dark material during digestion in both cores.

Interval	HF volume used	Tally (ODP Hole 982B)	Tally (IODP Hole U1313A)
Glacial	63 µL	10	8
	63 + 150 µL	13	4
Interglacial	63 µL	19	18
	63 + 150 µL	1	2

Carbonates were dissolved by the addition of 2 mL 6M hydrochloric acid (HCl), followed by 3 mL HNO_3 to create reverse aqua regia. This solution was then heated to dryness at 120°C. 1.5 mL hydrogen peroxide (H_2O_2) was then added to the residue in 0.5 mL increments to dissolve any remaining organic matter and slowly heated to dryness at 40°C to prevent loss of material through sputtering. Lastly, I added 0.5 mL concentrated HNO3 and 0.5 mL MQ to completely dissolve the sample in solution. If any solid material appeared to still be present at this stage on visual inspection, it was heated to dryness and the hydrogen peroxide step repeated until the sample reached full clarity.

All samples, standards, and blanks were diluted into a 2% HNO_3 solution by the addition of 24 mL MQ immediately prior to analysis.

3.2.1. ICP-MS analysis

Ba and Al concentrations were determined via inductively coupled plasma mass spectrometry (ICP-MS) using a PerkinElmer NexION 350D at the Department of Earth Sciences, University of Oxford in April 2023. All samples, standards, and blank 2% HNO_3 solutions were weighed in 50 mL centrifuge tubes and placed in an ESI prepFAST M5 alongside a preprepared internal Rh standard.

3.2.2. Ba_{XS} calculations

To calculate Ba_{XS} from the raw ICP-MS concentration outputs, the $Ba_{detrital}$ component must be calculated and subtracted, as shown in Equation 3.1.

$$Ba_{bio} = Ba_{XS} = Ba_{total} - Ba_{detrital} \quad \text{(Equation 3.1)}$$

Reitz et al. (2004) found that the regional average Ba/Al ratio of detrital aluminosilicates in equatorial pelagic Atlantic surface sediments is 0.0027, whilst the Ba/Al range measured in all modern terrestrial rocks is 0.005–0.010 (Taylor, 1964; Taylor and McLennan, 1985; Reitz *et al.*, 2004). Modern equatorial detrital material is unlikely to be a perfect analogue for the high- and mid-latitude Pleistocene North Atlantic, particularly if IRD is the dominant detrital phase (Ruddiman, 1977). I therefore use the analytically determined Ba/Al of 0.0027 as the primary value in calculations, but graphically present $Ba_{XS}AR$ values for Ba/Al ratios of 0.0014–0.01 in all figures. The lower bound (0.0014) is the smallest calculated detrital Ba/Al found by Reitz et al. (2004) from any Atlantic site. Changes in the primary source of detrital sediment (i.e. IRD or wind-blown dust) may deviate significantly from the mean

modern Atlantic Ba/Al ratio but are nonetheless likely to remain within these bounds. This is considered further in the discussion. The equation used to calculate Ba_{XS} is shown below:

$$Ba_{XS} = Ba_{total} - (Al_{total} * 0.0027) \quad \text{(Equation 3.2)}$$

It is then possible to calculate the accumulation rate of Ba_{XS} using the same method outlined for Equation 2.2 in the Chapter 2 and shown in Equation 3.3.

$$Ba_{XS}AR = Ba_{XS} * \rho * S \quad \text{(Equation 3.3)}$$

Where ρ is sediment dry bulk density (g cm^{-3}) and S is linear sedimentation rate (cm kyr^{-1}). The unit of Ba_{XS} is ppm (µg g^{-1}), so $Ba_{XS}AR$ values used in this chapter have the unit µg cm^{-2} kyr^{-1}. The methods for generating these values are described in Chapter 2.

3.2.3. Mann-Whitney U tests

I conducted all statistical tests using R version 4.4. I tested for significant differences between the mean NAR values in glacial and interglacial intervals using two-tailed Mann-Whitney U Tests (Mann and Whitney, 1947), as the data were nonparametric.

3.3. Results

3.3.1. Blanks and standards

Blanks contained a mean 1.09 ppm Al and 0.016 ppm Ba, which is less than 0.1% of the mean all-sample concentration measured for either core. This suggests negligible environmental contamination during processing.

Table 3.2 – Al and Ba concentrations for blanks processed in different crushing and digestion batches. Values in parts per million given to 3 decimal places.

	Al (ppm)	Ba (ppm)
Blank A	1.537	0.005
Blank B	0.529	0.015
Blank C	1.206	0.029

3.3.2. Standards

Concentrations of Al in USGS SGR-1 standards ranged between 28100–30800 ppm, which is 7.66-15.8% lower than minimum expected values. Ba concentrations in standards were 247–277 ppm, which is within the expected range for two out of three samples, whilst the third sample was 1% (2.6 ppm) below the minimum expected value.

These results may suggest that there may be a small underestimation of sample Al concentration for intervals where total Al is high. This is considered further in the Appendix**.**

3.3.3. Ba_{XS}

When discussing $Ba_{detrital}$ and Ba_{XS} values, I refer to values calculated using a Ba/Al value of 0.0027, as discussed in the methods, unless explicitly stated otherwise.

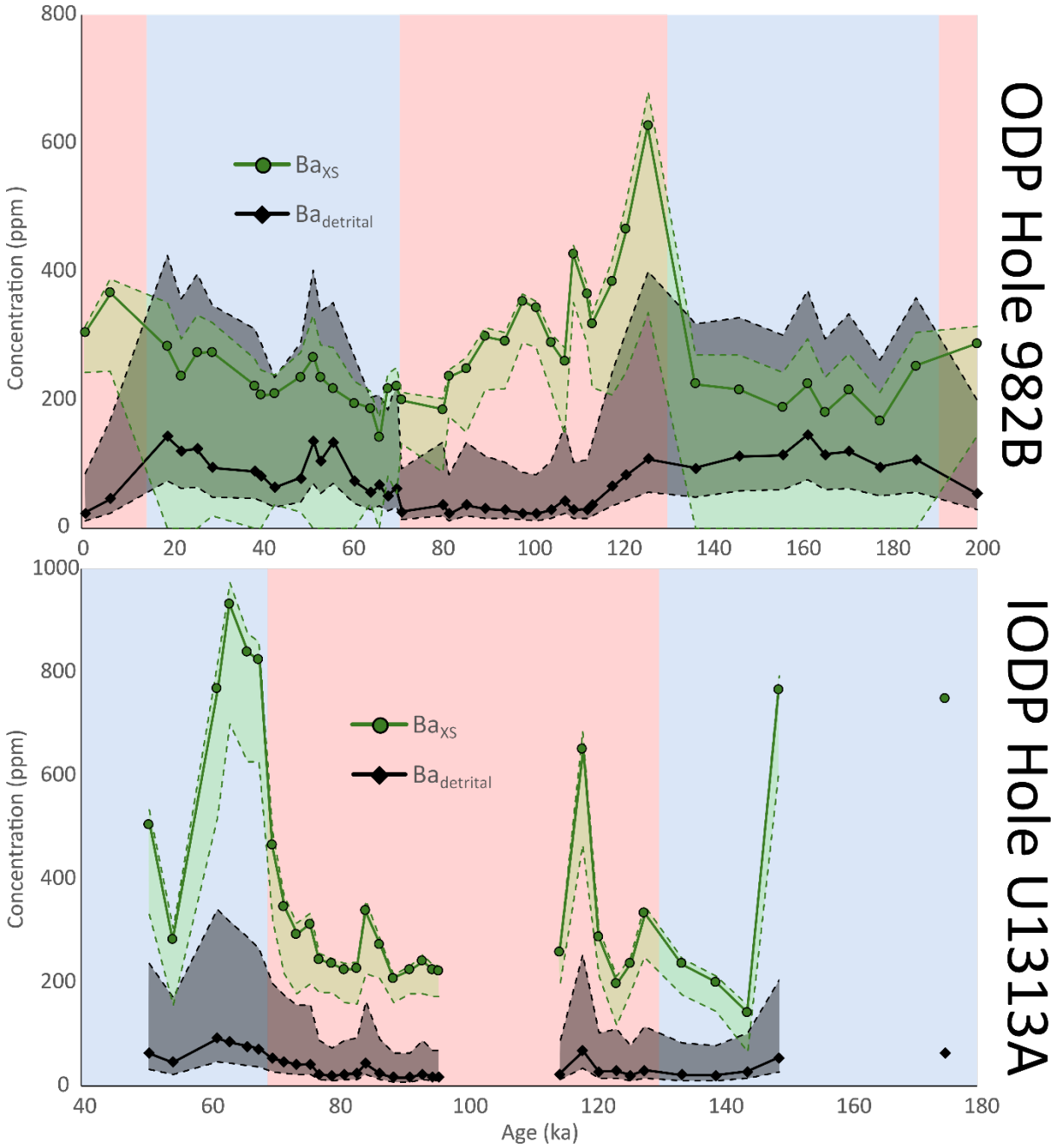

Figure 3.1 – Ba_{XS} (green circles) and $Ba_{detrital}$ (black diamonds) at ODP Hole 982B (top) and IODP Hole U1313A (bottom) over the past 200 ka. The range of plausible values based on detrital Ba/Al (Taylor, 1964; Taylor and McLennan, 1985; Reitz *et al.*, 2004) is shown shaded in the same colour and dashed lines show upper and lower bounds. Glacial intervals (LGP and PGP) are shown with a blue background and interglacial intervals (Holocene, LIG and MIS 7) are shown with a red background. Gaps exceeding 20 kyr between adjacent samples are not shown connected.

Al_{total} at ODP Hole 982B ranged from 8290–54100 ppm with a mean value of 27000 ppm. Mean Al_{total} was higher during glacial intervals (37200 ppm) than interglacial intervals (15300 ppm), shown in Figure 3.3. Ba_{total} ranged from 208–735 ppm, with a mean of 341 ppm. Ba_{XS} ranges from 141–627 ppm,

with a mean of 268 ppm, and there was significantly higher Ba_{XS} during glacial intervals relative to interglacial intervals ($n_{glacial}$=23, $n_{interglacial}$=20, U=63, p=5.03x10^{-5}). $Ba_{detrital}$ has a range of 22–146 ppm and a mean of 73 ppm.

The detrital Ba/Al value chosen for ODP Hole 982B is important as there is a large overlap between plausible Ba_{XS} and $Ba_{detrital}$. Assuming a constant Ba/Al ratio of detrital material across all glacial intervals and interglacial intervals, the maximum possible Ba/Al of this material (that does not lead to a negative Ba_{XS}) is 0.0068. Under this extreme scenario, Ba_{XS} is less than 70 ppm, and lower than $Ba_{detrital}$, in all glacial samples, and Ba_{XS} would be greater than $Ba_{detrital}$ in only 13 out of 20 interglacial samples. In contrast, using a Ba/Al of 0.0027 means that Ba_{XS} is greater than $Ba_{detrital}$ for every sample.

At IODP Hole U1313A, Al_{total} ranged from 6330–34300 ppm with a mean of 14800 ppm, and Ba_{total} was 170–1020 ppm with a mean of 425 ppm. Lower Al_{total} values in this core compared to ODP Hole 982B translate into lower $Ba_{detrital}$, which ranges from 17–93 ppm with a mean of 40 ppm. Ba_{XS} is 143–933 ppm, with a mean of 385 ppm.

Relatively low Al_{total} also produce a comparably small range of hypothetical values of $Ba_{detrital}$ and Ba_{XS} for IODP Hole U1313A, and even if detrital Ba/Al is at its maximum plausible value (0.01), Ba_{XS} would be greater than $Ba_{detrital}$ in 30 out of 32 samples (exceptions at 54 ka and 144 ka).

3.3.4. Ba_{XS}AR

Conversion of Ba_{XS} to accumulation rates (Ba_{XS}AR) does not cause significant changes to the overall trends seen in the concentration datasets for either core.

For ODP Hole 982B, Ba_{XS}AR ranges from 309–4380 µg cm^{-2} kyr^{-1}, with a mean of 885 µg cm^{-2} kyr^{-1} (Figure 3.2). The two youngest samples (1 ka and 7 ka) have Ba_{XS}AR values substantially greater than the mean for all samples because the sedimentation rate is four and two times greater, respectively, than the next highest sedimentation rate for all samples. Ba_{XS}AR more than quadrupled between the late PGP (137 ka) and early LIG (126 ka), and the 12 highest Ba_{XS}AR values occurred during interglacial intervals. Ba_{XS}AR declines through the LIG into the early LGP before increasing again after 66 ka. In contrast, the late PGP is characterised by persistently low Ba_{XS}AR, including the overall minima at 157 ka.

At IODP Hole U1313A, Ba_{XS}AR ranges from 910–7980 µg cm^{-2} kyr^{-1}, with a mean of 2720 µg cm^{-2} kyr^{-1} (Figure 3.2). The four highest Ba_{XS}AR values all occur in the early LGP between 68–61 ka. 7 of the 9 lowest Ba_{XS}AR values occur across the PGP–LIG transition between 144–115 ka.

Possible variation in detrital Ba/Al dominates uncertainly in Ba_{XS}AR calculations (rather than sedimentation rate or density), but values are better constrained for both cores during interglacial intervals than glacial intervals due to relatively low Al concentrations.

For the intervals where samples of comparable age are available for both cores, Ba_{XS}AR is always greater at IODP Site U1313 than ODP Site 982, except in the early LIG, where plausible values overlap. The sites see opposite trends during the second half of the LIG, when Ba_{XS}AR declines in ODP Hole 982B but increases in IODP Hole U1313A.

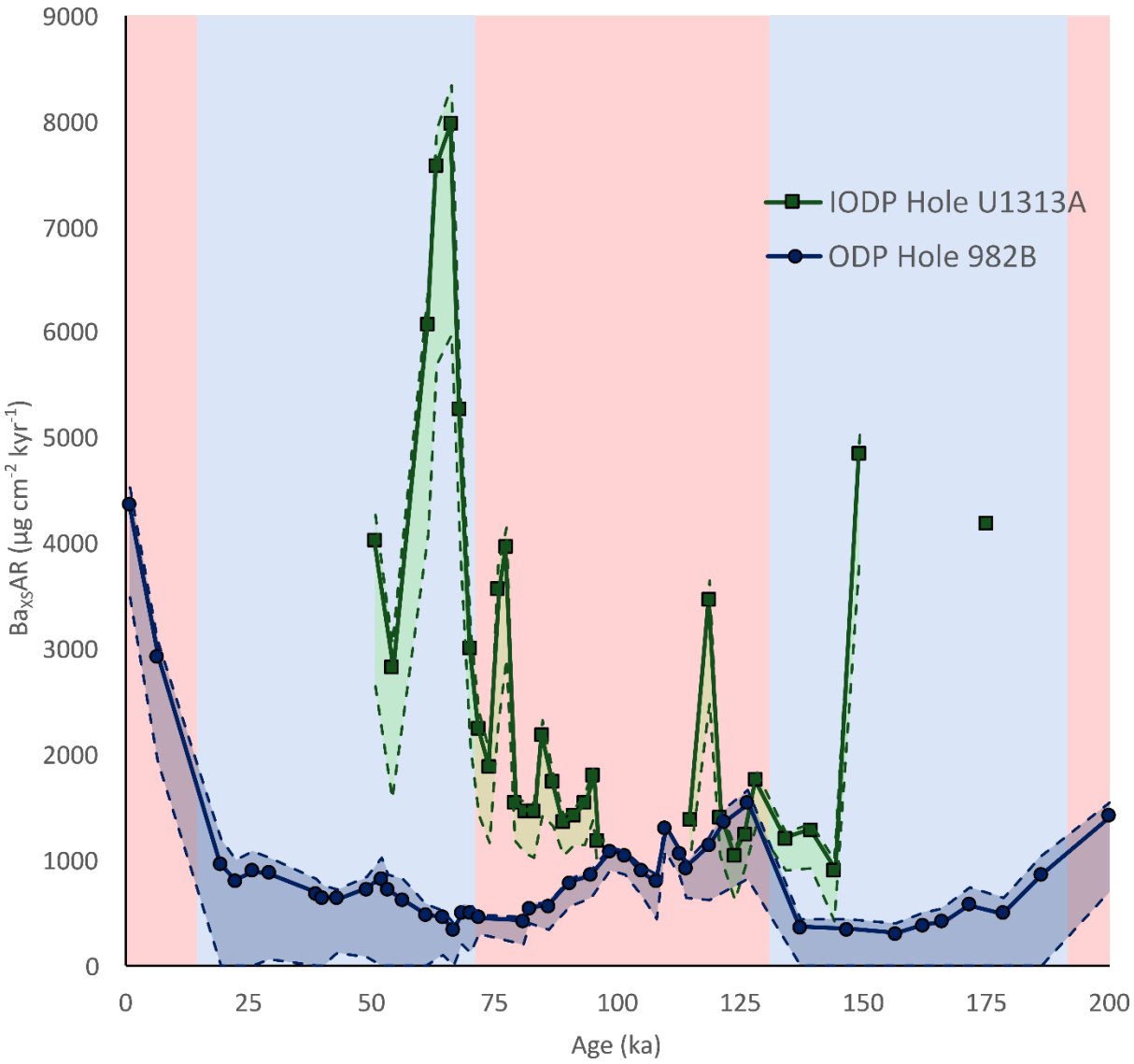

Figure 3.2 – $Ba_{XS}AR$ at IODP Site U1313 (green squares) and ODP Hole 982B (blue circles) between 0–200 ka. The range of plausible values based on detrital Ba/Al (Taylor, 1964; Taylor and McLennan, 1985; Reitz *et al.*, 2004) is shown shaded in the same colour and dashed lines show upper and lower bounds. Glacial intervals (LGP and PGP) are shown with a blue background and interglacial intervals (Holocene, LIG and MIS 7) are shown with a red background. Age gaps between samples that exceed 20 kyr are not connected.

3.3.5. Glacial-interglacial comparisons

In both cores, there are significant differences between the mean values of glacial and interglacial Ba_{XS} and $Ba_{XS}AR$, summarised in Table 3.3. At ODP Hole 982B, interglacial intervals experience significantly higher $Ba_{XS}AR$, even when the two youngest (anomalously high) samples are excluded. For IODP Hole U1313A, glacial values are higher than interglacial values, whilst the opposite is true for ODP Hole 982B (Figure 3.3).

Table 3.3 – Results of MWU tests to determine whether there are significant differences between glacial and interglacial mean values for Ba_{XS} and $Ba_{XS}AR$.

Core	Ba_{XS} or $Ba_{XS}AR$	$n_{glacial}$	$n_{interglacial}$	U	p
IODP Hole U1313A	Ba_{XS}	12	20	180	0.0206
IODP Hole U1313A	$Ba_{XS}AR$	12	20	179	0.0228
ODP Hole 982B	Ba_{XS}	23	20	63	$5.03x10^{-5}$
ODP Hole 982B	$Ba_{XS}AR$	23	20	92	$8.14x10^{-4}$
ODP Hole 982B	$Ba_{XS}AR$ (excluding 2 youngest samples)	21	18	92	$2.63x10^{-3}$

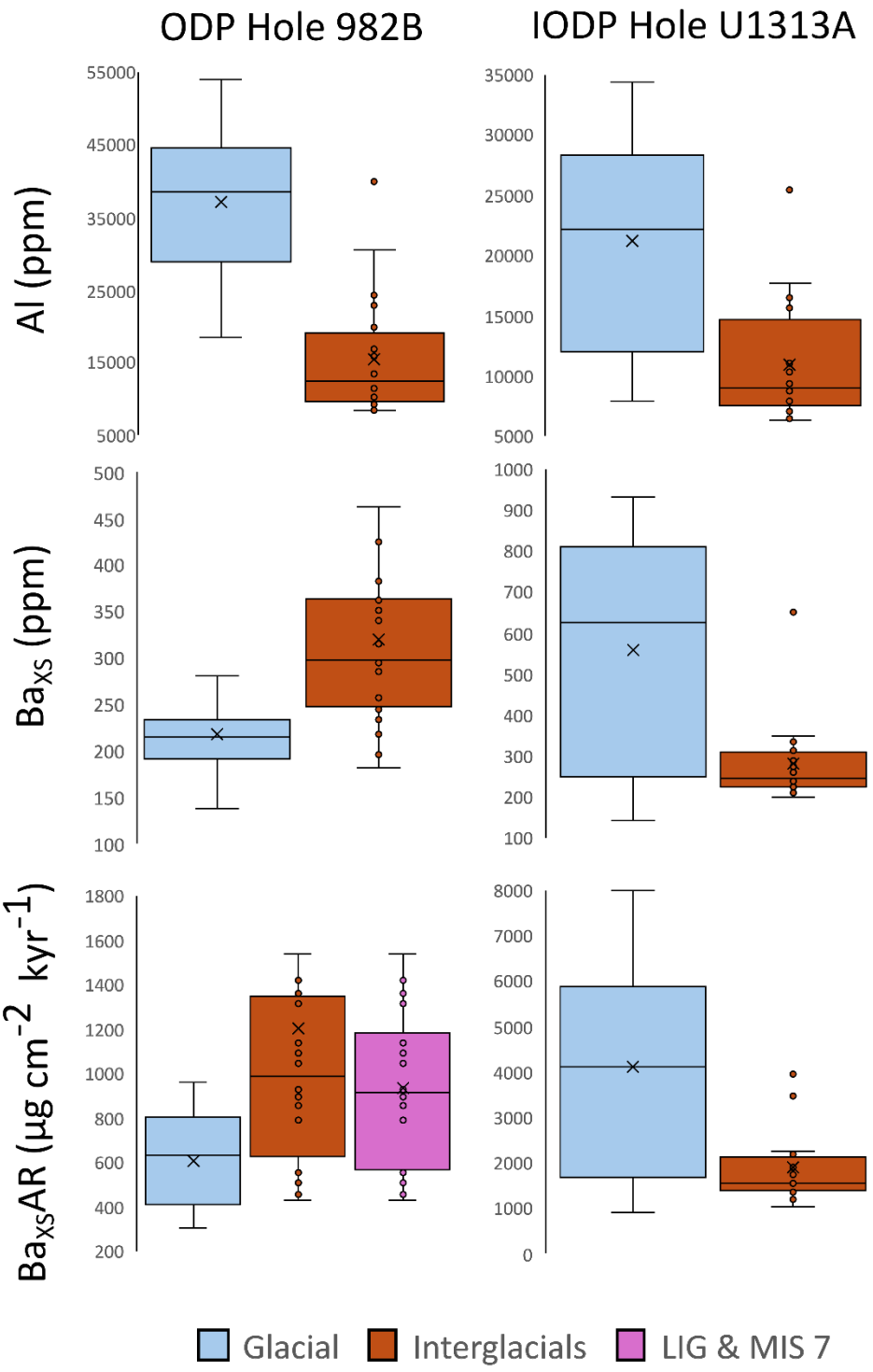

Figure 3.3 – Box plots showing distribution of sample values for Al (top row), Ba_{XS} (middle row), and $Ba_{XS}AR$ (bottom row) in ODP Hole 982B (left column) and IODP Hole U1313A (right column). Glacial values are indicated by blue boxes (left) in each case, and interglacial intervals are shown with red boxes (right). An additional pink box shows interglacial $Ba_{XS}AR$ at ODP Hole 982B excluding the two anomalously high Holocene values. Horizontal lines within boxes indicate the median value and black crosses show the mean.

3.3.6. Al-Ba_{XS} correlation

For IODP Hole U1313A, there is a strong positive correlation (R^2=0.855) between Al and Ba_{XS} during both glacial intervals (R^2=0.816) and interglacial intervals (R^2=0.794).

At ODP Hole 982B, there is no apparent correlation between Al and Ba_{XS} for all samples (R^2=0.0319). There are weak positive correlations between Al and Ba_{XS} during glacial intervals (R^2=0.226) and during interglacial intervals (R^2=0.420). Correlations for both sites are shown in Figure 3.4.

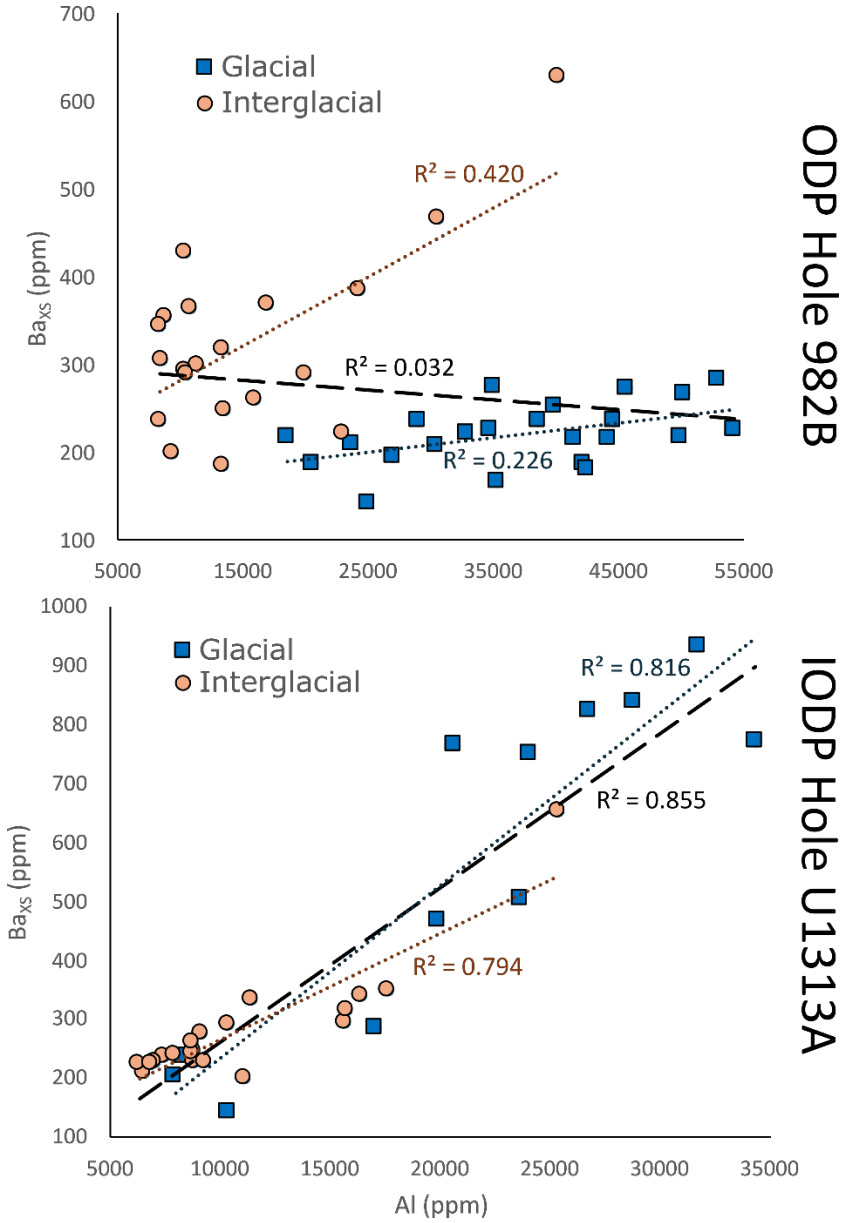

Figure 3.4 – Cross-plots showing correlation of Al and Ba_{XS} within samples during glacial intervals (blue squares) and interglacial intervals (red circles) in ODP Hole 982B (top) and IODP U1313A (bottom). Long black dashed lines show the best fit for all samples, whilst dotted blue and red lines show the best fit line for glacial and interglacial samples, respectively. Coefficients of determination are displayed next to each line in the same colour.

3.4. Discussion

3.4.1. Provenance of detrital material

The 'Ruddiman Belt' describes the accumulation of IRD during Pleistocene glacial intervals along a 40–55°N latitudinal band in the North Atlantic (Ruddiman, 1977; Peck *et al.*, 2007), likely due to the southward shift of cold oceanographic fronts that allowed icebergs to travel to temperate latitudes (e.g. McIntyre, Ruddiman and Jantzen, 1972; Didié and Bauch, 2000; Rasmussen et al., 2003; Holmes et al., 2022). Existing records for both ODP Site 982 and IODP Site U1313 demonstrate a substantial increase in IRD concentration during Late Pleistocene glacial intervals, relative to interglacial intervals (Baumann and Huber, 1999; Venz *et al.*, 1999; Naafs, Hefter and Stein, 2013; Smith *et al.*, 2013; Lang *et al.*, 2016). IRD records have been produced for both sites, permitting a comparison with Al concentrations to test whether aluminosilicates in iceberg-rafted terrestrial rocks were the dominant source of detrital material to North Atlantic sites.

For ODP Site 982, there is reasonable agreement between the Al record and IRD concentration (volume % of IRD grains in 250–2000 µm fraction; Venz et al., 1999**)** over the past 200 ka (Figure 3.5). Values for both Al and IRD decline rapidly following Termination I (LGP–Holocene) and Termination II (PGP–LIG), and IRD volumes remain below 2% through most of the LIG, when Al is similarly low. However, there are some divergences between these records, notably at 50–60 ka when Al is near its overall maximum (3.8–5.0%) but IRD remains low at around half the value seen in the late LGP. Similar differences are also seen in the early and late PGP. This implies one or more significant non-IRD sources of detrital Al to the mid-latitude pelagic region during glacial intervals, although it should also be noted that the IRD calculation method of Venz et al. (1999) does not record any IRD outside of the 250–2000 µm size fraction and therefore may underestimate total IRD.

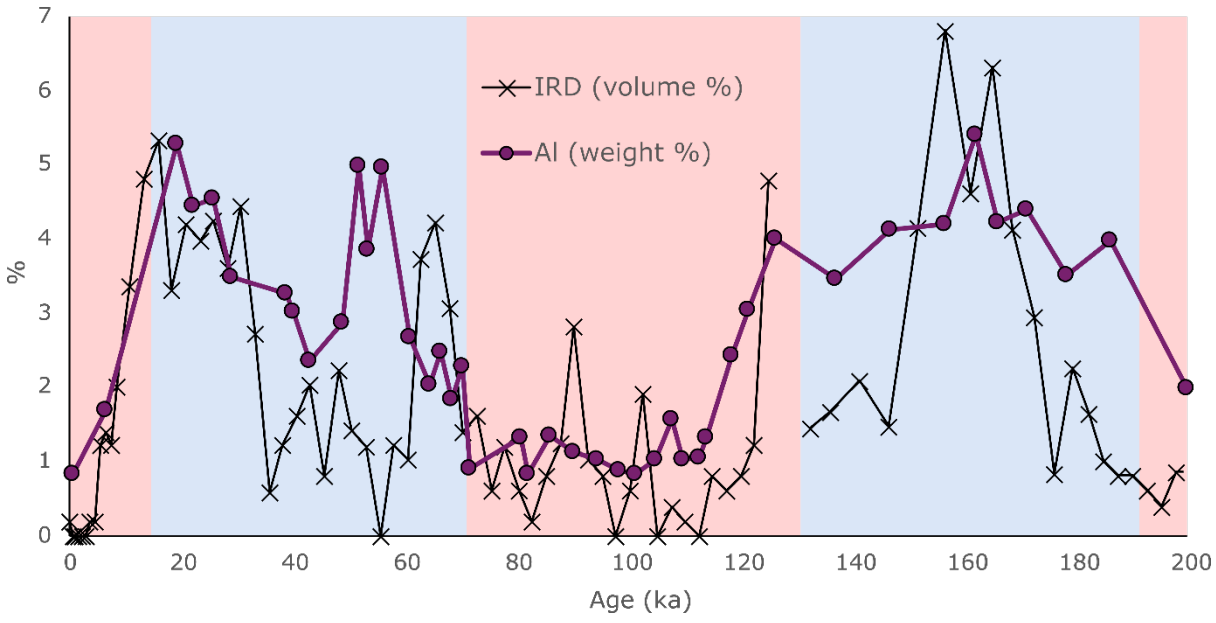

Figure 3.5 – Comparison of weight Al (weight percent; purple circles) and volume % IRD (volume percent; black crosses) from Venz et al. (1999) for ODP Site 982. A single 26% IRD point is excluded at 128 ka for scaling purposes. Red backgrounds indicate interglacial intervals and blue backgrounds show glacial intervals.

High-resolution IRD concentration records are available for the early LGP–Holocene (0–69 ka; Naafs et al., 2013; Lang et al., 2016) and late MIS 7–early LIG (110–194 ka; Smith et al., 2013) at IODP Site U1313, but not for the majority (70–110 ka) of the LIG. However, the available records show that significant IRD inputs to this location during the LGP were generally restricted to Heinrich events, given the location of this site at the southernmost edge of the Ruddiman Belt (Ruddiman, 1977; Expedition 306 Scientists, 2006; Naafs, Hefter and Stein, 2013). There is a noticeable increase in the ratio of the quartz/calcite ratio at IODP Site U1313 coincident with Heinrich event 6 (H6) around 60 ka (Hemming, 2004; Naafs *et al.*, 2013), which also coincides with the maximum Al concentration from this record and is probably associated with aluminosilicate-rich IRD delivery to this location from Greenland (McManus *et al.*, 1998; Hemming, 2004; Hodell *et al.*, 2008).

IRD likely makes a substantial contribution to total Al at IODP Site U1313, particularly during glacial intervals, but as Al concentrations are around 0.5–2.5% during interglacial intervals, when negligible ice rafting affected this site, it is probable that another detrital source played a significant role too.

Naafs et al. (2012) produced a high-resolution record of wind-blown dust deposition at IODP Site U1313 by measuring the concentration of higher plant leaf waxes (*n*-alkanl-1-ols and non-reworked *n*-alkanes) in sediment. Wax concentrations increased approximately fourfold between the late LIG (74–77 ka) and early LGP (54–62 ka), implying similar increases in the input of North American-sourced continental dust to the temperate North Atlantic. Numerous other authors have also recorded strong increases in dust delivery to the pelagic ocean during glacial intervals (e.g. Kumar et al., 1995; Jahn et al., 2003; Maher et al., 2010; Lang et al., 2014; Chen et al., 2023). For IODP Site U1313, aeolian dust increased alongside the change in the quartz/dolomite ratio in the early LGP (Figure 3.6; Naafs et al., 2012, 2013), suggesting contemporaneous increases in iceberg calving and glaciogenic dust formation in North America. These changes are further coincident with a 4°C surface cooling at both IODP Site U1313 (Stein *et al.*, 2009; Naafs *et al.*, 2013) and ODP Site 982 (Lawrence *et al.*, 2009; Herbert *et al.*, 2016), demonstrating the re-emergence of full glacial conditions in the North Atlantic.

The synchroneity of increased dust and IRD flux make it challenging to identify whether aeolian or glacial detritus was the more significant contributor to total Al at IODP Site U1313. Peaks in Al during the LIG are unlikely to be solely IRD-derived owing to the low total IRD flux throughout the interglacial, and interglacial Al peaks are consistent with increases in the aeolian dust flux within the error of the age model for this site (Naafs *et al.*, 2013). Hence it is likely that some, or perhaps even the majority, of interglacial Al content of this core was derived from wind-blown dust, whilst glacial Al has more variable provenance.

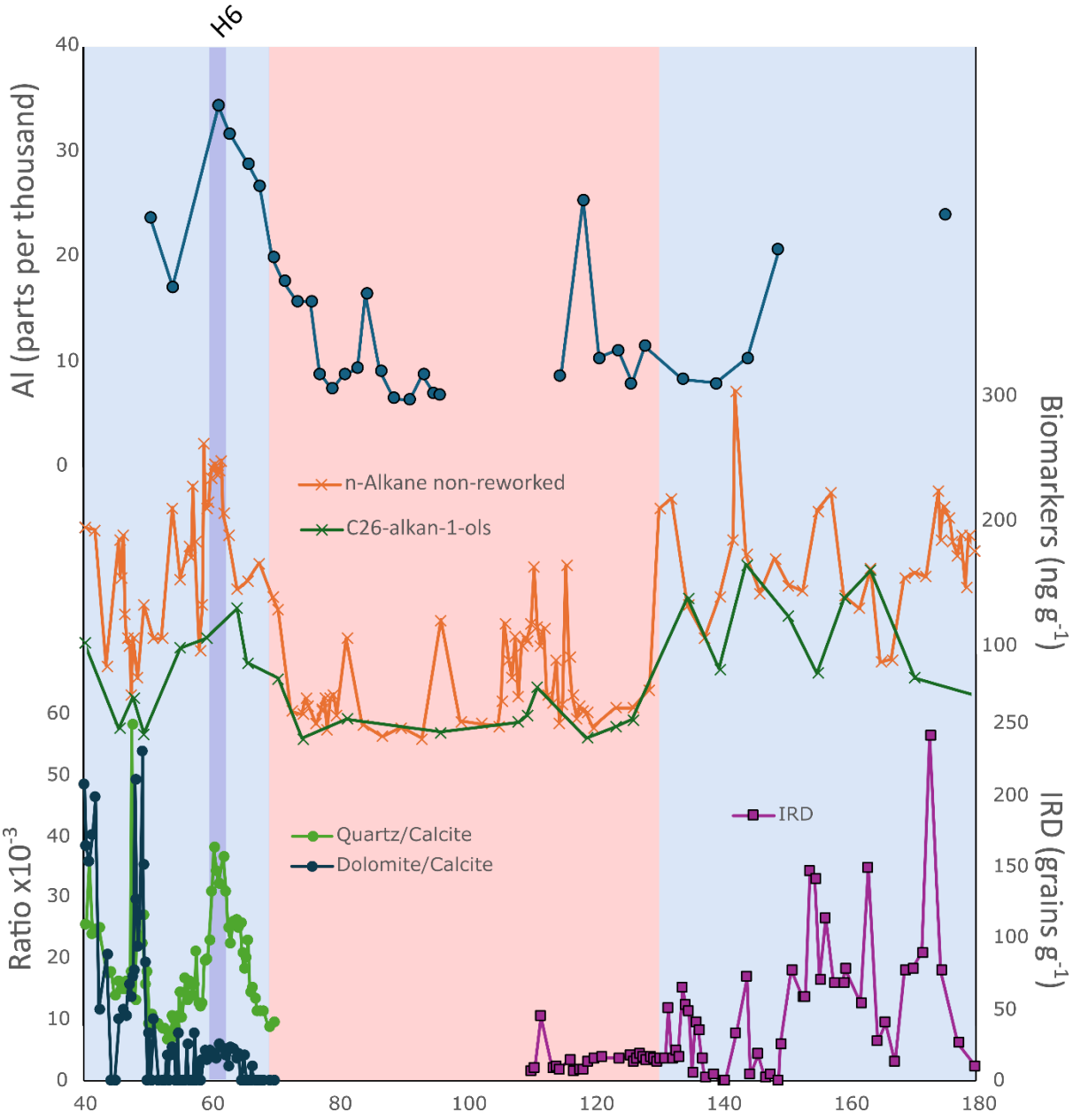

Figure 3.6 – Proxies for detrital input at IODP Site U1313. Al concentrations (blue circles; this study); aeolian dust proxy biomarkers (orange and green crosses; Naafs *et al.*, 2012); sediment quartz/calcite and dolomite/calcite ratios (Naafs *et al.*, 2013), and IRD counts (purple squares; Smith *et al.*, 2013). Approximate timing of Heinrich Event 6 (Hemming, 2004) is indicated by a vertical line marked 'H6' at the top. Gaps in the Al record exceeding 20 kyr have no connecting line. Glacial and interglacial intervals are indicated by a blue and red background, respectively.

3.4.2. Ba/Al ratios

North American wind-blown dust and high-latitude IRD are unlikely to have the same Ba/Al ratios (Taylor, 1964; Taylor and McLennan, 1985; Wedephl, 1991; Dymond, Suess and Lyle, 1992; Reitz *et al.*, 2004; House and Norris, 2020), implying that the variable provenance of the detrital sediment could exert an important caveat on the interpretation of Ba_{XS} and $Ba_{XS}AR$ over the past 200 ka.

Geochemical evidence suggests that the Hudson Strait was the dominant source of North Atlantic IRD during Heinrich events (Heinrich, 1988; Bond *et al.*, 1992; Hemming, 2004; Peck *et al.*, 2007; Naafs, Hefter and Stein, 2013; Zhou *et al.*, 2021), with a significant contribution from the Greenland and/or European ice sheets during H3 (~31 ka) and H6 (~60 ka) (McManus *et al.*, 1998; Hemming, 2004; Hodell *et al.*, 2008). Organic biomarker evidence indicates that IRD deposited during Hudson Strait Heinrich events was sourced from Upper Ordovician formations on Southampton Island and Baffin Island (Hefter, Naafs and Zhang, 2017), which consist of interbedded shales, limestones, and dolomites (Sandford and Grant, 1998; Zhang, 2008, 2012).

Bailey et al. (2012) used Pb-isotopes to show that ambient (i.e. non-Heinrich event) glacial and interglacial subpolar North Atlantic IRD had similar sources, which are not characteristic of any single region or formation, but are consistent with contributions from the Canadian Shield, Greenland, the British Isles, and Scandinavia. IRD source rocks therefore likely represent diverse geologies and ages (Figure 3.7), making the calculation of a 'typical' Ba/Al highly challenging. However, the consistent geochemical profiles of IRD between the LIG and PGP provide reassurance that Ba/Al had a small variance in ODP Site 982 between glacial and interglacial times if IRD was the dominant source of Al. The blending of multiple diverse lithologies into an overall IRD composition suggests that a terrestrial average Ba/Al may be more appropriate than the empirically determined Ba/Al value from detrital material in modern equatorial pelagic Atlantic sediment.

The choice of detrital Ba/Al at IODP Site U1313 is less significant than for the higher-latitude site, as even using the probable maximum ratio of 0.01 does not substantially change the patterns observed during any interval due to higher overall Ba and lower Al at this site. As with ODP Site 982, high Ba/Al in IRD would slightly lower estimates of Ba_{XS} and $Ba_{XS}AR$ for all samples. Establishing the Ba/Al of North American aeolian dust, which is likely to be significant in interglacial intervals, is more challenging. Limited measurements suggest that aeolian dust may be relatively Ba-depleted (Anderson and Winckler, 2005; Hull and Norris, 2011) and therefore Ba/Al ratios of this dust may more closely resemble the chemical profile of modern equatorial Atlantic pelagic detritus, which likely also has an aeolian origin (Reitz *et al.*, 2004).

The close correlation between Al and Ba in IODP Hole U1313A raises the possibility that the majority of Ba could have been derived from detrital material. However, the mean Ba_{total}/Al_{total} in all samples is 0.029, around three times greater than the highest ratio measured from continental rocks in the present day (Taylor, 1964; Taylor and McLennan, 1985; Eagle *et al.*, 2003; Reitz *et al.*, 2004). It is therefore highly unlikely that the correlation is a consequence of Ba-enriched detrital inputs.

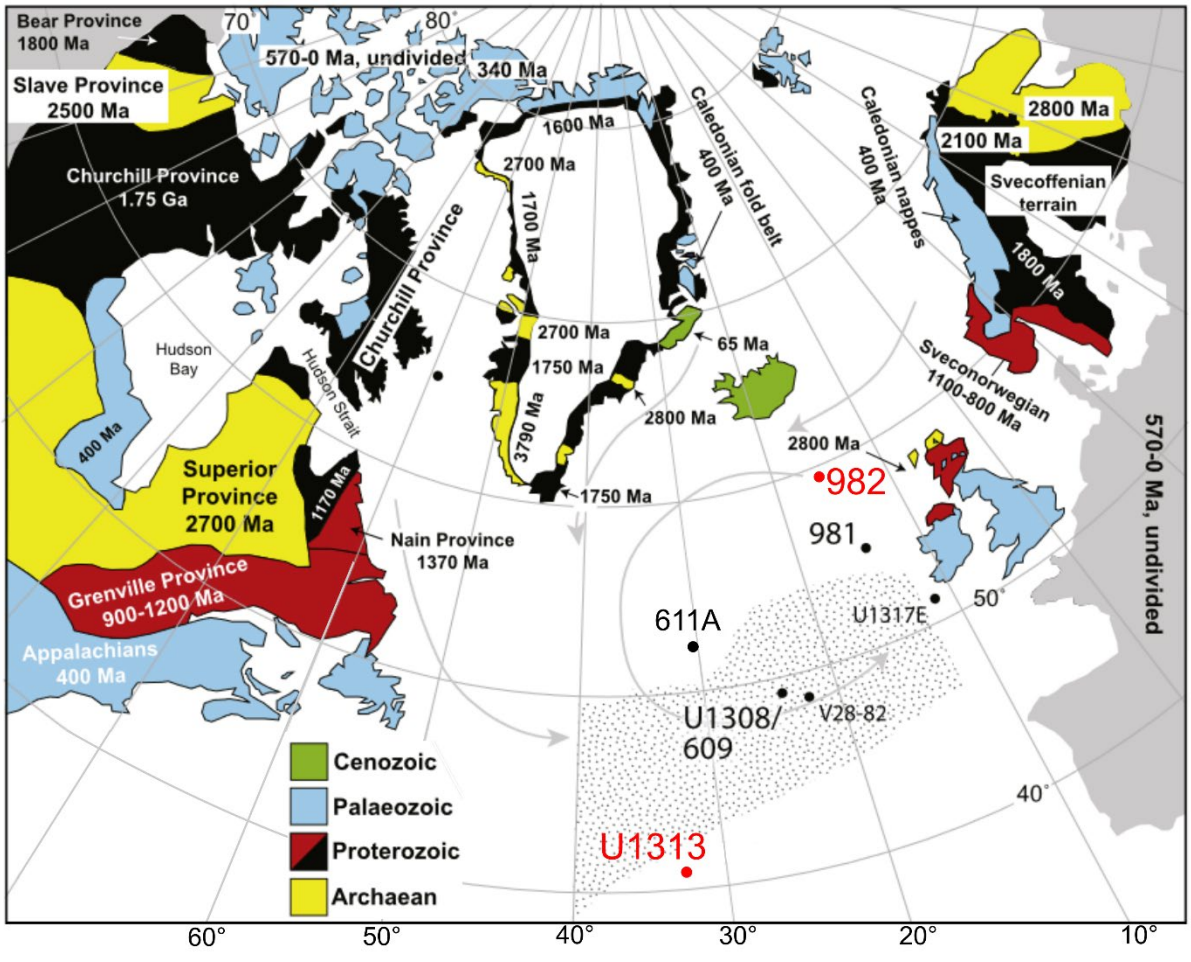

Figure 3.7 - Generalised geological map showing likely source regions for late Pleistocene North Atlantic IRD and sediment cores. Grey arrows show the generalised patterns of iceberg flow during the LGP (Ruddiman, 1977; Death *et al.*, 2006) and stippled area shows the Ruddiman IRD belt (Ruddiman, 1977; Hemming, 2004). The two sediment core sites used in this research, IODP Site U1313 and ODP Site 982, are shown in red. Figure modified from Bailey et al. (2012).

3.4.3. Trends in export production

Authors such as Dymond, Suess and Lyle (1992) and Pfeifer et al. (2001) developed algorithms for converting Ba_{XS} into estimates of carbon export using empirical patterns in the present day. I refrain from using those algorithms in this study due to the seemingly poor reliability of universal algorithms to accurately reconstruct export production in all marine settings, likely due to variable diagenetic impacts on barite preservation in time and space (Torres *et al.*, 1996; Schoepfer *et al.*, 2015). Instead, I restrict my interpretation of export production to relative changes within and between the two North Atlantic sites using Ba_{XS} and $Ba_{XS}AR$.

Despite the relatively close geographic proximity of IODP Site U1313 and ODP Site 982, two highly distinct glacial-interglacial patterns and controls are apparent.

ODP Site 982 is characterised by elevated interglacial export production, including abrupt increases across both glacial–interglacial transitions. For the LIG, there is a gradual decline in export production following peak interglacial conditions at the onset of MIS 5. These patterns occur independently of allochthonous inputs from glacial and/or aeolian sources and are therefore better explained by changes in ocean structure and consequential impacts on the marine biosphere.

The NATW region is defined by the influence of the NAC, which is a warm and relatively fast current that separates the subtropical gyre and subarctic front (Krauss, 1986; Fratantoni, 2001). In the modern, the subpolar North Atlantic is characterised by a deep winter mixed layer and strong NAC-induced vertical mixing that resupplies nutrients to the surface ocean, leading to seasonal blooms of large phytoplankton such as diatoms and coccolithophores and significant sinking of organic matter from the mixed layer to the deep ocean by biological processes including diel vertical migration (DVM) in zooplankton and fishes, sinking of large aggregates, and the production of faecal pellets (Turner, 2002; Frangoulis *et al.*, 2011; Archibald, Siegel and Doney, 2019; Nowicki, DeVries and Siegel, 2022). By comparison, the Arctic Ocean north of NATW has a pronounced summer peak in primary production and a high export ratio, but lower total export due to light limitation (caused by both latitude and sea ice cover) and strong stratification (Anderson, Jones and Swift, 2003; Forest *et al.*, 2010; Randelhoff and Guthrie, 2016; Nowicki, DeVries and Siegel, 2022). During late Pleistocene glacial intervals, the NAC and NATW moved southwards due to the expansion of cold polar waters (McIntyre, Ruddiman and Jantzen, 1972; Villanueva *et al.*, 2001; Schwab *et al.*, 2012). The expanded subpolar gyre had many of the properties that lead to low Arctic export production today, including strong vertical stratification and seasonal light limitation due to the expansion of sea ice, which likely reached as far south as ODP Site 982 intermittently during the LGP and PGP (Pedro *et al.*, 2022; Cauquoin *et al.*, 2023). Oceanographic changes during glacial intervals can therefore explain why export production at ODP Site 982 was lower during glacial intervals relative to interglacial intervals.

However, it is notable that export appears to have increased in the late LGP prior to the Last Glacial Maximum (LGM; Lawrence et al., 2009; Herbert et al., 2016), despite this being the time when stratification and sea ice extent would be expected to be at its greatest. Although no site-specific aeolian dust proxy record exists for ODP Site 982, dust fluxes to the temperate North Atlantic peaked in the late LGP (Naafs *et al.*, 2012), so simultaneous increases in the dust flux to the subpolar North Atlantic could have led to increased primary and export production sufficient to offset some of the negative changes caused by the incursion of polar water masses. Additionally, simulations suggest that lower water temperatures (as seen at ODP Site 982 during the late LGP) may reduce organic carbon remineralisation without impacting its production (Chikamoto *et al.*, 2012). Maximum IRD values are seen in the late LGP and iceberg-rafted iron also has the potential to alleviate nutrient limitation in the polar ocean, although the iron content of icebergs is highly variable (Hopwood *et al.*, 2019).

IODP Site U1313 is located in the southernmost region of NATW in the present day, proximal to the permanently stratified subtropical gyre. Total export production here is similar to ODP Site 982 in the present day, although modelling suggests that a higher proportion of export comes from faecal pellets and less from either sinking aggregates or the migrant pump (Nowicki, DeVries and Siegel, 2022) due to stronger vertical stratification (Bolton *et al.*, 2011; Guerreiro *et al.*, 2023). The area had low relative export production during the LIG that increased substantially during the early LGP. This work suggests that export production had more high-frequency variation here than at the higher latitude site.

The strong correlation between Al and Ba_{XS} during both glacial intervals and interglacial intervals could either be a result of allogenic nutrient inputs or oceanographic reconfiguration. A modern sediment trap study proximal to this site indicates that total barium flux to depth is a function of primary production changes, which in turn responds to natural dust deposition (Stern, Dellwig and Waniek, 2017).

IODP Site U1313 likely remained within NATW throughout the past 200 ka, although its position at the southernmost extent of the glacial IRD belt suggests it was proximal to cool polar waters, and hence near the northern edge of NATW, during the most extreme cold phases of past glacial intervals (Ruddiman, 1977; Expedition 306 Scientists, 2006; Stein *et al.*, 2009; Smith *et al.*, 2013). Changes to vertical ocean structure alone are therefore unlikely to explain the eightfold increase in export production that seems to have occurred between the mid-LIG and early LGP (assuming a linear relationship between $Ba_{XS}AR$ and export production).

Organic biomarker $\delta^{13}C$ evidence indicates that the glacial aeolian dust flux originated from the North American continent and was brought to this site by westerly winds in much greater quantities during glacial intervals than interglacial intervals (Naafs *et al.*, 2012; Hefter, Naafs and Zhang, 2017). The temperate North Atlantic is typically co-limited by iron and phosphate in southern NATW, and by nitrate in the subtropical gyre south of the Azores Current in the present day (Moore *et al.*, 2013; Browning and Moore, 2023). Relatively small increases in the flux of limiting micronutrients such as iron can significantly increase primary and export production in the open ocean on short timescales, as demonstrated by iron fertilisation experiments (Assmy *et al.*, 2007; Smetacek *et al.*, 2012; Martínez-García *et al.*, 2014; Yoon *et al.*, 2018) and contemporary observations of ecosystem response to allogenic inputs (e.g. Stern, Dellwig and Waniek, 2017). Evidence from glacial regions in western North America and Nepal suggests that glaciogenic dust is significantly more bioavailable in seawater than volcanic ash, and thus had high fertilisation potential (Koffman *et al.*, 2021).

Whilst iron fertilisation experiments in HNLC regions have consistently resulted in increased primary production, they do not always result in sustained increases in export production, as enhanced grazing by primary consumers such as zooplankton and small fishes may result in the rapid recycling of new production in the shallow ocean (Blain *et al.*, 2007; Smetacek *et al.*, 2012; Yoon *et al.*, 2018) However, it is likely that sustained aeolian dust inputs to the temperate North Atlantic may have resulted in long-term changes to ecosystem structure that promoted greater export by aggregate sinking and DVM (Quéguiner, 2013). Modern ocean regions that are rapidly resupplied with nutrients, such as upwelling zones, tend to have shorter, more efficient food webs and consequently higher export ratios than open ocean sites (Vargas *et al.*, 2007; Sigman and Hain, 2012; Armengol *et al.*, 2019; Massing *et al.*, 2022).

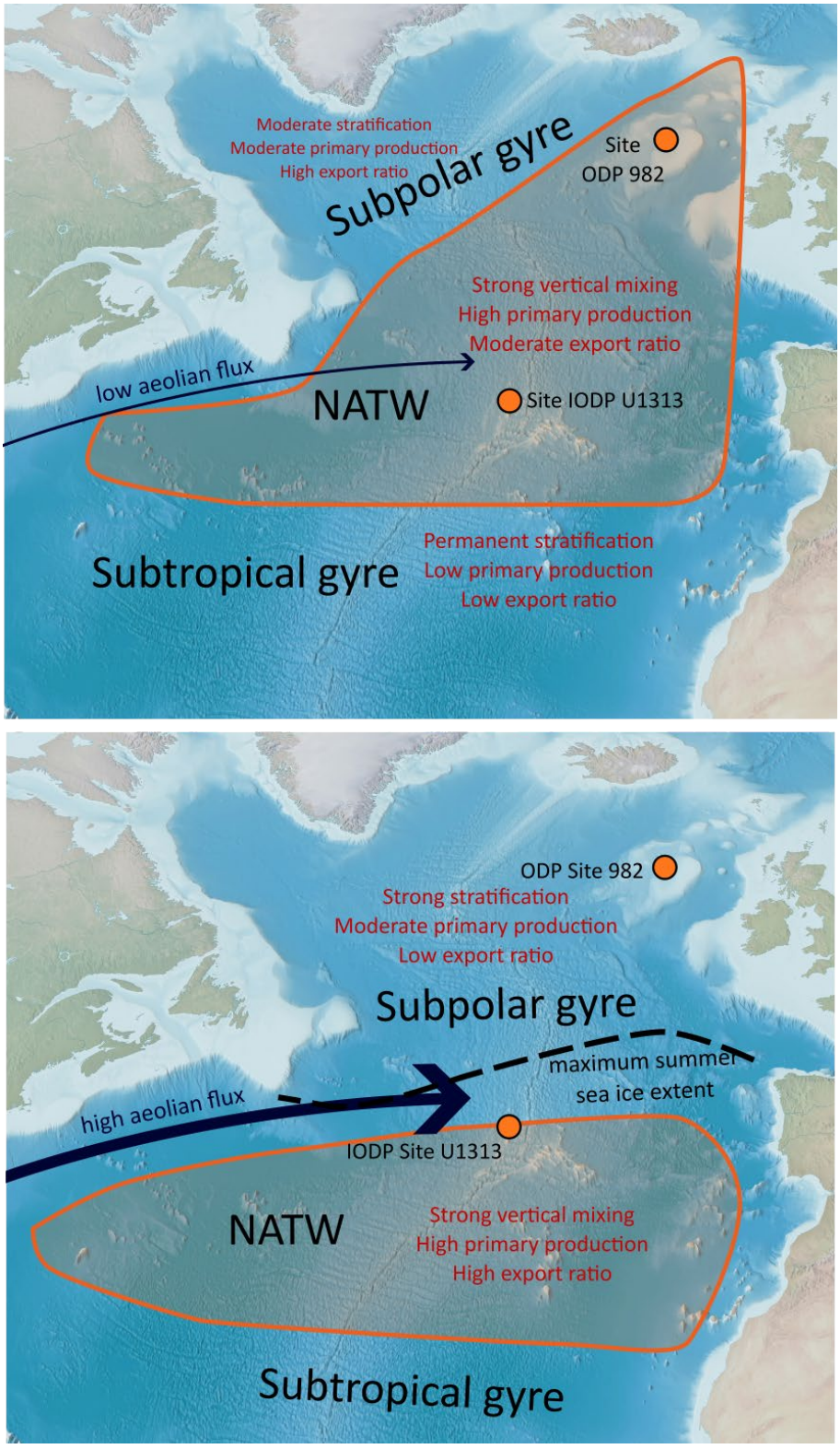

Figure 3.8 – Simplified schematic maps of the North Atlantic during interglacial intervals (top) and glacial intervals (bottom) based on the results of this study. The extent of NATW is shown in the shaded area with an orange outline. The two sites used in this study are shown with orange circles and modelled approximate limit of summer sea ice extent during LGP stadials (Pedro *et al.*, 2022) is indicated with a black dashed line. Modern coastlines, which are not reflective of contemporary geography, are shown in both cases.

3.4.4. Implications for global climate

Increases in export production in the temperate North Atlantic site in the LGP far exceed decreases in the subpolar site. If this was true across similar latitudes in the North Atlantic basin, it implies that the regional biological carbon pump could have acted as significant additional sink of atmospheric carbon dioxide during Pleistocene glacial intervals driven by aeolian dust fertilisation. Similar conclusions have been reported for the Pacific (Loveley *et al.*, 2017; Chen *et al.*, 2023; Zan *et al.*, 2023) and Southern Ocean (Jahn *et al.*, 2003; Blain *et al.*, 2007; Martínez-García *et al.*, 2014). This research indicates that the temperate North Atlantic may have been an additional contributor to the global pattern of enhanced removal of organic carbon by the marine biosphere during glacial intervals (Naafs *et al.*, 2012; Hefter, Naafs and Zhang, 2017; Saini *et al.*, 2023).

3.5. Conclusion

Organic carbon export in the open ocean plays an important role in the global carbon cycle and may have been significant in contributing to glacial-interglacial climate change. Using the excess barium proxy, I reconstructed North Atlantic carbon export over the past 200 ka in two pelagic sediment cores. The delivery of terrestrial detritus was significantly higher in the North Atlantic during glacial intervals relative to interglacial intervals due to ice-rafting both during and between Heinrich events. Major increases in export production occurred in the temperate North Atlantic during the last interglacial-glacial transition, likely driven by a significantly higher aeolian dust flux to the mid-latitude pelagic ocean. In contrast, export production in the subpolar North Atlantic was higher during each of the past three interglacial intervals than in the LGP or PGP, indicating that enhanced vertical stratification synchronous with the incursion of cold polar water masses exerted a major negative effect on productivity. The synchroneity of glacial intensification and a strengthening of the temperate organic carbon pump supports a global picture of enhanced biologically mediated transport of carbon into the deep ocean during glacial intervals.

Acknowledgements

I am grateful to Luke Bridgestock for sharing his extensive knowledge on the use of barium as a productivity proxy. I am indebted to Jane Barling for her advice on processing and digestion methods and to Phil Holdship for analysing the processed samples. This work would not have been possible without the generous real-time practical and emotional support of the many other Department of Earth Sciences clean lab users, and I am immensely thankful for their willingness to share wisdom with an amateur geochemist.

Appendix

Variable HF application

As shown in Table 3.1, I applied additional HF to 33% of ODP 982B and 19% of IODP U1313A samples as visual inspection indicated incomplete dissolution of silicates. Across both cores, 85% of samples that required additional treatment date from glacial intervals, which provides reassurance that the dark material was correctly identified as silicate, since silicate was proportionally more significant at these times (Baumann and Huber, 1999; Venz *et al.*, 1999; Naafs *et al.*, 2013; Smith *et al.*, 2013). However, further investigation is merited to test whether binary HF treatment of samples could have biased subsequent calculated concentrations.

With respect to binary HF addition, there are two hypotheses that must be rejected in order for the whole dataset to be seen as reliable:

1. Undissolved silicates were misidentified during digestions and the addition of HF was unnecessary. In this case, the samples with additional treatment would be expected to have Al concentrations that were not significantly higher than the samples that received basic treatment. In this case, HF addition may also result in the production of fluoride minerals that could remain out of solution, skewing calculated concentrations of solution.
2. Undissolved silicates were correctly identified within the samples that received additional treatment, but solid silicate phases were also present in samples that received basic treatment. In this case, samples with additional treatment would be expected to have significantly higher Al concentrations than those with basic treatment.

In ODP Hole 982B, Al concentrations in samples with additional HF treatment ranged from 28900–54100 ppm, compared to 8290–42000 ppm in samples with basic treatment. The eight higher Al concentrations for all samples all received additional treatment, but six basic treatment samples had higher Al concentrations than the lowest additional treatment.

For IODP Hole U1313A, samples with additional treatment had Al concentrations ranging from 17600–34300 ppm compared to 6330–31700 ppm in those with basic treatment. The higher overall Al concentration in these samples received additional treatment, but the next two highest were both those with basic treatment.

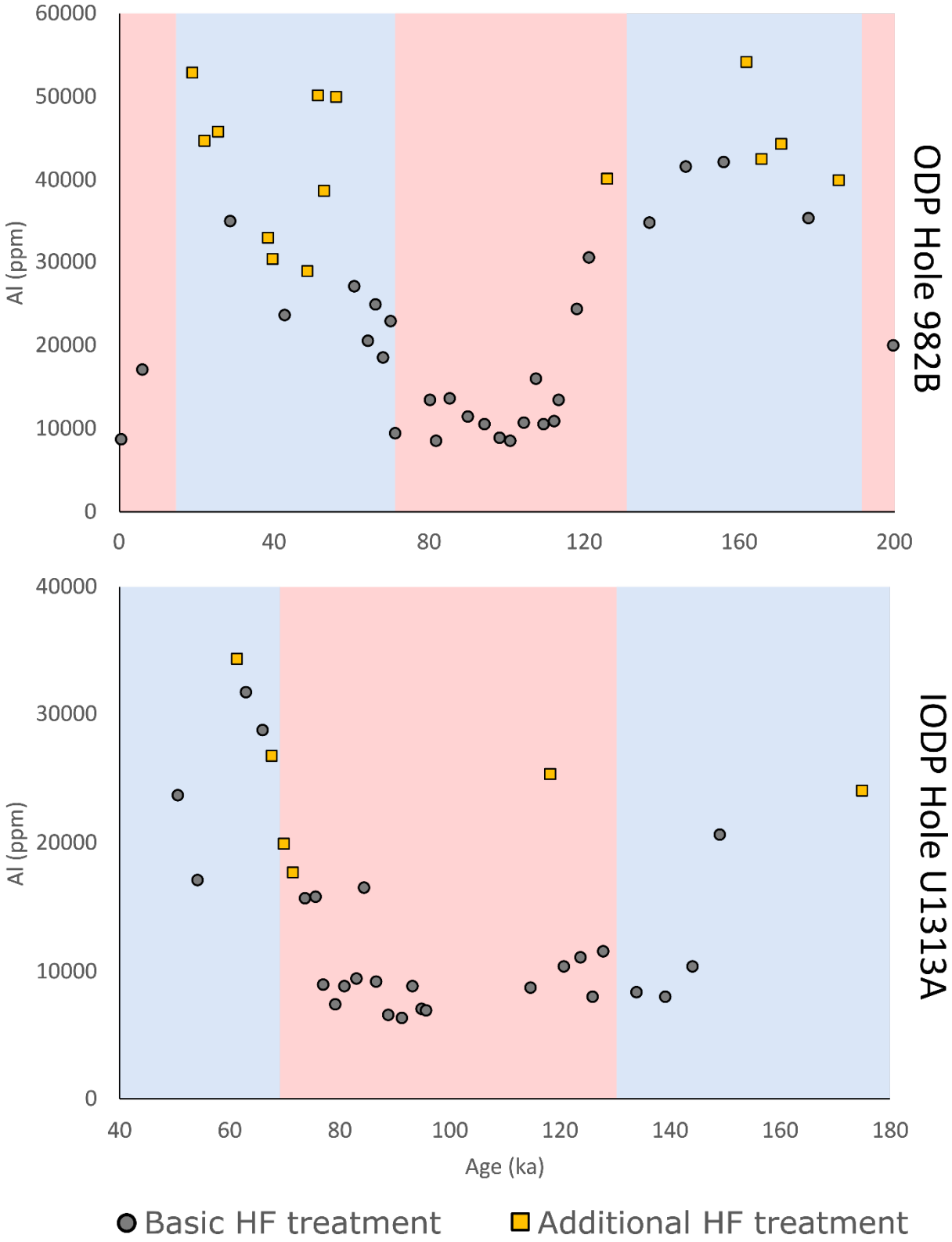

Figure 3.A1 – Al values for samples treated with standard (grey circles) and additional (yellow squares) HF in ODP Hole 982B (top) and IODP Hole U1313A (bottom).

The higher mean Al concentrations for additional HF treated samples in both cores suggest that hypothesis 1 can be rejected. The overlapping of Al concentrations in samples with basic and additional treatment for both locations provides reassurance that undissolved silicate was not present in all untreated samples. Without knowing what fraction of total Al was hosted in silicate and non-silicate phases, it remains challenging to wholly discount hypothesis 2. Significant differences in Al are still present between glacial and interglacial samples that received only basic treatment, but it is possible that true Al values (particularly during glacial intervals) may have been higher than those calculated in basic treatment samples. If this is the case, Al values may have been slightly underestimated, resulting in higher $Ba_{detrital}$ and lower Ba_{XS}. For ODP Hole 982B, such a revision would not have a major effect on reconstructed export production during glacial intervals since a $Ba_{XS}AR$ value of 0 μg cm^{-2} kyr^{-1} is within the range of plausible values for the majority of glacial samples. For IODP Site U1313, additional HF treatment does not appear to have significantly affected the calculated glacial Al concentrations, suggesting near-complete silicate digestion during glacial intervals.

Future studies could more reliably test hypothesis 2 by treating multiple subsamples of the same material with variable HF volumes and measuring the impact on Al concentrations. This would allow the development of a tailored digestion process for this sediment. Ba_{XS} could also be more reliably reconstructed by measuring the specific Ba/Al of detrital material in this sample using a sequential extraction process (e.g. Reitz et al., 2004), rather than a generalised value.

USGS SGR-1 standards

Al recovery and, to a lesser extent, Ba recovery in USGS SGR-1 standards is beneath the expected values, suggesting the incomplete digestion of aluminosilicate phases in prepared samples. The clustering of Al and Ba values across all three standards indicates that this was uniformly true. Using additional HF during digestion may have resulted in higher Al recovery closer. The lower-than-expected Ba values are likely also a result of Ba being bound to aluminosilicate phases in USGS SGR-1.

Table 3.A1 – Al and Ba concentrations for USGS SGR-1 standards processed in different crushing and digestion batches. Values in ppm given to 6 significant figures.

	Al (ppm)	Ba (ppm)
Published values	34500 ± 1100	290 ± 40
Standard A	28094.6	247.404
Standard B	30464.6	266.033
Standard C	30842.4	276.814

The implications of this on the completeness of sample digestion depends on the relative amount of aluminosilicate in samples. Looking only at samples that received additional HF treatment, one from IODP Hole U1313A and fourteen (out of fifteen) in ODP Hole 982B had higher Al than the mean recovered from USGS SGR-1 standards. This supports the same conclusion reached in the previous appendix section, that glacial Al may be underestimated at ODP Hole 982B, but the magnitude of those reductions is relatively minor and there is no change to the overall trends described.

References

Algeo, T.J. *et al.* (2013) 'Plankton and productivity during the Permian–Triassic boundary crisis: An analysis of organic carbon fluxes', *Global and Planetary Change*, 105, pp. 52–67. Available at: https://doi.org/10.1016/j.gloplacha.2012.02.008.

Anderson, L.G., Jones, E.P. and Swift, J.H. (2003) 'Export production in the central Arctic Ocean evaluated from phosphate deficits', *Journal of Geophysical Research: Oceans*, 108(C6), p. 3199. Available at: https://doi.org/10.1029/2001JC001057.

Anderson, R.F. and Winckler, G. (2005) 'Problems with paleoproductivity proxies', *Paleoceanography*, 20(3), pp. 1–7. Available at: https://doi.org/10.1029/2004PA001107.

Archibald, K.M., Siegel, D.A. and Doney, S.C. (2019) 'Modeling the Impact of Zooplankton Diel Vertical Migration on the Carbon Export Flux of the Biological Pump', *Global Biogeochemical Cycles*, 33(2), pp. 181–199. Available at: https://doi.org/10.1029/2018GB005983.

Armengol, L. *et al.* (2019) 'Planktonic food web structure and trophic transfer efficiency along a productivity gradient in the tropical and subtropical Atlantic Ocean', *Scientific Reports*, 9(1), pp. 1–19. Available at: https://doi.org/10.1038/s41598-019-38507-9.

Assmy, P. *et al.* (2007) 'Mechanisms determining species dominance in a phytoplankton bloom induced by the iron fertilization experiment EisenEx in the Southern Ocean', *Deep Sea Research Part I: Oceanographic Research Papers*, 54(3), pp. 340–362. Available at: https://doi.org/10.1016/j.dsr.2006.12.005.

Bailey, I. *et al.* (2012) 'Flux and provenance of ice-rafted debris in the earliest Pleistocene sub-polar North Atlantic Ocean comparable to the last glacial maximum', *Earth and Planetary Science Letters*, 341–344, pp. 222–233. Available at: https://doi.org/10.1016/j.epsl.2012.05.034.

Baumann, K.-H. and Huber, R. (1999) 'Sea-surface gradients between the North Atlantic and the Norwegian Sea during the last 3.1 m.y.: comparison of Sites 982 and 985', in *Proceedings of the Ocean Drilling Program, 162 Scientific Results*. Ocean Drilling Program, pp. 179–190. Available at: https://doi.org/10.2973/odp.proc.sr.162.014.1999.

Behrenfeld, M.J. (2014) 'Climate-mediated dance of the plankton', *Nature Climate Change*, 4(10), pp. 880–887. Available at: https://doi.org/10.1038/nclimate2349.

Biggs, T.E.G., Huisman, J. and Brussaard, C.P.D. (2021) 'Viral lysis modifies seasonal phytoplankton dynamics and carbon flow in the Southern Ocean', *The ISME Journal*, (June), pp. 1–8. Available at: https://doi.org/10.1038/s41396-021-01033-6.

Blain, S. *et al.* (2007) 'Effect of natural iron fertilization on carbon sequestration in the Southern Ocean', *Nature 2007 446:7139*, 446(7139), pp. 1070–1074. Available at: https://doi.org/10.1038/nature05700.

Bolton, C.T. *et al.* (2011) 'Biotic and geochemical evidence for a global latitudinal shift in ocean biogeochemistry and export productivity during the late Pliocene', *Earth and Planetary Science Letters*, 308(1–2), pp. 200–210. Available at: https://doi.org/10.1016/j.epsl.2011.05.046.

Bond, G. *et al.* (1992) 'Evidence for massive discharges of icebergs into the North Atlantic ocean during the last glacial period', *Nature 1992 360:6401*, 360(6401), pp. 245–249. Available at: https://doi.org/10.1038/360245a0.

Bond, G. *et al.* (1993) 'Correlations between climate records from North Atlantic sediments and Greenland ice', *Nature 1993 365:6442*, 365(6442), pp. 143–147. Available at: https://doi.org/10.1038/365143a0.

Bridgestock, L. *et al.* (2018) 'Controls on the barium isotope compositions of marine sediments', *Earth and Planetary Science Letters*, 481, pp. 101–110. Available at: https://doi.org/10.1016/j.epsl.2017.10.019.

Bridgestock, L. *et al.* (2019) 'Increased export production during recovery from the Paleocene–Eocene thermal maximum constrained by sedimentary Ba isotopes', *Earth and Planetary Science Letters*, 510, pp. 53–63. Available at: https://doi.org/10.1016/j.epsl.2018.12.036.

Browning, T.J. and Moore, C.M. (2023) 'Global analysis of ocean phytoplankton nutrient limitation reveals high prevalence of co-limitation', *Nature Communications 2023 14:1*, 14(1), pp. 1–12. Available at: https://doi.org/10.1038/s41467-023-40774-0.

Cauquoin, A. *et al.* (2023) 'Effects of Last Glacial Maximum (LGM) sea surface temperature and sea ice extent on the isotope-temperature slope at polar ice core sites', *Climate of the Past*, 19(6), pp. 1275–1294. Available at: https://doi.org/10.5194/CP-19-1275-2023.

Chen, T. *et al.* (2023) 'Thorium isotope evidence for glacial–interglacial dust storminess and productivity in the North Pacific gyre', *Geochimica et Cosmochimica Acta*, 346, pp. 15–28. Available at: https://doi.org/10.1016/J.GCA.2023.01.007.

Chikamoto, M.O. *et al.* (2012) 'Temperature-induced marine export production during glacial period', *Geophysical Research Letters*, 39(21). Available at: https://doi.org/10.1029/2012GL053828.

Davison, P.C. *et al.* (2013) 'Carbon export mediated by mesopelagic fishes in the northeast Pacific Ocean', *Progress in Oceanography*, 116, pp. 14–30. Available at: https://doi.org/10.1016/J.POCEAN.2013.05.013.

Death, R. *et al.* (2006) 'Modelling iceberg trajectories, sedimentation rates and meltwater input to the ocean from the Eurasian Ice Sheet at the Last Glacial Maximum', *Palaeogeography, Palaeoclimatology, Palaeoecology*, 236(1–2), pp. 135–150. Available at: https://doi.org/10.1016/J.PALAEO.2005.11.040.

Didié, C. and Bauch, H.A. (2000) 'Species composition and glacial–interglacial variations in the ostracode fauna of the northeast Atlantic during the past 200,000 years', *Marine Micropaleontology*, 40(1–2), pp. 105–129. Available at: https://doi.org/10.1016/S0377-8398(00)00034-7.

Dymond, J., Suess, E. and Lyle, M. (1992) 'Barium in Deep-Sea Sediment: A Geochemical Proxy for Paleoproductivity', *Paleoceanography*, 7(2), pp. 163–181. Available at: https://doi.org/10.1029/92PA00181.

Eagle, M. *et al.* (2003) 'A comparison between excess barium and barite as indicators of carbon export', *Paleoceanography*, 18(1). Available at: https://doi.org/10.1029/2002PA000793.

Expedition 306 Scientists (2006) 'Site U1313', in *Proceedings of the IODP, 303/306*. Integrated Ocean Drilling Program. Available at: https://doi.org/10.2204/iodp.proc.303306.112.2006.

Forest, A. *et al.* (2010) 'Relationships between primary production and vertical particle export at the Atlantic-Arctic boundary (Fram Strait, HAUSGARTEN)', *Polar Biology*, 33(12), pp. 1733–1746. Available at: https://doi.org/10.1007/S00300-010-0855-3/FIGURES/7.

Frangoulis, C. *et al.* (2011) 'Importance of copepod carcasses versus faecal pellets in the upper water column of an oligotrophic area', *Estuarine, Coastal and Shelf Science*, 92(3), pp. 456–463. Available at: https://doi.org/10.1016/j.ecss.2011.02.005.

Fratantoni, D.M. (2001) 'North Atlantic surface circulation during the 1990's observed with satellite-tracked drifters', *Journal of Geophysical Research: Oceans*, 106(C10), pp. 22067–22093. Available at: https://doi.org/10.1029/2000JC000730.

Fu, W., Randerson, J.T. and Moore, J.K. (2016) 'Climate change impacts on net primary production (NPP) and export production (EP) regulated by increasing stratification and phytoplankton community structure in the CMIP5 models', *Biogeosciences*, 13(18), pp. 5151–5170. Available at: https://doi.org/10.5194/bg-13-5151-2016.

Ganeshram, R.S. *et al.* (2003) 'An experimental investigation of barite formation in seawater', *Geochimica et Cosmochimica Acta*, 67(14), pp. 2599–2605. Available at: https://doi.org/10.1016/S0016-7037(03)00164-9.

Gasol, J.M., Del Giorgio, P.A. and Duarte, C.M. (1997) 'Biomass distribution in marine planktonic communities', *Limnology and Oceanography*, 42(6), pp. 1353–1363. Available at: https://doi.org/10.4319/lo.1997.42.6.1353.

Guerreiro, C. V. *et al.* (2023) 'Response of coccolithophore communities to oceanographic and atmospheric processes across the North- and Equatorial Atlantic', *Frontiers in Marine Science*, 10, p. 1119488. Available at: https://doi.org/10.3389/FMARS.2023.1119488/BIBTEX.

Guidi, L. *et al.* (2009) 'Effects of phytoplankton community on production, size, and export of large aggregates: A world-ocean analysis', *Limnology and Oceanography*, 54(6), pp. 1951–1963. Available at: https://doi.org/10.4319/lo.2009.54.6.1951.

Guidi, L. *et al.* (2016) 'Plankton networks driving carbon export in the oligotrophic ocean', *Nature*, 532(7600), pp. 465–470. Available at: https://doi.org/10.1038/nature16942.

Hefter, J., Naafs, B.D.A. and Zhang, S. (2017) 'Tracing the source of ancient reworked organic matter delivered to the North Atlantic Ocean during Heinrich Events', *Geochimica et Cosmochimica Acta*, 205, pp. 211–225. Available at: https://doi.org/10.1016/j.gca.2017.02.008.

Heinrich, H. (1988) 'Origin and consequences of cyclic ice rafting in the Northeast Atlantic Ocean during the past 130,000 years', *Quaternary Research*, 29(2), pp. 142–152. Available at: https://doi.org/10.1016/0033-5894(88)90057-9.

Hemming, S.R. (2004) 'Heinrich events: Massive late Pleistocene detritus layers of the North Atlantic and their global climate imprint', *Reviews of Geophysics*, 42(1), p. 1005. Available at: https://doi.org/10.1029/2003RG000128.

Henry, L.G. *et al.* (2016) 'North Atlantic ocean circulation and abrupt climate change during the last glaciation', *Science*, 353(6298), pp. 470–474. Available at: https://doi.org/10.1126/SCIENCE.AAF5529/SUPPL_FILE/PAPV2.PDF.

Henson, S.A., Sanders, R. and Madsen, E. (2012) 'Global patterns in efficiency of particulate organic carbon export and transfer to the deep ocean', *Global Biogeochemical Cycles*, 26(1), p. n/a-n/a. Available at: https://doi.org/10.1029/2011GB004099.

Herbert, T.D. *et al.* (2016) 'Late Miocene global cooling and the rise of modern ecosystems', *Nature Geoscience*, 9(11), pp. 843–847. Available at: https://doi.org/10.1038/ngeo2813.

Hitchen, K. (2004) 'The geology of the UK Hatton-Rockall margin', *Marine and Petroleum Geology*, 21(8), pp. 993–1012. Available at: https://doi.org/10.1016/J.MARPETGEO.2004.05.004.

Hodell, D.A. *et al.* (2008) 'Onset of "Hudson Strait" Heinrich events in the eastern North Atlantic at the end of the middle Pleistocene transition (~640 ka)?', *Paleoceanography*, 23(4). Available at: https://doi.org/10.1029/2008PA001591.

Holmes, D.E. *et al.* (2022) 'Reorganization of Atlantic Waters at sub-polar latitudes linked to deep-water overflow in both glacial and interglacial climate states', 18, pp. 989–1009. Available at: https://doi.org/10.5194/cp-18-989-2022.

Hopwood, M.J. *et al.* (2019) 'Highly variable iron content modulates iceberg-ocean fertilisation and potential carbon export', *Nature Communications 2019 10:1*, 10(1), pp. 1–10. Available at: https://doi.org/10.1038/s41467-019-13231-0.

House, B.M. and Norris, R.D. (2020) 'Unlocking the barite paleoproductivity proxy: A new high-throughput method for quantifying barite in marine sediments', *Chemical Geology*, 552, p. 119664. Available at: https://doi.org/10.1016/J.CHEMGEO.2020.119664.

Hull, P.M. and Norris, R.D. (2011) 'Diverse patterns of ocean export productivity change across the Cretaceous-Paleogene boundary: New insights from biogenic barium', *Paleoceanography*, 26(3). Available at: https://doi.org/10.1029/2010PA002082.

Iversen, M.H. (2023) 'Carbon Export in the Ocean: A Biologist's Perspective', *Annual Review of Marine Science*, 15(Volume 15, 2023), pp. 357–381. Available at: https://doi.org/10.1146/ANNUREV-MARINE-032122-035153/CITE/REFWORKS.

Jacobel, A.W. *et al.* (2019) 'No evidence for equatorial Pacific dust fertilization', *Nature Geoscience*, 12(3), pp. 154–155. Available at: https://doi.org/10.1038/s41561-019-0304-z.

Jahn, B. *et al.* (2003) 'Pleistocene variations in dust input and marine productivity in the northern Benguela Current: Evidence of evolution of global glacial–interglacial cycles', *Palaeogeography, Palaeoclimatology, Palaeoecology*, 193(3–4), pp. 515–533. Available at: https://doi.org/10.1016/S0031-0182(03)00264-5.

Joy-Warren, H.L. *et al.* (2019) 'Light Is the Primary Driver of Early Season Phytoplankton Production Along the Western Antarctic Peninsula', *Journal of Geophysical Research: Oceans*, 124(11), pp. 7375–7399. Available at: https://doi.org/10.1029/2019JC015295.

Kindler, P. *et al.* (2014) 'Climate of the Past Temperature reconstruction from 10 to 120 kyr b2k from the NGRIP ice core', 10, pp. 887–902. Available at: https://doi.org/10.5194/cp-10-887-2014.

Koffman, B.G. *et al.* (2021) 'Glacial Dust Surpasses Both Volcanic Ash and Desert Dust in Its Iron Fertilization Potential', *Global Biogeochemical Cycles*, 35(4), pp. 1–29. Available at: https://doi.org/10.1029/2020GB006821.

Krauss, W. (1986) 'The North Atlantic Current', *Journal of Geophysical Research: Oceans*, 91(C4), pp. 5061–5074. Available at: https://doi.org/10.1029/JC091IC04P05061.

Kumar, N. *et al.* (1995) 'Increased biological productivity and export production in the glacial Southern Ocean', *Nature 1995 378:6558*, 378(6558), pp. 675–680. Available at: https://doi.org/10.1038/378675a0.

Kuypers, M.M.M. *et al.* (2002) 'Enhanced productivity led to increased organic carbon burial in the euxinic North Atlantic basin during the late Cenomanian oceanic anoxic event', *Paleoceanography*, 17(4), pp. 3-1-3–13. Available at: https://doi.org/10.1029/2000PA000569.

Laber, C.P. *et al.* (2018) 'Coccolithovirus facilitation of carbon export in the North Atlantic', *Nature Microbiology*, 3(5), pp. 537–547. Available at: https://doi.org/10.1038/s41564-018-0128-4.

Lampitt, R.S. *et al.* (2010) 'Long-term variability of downward particle flux in the deep northeast Atlantic: Causes and trends', *Deep Sea Research Part II: Topical Studies in Oceanography*, 57(15), pp. 1346–1361. Available at: https://doi.org/10.1016/j.dsr2.2010.01.011.

Lang, D.C. *et al.* (2014) 'The transition on North America from the warm humid Pliocene to the glaciated Quaternary traced by eolian dust deposition at a benchmark North Atlantic Ocean drill site', *Quaternary Science Reviews*, 93, pp. 125–141. Available at: https://doi.org/10.1016/J.QUASCIREV.2014.04.005.

Lang, D.C. *et al.* (2016) 'Incursions of southern-sourced water into the deep North Atlantic during late Pliocene glacial intensification', *Nature Geoscience*, 9(5), pp. 375–379. Available at: https://doi.org/10.1038/ngeo2688.

Lawrence, K.T. *et al.* (2009) 'High-amplitude variations in North Atlantic sea surface temperature during the early Pliocene warm period', *Paleoceanography*, 24(2), p. n/a-n/a. Available at: https://doi.org/10.1029/2008PA001669.

Li, S. *et al.* (2024) 'Multifaceted Contributions of Coccolithophores to Ocean Carbon Export', *Ocean-Land-Atmosphere Research* [Preprint]. Available at: https://doi.org/10.34133/OLAR.0049.

Liguori, B.T.P., De Almeida, M.G. and de Rezende, C.E. (2016) 'Barium and its importance as an indicator of (Paleo)productivity', *Anais da Academia Brasileira de Ciencias*, 88(4), pp. 2093–2103. Available at: https://doi.org/10.1590/0001-3765201620140592.

Loveley, M.R. *et al.* (2017) 'Millennial-scale iron fertilization of the eastern equatorial Pacific over the past 100,000 years', *Nature Geoscience*, 10(10), pp. 760–764. Available at: https://doi.org/10.1038/ngeo3024.

Maher, B.A. *et al.* (2010) 'Global connections between aeolian dust, climate and ocean biogeochemistry at the present day and at the last glacial maximum', *Earth-Science Reviews*, 99(1–2), pp. 61–97. Available at: https://doi.org/10.1016/J.EARSCIREV.2009.12.001.

Mann, H.B. and Whitney, D.R. (1947) 'On a Test of Whether one of Two Random Variables is Stochastically Larger than the Other', *https://doi.org/10.1214/aoms/1177730491*, 18(1), pp. 50–60. Available at: https://doi.org/10.1214/AOMS/1177730491.

Martin, J.H. (1990) 'Glacial-interglacial CO 2 change: The Iron Hypothesis', *Paleoceanography*, 5(1), pp. 1–13. Available at: https://doi.org/10.1029/PA005i001p00001.

Martínez-García, A. *et al.* (2014) 'Iron Fertilization of the Subantarctic Ocean During the Last Ice Age', *Science*, 343(6177), pp. 1347–1350. Available at: https://doi.org/10.1126/science.1246848.

Massing, J.C. *et al.* (2022) 'Toward a Solution of the "Peruvian Puzzle": Pelagic Food-Web Structure and Trophic Interactions in the Northern Humboldt Current Upwelling System Off Peru', *Frontiers in Marine Science*, 8, p. 759603. Available at: https://doi.org/10.3389/FMARS.2021.759603/BIBTEX.

McIntyre, A., Ruddiman, W.F. and Jantzen, R. (1972) 'Southward penetrations of the North Atlantic polar front: faunal and floral evidence of large-scale surface water mass movements over the last 225,000 years', *Deep Sea Research and Oceanographic Abstracts*, 19(1), pp. 61–77. Available at: https://doi.org/10.1016/0011-7471(72)90073-3.

McManus, J.F. *et al.* (1998) 'Radiometrically determined sedimentary fluxes in the sub-polar North Atlantic during the last 140,000 years', *Earth and Planetary Science Letters*, 155(1–2), pp. 29–43. Available at: https://doi.org/10.1016/S0012-821X(97)00201-X.

Mitchell, B.G. *et al.* (1991) 'Light limitation of phytoplankton biomass and macronutrient utilization in the Southern Ocean', *Limnology and Oceanography*, 36(8), pp. 1662–1677. Available at: https://doi.org/10.4319/lo.1991.36.8.1662.

Moore, C.M. *et al.* (2013) 'Processes and patterns of oceanic nutrient limitation', *Nature Geoscience*, 6(9), pp. 701–710. Available at: https://doi.org/10.1038/ngeo1765.

Mouriño-Carballido, B. and Neuer, S. (2008) 'Regional Differences in the Role of Eddy Pumping in the North Atlantic Subtropical Gyre', *Source: Oceanography*, 21(2), pp. 52–61. Available at: https://doi.org/10.2307/24805610.

Murray, R.W. *et al.* (2000) 'Export production and carbonate dissolution in the central equatorial Pacific Ocean over the past 1 Myr', *Paleoceanography*, 15(6), pp. 570–592. Available at: https://doi.org/10.1029/1999PA000457.

Naafs, B.D.A. *et al.* (2012) 'Strengthening of North American dust sources during the late Pliocene (2.7 Ma)', *Earth and Planetary Science Letters*, 317–318, pp. 8–19. Available at: https://doi.org/10.1016/j.epsl.2011.11.026.

Naafs, B.D.A. *et al.* (2013) 'Warming of surface waters in the mid-latitude North Atlantic during Heinrich events', *Paleoceanography*, 28(1), pp. 153–163. Available at: https://doi.org/10.1029/2012PA002354.

Naafs, B.D.A., Hefter, J. and Stein, R. (2013) 'Millennial-scale ice rafting events and Hudson Strait Heinrich(-like) Events during the late Pliocene and Pleistocene: a review', *Quaternary Science Reviews*, 80, pp. 1–28. Available at: https://doi.org/10.1016/J.QUASCIREV.2013.08.014.

Nowicki, M., DeVries, T. and Siegel, D.A. (2022) 'Quantifying the Carbon Export and Sequestration Pathways of the Ocean's Biological Carbon Pump', *Global Biogeochemical Cycles*, 36(3). Available at: https://doi.org/10.1029/2021GB007083.

Passow, U. and Carlson, C. (2012) 'The biological pump in a high CO2 world', *Marine Ecology Progress Series*, 470(2), pp. 249–271. Available at: https://doi.org/10.3354/meps09985.

Pattan, J.N. *et al.* (2003) 'Productivity fluctuations in the southeastern Arabian Sea during the last 140 ka', *Palaeogeography, Palaeoclimatology, Palaeoecology*, 193(3–4), pp. 575–590. Available at: https://doi.org/10.1016/S0031-0182(03)00267-0.

Paytan, A. and Griffith, E.M. (2007) 'Marine barite: Recorder of variations in ocean export productivity', *Deep Sea Research Part II: Topical Studies in Oceanography*, 54(5–7), pp. 687–705. Available at: https://doi.org/10.1016/J.DSR2.2007.01.007.

Peck, V.L. *et al.* (2007) 'The relationship of Heinrich events and their European precursors over the past 60ka BP: a multi-proxy ice-rafted debris provenance study in the North East Atlantic', *Quaternary Science Reviews*, 26(7–8), pp. 862–875. Available at: https://doi.org/10.1016/j.quascirev.2006.12.002.

Pedro, J.B. *et al.* (2022) 'Dansgaard-Oeschger and Heinrich event temperature anomalies in the North Atlantic set by sea ice, frontal position and thermocline structure', *Quaternary Science Reviews*, 289, p. 107599. Available at: https://doi.org/10.1016/J.QUASCIREV.2022.107599.

Petit, J.R. *et al.* (1999) 'Climate and atmospheric history of the past 420,000 years from the Vostok ice core, Antarctica', *Nature*, 399(6735), pp. 429–436. Available at: https://doi.org/10.1038/20859.

Pfeifer, K. *et al.* (2001) 'Reconstruction of primary productivity from the barium contents in surface sediments of the South Atlantic Ocean', *Marine Geology*, 177(1–2), pp. 13–24. Available at: https://doi.org/10.1016/S0025-3227(01)00121-9.

Pöppelmeier, F. *et al.* (2021) 'Simulated stability of the Atlantic Meridional Overturning Circulation during the Last Glacial Maximum', *Climate of the Past*, 17(2), pp. 615–632. Available at: https://doi.org/10.5194/CP-17-615-2021.

Quéguiner, B. (2013) 'Iron fertilization and the structure of planktonic communities in high nutrient regions of the Southern Ocean', *Deep Sea Research Part II: Topical Studies in Oceanography*, 90, pp. 43–54. Available at: https://doi.org/10.1016/J.DSR2.2012.07.024.

Randelhoff, A. and Guthrie, J.D. (2016) 'Regional patterns in current and future export production in the central Arctic Ocean quantified from nitrate fluxes', *Geophysical Research Letters*, 43(16), pp. 8600–8608. Available at: https://doi.org/10.1002/2016GL070252.

Rasmussen, T.L. *et al.* (2003) 'Millennial-scale glacial variability versus Holocene stability: changes in planktic and benthic foraminifera faunas and ocean circulation in the North Atlantic during the last 60 000 years', *Marine Micropaleontology*, 47(1–2), pp. 143–176. Available at: https://doi.org/10.1016/S0377-8398(02)00115-9.

Reitz, A. *et al.* (2004) 'Biogenic barium and the detrital Ba/Al ratio: a comparison of their direct and indirect determination', *Marine Geology*, 204(3–4), pp. 289–300. Available at: https://doi.org/10.1016/S0025-3227(04)00004-0.

Ruddiman, W.F. (1977) 'Late Quaternary deposition of ice-rafted sand in the subpolar North Atlantic (lat 40° to 65°N)', *Geological Society of America Bulletin*, 88(12), p. 1813. Available at: https://doi.org/10.1130/0016-7606(1977)88<1813:LQDOIS>2.0.CO;2.

Saba, G.K. *et al.* (2021) 'Toward a better understanding of fish-based contribution to ocean carbon flux', *Limnology and Oceanography*, 66(5), pp. 1639–1664. Available at: https://doi.org/10.1002/lno.11709.

Saini, H. *et al.* (2023) 'Impact of iron fertilisation on atmospheric CO2 during the last glaciation', *Climate of the Past*, 19(7), pp. 1559–1584. Available at: https://doi.org/10.5194/CP-19-1559-2023.

Sandford, B. and Grant, A. (1998) 'Paleozoic and Mesozoic Geology of the Hudson Bay and southeast Arctic platforms'. Geological Survey of Canada. Available at: https://scholar.google.com/scholar?hl=en&as_sdt=0%2C5&q=Paleozoic+and+Mesozoic+Geology+of+the+Hudson+Bay+and+Southeast+Arctic+Platforms&btnG= (Accessed: 3 September 2024).

Schenau, S.J., Reichart, G.J. and De Lange, G.J. (2005) 'Phosphorus burial as a function of paleoproductivity and redox conditions in Arabian Sea sediments', *Geochimica et Cosmochimica Acta*, 69(4), pp. 919–931. Available at: https://doi.org/10.1016/J.GCA.2004.05.044.

Schmidt, K. *et al.* (2014) 'Not all calcite ballast is created equal: Differing effects of foraminiferan and coccolith calcite on the formation and sinking of aggregates', *Biogeosciences*, 11(1), pp. 135–145. Available at: https://doi.org/10.5194/BG-11-135-2014.

Schoepfer, S.D. *et al.* (2015) 'Total organic carbon, organic phosphorus, and biogenic barium fluxes as proxies for paleomarine productivity', *Earth-Science Reviews*, 149, pp. 23–52. Available at: https://doi.org/10.1016/j.earscirev.2014.08.017.

Schwab, C. *et al.* (2012) 'Coccolithophore paleoproductivity and ecology response to deglacial and Holocene changes in the Azores Current System', *Paleoceanography*, 27(3). Available at: https://doi.org/10.1029/2012PA002281.

Shackleton, N.J. (1987) 'OXYGEN ISOTOPES, ICE VOLUME AND SEA LEVEL', *Quaternary Science Reviews*, 6, pp. 183–90.

Shipboard Scientific Party (1996) 'Site 982', in *Proceedings of the Ocean Drilling Program, 162 Initial Reports*. Ocean Drilling Program, pp. 91–138. Available at: https://doi.org/10.2973/odp.proc.ir.162.104.1996.

Siegel, D.A. *et al.* (2014) 'Global assessment of ocean carbon export by combining satellite observations and food-web models', *Global Biogeochemical Cycles*, 28(3), pp. 181–196. Available at: https://doi.org/10.1002/2013GB004743.

Sigman, D.M. and Boyle, E.A. (2000) 'Glacial/interglacial variations in atmospheric carbon dioxide', *Nature*, 407(6806), pp. 859–869. Available at: https://doi.org/10.1038/35038000.

Sigman, D.M. and Hain, M.P. (2012) 'The Biological Productivity of the Ocean', *Nature Education*, 3(6), pp. 1–16.

Smetacek, V. *et al.* (2012) 'Deep carbon export from a Southern Ocean iron-fertilized diatom bloom', *Nature*, 487(7407), pp. 313–319. Available at: https://doi.org/10.1038/nature11229.

Smith, M.E. *et al.* (2013) 'Data report: oxygen isotopes and foraminifer abundance record for the last glacial-interglacial cycle and marine isotope Stage 6 at IODP Site U1313', in, pp. 1–11. Available at: https://doi.org/10.2204/iodp.proc.303306.216.2013.

Stein, R. *et al.* (2009) 'Variability of surface water characteristics and Heinrich-like events in the Pleistocene midlatitude North Atlantic Ocean: Biomarker and XRD records from IODP Site U1313 (MIS 16-9)', *Paleoceanography*, 24(2), p. n/a-n/a. Available at: https://doi.org/10.1029/2008PA001639.

Stern, J., Dellwig, O. and Waniek, J.J. (2017) 'Deep–sea fluxes of barium and lithogenic trace elements in the subtropical northeast Atlantic', *Deep Sea Research Part I: Oceanographic Research Papers*, 122, pp. 72–80. Available at: https://doi.org/10.1016/J.DSR.2017.02.002.

Talley, L.D. *et al.* (2011) 'Atlantic Ocean', *Descriptive Physical Oceanography*, pp. 245–301. Available at: https://doi.org/10.1016/B978-0-7506-4552-2.10009-5.

Taylor, S.R. (1964) 'Abundance of chemical elements in the continental crust: a new table', *Geochimica et Cosmochimica Acta*, 28(8), pp. 1273–1285. Available at: https://doi.org/10.1016/0016-7037(64)90129-2.

Taylor, S.R. and McLennan, S.M. (1985) The continental crust: Its composition and evolution: an examination of the geochemical record preserved in sedimentary rocks. Oxford: Blackwell Scientific Pub.,Palo Alto, CA.

Torfstein, A., Winckler, G. and Tripati, A. (2010) 'Productivity feedback did not terminate the Paleocene-Eocene Thermal Maximum (PETM)', *Climate of the Past*, 6(2), pp. 265–272. Available at: https://doi.org/10.5194/cp-6-265-2010.

Torres, M.E. *et al.* (1996) 'Barite fronts in continental margin sediments: A new look at barium remobilization in the zone of sulfate reduction and formation of heavy barites in diagenetic fronts', *Chemical Geology*, 127(1–3), pp. 125–139. Available at: https://doi.org/10.1016/0009-2541(95)00090-9.

Turner, J. (2002) 'Zooplankton fecal pellets, marine snow and sinking phytoplankton blooms', *Aquatic Microbial Ecology*, 27(1), pp. 57–102. Available at: https://doi.org/10.3354/ame027057.

Vargas, C.A. *et al.* (2007) 'The relative importance of microbial and classical food webs in a highly productive coastal upwelling area', *Limnology and Oceanography*, 52(4), pp. 1495–1510. Available at: https://doi.org/10.4319/LO.2007.52.4.1495.

Venz, K.A. *et al.* (1999) 'A 1.0 Myr Record of Glacial North Atlantic Intermediate Water Variability from ODP Site 982 in the Northeast Atlantic', *Paleoceanography*, 14(1), pp. 42–52. Available at: https://doi.org/10.1029/1998PA900013.

Villanueva, J. *et al.* (2001) 'A latitudinal productivity band in the Central North Atlantic over the last 270 kyr: An alkelone perspective', *Paleoceanography*, 16(6), pp. 617–626. Available at: https://doi.org/10.1029/2000PA000543.

Webb, P. (2021) 'Patterns of Primary Production', in *Introduction to Oceanography*. Roger Williams University. Available at: https://rwu.pressbooks.pub/webboceanography/chapter/7-4-patterns-of-primary-production/.

Wedephl, K. (1991) 'The composition of the upper earth's crust and the natural cycles of selected metals', in E. Merian (ed.) *Metals and Their Compounds in the Environment: Occurrence, Analysis and Biological Relevance*. Hoboken, New Jersey, pp. 3–17.

Williams, R.H. *et al.* (2016) 'Glacial to Holocene changes in trans-Atlantic Saharan dust transport and dust-climate feedbacks', *Science Advances*, 2(11). Available at: https://doi.org/10.1126/SCIADV.1600445/SUPPL_FILE/1600445_SM.PDF.

Worne, S. *et al.* (2019) 'Coupled climate and subarctic Pacific nutrient upwelling over the last 850,000 years', *Earth and Planetary Science Letters*, 522, pp. 87–97. Available at: https://doi.org/10.1016/J.EPSL.2019.06.028.

Yoon, J.-E. *et al.* (2018) 'Reviews and syntheses: Ocean iron fertilization experiments – past, present, and future looking to a future Korean Iron Fertilization Experiment in the Southern Ocean (KIFES) project', *Biogeosciences*, 15(19), pp. 5847–5889. Available at: https://doi.org/10.5194/bg-15-5847-2018.

Yu, J. *et al.* (2019) 'More efficient North Atlantic carbon pump during the Last Glacial Maximum', *Nature Communications*, 10(1), p. 2170. Available at: https://doi.org/10.1038/s41467-019-10028-z.

Zan, J. *et al.* (2023) 'Mid-pleistocene links between Asian dust, Tibetan glaciers, and pacific iron fertilization', *Proceedings of the National Academy of Sciences of the United States of America*, 120(24), p. e2304773120. Available at: https://doi.org/10.1073/PNAS.2304773120/SUPPL_FILE/PNAS.2304773120.SD01.PDF.

Zhang, S. (2008) 'New insights into Ordovician oil shales in Hudson Bay Basin: Their number, stratigraphic position, and petroleum potential', *Bulletin of Canadian Petroleum Geology*, 56(4), pp. 300–324. Available at: https://doi.org/10.2113/GSCPGBULL.56.4.300.

Zhang, S. (2012) Ordovician stratigraphy and oil shale, southern Baffin Island, Nunavut - preliminary field and post-field data. Natural Resources Canada. Available at: https://doi.org/10.4095/291521.

Zhou, Y. *et al.* (2021) 'Enhanced iceberg discharge in the western North Atlantic during all Heinrich events of the last glaciation', *Earth and Planetary Science Letters*, 564, p. 116910. Available at: https://doi.org/10.1016/J.EPSL.2021.116910.

Chapter 4: Late Pleistocene North Atlantic fish productivity reconstructed using ichthyoliths

Abstract

Fishes dominate the upper trophic levels of aquatic ecosystems, play an important role in the global carbon cycle, and are of vital importance to humanity as a food source. Using the accumulation rate of fish microfossils (ichthyoliths) from two North Atlantic sediment cores, I reconstruct the palaeoproductivity of fishes from the late penultimate glacial period (PGP) to the mid-late last glacial period (LGP). Mean ichthyolith accumulation rate (IAR) was around three times higher in the temperate North Atlantic compared to the subpolar site, and both cores show significantly higher IAR during the last interglacial (LIG) relative to adjacent glacial intervals. Comparison with existing proxies suggests that the overall IAR is positively correlated with local temperature, but substantial variability in IAR is frequent, particularly during intervals of rapid environmental change. Temperature increases may positively affect mesopelagic fish productivity by increasing trophic transfer efficiency, or by modifying the mean trophic level at which these fishes are feeding. Morphometric analysis of these ichthyoliths could permit a more holistic assessment of these hypotheses. These findings suggest that organic carbon exported through the faecal pellets of fish undergoing diel vertical migration (DVM) may act as a negative feedback on the carbon cycle over geological timescales. Long-term mesopelagic fish production could increase in response to anthropogenic warming, but high frequency variability may dominate on millennial timescales.

Chapter contents

4.1. Introduction

Fishes are a ubiquitous and diverse vertebrate group in the present day. They have important roles in ecosystem function as consumers (Nelson, Grande and Wilson, 2016; Berkovitz and Shellis, 2017), as well as influencing global climate by transporting organic carbon from the surface to deep ocean (Davison *et al.*, 2013; Anderson *et al.*, 2019; Saba *et al.*, 2021).

Fishes are consumers occupying intermediate and higher trophic levels through the full depth of the modern ocean. The mesopelagic ocean (200–1000m) is the most productive habitat for fishes globally (Gjøsaeter and Kawaguchi K., 1980; Kaiser, 2011; Dornan *et al.*, 2022). Lanternfishes (family *Myctophidae*) are an abundant clade of mesopelagic fishes, which typically feed on crustacean mesozooplankton, such as copepods, and are themselves a food source for larger pelagic fishes (Gjøsaeter and Kawaguchi K., 1980; Catul, Gauns and Karuppasamy, 2011; Pereira *et al.*, 2011; Hudson *et al.*, 2014; Schwarzhans and Carnevale, 2021). Notable mesopelagic species in the modern North Atlantic include the glacier lanternfish (*Benthosema glaciale*; the most abundant single species), the Arctic telescope lanternfish (*Protomyctophum arcticum*), and the tropical–subtropical Bermuda lanternfish (*Hygophum hygomii*; Hudson et al., 2014).

Fishes influence the carbon cycle via the vertical transport of carbon-rich organic matter from the surface ocean to depth through diel vertical migration (Davison *et al.*, 2013; Irigoien *et al.*, 2014; Anderson *et al.*, 2019; Behrenfeld *et al.*, 2019; Kelly *et al.*, 2019). Faecal pellets produced by fishes have relatively high sinking rate and export potential compared to the carcasses and faecal matter of their zooplankton prey (Turner, 2002; Frangoulis *et al.*, 2011). The contribution of fish faecal pellets to total export is poorly constrained (Davison *et al.*, 2013; Hudson *et al.*, 2014) but has been estimated at 3–29% of total export from the euphotic zone (Saba *et al.*, 2021), though modelling suggests the proportional contribution of faecal pellets to total export is highest in the stratified pelagic ocean (Nowicki, DeVries and Siegel, 2022).

The fossil record of fishes spans from the Cambrian to the present-day (Shu et al., 1999, 2003; Morris, 2008), and the fish macrofossil record has facilitated the reconstruction of fish palaeoecology and evolution throughout the Phanerozoic (e.g. Hurley et al., 2006; Friedman, 2010; Near et al., 2012; Giles et al., 2017). However, the microfossil record of fishes remains relatively underutilised in comparison. Fish microfossils from pelagic sediments have enormous potential to improve our understanding of the ecological and evolutionary history of open-ocean fishes, which are unlikely to be preserved in easily accessible (often shallow marine) sedimentary rocks.

Ichthyoliths are the robust microfossil remains of fishes, consisting of actinopterygian (ray-finned fishes) teeth and chondrichthyan (sharks and rays) dermal denticles. Both teeth and denticles, which are tooth-like scales that cover the skin of cartilaginous fishes, are composed of dissolution-resistant bioapatite (calcium phosphate) and are a common component of seafloor sediment throughout the global ocean (Doyle and Riedel, 1979, 1985; Johns, Barnes and Narayan, 2006; Sibert *et al.*, 2017). For example, ichthyolith concentrations are extremely high in Pacific red clays, where corrosive bottom waters dissolve almost all other biogenic sediment components (Doyle and Riedel, 1979, 1985; Sibert, Hull and Norris, 2014; Sibert *et al.*, 2016).

Extant actinopterygian fishes are polyphyodont, meaning their teeth are replaced continuously throughout life, and have two sets of dentitions – an oral and pharyngeal jaw (Nelson, Grande and Wilson, 2016; Berkovitz and Shellis, 2017; Huysseune and Witten, 2024). The nature of tooth replacement in actinopterygians remains poorly understood, but limited research suggests that tooth

resorption may be common in some lineages (Bemis, Giuliano and McGuire, 2005; Collins, 2023). The two dentitions may be functionally distinct, with the oral jaw used for predation and the pharyngeal jaw used for processing food (Wise and Stock, 2006; Nelson, Grande and Wilson, 2016; Carr, Summers and Cohen, 2021). Attributing fossil teeth to a phylogenetic lineage of actinopterygians is highly challenging due to the extreme diversity and strong convergence of morphotypes across and within clades (Nelson, Grande and Wilson, 2016; Berkovitz and Shellis, 2017; Martin and Davis, 2020; Huysseune and Witten, 2024). Although data is highly limited (particularly for deep sea species), tooth shedding rates are likely variable among species, and tooth resorption is common in both extant and ancient fishes (Bemis, Giuliano and McGuire, 2005; Johanson, 2017). However, the vast majority of teeth in prior ichthyolith studies are found in the <100 µm size fraction (Doyle and Riedel, 1985; Werner, 2019; Britten and Sibert, 2020; Sibert *et al.*, 2020), indicating that tooth flux to the seafloor is probably dominated by small species, juvenile fish, and the pharyngeal tooth battery (Sibert *et al.*, 2017). The high relative abundance of small teeth in ichthyolith assemblages reflects the dominant contribution of small mesopelagic fishes to total marine vertebrate biomass (Gjøsaeter and Kawaguchi K., 1980; Irigoien, Hulsman and Harris, 2004; Anderson *et al.*, 2019; Clavel-Henry *et al.*, 2020). Tooth structure may also be an important factor in preservation over geological timescales, with possibly increased preservation for teeth with high enamel to dentine ratios (Sibert *et al.*, 2017).

Chondrichthyan dermal denticles were a significant component of pelagic ichthyolith assemblages throughout the Mesozoic and early Cenozoic (Doyle and Riedel, 1985; Sibert, Hull and Norris, 2014; Sibert and Norris, 2015; Sibert *et al.*, 2016; Britten and Sibert, 2020), but declined substantially during the early Miocene, likely due to a global extinction of pelagic sharks (Sibert and Rubin, 2021). No denticles were found in the Pleistocene samples used in the current work.

Ichthyolith accumulation rate is a proxy for fish biomass production, allowing for comparisons in the productivity of fishes in both space and time (Sibert *et al.*, 2017). This approach has been used to reconstruct fish productivity across the end-Cretaceous mass extinction (Sibert, Hull and Norris, 2014; Sibert and Norris, 2015; Sibert *et al.*, 2018), the early Palaeogene (Britten and Sibert, 2020), the Eocene-Oligocene (Sibert *et al.*, 2017), the past 85 Myr (Sibert *et al.*, 2016), and the Pleistocene (Werner, 2019).

Only one of these previous studies has used ichthyoliths to investigate open ocean fish ecology during the Pleistocene. Werner (2019) produced a low-resolution dataset of Pleistocene IAR at ODP Site 982, IODP Site U1313, and three other global sites that found high latitude IAR was approximately one order of magnitude lower than equatorial and subtropical IAR in the pelagic ocean, positing that the subpolar ocean may be less productive for fishes than modern observations have suggested. However, Werner (2019) did not use the 38–63 µm sediment size fraction, which was the most common ichthyolith size fraction found in the current work, and utilised an alternative processing method that is likely to result in the loss of a higher proportion of total ichthyoliths (Sibert *et al.*, 2017). IAR measurements were also conducted at a relatively coarse temporal resolution, which did not permit analysis of changes between glacial and interglacial intervals. Previous work has shown a positive correlation of IAR with water temperature across latitudes (Sibert and Norris, 2015), and through time (Britten and Sibert, 2020) in the early Cenozoic. Pelagic IAR was relatively stable across intervals of major environmental change in the geological past, such as the end-Cretaceous mass extinction event (Sibert, Hull and Norris, 2014) and the Eocene-Oligocene transition (Sibert *et al.*, 2020).

In this chapter, I produce a new high-resolution ichthyolith accumulation rate (IAR) record for the late Pleistocene North Atlantic using two sediment cores: IODP Hole U1313A and ODP Hole 982B. I use this

new dataset to describe changes in fish biomass production and its relationship to environmental change during glacial-interglacial cycles over the past 200 kyr. I test the following hypotheses:

- Fish production declined following episodes of more rapid environmental change, such as glacial-interglacial transitions.
- Glacial and interglacial intervals experienced significantly different IAR.
    - IAR declines during glacial intervals.
    - IAR increases during interglacial intervals.

4.2. Methods

I extracted ichthyoliths from samples with an approximate volume of 15cc from two North Atlantic sediment cores: 23 from ODP Hole 982B and 32 from IODP Hole U1313A. These samples are pelagic carbonates, as described in Chapter 1. Each 15 cc sample underwent multi-step processing modified from Sibert et al. (2017), which is described in detail in this section. Sample drying, washing, sieving and dissolution took place in the Oxford University Museum of Natural History research lab, University of Oxford, and in the Elemental and Chemistry Labs at the Department of Earth Sciences, University of Oxford, between November 2020 and December 2023.

Samples were placed in an oven at 50°C until they dried, which was determined by their weight remaining constant for two consecutive days. The dry sample was then wet washed over a 38 µm sieve until water passing through the sieve became visibly clear. At this point the remaining sample was transferred to a filter paper and dried overnight at 50°C. The sample was then dry sieved in a brass 38 µm and 125 µm sieve stack. The >125 µm sediment fraction was stored for future analysis of foraminifera. Earlier work has indicated that the vast majority of ichthyoliths are found in the 38–125 µm size range (Britten and Sibert, 2020; Sibert *et al.*, 2020). Nonetheless, to test the possibility of ichthyoliths being retained in the coarsest size fraction, I picked three >125 µm fractions for both cores, including glacial and interglacial intervals. I found no ichthyoliths in any of the three >125 µm fractions from ODP Hole 982B, and only zero, three, and four ichthyoliths in the three >125 µm fractions from IODP Hole U1313A. For the latter core, this represents a maximum underestimate of total ichthyolith counts of up to 8%. Whilst it would be preferable to pick the entire >38 µm fraction, including the >125 µm fraction, the value of retaining the calcareous coarse fraction for future study was deemed preferable to destroying this relatively limited sample.

I dissolved the 38-125 µm fraction in 5-10% acetic acid for 2–4 hours to remove the proportionally dominant carbonate component of the sediment. Any remaining undissolved sample was rinsed into filter paper and left to dry at 50°C overnight.

I then stained the remaining sample by submerging it in a 1% potassium hydroxide (KOH) solution with a small amount of Alizarin Red S dye powder for 24–48 hours (Sibert *et al.*, 2017), which was added until the solution turned a deep purple colour. Applying this calcium-specific dye permits easier recognition of the usually-transparent teeth at the picking stage. The remaining sample was again rinsed into filter paper and left in an oven at 50°C overnight.

For the earliest processed samples, the dyed sediment was transferred into a sieve stack containing a base catcher, 63 µm, and 90 µm sieves. The 38–63 µm, 63–90 µm, and 90–125 µm sediment fractions were then each picked separately by distributing a small amount of material in a black-backed metal

picking tray and identifying dyed ichthyoliths using a stereo microscope. Using three size fractions allows quantification of the relative contribution of each size to the total ichthyolith assemblage, yielding morphological information of potential biomechanical relevance (e.g. Sibert and Norris, 2015; Britten and Sibert, 2020). However, compared to transferring material directly from the filter paper to the picking tray, these additional steps also increased the time taken to process and pick samples, sieve cleaning time, and the possibility of losing teeth during processing. Therefore, for later samples, I picked the 38–125 µm size fraction without segregating the sediment by size by transferring directly from filter paper on to the picking tray. This approach does not prohibit the future acquisition of ichthyolith size information through imaging. I identified ichthyoliths on the picking tray using a stereo microscope and transferred them onto a separate carboard-backed slide for retention.

I imaged all extracted material using a Keyence VHX 7100 microscope at the Woods Hole Oceanographic Institution in January 2024 and used these images to screen putative ichthyoliths and subtract any misidentified material from the final counts ichthyolith totals.

4.2.1. LST method

Most ODP Hole 982B samples retained a significant proportion of non-biogenic silicate grains following the processing outlined above. This silicate material is likely to have originated from icebergs due to the high IRD flux to this location (Baumann and Huber, 1999; Venz *et al.*, 1999). I therefore used heavy liquid separation to further reduce the non-ichthoylith component of sediment for eight remaining ODP Hole 982B samples that had been processed but not yet picked, to improve the efficiency of subsequent picking.

I used LST Fastfloat (sodium heteropolytungstate; $Na_6W_{12}O_{39}$ xH_2O), which is a heavy liquid with a density of 2.80 ± 0.02 g/mL, to separate the fully processed but unpicked ODP Hole 982B samples at the Earth Sciences General Chemistry Laboratory at the University of Birmingham in March 2023. LST Fastfloat has a density lower than ichthyolith-bound calcium phosphate (3.1 g/mL) but denser than quartz silt (2.6-2.7 g/mL; Sibert et al., 2017).

I transferred dry samples to a 15 mL test tube. In a fume hood, I added 10 mL LST Fastfloat to the sample in 1 mL increments, agitating the solution between additions of LST and then allowing the solution to settle for at least five hours. Subsequently, I extracted the low-density material (floats) and high density ichthyolith-bearing material (sinks) from solution using a pipette. I placed floats and sinks into different filter papers and allowed them to dry in an oven at 45°C overnight. I then transferred both floats and sinks into glass vials prior to picking.

I measured the post-separation mass of all sinks and floats to test the efficacy of the process. A mean of 90.0% (ranging from 82.4% to 95.8%) of all material mass was found in floats, whilst a mean of only 10.0% was in the ichthyolith-bearing sinks. I picked three of the eight floats and found no ichthyoliths retained in this portion, yielding high confidence that the separation was successful.

It was not necessary to apply LST to the U1313A samples, as terrigenous silica formed a much smaller proportion of the total processed sample, probably due to the southerly location and comparatively low IRD flux to this site (Smith *et al.*, 2013; Lang *et al.*, 2016). Total picking time was therefore much lower than for ODP Hole 982B. Every additional processing step yields the possibility of losing ichthyoliths in transfer, and so it is preferable to minimise these as much as possible (Sibert *et al.*, 2017).

4.2.2. Ichthyolith accumulation rate

Ichthyolith counts were converted into ichthyolith accumulation rates to enable comparisons between samples using Equation 4.1.

$$IAR = N * \rho * S \qquad \text{(Equation 4.1)}$$

where N is ichthyolith concentration (ich g^{-1}), ρ is sediment dry bulk density (g cm^{-3}), and S is linear sedimentation rate (cm kyr^{-1}). I determined the density of samples using a linear interpolation of discrete dry density values published in the initial reports for IODP Site U1313 (Expedition 306 Scientists, 2006) and ODP Site 982 (Shipboard Scientific Party, 1996). Sample sedimentation rates were calculated using the age models described in Chapter 1. IAR has the unit ichthyoliths cm^{-2} kyr^{-1}.

4.2.3. Statistical tests

I conducted all statistical tests using R version 4.4. I tested for significant differences between the mean NAR values in glacial and interglacial intervals using two-tailed Mann-Whitney U Tests (MWU; Mann and Whitney, 1947), as the data were nonparametric.

4.3. Results

For samples from the past 200 ka, I counted a total of 470 and 980 ichthyoliths in ODP Hole 982B and IODP Hole U1313A, respectively (Figure 4.1), with a mean number of ichthyoliths per sample of 20 and 31, respectively. I counted an additional 115 and 74 ichthyoliths in ODP Hole 982B and IODP Hole U1313A, respectively, from samples excluded from the final analysis due to either the sample age being greater than 200 ka (3 samples) or problems during sample processing, such as irretrievable loss of a sample portion (3 samples). Screening of extracted ichthyoliths after imaging resulted in the deduction of 65 ichthyoliths from the initial total, meaning an accurate initial ichthyolith identification rate of 95.5%. This value does not include ichthyoliths that may have been missed during picking.

4.3.1. Ichthyolith abundance

For ODP Hole 982B, ichthyoliths per sample ranged from 0 to 43, resulting in an abundance of 0–3.0 ich g^{-1}, with a mean 1.3 ich g^{-1}. For IODP Hole U1313A, total ichthyoliths per sample ranged from 4–66, resulting in an abundance of 0.4–4.3 ich g^{-1} and a mean 2.1 ich g^{-1}. All ichthyoliths were identified either as teeth or jaw elements containing teeth, while no denticles were identified in the 1,639 total ichthyoliths, including those not included in final analyses.

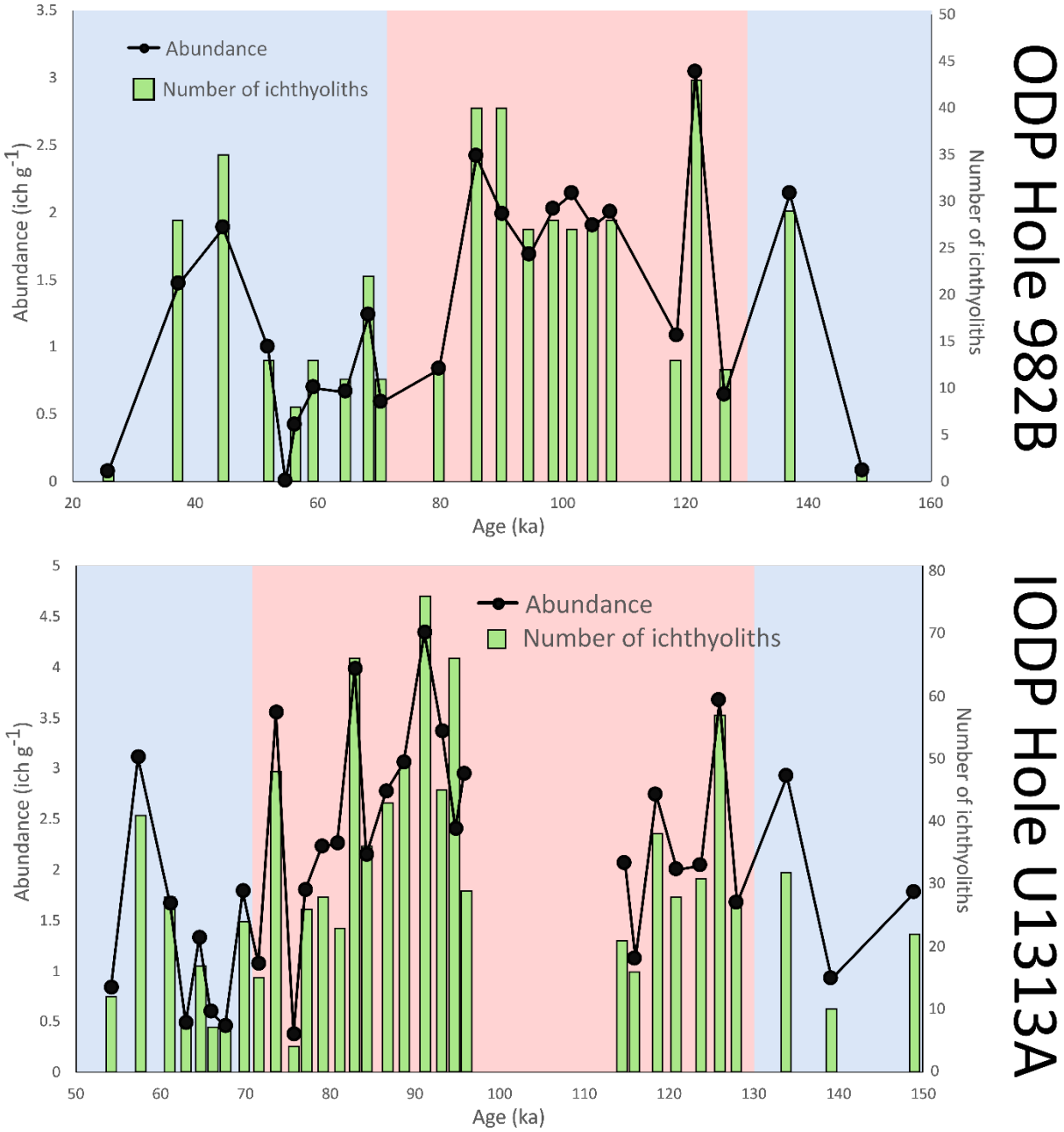

Figure 4.1 – Ichthyolith counts (green bars) and abundances (black circles) for ODP Hole 982B (top) and IODP Hole U1313A (bottom). Background colours indicate glacial intervals (blue) or the LIG (red).

4.3.2. Ichthyolith sizes

For those samples that were split into three size fractions prior to picking (n_{982B}=15, n_{U1313A}=10), the finest (38–63 µm) size fraction contained more ichthyoliths than either the 63–90 µm or 90–125 µm size fractions in both cores. The majority (65%) of ichthyoliths were present in this size fraction in ODP Hole 982B, and a plurality (42%) of ichthyoliths were found in the finest fraction for IODP Hole U1313A. The finest size fraction contained the greatest or equal greatest number of ichthyoliths for all ODP Hole 982B samples and for seven of ten IODP Hole U1313A samples. Medium (63–90 µm) and coarse (90–125 µm) ichthyoliths contributed a substantially-higher proportion of total ichthyoliths at IODP Hole

U1313A (34% and 24% respectively) compared to ODP Hole 982B (25% and 10% respectively), which is shown in Figure 4.2.

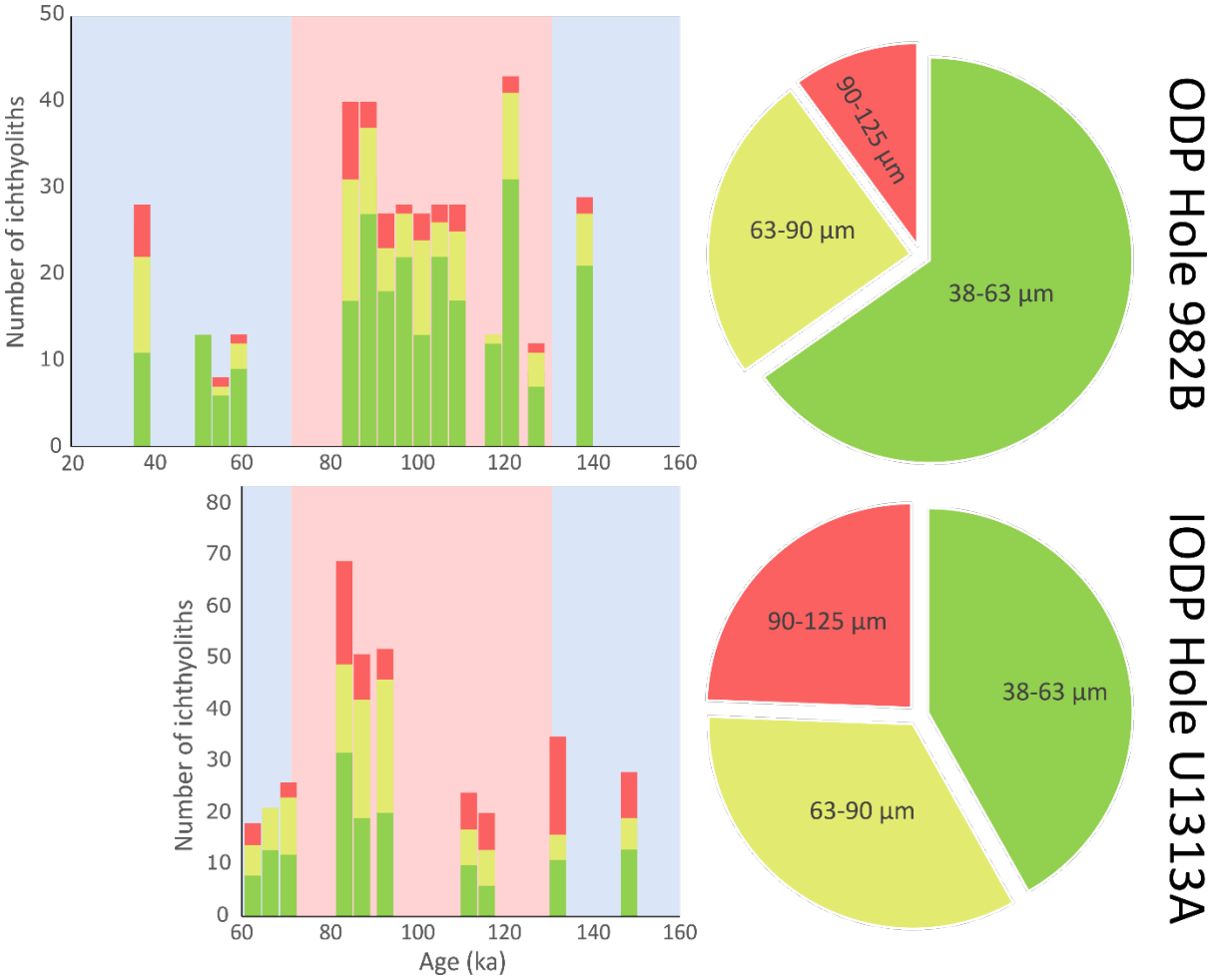

Figure 4.2 – Detail of ichthyolith size fractions in ODP Hole 982B (top) and IODP Hole U1313A (bottom). Stacked columns show the number of 38–63 µm (green), 63–90 µm (yellow), and 90–125 µm (red) ichthyoliths in each sample and the age of that sample. Bar chart background colours indicate glacial intervals (blue) or the LIG (red). Pie charts show the proportions of each ichthyolith size fraction for the full, size-separated dataset.

4.3.3. Ichthyolith accumulation rate

Maximum IAR at ODP Hole 982B is 8.9 ich cm^{-2} ka^{-1}, which occurred in the early LIG at 122 ka. Mean IAR for ODP Hole 982B is 3.7 ich cm^{-2} ka^{-1} and the standard deviation across all samples is 2.4 ich cm^{-2} ka^{-1}. IAR variation is mainly driven by changes in ichthyolith abundance rather than dry bulk density (1.4–1.5 g cm^{-3}) or sedimentation rate (1.0–2.2 cm kyr^{-1}). High and stable IAR is sustained in six adjacent samples in the mid-LIG (108–86 ka), but IAR more than halves in the late LIG at 80 ka, where it remains low into the early LGP before increasing again after 52 ka.

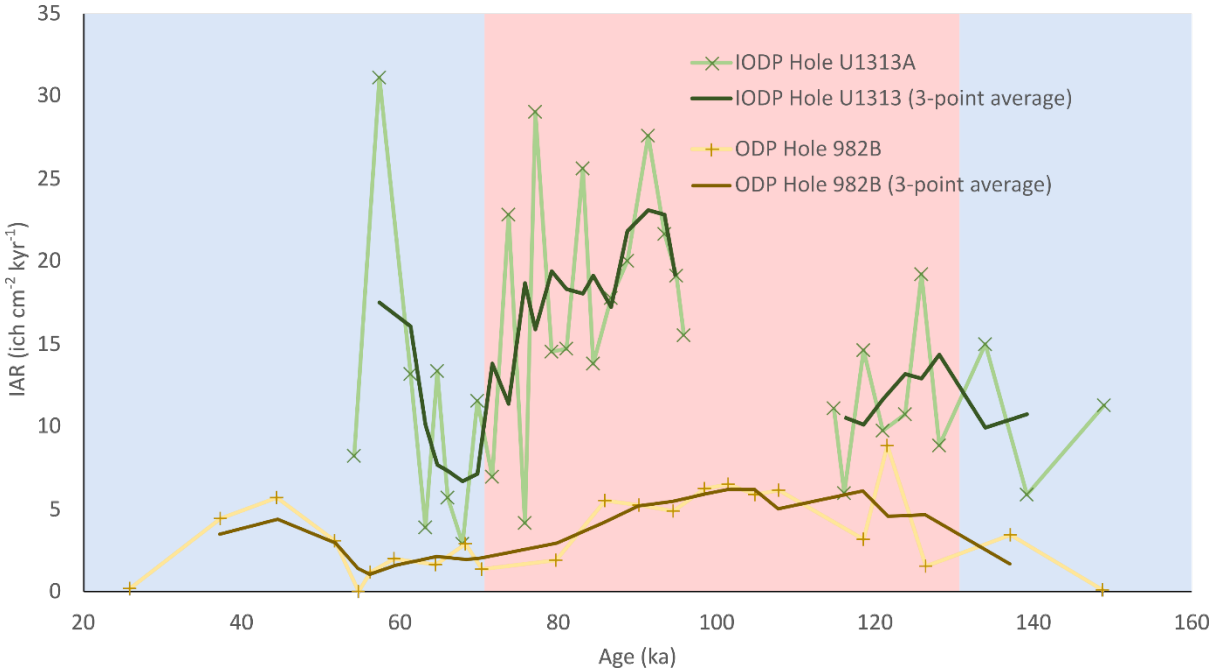

Figure 4.3 – IAR measurements for IODP Hole U1313A (green crosses) and ODP Hole 982B (yellow pluses), including 3-point running averages (dark green and dark yellow lines, respectively). Background colours show glacial intervals in blue and the LIG in red.

For IODP Hole U1313A, IAR ranges from 2.9 ich cm^{-2} ka^{-1} at 68 ka, to 31.1 ich cm^{-2} ka^{-1} at 57 ka, with a mean of 13.8 ich cm^{-2} ka^{-1}, which is almost four times greater than the subpolar core. The standard deviation of 7.4 ich cm^{-2} ka^{-1} for IAR at this site is over three times greater than the subpolar site. As with ODP Site 982, IAR variation is predominantly driven by changes in ichthyolith abundance rather than dry bulk density (1.4–1.6 g cm^{-3}) or sedimentation rate (2.0–10.9 cm kyr^{-1}). Whilst the highest IAR in the dataset for this core occurred during the LGP, the next 11 highest IARs all occur during the LIG. The late LIG sees the highest sustained IAR in the dataset, with IAR in all 11 samples from 77–96 ka above the mean. Five of the seven lowest IAR values occur in between 63–76 ka across the LIG–LGP boundary, although none of these samples are adjacent.

MWU tests show that there were significant differences between glacial and interglacial IAR for ODP Hole 982B ($n_{glacial}$=12, $n_{interglacial}$=11, W=19, p=0.004) and IODP Hole U1313A ($n_{glacial}$=11, $n_{interglacial}$=21, W=65, p=0.04728). In both cases, interglacial (LIG) IAR is higher than glacial (combined LGP and PGP) IAR. A comparison of glacial and interglacial IAR for both cores is shown in Figure 4.4.

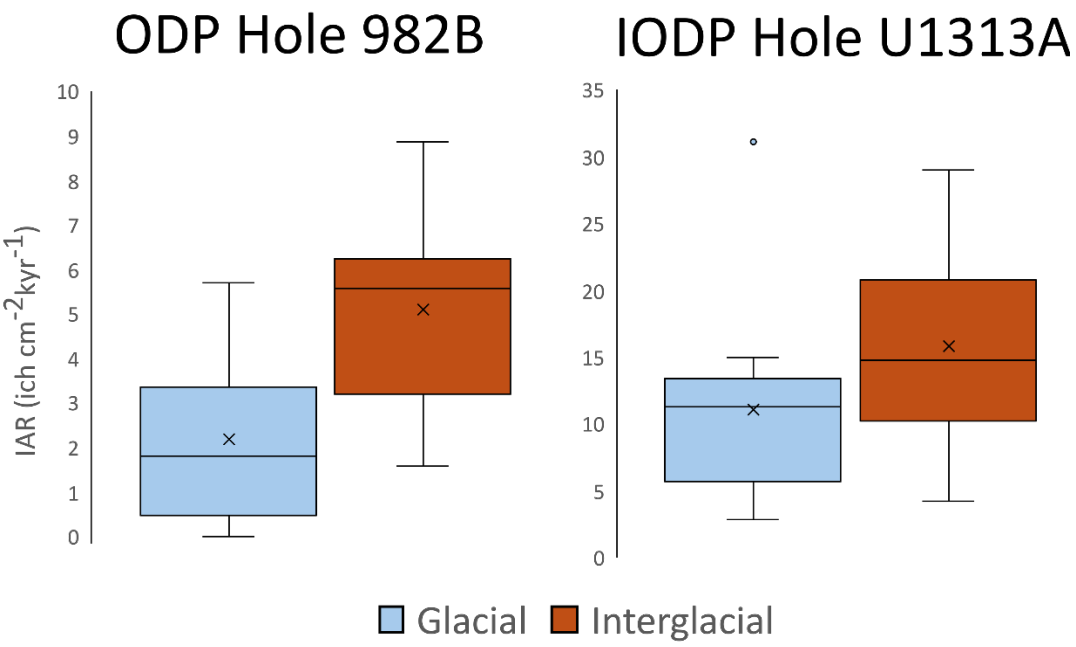

Figure 4.4 – Box plots of IAR in ODP Hole 982B (left) and IODP Hole U1313A (right) for glacial (LGP and PGP) and interglacial (LIG) intervals. Horizontal lines with boxes show mean and crosses indicate median values.

4.3.4. Diagenesis and preservation

Ichthyolith preservation was good throughout the sections in both cores with no evidence of surface corrosion, suggesting no large-scale impact from changing bottom water or pore water conditions across glacial-interglacial cycles. Most teeth preserve both a dentine body and enameloid tip, although in some cases one of the two of these was absent, implying that the whole tooth would be of a larger size than the remaining fragment. Basal fragmentation of teeth was common, particularly in teeth with a wide pulp cavity, but this did not prevent their identification.

Objects that were initially misidentified as ichthyoliths and later subtracted from the final counts predominantly consisted of bone fragments, which were far more abundant in these samples than other ichthyolith studies using older sediments (Sibert, personal communication). This is perhaps unsurprising, given the short diagenetic history of these samples relative to the late Mesozoic and early Cenozoic material used in earlier studies (e.g. Sibert, Hull and Norris, 2014; Sibert et al., 2020; Sibert and Rubin, 2021). In older sediments, fish tooth enameloid can sometimes be the sole remaining piscine fossil content in sediment (Sibert *et al.*, 2017).

Eleven ichthyoliths (0.7%) in the dataset consist of jaw elements containing one or more teeth (Figure 4.5), nine of which were found in IODP Hole U1313A and two in ODP Hole 982B. I also found numerous other potential jaw elements in samples from both cores, but did not count these as ichthyoliths as none of them contained obvious teeth. Despite sometimes containing more than one tooth, jaw elements were counted as individual ichthyoliths as many of the visible teeth were finer than 38 µm and would therefore not otherwise have been retained and counted. These jaw elements demonstrate that an unquantified portion of <38 µm are lost using standard ichthyolith processing procedures. The

<38 µm fraction is not counted due to the difficulty in extracting teeth from finer material, but this may bias interpretations that use the IAR proxy.

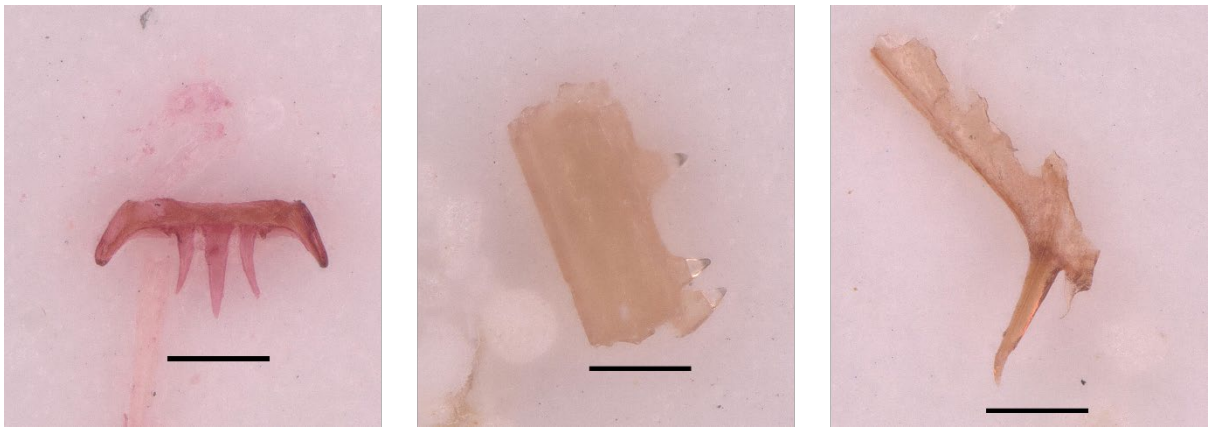

Figure 4.5 – Segments of fish jaws containing in-situ teeth, some of which have at least one axis smaller than 38 µm. The black bar has a width of 100 µm.

4.4. Discussion

In this chapter, I set out to assess whether fish production varied between glacial intervals and interglacial intervals in the late Pleistocene, and to establish whether there was a relationship between environmental variables and fish production as reconstructed using IAR.

4.4.1. IAR comparison to existing records

Werner (2019) found a mean Pleistocene IAR of 4.5 ich cm^{-2} kyr^{-1} at IODP Site U1313 and 0.7 ich cm^{-2} kyr^{-1} at ODP Site 982, compared to the 13.8 ich cm^{-2} kyr^{-1} and 3.7 ich cm^{-2} kyr^{-1}, respectively, in this study. Whilst the low relative IAR at ODP Site 982 is a consistent finding between both studies, mean IAR in this study is between three to five times greater than the older work. This is likely because Werner (2019) did not retain and count ichthyoliths finer than 63 µm, which were a plurality of teeth in both sites, thus producing a substantial underestimate relative to this research.

Published IAR records for comparable (i.e. >38 µm fraction) size fractions exist for a variety of pelagic sediment cores spanning the Cretaceous-Palaeogene (Sibert, Hull and Norris, 2014) and Eocene-Oligocene (Sibert *et al.*, 2020). For ODP Site 982, IAR range is comparable to that of the Eocene-Oligocene North Atlantic (IODP Site U1406) and South Atlantic (ODP Site 522). Mean IAR at IODP Site U1313 is over three times greater than the next highest published IAR (Figure 4.6).

The relatively high IAR recorded at IODP Site U1313 could be because this ichthyolith assemblage captures a greater breadth of trophic levels than other sites – a possibility considered in greater detail in section 4.4.2. IODP Site U1313 also has a relatively high sedimentation rate (Expedition 306 Scientists, 2006; Naafs, Hefter and Stein, 2013) compared to the other sites in the Figure 4.6 comparison (including ODP Site 982), so it is possible that sedimentation rates exert a significant control on the likelihood of ichthyolith preservation over geological timescales.

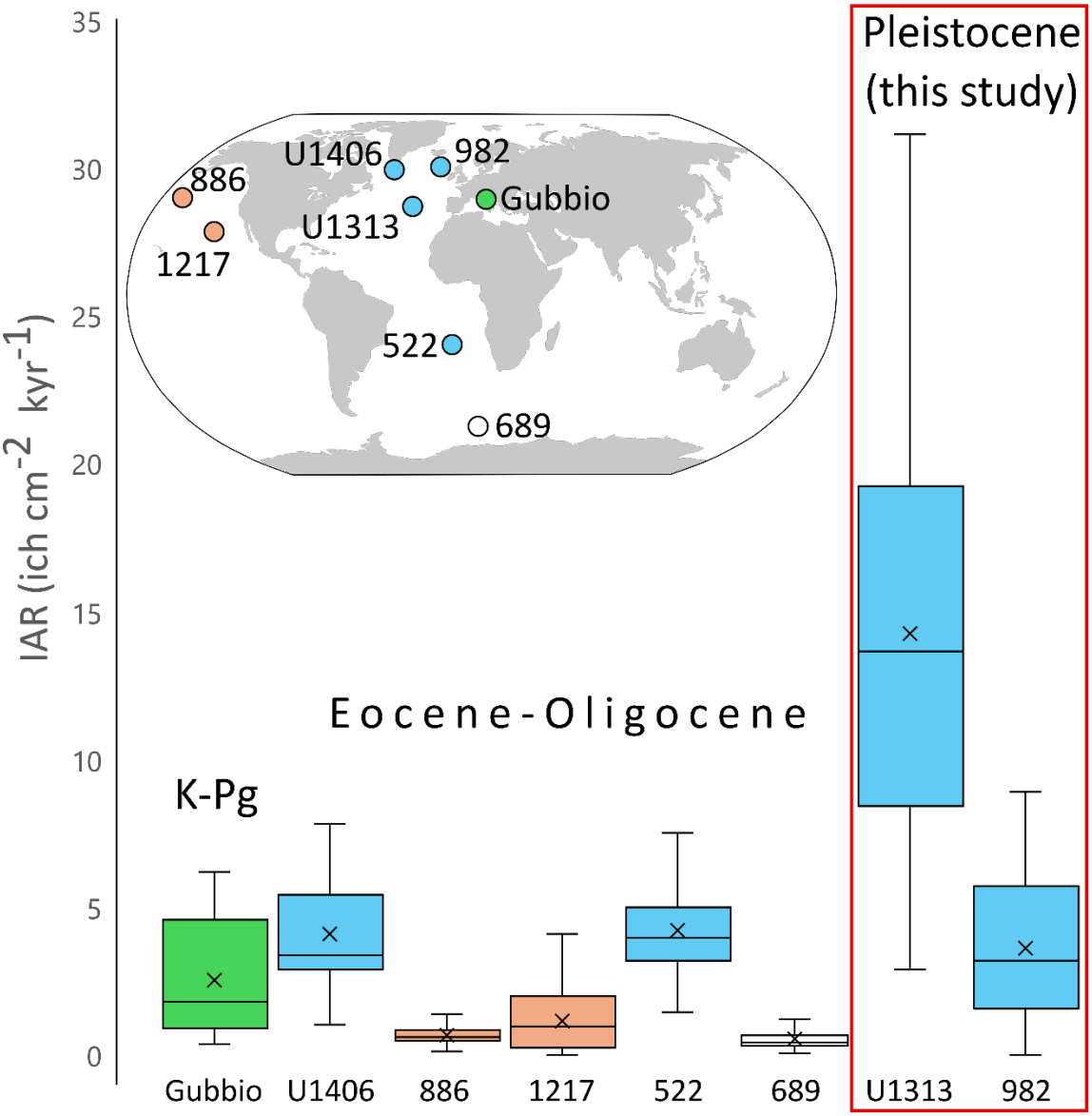

Figure 4.6 – Comparison of IAR from the two sites in this study (outlined in a red box on the far right) with existing published IAR values from the Cretaceous-Palaeogene Tethys Sea (Sibert, Hull and Norris, 2014), and the Eocene-Oligocene Pacific, Atlantic, and Southern Ocean (Sibert *et al.*, 2020). Sites are shown in the modern world map (whose geography differs), and site names are listed beneath corresponding boxes. Box and map fill colours indicate contemporary IAR reconstruction ocean basin: Atlantic (blue), Pacific (red), Tethys (green), Pacific (red), and Southern (white). Horizontal line within a box shows the mean IAR and crosses show median values. Upper and lower bounds of boxes show upper and lower quartile, respectively, and whiskers show full range of values.

4.4.2. Comparing IAR between sites

An extensive body of prior research has established that the high latitude ocean is a generally more biologically productive environment than the oligotrophic subtropical ocean, as demonstrated by the strong seasonal resupply of allochthonous nutrients to the mixed layer (Moore *et al.*, 2013; Behrenfeld

and Boss, 2014; Poulton *et al.*, 2017; Browning and Moore, 2023), higher annual primary production (Webb, 2021; NASA Goddard Space Flight Center, Ocean Ecology Laboratory and Ocean Biology Processing Group, 2022) , and fewer average trophic steps between primary producers and apex predators (Sommer *et al.*, 2002; Sigman and Hain, 2012; Armengol *et al.*, 2019). Ichthyolith accumulation rates resolved in this study initially appear to contradict these findings, as mid-latitude IAR is substantially higher than subpolar IAR throughout almost the entirety of the study interval, including the early LIG when oceanic conditions were likely comparable to those of the Holocene (Shackleton, 1969; Tzedakis *et al.*, 2009; Kleinen, Brovkin and Munhoven, 2016). If IAR is taken as a proxy for fish biomass (e.g. Sibert et al., 2016, 2017; Britten and Sibert, 2020), this would appear to suggest that the mid-latitude North Atlantic is more productive for fishes than the subpolar region during the Pleistocene, as was previously suggested by Werner (2019).

This analysis is highly dependent on how IAR is interpreted as a proxy (see Methodological caveats section below). As this study only uses fine sediment (<125 µm), and small mesopelagic fishes dominate the total abundance of piscine fauna in the global ocean (Gjøsaeter and Kawaguchi K., 1980; Kaiser, 2011; Dornan *et al.*, 2022), IAR is likely to be primarily a signal of the abundance of these small, often planktivorous fauna. Higher relative proportions of coarser (63–90 µm and 90–125 µm) ichthyoliths could indicate that abundant mid-latitude fish fauna may occupy a broader range of body sizes and trophic levels compared to the subpolar site, assuming allometric scaling of tooth and body size in mesopelagic fishes (Sibert and Norris, 2015; Britten and Sibert, 2020). Whilst it is not possible to confidently test the hypothesis of greater functional diversity among midlatitude mesopelagic fishes compared to those in the subpolar ocean using the data generated in this study, this could be tested in future through morphometric analysis (Sibert and Norris, 2015; Sibert *et al.*, 2018, 2020).

4.4.3. Temporal IAR changes

As with other ecosystem proxies considered in Chapter 2 and Chapter 3, the IAR record here demonstrates distinct differences between glacial and interglacial intervals. At both sites, mean IAR is significantly higher during the LIG relative to glacial intervals (Figure 4.4), although it should be noted these IAR records span a shorter interval than proxies generated in the previous two chapters. For example, due to sediment core depletion, no samples in either core are coincident with the Last Glacial Maximum, which was the most extreme glacial climate of the LGP and occurred close to its conclusion (Rasmussen *et al.*, 2003; Lisiecki and Raymo, 2005; Annan and Hargreaves, 2013), although the youngest sample (26 ka) in ODP Hole 982B has the lowest non-zero IAR of any sample. These findings indicate that a notable relationship exists between climate state and fish production in the pelagic ocean, with IAR being positively correlated with warmer temperatures.

Earlier studies have shown that, as well as abundance, fish body sizes may have changed significantly through time in response to environmental change. Agiadi et al. (2023) found, using otoliths, that the median size of Mediterranean lanternfishes decreased during a mid-Pleistocene interglacial (MIS 19) relative to adjacent glacial intervals. A similar trend on a spatial axis has also been reported in modern Southern Ocean lanternfish populations, where mesopelagic fish body size relative to zooplankton prey tends to decrease as deep-water temperature increases (Eskuche-Keith *et al.*, 2024). If a similar trend occurred in late Pleistocene North Atlantic mesopelagic fish populations, IARs reported in the current study may be underestimated during the LIG relative to glacial intervals due to the proportionally greater loss of ichthyoliths finer than 38 µm during processing (assuming allometric scaling of fish and tooth size), hence increasing the overall IAR disparity between glacial intervals and interglacial intervals. However, evidence from size distributions in the generated datasets for these

cores (Figure 4.2) does not indicate a reduction in the median size of interglacial ichthyoliths in the North Atlantic.

Primary production has strong potential to produce amplified impacts on fish productivity through bottom-up trophic controls, which may be either independent or co-varying with temperature (Chassot *et al.*, 2010; Blanchard *et al.*, 2012; Atkinson *et al.*, 2024). A full comparison of the productivity datasets generated in this thesis is the subject of Chapter 5, so discussion here is limited to comparisons of IAR with pre-existing productivity datasets, graphically summarised in Figure 4.7 and Figure 4.8. These datasets consist of: C37-alkenone accumulation rate at ODP Site 982 (Bolton *et al.*, 2011), which are produced by haptophyte algae and have been used to reconstruct phytoplankton biomass (Volkman *et al.*, 1995; Raja and Rosell-Melé, 2021); and benthic (*Cibicidoides* spp.) $\delta^{13}C$ for both ODP Site 982 (Venz *et al.*, 1999) and ODP Site 607 (the site reoccupied by IODP Site U1313; Raymo et al., 1990).

Correlation between C_{37}-alkenone accumulation rate (Bolton *et al.*, 2011) and IAR for ODP Site 982 is generally weak, suggesting that fish production is not a function of haptophyte algae productivity, though there are notable increases in both metrics during the onset of interglacial climate in the early LIG. Similarly, the benthic $\delta^{13}C$ record (Venz *et al.*, 1999) for this site shows negative excursions during the early LIG of up to 1‰, with a similar excursion documented for ODP Site 607 (the precursor to IODP Site U1313; Raymo et al., 1990), but this is likely a result of the elevated influence of low $\delta^{13}C$ southern-sourced bottom waters, rather than a function of surface productivity (Venz *et al.*, 1999). Beyond the early LIG, benthic $\delta^{13}C$ has weak agreement with the IAR record (Figure 4.7). Whilst these two proxies do not capture all surface ocean productivity, the evidence presented here does not support the conclusion that late Pleistocene North Atlantic fish productivity is solely a function of primary production.

Elevated fish production during warm intervals was previously documented by Britten and Sibert (2020), who found a positive nonlinear relationship between deep water temperature and pelagic Pacific IAR during the Palaeogene greenhouse climate. Using a simple ecosystem model, they found that this relationship was most parsimoniously explained by small changes in trophic transfer efficiency, with weaker significance relationships between IAR and either ecosystem structure, or primary production. Modern observations indicate that zooplankton grazing rates can be increased by elevated water temperature (Chen *et al.*, 2012; Schmoker, Hernández-León and Calbet, 2013), which may in turn increase energetic transfer to higher trophic levels and allow a greater proportion of energy produced by primary production to become fish biomass. Fishes in warm freshwater systems have been reported to feed higher in the food web than the same species in colder waters, functionally leading to a decrease in the trophic level of those fishes and thus increased energy transfer with temperature (O'Gorman *et al.*, 2016). However, warming on anthropogenic timescales is generally predicted to lead to a reduced fish biomass on decadal-centurial timescales through a combination of increased metabolic costs on aquatic organisms (Barneche *et al.*, 2021; Eddy *et al.*, 2021), stratification-induced reduction in nutrient supply at low latitudes (Brander, 2007; Dulvy and Heymans, 2009; Fu, Randerson and Moore, 2016), and deoxygenation (Gallo and Levin, 2016; Limburg *et al.*, 2020; Kim, Franco and Sumaila, 2023).

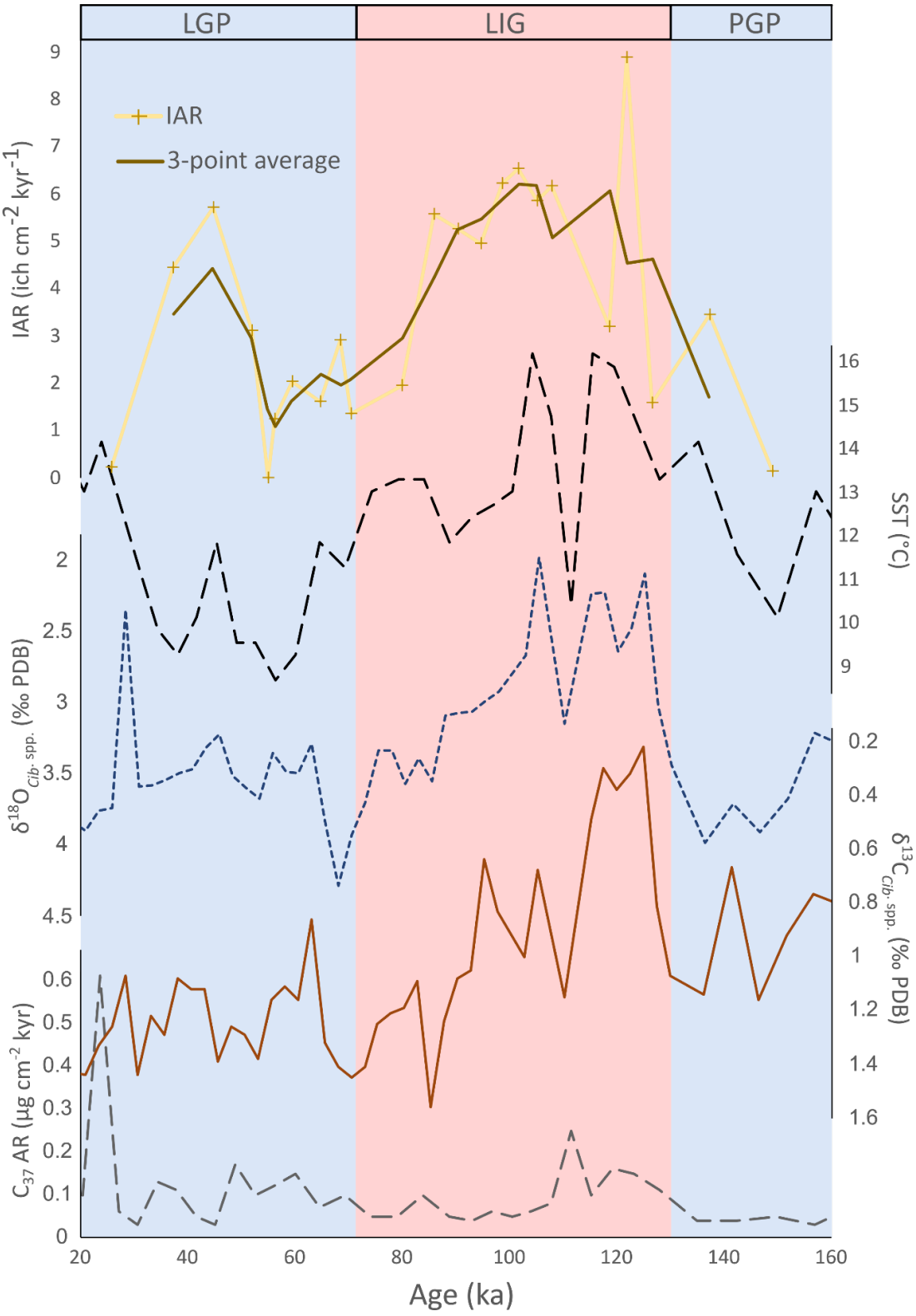

Figure 4.7 – Compilation of relevant palaeoenvironmental records for ODP Site 982. From top to bottom: ichthyolith accumulation rate (this work), sea surface temperature (Lawrence *et al.*, 2009), *Cibicidoides* spp. $\delta^{18}O$, and $\delta^{13}C$ (Venz *et al.*, 1999), and C_{37} alkenone accumulation rate (Bolton *et al.*, 2011). Background colour and top label indicate glacial or interglacial interval for the last glacial period (LGP), last interglacial (LIG), and penultimate glacial period (PGP).

Sea surface temperature records have been produced for both ODP Hole 982B (Lawrence *et al.*, 2009; Herbert *et al.*, 2016) and IODP Site U1313 (Stein *et al.*, 2009; Naafs *et al.*, 2013). Additionally, a benthic (*Cibicidoides* spp.) $\delta^{18}O$ record has been produced for ODP Hole 982B (Venz *et al.*, 1999), which records components of both deep-water temperature and terrestrial ice volume (Pearson, 2012). For ODP Hole 982B, the benthic $\delta^{18}O$ record closely resembles the SST record, suggesting a close relationship between the magnitude of temperature change in the North Atlantic above and below the thermocline during the late Pleistocene. Both SST and $\delta^{18}O$ records show a high degree of similarity to the IAR record here, with a 3°C decline in SST and 1.5‰ increase in $\delta^{18}O$ between from the early to late LIG, followed by a further 4°C decline in SST into the early LGP, which approximately co-varies with an IAR decline.

Similarly, a relatively stable SST of 16–18°C persists at IODP Site U1313 during a high IAR interval. An abrupt SST decline of 4°C occurs during the earliest LGP followed by a recovery to temperatures comparable to the late LIG over a 10 kyr interval, which is comparable to a strong decline and recovery in IAR seen at the same site. However, the SST trend appears to lag the decline in IAR. It is possible that this is due to a minor mismatch between the age models of these two cores (core A for IAR and core B for SST; Naafs et al., 2013). The suggestion of a mismatch is supported by a separate planktic (*G. bulloides*) $\delta^{18}O$ record (Smith *et al.*, 2013) generated from the same core (A) as was used in this study, which shows a 1.1 ‰ increase between 72–65 ka, predating the implied SST decline and coincident with the steep decline in IAR (Figure 4.8). Unlike the alkenone-derived SST record, planktic $\delta^{18}O$ records environmental changes in the temperature of the mixed layer alongside a global ice volume and surface salinity signal (Pearson, 2012). Therefore, whilst it is plausible that there is a minor mismatch between cores A and B, it is also possible that the fish productivity signal is a function of increased salinity in the mid-latitude North Atlantic preceding a significant decline in surface temperature. In either case, rapid IAR decline is coincident with environmental change at the onset of full glacial conditions.

Differences in sample resolution make it challenging to directly compare IAR and temperature reconstructions, and for both sites these surface temperature reconstructions were made using different cores to the one used to generate IAR (Lawrence *et al.*, 2009; Herbert *et al.*, 2016), increasing the likelihood of offsets between the age models of both sites, which may have a pronounced effect for high resolution studies such as this one. Surface temperature is also not an ideal proxy, as the majority of mesopelagic fish biomass is usually located below the thermocline (Irigoien *et al.*, 2014) and therefore relevant environmental temperature changes will likely resemble those of the deep, rather than surface, ocean. Nonetheless, the temperature records for both sites show a distinct similarity to IAR trends, unlike the productivity proxies discussed previously, but in agreement with the earlier findings of Britten and Sibert (2020). It therefore appears that, on multi-millennial timescales, water temperature changes are strongly associated with the magnitude of mesopelagic fish production.

The causes of this trend could be investigated further by gathering morphometric information about extracted teeth and determining whether there were any changes to the occupied functional space of fish communities over time that might indicate changes in prey type or trophic position, as well as changes in the diversity and disparity of fishes represented by the microfossil record.

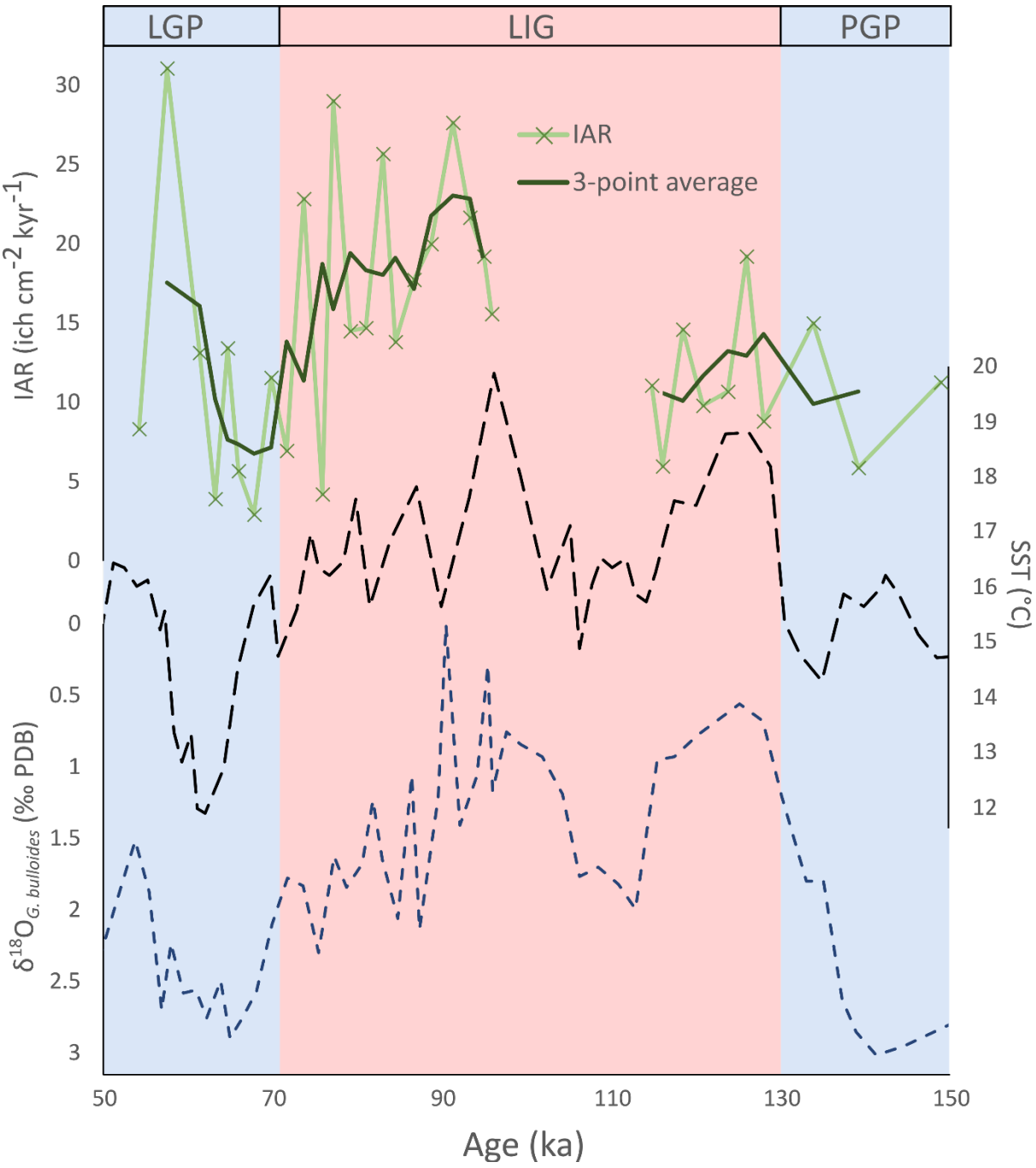

Figure 4.8 – Dataset comparison for IODP Site U1313. From top to bottom: ichthyolith accumulation rate (this work), sea surface temperature (Naafs *et al.*, 2013), and $\delta^{18}O_{G.\ bulloides}$ (Smith *et al.*, 2013). Background colour indicates glacial or interglacial interval, which are also labelled at the top: last glacial period (LGP), last interglacial (LIG), and penultimate glacial period (PGP). The IAR line is disconnected due to an 18 kyr gap between adjacent samples in the early LIG.

Standard deviation in IAR at IODP Site U1313 is over three times greater than ODP Site 982, suggesting abrupt high-magnitude changes in fish production over relatively short timescales, particularly during the late LIG and early PGP. As discussed in earlier chapters, this site is presently near the southernmost part of North Atlantic Transitional Waters (NATW), the region directly influenced by the North Atlantic Current (NAC; Krauss, 1986; Rossby, 1996). During warmer intervals in the Pleistocene, it is likely that NATW were displaced southwards due to the expansion of cold water masses from the high latitude Atlantic basin (McIntyre, Ruddiman and Jantzen, 1972; Ruddiman and McIntyre, 1976; Schwab *et al.*, 2012). Therefore, mesopelagic fish production (which is likely tertiary or quaternary production; Sommer et al., 2002) in this region is likely highly sensitive to changes in environmental and ecosystem variables (such as primary production, trophic transfer efficiency and ecosystem structure) that themselves are influenced by changes in overall climate state and particularly the strength and position of the NAC. Ice-ocean feedbacks resulted in high-amplitude, high-frequency changes to North Atlantic climate during past glacial intervals (Dansgaard *et al.*, 1993; Schmidt, Vautravers and Spero, 2006; Naafs *et al.*, 2013; Naafs, Hefter and Stein, 2013; Pedro *et al.*, 2022), and these frequent perturbations likely exerted strong second-order effects on fish production at intermediate latitudes, atop the overall temperature trend, that are not fully captured within the resolution of most existing proxy records.

4.4.4. Implications for climate and ecosystems

Fish DVM and faecal pellet production is presently responsible for up to 29% of organic carbon export in the global ocean (Saba *et al.*, 2021). The results here, alongside earlier works, suggest that pelagic fish biomass is positively correlated with ocean temperature. Past glacial intervals were characterized by lower fish biomass in both the temperate and high-latitude North Atlantic, implying that fish-mediated organic carbon export may be a hitherto unrecognised negative feedback mechanism in the global carbon cycle. The significance of the negative feedback depends strongly on the relative contribution of fish faecal pellets to total organic carbon export, which remains poorly constrained in the present day (Davison *et al.*, 2013; Anderson *et al.*, 2019; Saba *et al.*, 2021). Contemporary estimates suggest that faecal pellet export is most proportionally significant in the stratified mid-latitude ocean (Nowicki, DeVries and Siegel, 2022), whose spatial extent likely decreased during past glacial intervals due to the equatorward migration of oceanographic fronts (McIntyre, Ruddiman and Jantzen, 1972; Lang *et al.*, 2016). Hence changes in ecosystem structure, nutrient flux, and primary production are probably more quantitatively significant in influencing the strength of the biological pump on glacial-interglacial timescales relative to fish biomass. Nonetheless, these results highlight the potential value of including fish biomass changes in Pleistocene palaeoclimate and biogeochemical models.

Future climate change is expected to have negative impacts on global fish production (Brander, 2007; Dulvy and Heymans, 2009; Blanchard *et al.*, 2012; Kim, Franco and Sumaila, 2023). Since the pre-industrial era, average ocean surface temperatures have warmed by around 1°C, and additional warming of 1–4°C relative to the 1986–2005 baseline is expected by the end of the century (IPCC, 2019; Messias and Mercier, 2022). Extreme surface ocean warming during 2023 demonstrates that changes in regional or global ocean temperature can significantly exceed interdecadal averages on short timescales (Kuhlbrodt *et al.*, 2024), particularly due to cyclical phenomena such as the El Nino–Southern Oscillation (Jiang *et al.*, 2024) and North Atlantic Oscillation (Messias and Mercier, 2022). Deep ocean temperature has typically fluctuated by around 2°C between glacial and interglacial maxima over the past 400 kyr (Cutler *et al.*, 2003; Hansen *et al.*, 2013), and is currently increasing by around 0.02–0.04°C decade^{-1} in response to anthropogenic heating (Meinen *et al.*, 2020). The rate of

deep ocean warming is likely to increase in the future as additional surface ocean heat is transported to depth through overturning circulation (Durack *et al.*, 2018; IPCC, 2019). Even under the most optimistic future climate projections, the anthropogenic ocean heat excursion is likely to persist for millennia beyond the point of net zero anthropogenic carbon emissions (Matthews and Weaver, 2010), with profound consequences for deep ocean ecosystems (Gattuso *et al.*, 2015). Based on the current and prior research (Britten and Sibert, 2020), sustained increases in deep and surface ocean temperatures are likely to result in positive changes in mesopelagic fish biomass on multi-millennial timescales. However, intervals of rapid climate change during the late LIG–early PGP and last deglaciation are characterised by highly variable fish production in both the mid- and high-latitude North Atlantic, highlighting the potentially negative impact of rapid climate change on ecosystem stability on shorter timescales, even if higher temperatures exert a positive long-term effect on fish production.

Open ocean mesopelagic fishes have hitherto been relatively unaffected by direct human impacts (Catul, Gauns and Karuppasamy, 2011; Grimaldo *et al.*, 2020), in contrast to the substantial declines in many commercial fish species in fisheries worldwide (Dulvy and Heymans, 2009; FAO, 2020). This work shows the sensitivity of mesopelagic fishes to environmental change in the recent geological past, and highlights that similar changes are likely to result from near-future anthropogenic climate perturbations.

4.4.5. Methodological caveats

The results of this work assume that there is a positive correlation between IAR and fish production in the open ocean (Sibert *et al.*, 2017). Additional future work could improve the reliability of this assumption as well as the inferences that can be derived from it.

It would be highly beneficial to the interpretation of the IAR proxy to determine whether fish teeth reaching deep sea sediment do so directly through shedding, or by consumption and excretion of faecal pellets. Limited research to-date suggests that tooth resorption may be common in actinopterygian fishes (Bemis, Giuliano and McGuire, 2005; Johanson, 2017; Collins, 2023), supporting the latter hypothesis.

As discussed previously, ichthyolith research to-date utilises teeth in the >38 µm size fraction, as it is impractical to pick teeth at any smaller fraction. However, the retention of fish jaws in the samples used for the current research highlight that there are teeth finer than 38 µm that are typically lost during processing (Figure 4.5). Whilst their habitat and net avoidance behavior presents distinct challenges in acquiring physical samples of modern mesopelagic fish (Kaartvedt, Staby and Aksnes, 2012), it would be advantageous to assess the size distribution of teeth for the most abundant species so that the proportion of lost ichthyoliths can be better-constrained.

Similarly, estimating variation in number of teeth and (assuming shedding is an important mechanism in the transport of teeth to sediment) the shedding rate of teeth within the most common small open ocean species will also provide constraint on how to interpret IAR in the geological record. Whilst the diversity of tooth morphotypes found in this work provides some reassurance that ichthyolith retention in sediment is not strongly biased towards a small number of species or functional niches, it would be useful to assess how differences in habitat (e.g. benthic vs pelagic) or tooth shedding rate relate to IAR. The low accumulation rate of teeth on human timescales renders proxy validation methods such as sediment traps impractical. For example, assuming a modern IAR equal to the late Pleistocene mean for IODP Hole U1313A (13.8 ich cm^{-2} kyr^{-1}), it would be expected to take an average

of 72 years for a single tooth to fall in a given square centimetre of sediment. Relatively high IAR (Figure 4.6) and the similarity of palaeo-fauna to those still extant indicates that the late Pleistocene–Holocene North Atlantic is an ideal location to further refine the IAR proxy.

Ichthyolith morphometrics were not analysed in this work, but if done in the future, these would permit a more detailed and reliable assessment of some of the causes of IAR change over time (e.g. Sibert and Norris, 2015; Sibert et al., 2016). For example, if changes in the occupied morphospace of ichthyoliths changed synchronously with IAR, this might indicate that IAR is related to changes in trophic level occupation by mesopelagic fishes. If temperature rise leads to a decrease in the average trophic level of mesopelagic fishes, this could explain why fish production appears to increase with temperature (Sommer *et al.*, 2002; O'Gorman *et al.*, 2016) without needing to invoke changes in the trophic transfer efficiency of feeding at the same trophic level, as I have suggested in this work.

4.5. Conclusion

To test how fish production changed responded to glacial-interglacial climate change, I processed sediment samples from two pelagic North Atlantic cores to produce new datasets for IAR during the late Pleistocene. IODP Site U1313, in the temperate ocean, has a mean IAR three times greater than any previously investigated site assessed using a similar methodology from any time interval or region, suggesting very high overall fish production in the mid-latitude North Atlantic. Fish production is higher at the mid-latitude site relative to the subpolar site throughout the study interval. Both cores show significantly higher IAR during the LIG relative to glacial intervals and an apparent positive correlation to water temperature. Both locations saw a substantial reduction in fish production during the last glacial inception, coincident with a steep decline in ocean temperature. IAR variance is high at IODP Site U1313 during the late LIG and early PGP, suggesting high sensitivity of fish biomass to rapidly changing regional climate, including the strength and position of the NAC. The overall glacial-interglacial trend is likely a function of some combination of temperature-induced changes in trophic transfer efficiency, primary production, and ecosystem structure, but confidently distinguishing between these may require assessment of functional diversity through morphometric analyses of extracted ichthyoliths.

The positive correlation between ocean temperature and fish production, which is consistent with earlier findings from the early Cenozoic Pacific Ocean, highlights a potential role of fish faecal pellet organic matter export as a negative feedback in the global climate system on glacial-interglacial timescales. The significance of this feedback will be improved by refining estimates of the quantitative significance of fish-mediated organic carbon flux in the present day.

Unlike many larger groups, mesopelagic fishes have thus far avoided large-scale commercial overexploitation, and their biomass is likely to respond positively to future anthropogenic warming on multi-millennial timescales. Fish community response to warming on century-millennial timescales is less predictable, as intervals of rapid climate change during the late Pleistocene were coincident with highly variable fish production in the open ocean.

Acknowledgements

I am immensely grateful to Elizabeth Sibert for teaching me everything I know about ichthyolith extraction, analysis, and interpretation, as well as for generously hosting me at WHOI in January 2024 to image the ichthyoliths that I had extracted. Ivo Leonard, Yingbo Li, Emilia Miller, Manreet Jassal, and Ella Kyle collectively spent thousands of hours helping me to process and pick samples, for which I am hugely grateful. I am indebted to Paul Smith and Juliet Hay at the Oxford University Museum of Natural History for generously facilitating sample processing safely in the midst of a global pandemic. Owen Green was an invaluable source of wisdom on microfossil processing at the Oxford University Department of Earth Sciences. I am also very grateful to Hannah Bird and Kirsty Edgar at the University of Birmingham for hosting me and allowing me to work in their lab to undertake heavy liquid separation.

References

Agiadi, K. *et al.* (2023) 'Palaeontological evidence for community-level decrease in mesopelagic fish size during Pleistocene climate warming in the eastern Mediterranean', *Proceedings of the Royal Society B: Biological Sciences*, 290(1990). Available at: https://doi.org/10.1098/rspb.2022.1994.

Anderson, T.R. *et al.* (2019) 'Quantifying carbon fluxes from primary production to mesopelagic fish using a simple food web model', *ICES Journal of Marine Science*, 76(3), pp. 690–701. Available at: https://doi.org/10.1093/ICESJMS/FSX234.

Annan, J.D. and Hargreaves, J.C. (2013) 'A new global reconstruction of temperature changes at the Last Glacial Maximum', *Climate of the Past*, 9(1), pp. 367–376. Available at: https://doi.org/10.5194/cp-9-367-2013.

Armengol, L. *et al.* (2019) 'Planktonic food web structure and trophic transfer efficiency along a productivity gradient in the tropical and subtropical Atlantic Ocean', *Scientific Reports*, 9(1), pp. 1–19. Available at: https://doi.org/10.1038/s41598-019-38507-9.

Atkinson, A. *et al.* (2024) 'Steeper size spectra with decreasing phytoplankton biomass indicate strong trophic amplification and future fish declines', *Nature Communications*, 15(1), p. 381. Available at: https://doi.org/10.1038/s41467-023-44406-5.

Barneche, D.R. *et al.* (2021) 'Warming impairs trophic transfer efficiency in a long-term field experiment', *Nature*, 592(7852), pp. 76–79. Available at: https://doi.org/10.1038/s41586-021-03352-2.

Baumann, K.-H. and Huber, R. (1999) 'Sea-surface gradients between the North Atlantic and the Norwegian Sea during the last 3.1 m.y.: comparison of Sites 982 and 985', in *Proceedings of the Ocean Drilling Program, 162 Scientific Results*. Ocean Drilling Program, pp. 179–190. Available at: https://doi.org/10.2973/odp.proc.sr.162.014.1999.

Behrenfeld, M.J. *et al.* (2019) 'Global satellite-observed daily vertical migrations of ocean animals', *Nature 2019 576:7786*, 576(7786), pp. 257–261. Available at: https://doi.org/10.1038/s41586-019-1796-9.

Behrenfeld, M.J. and Boss, E.S. (2014) 'Resurrecting the Ecological Underpinnings of Ocean Plankton Blooms', *Annual Review of Marine Science*, 6(1), pp. 167–194. Available at: https://doi.org/10.1146/annurev-marine-052913-021325.

Bemis, W.E., Giuliano, A. and McGuire, B. (2005) 'Structure, attachment, replacement and growth of teeth in bluefish, Pomatomus saltatrix (Linnaeus, 1766), a teleost with deeply socketed teeth', *Zoology*, 108(4), pp. 317–327. Available at: https://doi.org/10.1016/j.zool.2005.09.004.

Berkovitz, B. and Shellis, P. (2017) 'Bony fishes', *The Teeth of Non-Mammalian Vertebrates*, pp. 43–111. Available at: https://doi.org/10.1016/B978-0-12-802850-6.00004-7.

Blanchard, J.L. *et al.* (2012) 'Potential consequences of climate change for primary production and fish production in large marine ecosystems', *Philosophical Transactions of the Royal Society B: Biological Sciences*, 367(1605), pp. 2979–2989. Available at: https://doi.org/10.1098/rstb.2012.0231.

Bolton, C.T. *et al.* (2011) 'Biotic and geochemical evidence for a global latitudinal shift in ocean biogeochemistry and export productivity during the late Pliocene', *Earth and Planetary Science Letters*, 308(1–2), pp. 200–210. Available at: https://doi.org/10.1016/j.epsl.2011.05.046.

Brander, K.M. (2007) 'Global fish production and climate change', *Proceedings of the National Academy of Sciences*, 104(50), pp. 19709–19714. Available at: https://doi.org/10.1073/PNAS.0702059104.

Britten, G.L. and Sibert, E.C. (2020) 'Enhanced fish production during a period of extreme global warmth', *Nature Communications*, 11(1), p. 5636. Available at: https://doi.org/10.1038/s41467-020-19462-w.

Browning, T.J. and Moore, C.M. (2023) 'Global analysis of ocean phytoplankton nutrient limitation reveals high prevalence of co-limitation', *Nature Communications 2023 14:1*, 14(1), pp. 1–12. Available at: https://doi.org/10.1038/s41467-023-40774-0.

Carr, E.M., Summers, A.P. and Cohen, K.E. (2021) 'The moment of tooth: rate, fate and pattern of Pacific lingcod dentition revealed by pulse-chase', *Proceedings of the Royal Society B: Biological Sciences*, 288(1960). Available at: https://doi.org/10.1098/RSPB.2021.1436.

Catul, V., Gauns, M. and Karuppasamy, P.K. (2011) 'A review on mesopelagic fishes belonging to family Myctophidae', *Reviews in Fish Biology and Fisheries*, 21(3), pp. 339–354. Available at: https://doi.org/10.1007/S11160-010-9176-4/FIGURES/9.

Chassot, E. *et al.* (2010) 'Global marine primary production constrains fisheries catches', *Ecology Letters*, 13(4), pp. 495–505. Available at: https://doi.org/10.1111/j.1461-0248.2010.01443.x.

Chen, B. *et al.* (2012) 'Does warming enhance the effect of microzooplankton grazing on marine phytoplankton in the ocean?', *Limnology and Oceanography*, 57(2), pp. 519–526. Available at: https://doi.org/10.4319/LO.2012.57.2.0519.

Clavel-Henry, M. *et al.* (2020) 'Spatial Distribution and Abundance of Mesopelagic Fish Biomass in the Mediterranean Sea', *Frontiers in Marine Science*, 7, p. 573986. Available at: https://doi.org/10.3389/FMARS.2020.573986/BIBTEX.

Collins, S.E. (2023) *Understanding the mechanisms of polyphyodonty: insights gained from tooth replacement in fish*. Birkbeck, University of London. Available at: https://doi.org/10.18743/PUB.00052277.

Cutler, K.B. *et al.* (2003) 'Rapid sea-level fall and deep-ocean temperature change since the last interglacial period', *Earth and Planetary Science Letters*, 206(3–4), pp. 253–271. Available at: https://doi.org/10.1016/S0012-821X(02)01107-X.

Dansgaard, W. *et al.* (1993) 'Evidence for general instability of past climate from a 250-kyr ice-core record', *Nature 1993 364:6434*, 364(6434), pp. 218–220. Available at: https://doi.org/10.1038/364218a0.

Davison, P.C. *et al.* (2013) 'Carbon export mediated by mesopelagic fishes in the northeast Pacific Ocean', *Progress in Oceanography*, 116, pp. 14–30. Available at: https://doi.org/10.1016/J.POCEAN.2013.05.013.

Dornan, T. *et al.* (2022) 'Large mesopelagic fish biomass in the Southern Ocean resolved by acoustic properties', *Proceedings of the Royal Society B: Biological Sciences*, 289(1967). Available at: https://doi.org/10.1098/rspb.2021.1781.

Doyle, P.S. and Riedel, W.R. (1979) *Ichthyoliths: present status of taxonomy and stratigraphy of microscopic fish skeletal debris*. University of California at San Diego.

Doyle, P.S. and Riedel, W.R. (1985) 'Cenozoic and Late Cretaceous Ichthyoliths', in H.M. Bolli, J.B. Saunders, and K. Perch-Nielsen (eds) *Plankton Stratigraphy*. Cambridge: Cambridge University Press.

Dulvy, N.K. and Heymans, J.J. (2009) 'Climate change, ecosystem variability and fisheries productivity'. Available at: https://www.researchgate.net/publication/286946937 (Accessed: 15 October 2024).

Durack, P.J. *et al.* (2018) 'Ocean warming from the surface to the deep in observations and models', *Oceanography*, 31(2 Special Issue), pp. 41–51. Available at: https://doi.org/10.5670/OCEANOG.2018.227.

Eddy, T.D. *et al.* (2021) 'Energy Flow Through Marine Ecosystems: Confronting Transfer Efficiency', *Trends in Ecology and Evolution*, 36(1), pp. 76–86. Available at: https://doi.org/10.1016/J.TREE.2020.09.006/ASSET/3BC101A6-257D-41C0-995E-9668E26D772A/MAIN.ASSETS/GR1.SML.

Eskuche-Keith, P. *et al.* (2024) 'Temperature alters the predator-prey size relationships and size-selectivity of Southern Ocean fish', *Nature Communications*, 15(1), p. 3979. Available at: https://doi.org/10.1038/s41467-024-48279-0.

Expedition 306 Scientists (2006) 'Site U1313', in *Proceedings of the IODP, 303/306*. Integrated Ocean Drilling Program. Available at: https://doi.org/10.2204/iodp.proc.303306.112.2006.

FAO (2020) *The State of World Fisheries and Aquaculture*, *Fisheries Oceanography*. Available at: https://doi.org/10.1111/fog.12466.

Frangoulis, C. *et al.* (2011) 'Importance of copepod carcasses versus faecal pellets in the upper water column of an oligotrophic area', *Estuarine, Coastal and Shelf Science*, 92(3), pp. 456–463. Available at: https://doi.org/10.1016/j.ecss.2011.02.005.

Friedman, M. (2010) 'Explosive morphological diversification of spiny-finned teleost fishes in the aftermath of the end-Cretaceous extinction', *Proceedings of the Royal Society B: Biological Sciences*, 277(1688), pp. 1675–1683. Available at: https://doi.org/10.1098/rspb.2009.2177.

Fu, W., Randerson, J.T. and Moore, J.K. (2016) 'Climate change impacts on net primary production (NPP) and export production (EP) regulated by increasing stratification and phytoplankton community structure in the CMIP5 models', *Biogeosciences*, 13(18), pp. 5151–5170. Available at: https://doi.org/10.5194/bg-13-5151-2016.

Gallo, N.D. and Levin, L.A. (2016) 'Fish Ecology and Evolution in the World's Oxygen Minimum Zones and Implications of Ocean Deoxygenation', *Advances in Marine Biology*, 74, pp. 117–198. Available at: https://doi.org/10.1016/BS.AMB.2016.04.001.

Gattuso, J.P. *et al.* (2015) 'Contrasting futures for ocean and society from different anthropogenic CO2 emissions scenarios', *Science*, 349(6243). Available at: https://doi.org/10.1126/SCIENCE.AAC4722/SUPPL_FILE/GATTUSO.SM.PDF.

Giles, S. *et al.* (2017) 'Early members of "living fossil" lineage imply later origin of modern ray-finned fishes', *Nature 2017 549:7671*, 549(7671), pp. 265–268. Available at: https://doi.org/10.1038/nature23654.

Gjøsaeter, J. and Kawaguchi K. (1980) *A review of the world resources of mesopelagic fish*. Rome.

Grimaldo, E. *et al.* (2020) 'Investigating the potential for a commercial fishery in the Northeast Atlantic utilizing mesopelagic species', *ICES Journal of Marine Science*, 77(7–8), pp. 2541–2556. Available at: https://doi.org/10.1093/ICESJMS/FSAA114.

Hansen, J. *et al.* (2013) 'Climate sensitivity, sea level and atmospheric carbon dioxide', *Philosophical Transactions of the Royal Society A: Mathematical, Physical and Engineering Sciences*, 371(2001). Available at: https://doi.org/10.1098/RSTA.2012.0294.

Herbert, T.D. *et al.* (2016) 'Late Miocene global cooling and the rise of modern ecosystems', *Nature Geoscience*, 9(11), pp. 843–847. Available at: https://doi.org/10.1038/ngeo2813.

Hudson, J.M. *et al.* (2014) 'Myctophid feeding ecology and carbon transport along the northern Mid-Atlantic Ridge', *Deep Sea Research Part I: Oceanographic Research Papers*, 93, pp. 104–116. Available at: https://doi.org/10.1016/j.dsr.2014.07.002.

Hurley, I.A. *et al.* (2006) 'A new time-scale for ray-finned fish evolution', *Proceedings of the Royal Society B: Biological Sciences*, 274(1609), pp. 489–498. Available at: https://doi.org/10.1098/RSPB.2006.3749.

Huysseune, A. and Witten, P.E. (2024) 'Continuous tooth replacement: what can teleost fish teach us?', *Biological Reviews*, 99(3), pp. 797–819. Available at: https://doi.org/10.1111/BRV.13045.

IPCC (2019) *IPCC Special Report on the Ocean and Cryosphere in a Changing Climate*, *The Ocean and Cryosphere in a Changing Climate: Special Report of the Intergovernmental Panel on Climate Change*. Cambridge University Press. Available at: https://doi.org/10.1017/9781009157964.

Irigoien, X. *et al.* (2014) 'Large mesopelagic fishes biomass and trophic efficiency in the open ocean', *Nature Communications 2014 5:1*, 5(1), pp. 1–10. Available at: https://doi.org/10.1038/ncomms4271.

Irigoien, X., Hulsman, J. and Harris, R.P. (2004) 'Global biodiversity patterns of marine phytoplankton and zooplankton', *Nature*, 429(6994), pp. 863–867. Available at: https://doi.org/10.1038/nature02593.

Jiang, N. *et al.* (2024) 'Enhanced risk of record-breaking regional temperatures during the 2023–24 El Niño', *Scientific Reports 2024 14:1*, 14(1), pp. 1–10. Available at: https://doi.org/10.1038/s41598-024-52846-2.

Johanson, Z. (2017) 'Paleobiology: A Tooth for a Tooth', *Current Biology*, 27(3), pp. R117–R119. Available at: https://doi.org/10.1016/J.CUB.2016.12.011.

Johns, M.J., Barnes, C.R. and Narayan, Y.R. (2006) 'Cenozoic ichthyolith biostratigraphy: Tofino Basin, British Columbia', *Canadian Journal of Earth Sciences*, 43(2), pp. 177–204. Available at: https://doi.org/10.1139/E05-102.

Kaartvedt, S., Staby, A. and Aksnes, D.L. (2012) 'Efficient trawl avoidance by mesopelagic fishes causes large underestimation of their biomass', *Marine Ecology Progress Series*, 456, pp. 1–6. Available at: https://doi.org/10.3354/MEPS09785.

Kaiser, M.J. (2011) *Marine Ecology: Processes, Systems and Impacts*. Oxford University Press. Available at: https://doi.org/10.1017/S0376892906253244.

Kelly, T.B. *et al.* (2019) 'The Importance of Mesozooplankton Diel Vertical Migration for Sustaining a Mesopelagic Food Web', *Frontiers in Marine Science*, 6. Available at: https://doi.org/10.3389/fmars.2019.00508.

Kim, H., Franco, A.C. and Sumaila, U.R. (2023) 'A Selected Review of Impacts of Ocean Deoxygenation on Fish and Fisheries', *Fishes*, 8(6), p. 316. Available at: https://doi.org/10.3390/fishes8060316.

Kleinen, T., Brovkin, V. and Munhoven, G. (2016) 'Modelled interglacial carbon cycle dynamics during the Holocene, the Eemian and Marine Isotope Stage (MIS) 11', *Climate of the Past*, 12(12), pp. 2145–2160. Available at: https://doi.org/10.5194/CP-12-2145-2016.

Krauss, W. (1986) 'The North Atlantic Current', *Journal of Geophysical Research: Oceans*, 91(C4), pp. 5061–5074. Available at: https://doi.org/10.1029/JC091IC04P05061.

Kuhlbrodt, T. *et al.* (2024) 'A Glimpse into the Future: The 2023 Ocean Temperature and Sea Ice Extremes in the Context of Longer-Term Climate Change', *Bulletin of the American Meteorological Society*, 105(3), pp. E474–E485. Available at: https://doi.org/10.1175/BAMS-D-23-0209.1.

Lang, D.C. *et al.* (2016) 'Incursions of southern-sourced water into the deep North Atlantic during late Pliocene glacial intensification', *Nature Geoscience*, 9(5), pp. 375–379. Available at: https://doi.org/10.1038/ngeo2688.

Lawrence, K.T. *et al.* (2009) 'High-amplitude variations in North Atlantic sea surface temperature during the early Pliocene warm period', *Paleoceanography*, 24(2), p. n/a-n/a. Available at: https://doi.org/10.1029/2008PA001669.

Limburg, K.E. *et al.* (2020) 'Ocean Deoxygenation: A Primer', *One Earth*, 2(1), pp. 24–29. Available at: https://doi.org/10.1016/j.oneear.2020.01.001.

Lisiecki, L.E. and Raymo, M.E. (2005) 'A Pliocene-Pleistocene stack of 57 globally distributed benthic δ 18O records', *Paleoceanography*, 20(1), pp. 1–17. Available at: https://doi.org/10.1029/2004PA001071.

Mann, H.B. and Whitney, D.R. (1947) 'On a Test of Whether one of Two Random Variables is Stochastically Larger than the Other', *https://doi.org/10.1214/aoms/1177730491*, 18(1), pp. 50–60. Available at: https://doi.org/10.1214/AOMS/1177730491.

Martin, R.P. and Davis, M.P. (2020) 'The evolution of specialized dentition in the deep-sea lanternfishes (Myctophiformes)', *Journal of Morphology*, 281(4–5), pp. 536–555. Available at: https://doi.org/10.1002/JMOR.21120.

Matthews, H.D. and Weaver, A.J. (2010) 'Committed climate warming', *Nature Geoscience 2010 3:3*, 3(3), pp. 142–143. Available at: https://doi.org/10.1038/ngeo813.

McIntyre, A., Ruddiman, W.F. and Jantzen, R. (1972) 'Southward penetrations of the North Atlantic polar front: faunal and floral evidence of large-scale surface water mass movements over the last 225,000 years', *Deep Sea Research and Oceanographic Abstracts*, 19(1), pp. 61–77. Available at: https://doi.org/10.1016/0011-7471(72)90073-3.

Meinen, C.S. *et al.* (2020) 'Observed Ocean Bottom Temperature Variability at Four Sites in the Northwestern Argentine Basin: Evidence of Decadal Deep/Abyssal Warming Amidst Hourly to Interannual Variability During 2009–2019', *Geophysical Research Letters*, 47(18), p. e2020GL089093. Available at: https://doi.org/10.1029/2020GL089093.

Messias, M.J. and Mercier, H. (2022) 'The redistribution of anthropogenic excess heat is a key driver of warming in the North Atlantic', *Communications Earth & Environment 2022 3:1*, 3(1), pp. 1–14. Available at: https://doi.org/10.1038/s43247-022-00443-4.

Moore, C.M. *et al.* (2013) 'Processes and patterns of oceanic nutrient limitation', *Nature Geoscience*, 6(9), pp. 701–710. Available at: https://doi.org/10.1038/ngeo1765.

Morris, S.C. (2008) 'A redescription of a rare chordate, Metaspriggina Walcotti Simonetta and Insom, from the Burgess Shale (Middle Cambrian), British Columbia, Canada', *Journal of Paleontology*, 82(2), pp. 424–430. Available at: https://doi.org/10.1666/06-130.1.

Naafs, B.D.A. *et al.* (2013) 'Warming of surface waters in the mid-latitude North Atlantic during Heinrich events', *Paleoceanography*, 28(1), pp. 153–163. Available at: https://doi.org/10.1029/2012PA002354.

Naafs, B.D.A., Hefter, J. and Stein, R. (2013) 'Millennial-scale ice rafting events and Hudson Strait Heinrich(-like) Events during the late Pliocene and Pleistocene: a review', *Quaternary Science Reviews*, 80, pp. 1–28. Available at: https://doi.org/10.1016/J.QUASCIREV.2013.08.014.

NASA Goddard Space Flight Center, Ocean Ecology Laboratory and Ocean Biology Processing Group (2022) *Moderate-resolution Imaging Spectroradiometer (MODIS) Chlorophyll concentration*.

Near, T.J. *et al.* (2012) 'Resolution of ray-finned fish phylogeny and timing of diversification', *Proceedings of the National Academy of Sciences of the United States of America*, 109(34), pp. 13698–13703. Available at: https://doi.org/10.1073/PNAS.1206625109/SUPPL_FILE/ST02.DOC.

Nelson, J.S., Grande, T.C. and Wilson, M.V.H. (2016) *Fishes of the World*. 5th edn. John Wiley & Sons.

Nowicki, M., DeVries, T. and Siegel, D.A. (2022) 'Quantifying the Carbon Export and Sequestration Pathways of the Ocean's Biological Carbon Pump', *Global Biogeochemical Cycles*, 36(3). Available at: https://doi.org/10.1029/2021GB007083.

O'Gorman, E.J. *et al.* (2016) 'Temperature effects on fish production across a natural thermal gradient', *Global Change Biology*, 22(9), pp. 3206–3220. Available at: https://doi.org/10.1111/GCB.13233.

Pearson, P.N. (2012) 'Oxygen Isotopes in Foraminifera: Overview and Historical Review', *The Paleontological Society Papers*, 18, pp. 1–38. Available at: https://doi.org/10.1017/S1089332600002539.

Pedro, J.B. *et al.* (2022) 'Dansgaard-Oeschger and Heinrich event temperature anomalies in the North Atlantic set by sea ice, frontal position and thermocline structure', *Quaternary Science Reviews*, 289, p. 107599. Available at: https://doi.org/10.1016/J.QUASCIREV.2022.107599.

Pereira, J.N. *et al.* (2011) 'Diet of mid-Atlantic Sowerby's beaked whales Mesoplondon bidens', *Deep Sea Research Part I: Oceanographic Research Papers*, 58(11), pp. 1084–1090. Available at: https://doi.org/10.1016/J.DSR.2011.08.004.

Poulton, A.J. *et al.* (2017) 'Coccolithophore ecology in the tropical and subtropical Atlantic Ocean: New perspectives from the Atlantic meridional transect (AMT) programme', *Progress in Oceanography*, 158, pp. 150–170. Available at: https://doi.org/10.1016/j.pocean.2017.01.003.

Raja, M. and Rosell-Melé, A. (2021) 'Appraisal of sedimentary alkenones for the quantitative reconstruction of phytoplankton biomass', *Proceedings of the National Academy of Sciences*, 118(2). Available at: https://doi.org/10.1073/PNAS.2014787118.

Rasmussen, T.L. *et al.* (2003) 'Millennial-scale glacial variability versus Holocene stability: changes in planktic and benthic foraminifera faunas and ocean circulation in the North Atlantic during the last 60 000 years', *Marine Micropaleontology*, 47(1–2), pp. 143–176. Available at: https://doi.org/10.1016/S0377-8398(02)00115-9.

Raymo, M.E. *et al.* (1990) 'Evolution of Atlantic-Pacific δ13C gradients over the last 2.5 m.y.', *Earth and Planetary Science Letters*, 97(3–4), pp. 353–368. Available at: https://doi.org/10.1016/0012-821X(90)90051-X.

Rossby, T. (1996) 'The North Atlantic Current and surrounding waters: At the crossroads', *Reviews of Geophysics*, 34(4), pp. 463–481. Available at: https://doi.org/10.1029/96RG02214.

Ruddiman, W.F. and McIntyre, A. (1976) 'Northeast Atlantic Paleoclimatic Changes over the Past 600,000 Years', *Memoir of the Geological Society of America*, 145, pp. 111–146. Available at: https://doi.org/10.1130/MEM145-P111.

Saba, G.K. *et al.* (2021) 'Toward a better understanding of fish-based contribution to ocean carbon flux', *Limnology and Oceanography*, 66(5), pp. 1639–1664. Available at: https://doi.org/10.1002/lno.11709.

Schmidt, M.W., Vautravers, M.J. and Spero, H.J. (2006) 'Rapid subtropical North Atlantic salinity oscillations across Dansgaard–Oeschger cycles', *Nature 2006 443:7111*, 443(7111), pp. 561–564. Available at: https://doi.org/10.1038/nature05121.

Schmoker, C., Hernández-León, S. and Calbet, A. (2013) 'Microzooplankton grazing in the oceans: impacts, data variability, knowledge gaps and future directions', *Journal of Plankton Research*, 35(4), pp. 691–706. Available at: https://doi.org/10.1093/PLANKT/FBT023.

Schwab, C. *et al.* (2012) 'Coccolithophore paleoproductivity and ecology response to deglacial and Holocene changes in the Azores Current System', *Paleoceanography*, 27(3). Available at: https://doi.org/10.1029/2012PA002281.

Schwarzhans, W. and Carnevale, G. (2021) 'The rise to dominance of lanternfishes (Teleostei: Myctophidae) in the oceanic ecosystems: a paleontological perspective', *Paleobiology*, 47(3), pp. 446–463. Available at: https://doi.org/10.1017/pab.2021.2.

Shackleton, N.J. (1969) 'The last interglacial in the marine and terrestrial records', *Proceedings of the Royal Society of London. Series B. Biological Sciences*, 174(1034), pp. 135–154. Available at: https://doi.org/10.1098/rspb.1969.0085.

Shipboard Scientific Party (1996) 'Site 982', in *Proceedings of the Ocean Drilling Program, 162 Initial Reports*. Ocean Drilling Program, pp. 91–138. Available at: https://doi.org/10.2973/odp.proc.ir.162.104.1996.

Shu, D.G. *et al.* (1999) 'Lower Cambrian vertebrates from south China', *Nature 1999 402:6757*, 402(6757), pp. 42–46. Available at: https://doi.org/10.1038/46965.

Shu, D.G. *et al.* (2003) 'Head and backbone of the Early Cambrian vertebrate Haikouichthys', *Nature*, 421(6922), pp. 526–529. Available at: https://doi.org/10.1038/NATURE01264.

Sibert, E. *et al.* (2016) 'Eighty-five million years of Pacific Ocean gyre ecosystem structure: long-term stability marked by punctuated change', *Proceedings of the Royal Society B: Biological Sciences*, 283(1831), p. 20160189. Available at: https://doi.org/10.1098/rspb.2016.0189.

Sibert, E. *et al.* (2018) 'Two pulses of morphological diversification in Pacific pelagic fishes following the Cretaceous-Palaeogene mass extinction', *Proceedings of the Royal Society B: Biological Sciences*, 285(1888). Available at: https://doi.org/10.1098/RSPB.2018.1194.

Sibert, E.C. *et al.* (2017) 'Methods for isolation and quantification of microfossil fish teeth and elasmobranch dermal denticles (Ichthyoliths) from marine sediments', *Palaeontologia Electronica*, 20(1), pp. 1–14. Available at: https://doi.org/10.26879/677.

Sibert, E.C. *et al.* (2020) 'No state change in pelagic fish production and biodiversity during the Eocene–Oligocene transition', *Nature Geoscience*, 13(3), pp. 238–242. Available at: https://doi.org/10.1038/s41561-020-0540-2.

Sibert, E.C., Hull, P.M. and Norris, R.D. (2014) 'Resilience of Pacific pelagic fish across the Cretaceous/Palaeogene mass extinction', *Nature Geoscience*, 7(9), pp. 667–670. Available at: https://doi.org/10.1038/ngeo2227.

Sibert, E.C. and Norris, R.D. (2015) 'New age of fishes initiated by the Cretaceous-Paleogene mass extinction', *Proceedings of the National Academy of Sciences of the United States of America*, 112(28), pp. 8537–8542. Available at: https://doi.org/10.1073/PNAS.1504985112/-/DCSUPPLEMENTAL/PNAS.201504985SI.PDF.

Sibert, E.C. and Rubin, L.D. (2021) 'An early Miocene extinction in pelagic sharks', *Science*, 372(6546), pp. 1105–1107. Available at: https://doi.org/10.1126/science.aaz3549.

Sigman, D.M. and Hain, M.P. (2012) 'The Biological Productivity of the Ocean', *Nature Education*, 3(6), pp. 1–16.

Smith, M.E. *et al.* (2013) 'Data report: oxygen isotopes and foraminifer abundance record for the last glacial-interglacial cycle and marine isotope Stage 6 at IODP Site U1313', in, pp. 1–11. Available at: https://doi.org/10.2204/iodp.proc.303306.216.2013.

Sommer, U. *et al.* (2002) 'Pelagic food web configurations at different levels of nutrient richness and their implications for the ratio fish production:primary production', *Hydrobiologia*, 484(1), pp. 11–20. Available at: https://doi.org/10.1023/A:1021340601986/METRICS.

Stein, R. *et al.* (2009) 'Variability of surface water characteristics and Heinrich-like events in the Pleistocene midlatitude North Atlantic Ocean: Biomarker and XRD records from IODP Site U1313 (MIS 16-9)', *Paleoceanography*, 24(2), p. n/a-n/a. Available at: https://doi.org/10.1029/2008PA001639.

Turner, J. (2002) 'Zooplankton fecal pellets, marine snow and sinking phytoplankton blooms', *Aquatic Microbial Ecology*, 27(1), pp. 57–102. Available at: https://doi.org/10.3354/ame027057.

Tzedakis, P.C. *et al.* (2009) 'Interglacial diversity', *Nature Geoscience*, 2(11), pp. 751–755. Available at: https://doi.org/10.1038/ngeo660.

Venz, K.A. *et al.* (1999) 'A 1.0 Myr Record of Glacial North Atlantic Intermediate Water Variability from ODP Site 982 in the Northeast Atlantic', *Paleoceanography*, 14(1), pp. 42–52. Available at: https://doi.org/10.1029/1998PA900013.

Volkman, J.K. *et al.* (1995) 'Alkenones in Gephyrocapsa oceanica: Implications for studies of paleoclimate', *Geochimica et Cosmochimica Acta*, 59(3), pp. 513–520. Available at: https://doi.org/10.1016/0016-7037(95)00325-T.

Webb, P. (2021) 'Patterns of Primary Production', in *Introduction to Oceanography*. Roger Williams University. Available at: https://rwu.pressbooks.pub/webboceanography/chapter/7-4-patterns-of-primary-production/.

Werner, L.K. (2019) *A Pleistocene record of global fish production and implications for sustainability of polar fisheries*. Masters Thesis. University of California San Diego. Available at: https://escholarship.org/uc/item/41w8n1cw#main (Accessed: 19 September 2024).

Wise, S.B. and Stock, D.W. (2006) 'Conservation and divergence of Bmp2a, Bmp2b, and Bmp4 expression patterns within and between dentitions of teleost fishes', *Evolution & development*, 8(6), pp. 511–523. Available at: https://doi.org/10.1111/J.1525-142X.2006.00124.X.

Chapter 5: Relationships between late Pleistocene North Atlantic primary, export, and fish production

Abstract

In the prior three chapters, I produced new records of productivity to reconstruct changes in specific components of the North Atlantic marine ecosystem across glacial-interglacial cycles during the late Pleistocene. In this chapter, I use linear regressions to test whether significant relationships existed between primary, export, and fish production over the past 200 kyrs. I find a positive relationship between coccolith and export production during the Last Interglacial at ODP Site 982 and during glacial intervals at IODP Site U1313, suggesting that coccolithophores contribute significantly to organic carbon export during intervals when total export is relatively low. I also resolve a mixture of negative and insignificant relationships between fish and export production at both sites, suggesting that fish-mediated organic carbon export did not contribute significantly during times of elevated export production. Lastly, I find no significant relationships between fish and coccolithophore production during the past 200 kyrs, which may indicate either that fish production is more strongly influenced by environmental factors such as temperature as opposed to primary production, or that coccolith accumulation provides an incomplete view of total primary production in the pelagic North Atlantic Ocean.

Chapter contents

5.1. Introduction

The prior three chapters have presented new datasets concerning different aspects of biological productivity from the late Pleistocene North Atlantic Ocean. The purpose of this chapter is test for relationships between these independent datasets and therefore provide a more integrated and holistic view of North Atlantic ecosystem change over the past 200 kyr.

Understanding large-scale ecosystem changes requires a consideration of how energy is transferred between organisms and trophic levels in the marine environment. In the simplest sense, energy transfer to upper trophic levels is constrained by primary production (Chassot *et al.*, 2010) and trophic transfer efficiency (Blanchard *et al.*, 2012). The latter may itself vary as a function of both environmental variables such as temperature (Barneche *et al.*, 2021; Atkinson *et al.*, 2024), and ecological factors such as number of intermediate trophic levels (Sigman and Hain, 2012; Armengol *et al.*, 2019; Massing *et al.*, 2022). For example, the persistence of a strong microbial loop is thought to limit energy transfer to higher trophic levels in many open ocean oligotrophic environments, producing both low primary production and low fish production that characterises much of the open ocean (Platt, Rao and Irwin, 1983; Pomeroy *et al.*, 2007; Rousseaux and Gregg, 2013; Webb, 2021).

In modern marine environments, primary production has been shown to display a clear limit on fish production on a local (Knight and Jiang, 2009; Piroddi, Giovanni and Villy, 2010; Feng *et al.*, 2021), regional (Conti and Scardi, 2010; Marshak and Link, 2021), and global scale (Chassot *et al.*, 2010). The emphasis of contemporary research has tended to be on commercially harvested fishes, which represent a minute fraction of approximately 30,000 total extant fish species (Nelson, Grande and Wilson, 2016; FAO, 2020). There has been limited exploration in prior literature of the relationship between primary production and mesopelagic fishes (with exceptions, e.g. Anderson et al., 2019), despite these fishes likely composing the majority of total vertebrate biomass on Earth (Gjøsaeter and Kawaguchi K., 1980; Irigoien, Hulsman and Harris, 2004; Irigoien *et al.*, 2014; Clavel-Henry *et al.*, 2020). As discussed in Chapter 4, the dominance of mesopelagic fishes in overall fish biomass suggests that they may similarly dominate pelagic ichthyolith record (Sibert *et al.*, 2017), and prior research suggests that primary production was less significant than temperature in explaining patterns of fish production in the early Cenozoic (Britten and Sibert, 2020). This research is the first to directly compare fish and primary production using proxies generated from the same sample material.

As well as constraining fish production, primary production also limits the maximum amount of organic carbon that can be exported to depth. However, primary production is often nonlinearly related to export production. Export ratios (export production/primary production) vary from less than 0.1 in the stratified subtropical gyres, to 0.4 in productive polar waters (Nowicki, DeVries and Siegel, 2022). For example, Lopes, Kucera and Mix (2015) found an inverse relationship between primary and export production in the North Pacific across the last glacial termination using fossil diatom flora, attributing this to changing ecosystem structure and seafloor preservation.

Ocean warming is likely to lead to enhanced vertical stratification, which may negatively impact primary production by reducing the resupply of limiting nutrients to the mixed layer (Lozier *et al.*, 2011; Fu, Randerson and Moore, 2016; Li *et al.*, 2020). Nutrient stress further favours the proliferation of ecosystems dominated by small phytoplankton with weak export potential (Fu, Randerson and Moore, 2016). The productivity characteristics of the North Atlantic are also strongly influenced by the North Atlantic Current (NAC), which raises the temperature of the midlatitude and subpolar region and supports nutrient resupply to the shallow ocean through physical mixing (Krauss, 1986; Rossby, 1996; Naafs *et al.*, 2010). Taken together, warming is predicted to reduce both primary and export production in the midlatitude ocean, with changes to vertical structure and ecosystem structure likely to dominate change.

As discussed in the Chapter 4, the contribution of fish faecal pellets to export production is estimated at 3–29% of total export from the euphotic zone (Davison *et al.*, 2013; Hudson *et al.*, 2014; Saba *et al.*, 2021). The proportional contribution of faecal pellets (including those produced by zooplankton) is highest in the stratified gyres and relatively low in productive low-latitude waters (Nowicki, DeVries and Siegel, 2022). No previous research has compared geological proxy reconstructions of fish and export production to assess the potential significance of fish faecal pellets to organic carbon export during intervals of past climate change.

In this chapter, I will test the following hypotheses:

- A positive relationship existed between primary and fish production in the geological past.
- Fish production is more strongly associated with ocean temperature than primary production.
- There is strong positive relationship between primary and export production.
- Fish production is positively correlated with export production, and the relationship is stronger at temperate latitudes than in the subpolar ocean.

5.2. Methods

To synthesise across datasets, I test for relationships between nannofossil accumulation rate (NAR), excess barium accumulation rate ($Ba_{XS}AR$), and ichthyolith accumulation rate (IAR) for IODP Hole U1313A and ODP Hole 982B

For each variable pairing, regressions were produced for: the entire dataset, glacial intervals, and interglacial intervals. Regressions only include samples where data was generated for both productivity variables, which is a subset of the total dataset since data were not generated for all samples for all proxies. This results in variable total, glacial, and interglacial sample size in each case (listed in Table 5.1 and Table 5.2), with potential to influence the coefficient of determination (R^2). This means that, for some regressions, sample sizes are too

small to permit a meaningful reconstruction of the relationships between variables. Specific cases of this are considered in the Discussion.

For both sites, glacial intervals include the Last Glacial period (LGP) and Penultimate Glacial Period (PGP). For ODP Hole 982B, samples from the Last Interglacial (LIG) constitute the vast majority of all samples, but Ba_{XS}AR–NAR regressions also include a single sample from both the Holocene and Marine Isotope Stage 7 (MIS 7). All interglacial samples from IODP Hole U1313A are from the LIG.

5.3. Results

Full coefficient of determination (R^2) value for all regressions are listed in Table 5.1 and Table 5.2 (to 3 decimal places) and are described in greater detail in each related subsection below.

Table 5.1 – R^2 values for ODP Hole 982B samples with measurements for both variables shown in the corresponding heading, with sample size (n) shown in brackets.

ODP Hole 982B	IAR–Ba_{XS}AR	IAR–NAR	Ba_{XS}AR–NAR
All values	0.107 (n=17)	0.068 (n=12)	0.516 (n=24)
Glacial	0.182 (n=7)	0.967 (n=3)	0.182 (n=11)
Interglacial	0.052 (n=10)	0.012 (n=9)	0.410 (n=13)

Table 5.2 – R^2 values for IODP Hole U1313A samples with measurements for both variables shown in the corresponding heading, with sample size (n) shown in brackets.

IODP Hole U1313A	IAR–Ba_{XS}AR	IAR–NAR	Ba_{XS}AR–NAR
All values	0.181 (n=29)	0.004 (n=23)	0.014 (n=27)
Glacial	0.182 (n=9)	0.042 (n=7)	0.067 (n=10)
Interglacial	0.001 (n=20)	0.001 (n=16)	0.579 (n=17)

5.3.1. IAR and Ba_{XS}AR

For both ODP Hole 982B and IODP Hole U1313A, R^2 values were higher (0.182 and 0.182 respectively) for glacial samples compared to interglacial intervals (0.052 and 0.001 respectively). All glacial and interglacial regression coefficients are negative, but coefficients are more negative for glacial intervals in both cores. The regression coefficient for all samples is negative for IODP Hole U1313A and positive for ODP Hole 982B. R^2 values for all samples are intermediate compared to those for glacial intervals and interglacial intervals for both ODP Hole 982B (0.107) and IODP Hole U1313A (0.181).

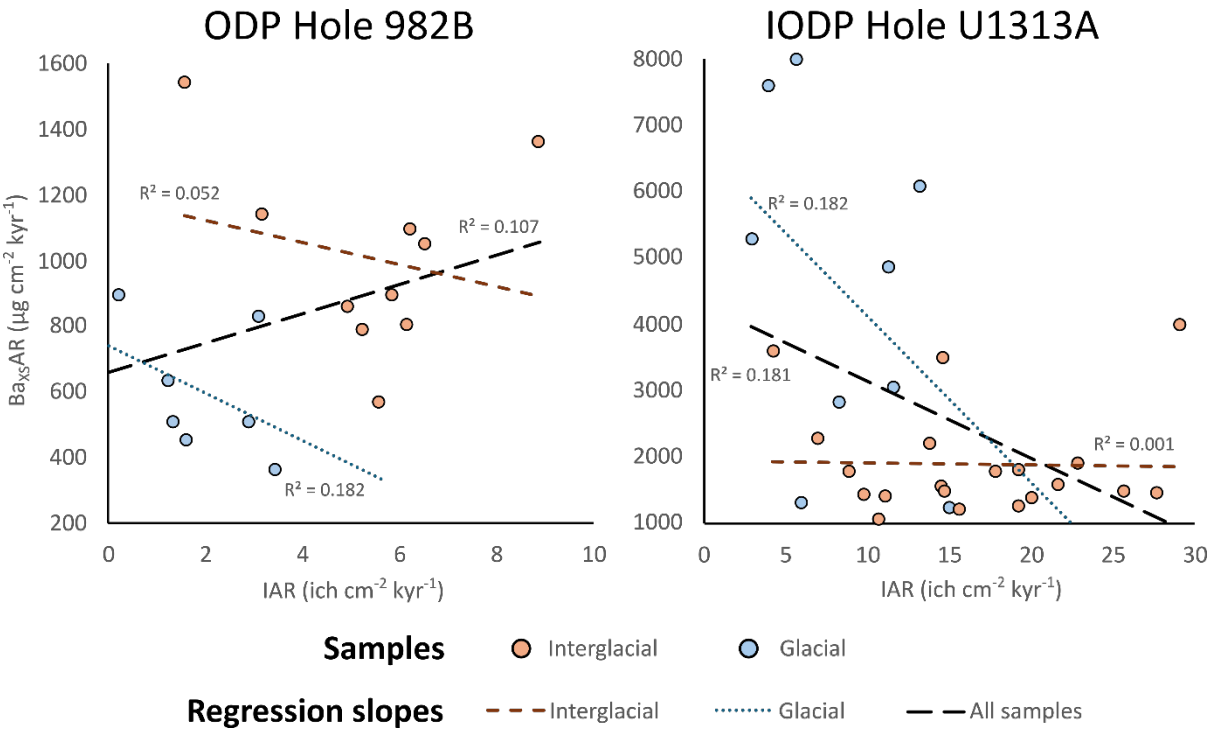

Figure 5.1 – Scatter plots for IAR and $Ba_{XS}AR$ showing glacial (blue) and interglacial (red) samples for ODP Hole 982B (left) and IODP Hole U1313A (right). Regression lines are indicated by long dashed black lines, short dashed red lines, and blue dotted lines for all samples, interglacial intervals, and glacial intervals respectively.

5.3.2. IAR and NAR

Only 12 data points for IAR and NAR were available for ODP Hole 982B. Very low R^2 values were found for all samples (0.068) and for interglacial intervals (0.012). The R^2 value for glacial samples, however, was the highest of any variable pair investigated (0.967), but only three samples are included in this dataset. The regression coefficients are low and positive for all samples and interglacial intervals, and relatively high and negative for glacial intervals.

For IODP Hole U1313A, R^2 values are below 0.05 for all three linear regressions. The regression coefficient is positive for glacial intervals and all samples, whilst the interglacial coefficient is relatively low and negative. The interglacial dataset is strongly influenced by a single sample at 77 ka that has both the highest NAR and IAR of all samples. If this sample is excluded, the interglacial coefficient of determination is increased (n_{IG}=15, R^2=0.342) and the regression coefficient becomes more negative.

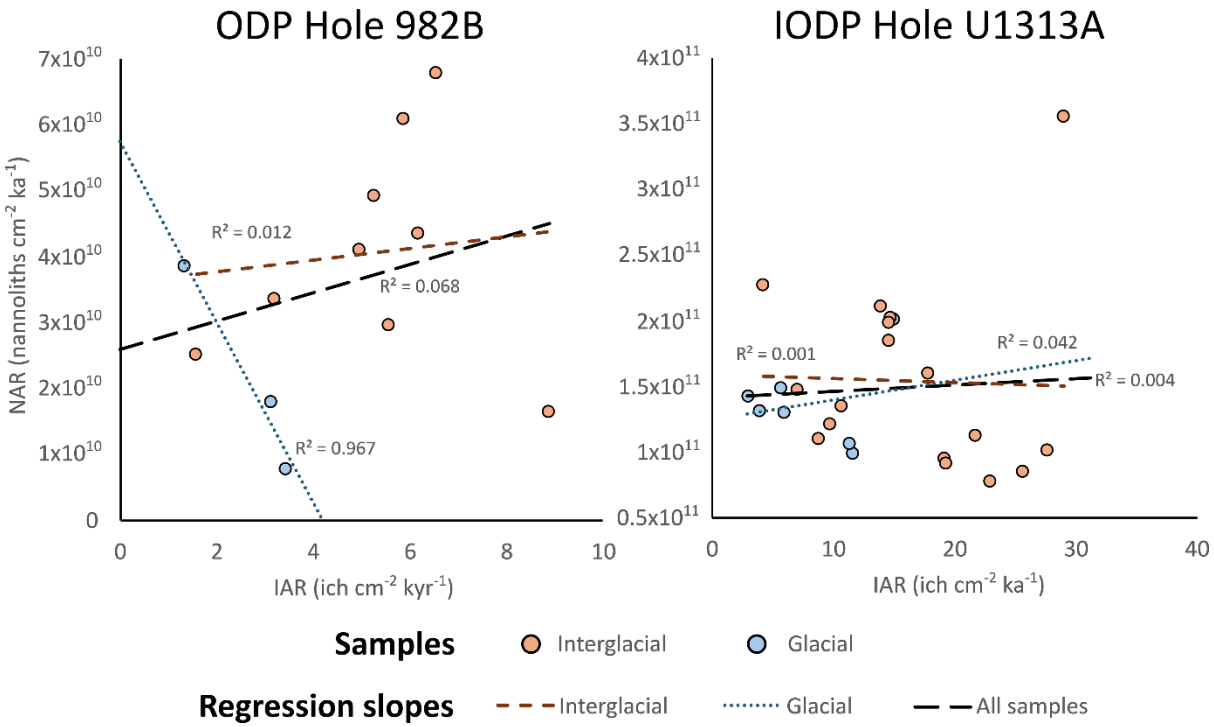

Figure 5.2 – Scatter plots for IAR and NAR showing glacial (blue) and interglacial (red) samples for ODP Hole 982B (left) and IODP Hole U1313A (right). Regression lines are indicated by long dashed black lines, short dashed red lines, and blue dotted lines for all samples, interglacial intervals, and glacial intervals respectively.

5.3.3. $Ba_{XS}AR$–NAR

Aside from the ODP Hole 982B glacial IAR–NAR regression (n=3 samples), the two highest R^2 values for any of the 18 total regressions occur in the interglacial relationship between $Ba_{XS}AR$ and NAR at both ODP Hole 982B (0.410) and IODP Hole U1313A (0.579). In both cases, the regression coefficient between $Ba_{XS}AR$ and NAR is positive, which is also the case for glacial intervals at the former site (R^2=0.183) but not the latter (R^2=0.0666). For ODP Hole 982B, the relationship is highly sensitive to a Holocene (6.5 ka) sample with a $Ba_{XS}AR$ value almost twice as high as the next highest value and NAR 38% higher than the next largest (from MIS7 at 200 ka). If the Holocene sample is excluded from the dataset, the ODP Hole 982B interglacial regression coefficient between $Ba_{XS}AR$ and NAR becomes negative (n_{IG}=12, R^2=0.188), although the relationship for all samples remains positive (n=23, R^2=0.180).

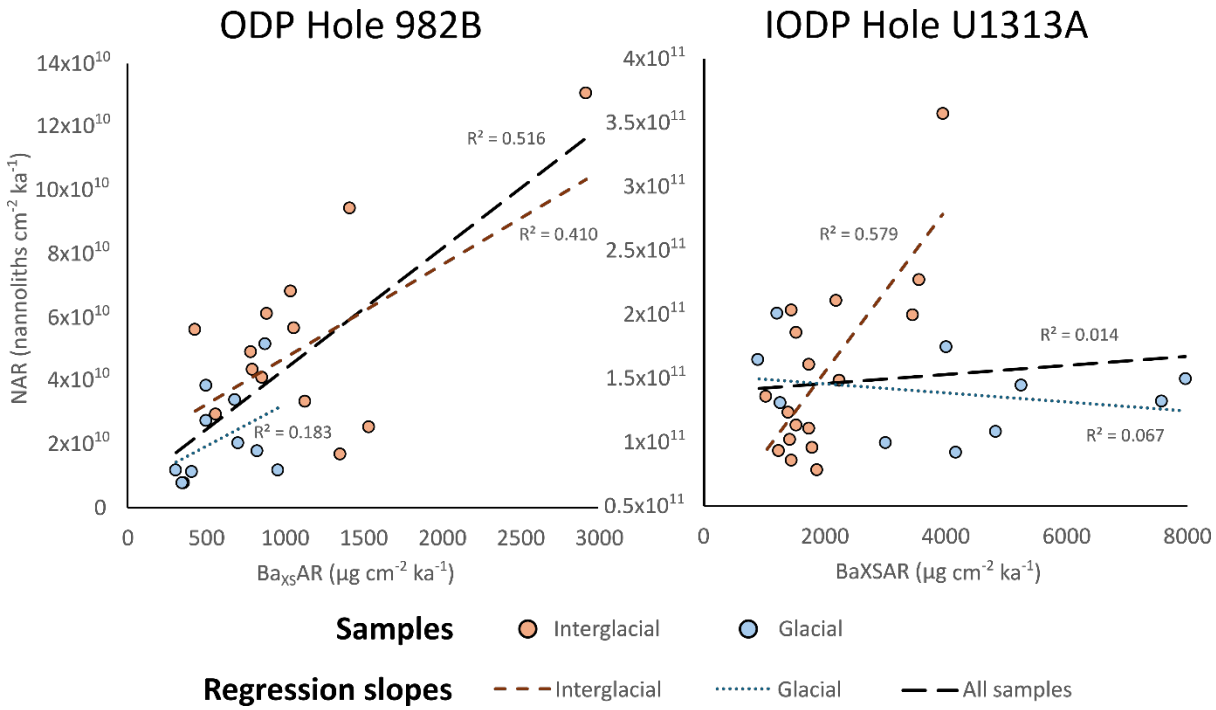

Figure 5.3 – Scatter plots for $Ba_{XS}AR$ and NAR showing glacial (blue) and interglacial (red) samples for ODP Hole 982B (left) and IODP Hole U1313A (right). Regression lines are indicated by long dashed black lines, short dashed red lines, and blue dotted lines for all samples, interglacial intervals, and glacial intervals respectively.

5.4. Discussion

Most relationships that were investigated using these regressions are of very low significance, suggesting that changes in coccolithophore production, export production, and fish production are often independent of each other, or weakly related. However, there are also some examples of where these relationships are more significant. Notably, there is an apparently positive interglacial relationship between coccolithophore production and export production, which permits an insight into the ecosystem factors that influence organic carbon export in the North Atlantic. Relationships that were generally or entirely insignificant, such as those between fish production and coccolithophore production, are also considered as these help to inform the functioning of both ecosystems and the organic carbon pump during the late Pleistocene.

5.4.1. Trophic connections between autotrophs and fishes

Chapter 4 established that fish production is suppressed during glacial intervals relative to interglacial intervals in both the temperate and subpolar North Atlantic. The results of the current chapter indicate that no systematic relationship existed between fish and coccolithophore production in the late Pleistocene. The only significant relationship between IAR and NAR was found in a regression containing three samples, which is far too small to make meaningful conclusions. During all other intervals, there is no significant relationship between these two variables.

Omitting the outlying sample at 77 ka for interglacial intervals at IODP Site U1313 produces a negative relationship between the NAR and IAR, which might have been explained through a transition to more oligotrophic conditions favourable to coccolithophore propagation (Jordan, 2009; Poulton *et al.*, 2017) and the persistence of a strong microbial loop resulting in the retention of energy in low and predominantly planktonic trophic levels (Sigman and Hain, 2012; Eddy *et al.*, 2021). This transition could result in a reduction in the proportion of energy produced through primary production that reaches those higher trophic steps occupied by fishes. However, there is no methodological reason to omit the outlying datapoint, and hence it coccolithophore primary production and fish production may vary independently.

There are two likely explanations for the absence of a significant relationship between coccolithophores and fishes, either: primary production is not the main control on mesopelagic fish production; and/or coccolithophore production is an unreliable proxy for total primary production.

Though contemporary studies indicate that primary production does provide a control on total fish production (e.g. Chassot et al., 2010; Blanchard et al., 2012), this result has not been replicated to-date using the fish microfossil record (e.g. Britten and Sibert, 2020; Sibert et al., 2020). Britten and Sibert (2020) found that primary production was a weak explanatory variable for reconstructed fish production in the early Cenozoic using a basic ecosystem model, and that deepwater temperature changes showed a stronger relationship with fish biomass as reconstructed using ichthyolith accumulation rates. Chapter 4 highlighted that alkenone accumulation rate, which has been suggested to reflect total primary production, and not only primary production by haptophyte algae (Bolton *et al.*, 2010; Raja and Rosell-Melé, 2021), displays poor agreement with the ichthyolith record, further supporting the independence of fish and autotroph productivity.

It is also probable that autotroph palaeoproductivity proxies imperfectly capture primary production (Anderson and Winckler, 2005; Schoepfer *et al.*, 2015; Hernández-Almeida *et al.*, 2019) The NAR record used in this work uses the accumulation rate of coccoliths that have been exported to the seafloor, either through direct sinking (Klaas and Archer, 2002; Schmidt *et al.*, 2014) or by aggregation in zooplankton faecal pellets (Roth, Mullin and Berger, 1975; Turner, 2002; Menschel, González and Giesecke, 2016; White *et al.*, 2018). Hence NAR is likely to record variations only in the productivity of coccolith-producing haptophyte algae, which comprise 10–20% of modern standing chlorophyll *a* biomass in the tropical and subtropical Atlantic (Poulton *et al.*, 2006, 2007), and up to 40% of total primary production at lower latitudes during blooming events (Broerse *et al.*, 2000; Poulton *et al.*, 2013; Rousseaux and Gregg, 2013). Whilst numerous studies have used surface sediment alkenone concentration as proxy for primary production or chlorophyll-*a* biomass (e.g. Volkman et al., 1995; Bolton et al., 2010; Marino et al., 2022), this relationship appears to be more significant in the subtropical ocean relative to the tropical or polar ocean (Raja and Rosell-Melé, 2021). Given that the vast majority of marine autotrophic and mixotrophic clades do not produce either alkenones or robust biomineralized exoskeletal components, the marine microfossil record will necessarily only enable a partial reconstruction of past ecosystems. It is therefore

important that palaeoecological reconstructions such as this one acknowledge that many clades and trophic steps will be absent from the sedimentary record (Woodhouse *et al.*, 2024).

This study had originally intended to produce a diatom palaeoproductivity record to give a more holistic view of autotroph dynamics over the past 200 kyr. However, initial investigations for determining sedimentary diatom concentrations through settling (Warnock and Scherer, 2014) yielded extremely low total abundances, implying very low accumulation of diatom frustules. Geochemical measurements of bulk silica were considered as an alternative means of reconstructing diatom abundances (e.g. Cortese et al., 2004; Etourneau et al., 2012; Worne et al., 2019), but these are also unlikely to provide useful information owing to silica content from ice-rafted debris deposition (Baumann and Huber, 1999; Venz *et al.*, 1999; Smith *et al.*, 2013; Lang *et al.*, 2016), particularly during glacial intervals and at the subpolar site.

It is additionally possible that ichthyolith accumulation rate imperfectly captures mesopelagic fish productivity, as was discussed in detail in Chapter 4.

5.4.2. Significance of fish-mediated organic carbon export

The consistently negative relationships between IAR and $Ba_{XS}AR$ indicates that the higher mean interglacial export at ODP Site 982 and higher glacial export at IODP Site U1313 was not primarily driven by changes in mesopelagic fish-mediated organic carbon transport to depth.

At the temperate site, intervals of highest fish production tend to coincide with weak export production and there is only one sample in which both reconstructed export and fish production are simultaneously higher than the mean for all samples. The most significant regressions at IODP Site U1313 are those with more negative coefficients, indicating that fishes contribute a relatively small fraction of total organic carbon in highly productive temperate regimes.

At the subpolar site, negative coefficients are also seen in both glacial and interglacial regressions, with glacial intervals being more significant. However, there is notably higher incidence of both elevated fish and export production compared to the temperate site.

This suggests that any increased magnitude of fish-mediated organic carbon export during interglacial intervals is weak relative to changes in other components of the organic carbon pump, such as aggregate sinking and physical mixing. For example, greater stratification during interglacial intervals may be more quantitatively significant in suppressing export at IODP Site U1313 (Fu, Randerson and Moore, 2016). These results are consistent with models suggesting that faecal pellets make a more proportionally significant contribution to total organic carbon export in unproductive, oligotrophic environments, whereas their contribution to overall export is low in eutrophic, productive environments (Anderson *et al.*, 2019; Nowicki, DeVries and Siegel, 2022).

5.4.3. Coccolithophore and organic carbon export

These regressions resolved a positive relationship between $Ba_{XS}AR$ and NAR during interglacial intervals at IODP Site U1313, suggesting that primary production by coccolith-producing

haptophyte algae is a direct or indirect driver of enhanced organic carbon export. Insignificant weak positive and negative relationships are seen for all samples and glacial intervals respectively, suggesting little influence of coccoliths of total export production in the midlatitude North Atlantic during glacial intervals.

All three regressions for ODP Site 982 produced moderately significant positive relationships. However, if looking only at samples from the LIG, the interglacial relationship between NAR and $Ba_{XS}AR$ becomes negative and moderately significant. This indicates that coccoliths productivity was negatively associated with total export during the LIG, in sharp contrast with the opposite finding at IODP Site U1313.

These results indicate that the contribution of coccolithophores in the organic carbon pump, either directly through sinking or by fuelling production at higher trophic levels, is more significant when total organic carbon export is low, i.e. during interglacial intervals at IODP Site U1313 and glacial intervals at ODP Site 982. For IODP Site U1313, the LIG was characterised by more oligotrophic, subtropical conditions due to weak allogenic nutrient inputs from both continental dust and vertical mixing, the latter due to the northward displacement of North Atlantic Transitional Waters (NATW; McIntyre, Ruddiman and Jantzen, 1972; Villanueva et al., 2001; Schwab et al., 2012) and subsequent enhanced vertical ocean stratification. At ODP Site 982 greater oligotrophy during glacial intervals is similarly related to the movement of the NATW, but in this case the NATW move southwards due the expansion of the subpolar gyre. The relationship between coccolithophore production and organic carbon export is weaker at ODP Site 982 however, due to the smaller contribution of coccolithophores to primary production in cold, high-latitude waters (Rousseaux and Gregg, 2013; Poulton *et al.*, 2017).

5.5. Conclusion

Using linear regressions, I compared the relationship between NAR, $Ba_{XS}AR$, and IAR in the late Pleistocene North Atlantic in two sediment cores for glacial intervals and interglacial intervals to test whether and how primary, fish, and export production were related during the late Pleistocene. Weak relationships between IAR and $Ba_{XS}AR$ suggest the fishes did not play a significant role in driving organic carbon export to depth, particularly in more oligotrophic systems. NAR is positively correlated with $Ba_{XS}AR$ at during the LIG at IODP Site U1313 and during glacial intervals at ODP Site 982, suggesting an important contribution of sinking aggregated coccolith biomass to export in stratified and oligotrophic waters. No notable relationships exist between IAR and NAR, supporting the idea that fish production is more strongly influenced by environmental variables relative to basal ecosystem changes. This research highlights the potential, but also the limitations of using the fossil and geochemical record holistically to try and reconstruct ecosystem change through time.

References

Anderson, R.F. and Winckler, G. (2005) 'Problems with paleoproductivity proxies', *Paleoceanography*, 20(3), pp. 1–7. Available at: https://doi.org/10.1029/2004PA001107.

Anderson, T.R. *et al.* (2019) 'Quantifying carbon fluxes from primary production to mesopelagic fish using a simple food web model', *ICES Journal of Marine Science*, 76(3), pp. 690–701. Available at: https://doi.org/10.1093/ICESJMS/FSX234.

Armengol, L. *et al.* (2019) 'Planktonic food web structure and trophic transfer efficiency along a productivity gradient in the tropical and subtropical Atlantic Ocean', *Scientific Reports*, 9(1), pp. 1–19. Available at: https://doi.org/10.1038/s41598-019-38507-9.

Atkinson, A. *et al.* (2024) 'Steeper size spectra with decreasing phytoplankton biomass indicate strong trophic amplification and future fish declines', *Nature Communications*, 15(1), p. 381. Available at: https://doi.org/10.1038/s41467-023-44406-5.

Barneche, D.R. *et al.* (2021) 'Warming impairs trophic transfer efficiency in a long-term field experiment', *Nature*, 592(7852), pp. 76–79. Available at: https://doi.org/10.1038/s41586-021-03352-2.

Baumann, K.-H. and Huber, R. (1999) 'Sea-surface gradients between the North Atlantic and the Norwegian Sea during the last 3.1 m.y.: comparison of Sites 982 and 985', in *Proceedings of the Ocean Drilling Program, 162 Scientific Results*. Ocean Drilling Program, pp. 179–190. Available at: https://doi.org/10.2973/odp.proc.sr.162.014.1999.

Blanchard, J.L. *et al.* (2012) 'Potential consequences of climate change for primary production and fish production in large marine ecosystems', *Philosophical Transactions of the Royal Society B: Biological Sciences*, 367(1605), pp. 2979–2989. Available at: https://doi.org/10.1098/rstb.2012.0231.

Bolton, C.T. *et al.* (2010) 'Glacial–interglacial productivity changes recorded by alkenones and microfossils in late Pliocene eastern equatorial Pacific and Atlantic upwelling zones', *Earth and Planetary Science Letters*, 295(3–4), pp. 401–411. Available at: https://doi.org/10.1016/j.epsl.2010.04.014.

Britten, G.L. and Sibert, E.C. (2020) 'Enhanced fish production during a period of extreme global warmth', *Nature Communications*, 11(1), p. 5636. Available at: https://doi.org/10.1038/s41467-020-19462-w.

Broerse, A.T.C. *et al.* (2000) 'Coccolithophore export production, species composition, and coccolith-CaCO3 fluxes in the NE Atlantic (34°N21°W and 48°N21°W)', *Deep Sea Research Part II: Topical Studies in Oceanography*, 47(9–11), pp. 1877–1905. Available at: https://doi.org/10.1016/S0967-0645(00)00010-2.

Chassot, E. *et al.* (2010) 'Global marine primary production constrains fisheries catches', *Ecology Letters*, 13(4), pp. 495–505. Available at: https://doi.org/10.1111/j.1461-0248.2010.01443.x.

Clavel-Henry, M. *et al.* (2020) 'Spatial Distribution and Abundance of Mesopelagic Fish Biomass in the Mediterranean Sea', *Frontiers in Marine Science*, 7, p. 573986. Available at: https://doi.org/10.3389/FMARS.2020.573986/BIBTEX.

Conti, L. and Scardi, M. (2010) 'Fisheries yield and primary productivity in large marine ecosystems', *Marine Ecology Progress Series*, 410, pp. 233–244. Available at: https://doi.org/10.3354/meps08630.

Cortese, G. *et al.* (2004) 'Opal sedimentation shifts in the World Ocean over the last 15 Myr', *Earth and Planetary Science Letters*, 224(3–4), pp. 509–527. Available at: https://doi.org/10.1016/J.EPSL.2004.05.035.

Davison, P.C. *et al.* (2013) 'Carbon export mediated by mesopelagic fishes in the northeast Pacific Ocean', *Progress in Oceanography*, 116, pp. 14–30. Available at: https://doi.org/10.1016/J.POCEAN.2013.05.013.

Eddy, T.D. *et al.* (2021) 'Energy Flow Through Marine Ecosystems: Confronting Transfer Efficiency', *Trends in Ecology and Evolution*, 36(1), pp. 76–86. Available at: https://doi.org/10.1016/J.TREE.2020.09.006/ASSET/3BC101A6-257D-41C0-995E-9668E26D772A/MAIN.ASSETS/GR1.SML.

Etourneau, J. *et al.* (2012) 'Contribution of changes in opal productivity and nutrient distribution in the coastal upwelling systems to Late Pliocene/Early Pleistocene climate cooling', *Climate of the Past*, 8(5), pp. 1435–1445. Available at: https://doi.org/10.5194/CP-8-1435-2012.

FAO (2020) *The State of World Fisheries and Aquaculture*, *Fisheries Oceanography*. Available at: https://doi.org/10.1111/fog.12466.

Feng, M. *et al.* (2021) 'Multi-year marine cold-spells off the west coast of Australia and effects on fisheries', *Journal of Marine Systems*, 214, p. 103473. Available at: https://doi.org/10.1016/j.jmarsys.2020.103473.

Fu, W., Randerson, J.T. and Moore, J.K. (2016) 'Climate change impacts on net primary production (NPP) and export production (EP) regulated by increasing stratification and phytoplankton community structure in the CMIP5 models', *Biogeosciences*, 13(18), pp. 5151–5170. Available at: https://doi.org/10.5194/bg-13-5151-2016.

Gjøsaeter, J. and Kawaguchi K. (1980) *A review of the world resources of mesopelagic fish*. Rome.

Hernández-Almeida, I. *et al.* (2019) 'A dataset of modern and fossil distribution of coccolithophore species Florisphaera profunda in the world's ocean', *Data in Brief*, 22, pp. 826–829. Available at: https://doi.org/10.1016/J.DIB.2018.12.079.

Hudson, J.M. *et al.* (2014) 'Myctophid feeding ecology and carbon transport along the northern Mid-Atlantic Ridge', *Deep Sea Research Part I: Oceanographic Research Papers*, 93, pp. 104–116. Available at: https://doi.org/10.1016/j.dsr.2014.07.002.

Irigoien, X. *et al.* (2014) 'Large mesopelagic fishes biomass and trophic efficiency in the open ocean', *Nature Communications 2014 5:1*, 5(1), pp. 1–10. Available at: https://doi.org/10.1038/ncomms4271.

Irigoien, X., Hulsman, J. and Harris, R.P. (2004) 'Global biodiversity patterns of marine phytoplankton and zooplankton', *Nature*, 429(6994), pp. 863–867. Available at: https://doi.org/10.1038/nature02593.

Jordan, R.W. (2009) 'Coccolithophores', in *Encyclopedia of Microbiology*. Elsevier, pp. 593–605. Available at: https://doi.org/10.1016/B978-012373944-5.00249-2.

Klaas, C. and Archer, D.E. (2002) 'Association of sinking organic matter with various types of mineral ballast in the deep sea: Implications for the rain ratio', *Global Biogeochemical Cycles*, 16(4), pp. 63-1-63–14. Available at: https://doi.org/10.1029/2001gb001765.

Knight, B.R. and Jiang, W. (2009) 'Assessing primary production constraints in New Zealand fisheries', *Fisheries Research*, 100(1), pp. 15–25. Available at: https://doi.org/10.1016/j.fishres.2009.06.001.

Krauss, W. (1986) 'The North Atlantic Current', *Journal of Geophysical Research: Oceans*, 91(C4), pp. 5061–5074. Available at: https://doi.org/10.1029/JC091IC04P05061.

Lang, D.C. *et al.* (2016) 'Incursions of southern-sourced water into the deep North Atlantic during late Pliocene glacial intensification', *Nature Geoscience*, 9(5), pp. 375–379. Available at: https://doi.org/10.1038/ngeo2688.

Li, G. *et al.* (2020) 'Increasing ocean stratification over the past half-century', *Nature Climate Change 2020 10:12*, 10(12), pp. 1116–1123. Available at: https://doi.org/10.1038/s41558-020-00918-2.

Lopes, C., Kucera, M. and Mix, A.C. (2015) 'Climate change decouples oceanic primary and export productivity and organic carbon burial', *Proceedings of the National Academy of Sciences of the United States of America*, 112(2), pp. 332–335. Available at: https://doi.org/https://doi.org/10.1073/pnas.141048011.

Lozier, M.S. *et al.* (2011) 'On the relationship between stratification and primary productivity in the North Atlantic', *Geophysical Research Letters*, 38(18), p. n/a-n/a. Available at: https://doi.org/10.1029/2011GL049414.

Marino, M. *et al.* (2022) 'Paleoproductivity proxies and alkenone precursors in the Western Mediterranean during the Early-Middle Pleistocene transition', *Palaeogeography, Palaeoclimatology, Palaeoecology*, 601, p. 111104. Available at: https://doi.org/10.1016/J.PALAEO.2022.111104.

Marshak, A.R. and Link, J.S. (2021) 'Primary production ultimately limits fisheries economic performance', *Scientific Reports*, 11(1), p. 12154. Available at: https://doi.org/10.1038/s41598-021-91599-0.

Massing, J.C. *et al.* (2022) 'Toward a Solution of the "Peruvian Puzzle": Pelagic Food-Web Structure and Trophic Interactions in the Northern Humboldt Current Upwelling System Off Peru', *Frontiers in Marine Science*, 8, p. 759603. Available at: https://doi.org/10.3389/FMARS.2021.759603/BIBTEX.

McIntyre, A., Ruddiman, W.F. and Jantzen, R. (1972) 'Southward penetrations of the North Atlantic polar front: faunal and floral evidence of large-scale surface water mass movements over the last 225,000 years', *Deep Sea Research and Oceanographic Abstracts*, 19(1), pp. 61–77. Available at: https://doi.org/10.1016/0011-7471(72)90073-3.

Menschel, E., González, H.E. and Giesecke, R. (2016) 'Coastal-oceanic distribution gradient of coccolithophores and their role in the carbonate flux of the upwelling system off Concepción, Chile (36°S)', *Journal of Plankton Research*, 38(4), pp. 798–817. Available at: https://doi.org/10.1093/PLANKT/FBW037.

Naafs, B.D.A. *et al.* (2010) 'Late Pliocene changes in the North Atlantic Current', *Earth and Planetary Science Letters*, 298(3–4), pp. 434–442. Available at: https://doi.org/10.1016/j.epsl.2010.08.023.

Nelson, J.S., Grande, T.C. and Wilson, M.V.H. (2016) *Fishes of the World*. 5th edn. John Wiley & Sons.

Nowicki, M., DeVries, T. and Siegel, D.A. (2022) 'Quantifying the Carbon Export and Sequestration Pathways of the Ocean's Biological Carbon Pump', *Global Biogeochemical Cycles*, 36(3). Available at: https://doi.org/10.1029/2021GB007083.

Piroddi, C., Giovanni, B. and Villy, C. (2010) 'Effects of local fisheries and ocean productivity on the northeastern Ionian Sea ecosystem', *Ecological Modelling*, 221(11), pp. 1526–1544. Available at: https://doi.org/10.1016/j.ecolmodel.2010.03.002.

Platt, T., Rao, D.V.S. and Irwin, B. (1983) 'Photosynthesis of picoplankton in the oligotrophic ocean', *Nature*, 301(5902), pp. 702–704. Available at: https://doi.org/10.1038/301702a0.

Pomeroy, L.R. *et al.* (2007) 'The Microbial Loop', *Oceanography*, 20(2), pp. 28–33. Available at: http://www.jstor.com/stable/24860040 (Accessed: 15 November 2024).

Poulton, A.J. *et al.* (2006) 'Phytoplankton mineralization in the tropical and subtropical Atlantic Ocean', *Global Biogeochemical Cycles*, 20(4). Available at: https://doi.org/10.1029/2006GB002712.

Poulton, A.J. *et al.* (2007) 'Relating coccolithophore calcification rates to phytoplankton community dynamics: Regional differences and implications for carbon export', *Deep Sea Research Part II: Topical Studies in Oceanography*, 54(5–7), pp. 538–557. Available at: https://doi.org/10.1016/J.DSR2.2006.12.003.

Poulton, A.J. *et al.* (2013) 'The 2008 Emiliania huxleyi bloom along the Patagonian Shelf: Ecology, biogeochemistry, and cellular calcification', *Global Biogeochemical Cycles*, 27(4), pp. 1023–1033. Available at: https://doi.org/10.1002/2013GB004641.

Poulton, A.J. *et al.* (2017) 'Coccolithophore ecology in the tropical and subtropical Atlantic Ocean: New perspectives from the Atlantic meridional transect (AMT) programme', *Progress in Oceanography*, 158, pp. 150–170. Available at: https://doi.org/10.1016/j.pocean.2017.01.003.

Raja, M. and Rosell-Melé, A. (2021) 'Appraisal of sedimentary alkenones for the quantitative reconstruction of phytoplankton biomass', *Proceedings of the National Academy of Sciences*, 118(2). Available at: https://doi.org/10.1073/PNAS.2014787118.

Rossby, T. (1996) 'The North Atlantic Current and surrounding waters: At the crossroads', *Reviews of Geophysics*, 34(4), pp. 463–481. Available at: https://doi.org/10.1029/96RG02214.

Roth, P.H., Mullin, M.M. and Berger, W.H. (1975) 'Coccolith Sedimentation by Fecal Pellets: Laboratory Experiments and Field Observations', *Geological Society of America Bulletin*, 86(8), p. 1079. Available at: https://doi.org/10.1130/0016-7606(1975)86<1079:CSBFPL>2.0.CO;2.

Rousseaux, C. and Gregg, W. (2013) 'Interannual Variation in Phytoplankton Primary Production at A Global Scale', *Remote Sensing*, 6(1), pp. 1–19. Available at: https://doi.org/10.3390/rs6010001.

Saba, G.K. *et al.* (2021) 'Toward a better understanding of fish-based contribution to ocean carbon flux', *Limnology and Oceanography*, 66(5), pp. 1639–1664. Available at: https://doi.org/10.1002/lno.11709.

Schmidt, K. *et al.* (2014) 'Not all calcite ballast is created equal: Differing effects of foraminiferan and coccolith calcite on the formation and sinking of aggregates', *Biogeosciences*, 11(1), pp. 135–145. Available at: https://doi.org/10.5194/BG-11-135-2014.

Schoepfer, S.D. *et al.* (2015) 'Total organic carbon, organic phosphorus, and biogenic barium fluxes as proxies for paleomarine productivity', *Earth-Science Reviews*, 149, pp. 23–52. Available at: https://doi.org/10.1016/j.earscirev.2014.08.017.

Schwab, C. *et al.* (2012) 'Coccolithophore paleoproductivity and ecology response to deglacial and Holocene changes in the Azores Current System', *Paleoceanography*, 27(3). Available at: https://doi.org/10.1029/2012PA002281.

Sibert, E.C. *et al.* (2017) 'Methods for isolation and quantification of microfossil fish teeth and elasmobranch dermal denticles (Ichthyoliths) from marine sediments', *Palaeontologia Electronica*, 20(1), pp. 1–14. Available at: https://doi.org/10.26879/677.

Sibert, E.C. *et al.* (2020) 'No state change in pelagic fish production and biodiversity during the Eocene–Oligocene transition', *Nature Geoscience*, 13(3), pp. 238–242. Available at: https://doi.org/10.1038/s41561-020-0540-2.

Sigman, D.M. and Hain, M.P. (2012) 'The Biological Productivity of the Ocean', *Nature Education*, 3(6), pp. 1–16.

Smith, M.E. *et al.* (2013) 'Data report: oxygen isotopes and foraminifer abundance record for the last glacial-interglacial cycle and marine isotope Stage 6 at IODP Site U1313', in, pp. 1–11. Available at: https://doi.org/10.2204/iodp.proc.303306.216.2013.

Turner, J. (2002) 'Zooplankton fecal pellets, marine snow and sinking phytoplankton blooms', *Aquatic Microbial Ecology*, 27(1), pp. 57–102. Available at: https://doi.org/10.3354/ame027057.

Venz, K.A. *et al.* (1999) 'A 1.0 Myr Record of Glacial North Atlantic Intermediate Water Variability from ODP Site 982 in the Northeast Atlantic', *Paleoceanography*, 14(1), pp. 42–52. Available at: https://doi.org/10.1029/1998PA900013.

Villanueva, J. *et al.* (2001) 'A latitudinal productivity band in the Central North Atlantic over the last 270 kyr: An alkelone perspective', *Paleoceanography*, 16(6), pp. 617–626. Available at: https://doi.org/10.1029/2000PA000543.

Volkman, J.K. *et al.* (1995) 'Alkenones in Gephyrocapsa oceanica: Implications for studies of paleoclimate', *Geochimica et Cosmochimica Acta*, 59(3), pp. 513–520. Available at: https://doi.org/10.1016/0016-7037(95)00325-T.

Warnock, J.P. and Scherer, R.P. (2014) 'A revised method for determining the absolute abundance of diatoms', *Journal of Paleolimnology*, 53(1), pp. 157–163. Available at: https://doi.org/10.1007/s10933-014-9808-0.

Webb, P. (2021) 'Patterns of Primary Production', in *Introduction to Oceanography*. Roger Williams University. Available at: https://rwu.pressbooks.pub/webboceanography/chapter/7-4-patterns-of-primary-production/.

White, M.M. *et al.* (2018) 'Coccolith dissolution within copepod guts affects fecal pellet density and sinking rate', *Scientific Reports 2018 8:1*, 8(1), pp. 1–6. Available at: https://doi.org/10.1038/s41598-018-28073-x.

Woodhouse, A. *et al.* (2024) 'The Micropaleoecology Framework: Evaluating Biotic Responses to Global Change Through Paleoproxy, Microfossil, and Ecological Data Integration', *Ecology and Evolution*, 14(11), p. e70470. Available at: https://doi.org/10.1002/ece3.70470.

Worne, S. *et al.* (2019) 'Coupled climate and subarctic Pacific nutrient upwelling over the last 850,000 years', *Earth and Planetary Science Letters*, 522, pp. 87–97. Available at: https://doi.org/10.1016/J.EPSL.2019.06.028.

Chapter 6: Pelagic marine ecosystem responses to late Pleistocene climate change

Abstract

This thesis examined how pelagic marine ecosystems responded to glacial-interglacial climate change in the late Pleistocene. I generated new palaeo-productivity proxy datasets for coccolithophores, mesopelagic fishes, and export production in two North Atlantic sediment cores. I found distinct trends in each of the three productivity proxies during the late Pleistocene, as well as distinct changes in the subpolar and midlatitude ocean. The North Atlantic Current, which defines regional ocean temperature and vertical mixing in this basin, appears to have had an important role in coccolithophore and export production for both regions. Fish production was strongly influenced by ocean temperature, and regional changes were more synchronous than those seen in coccolithophores or organic carbon export. Organic carbon export production had opposite trends in the two regions, in that subpolar export increased sharply after the past two glacial terminations and remained high during the Last Interglacial, whereas high midlatitude export coincide with strong allogenic nutrient inputs during glacial intervals. I found that coccolithophores contributed more significantly to total organic carbon export in stratified, oligotrophic conditions. These findings suggest that abrupt ecological changes may accompany future anthropogenic climate change in the North Atlantic. The strength and direction of regional North Atlantic climate change has high uncertainty, with the potential to either track global warming trends or undergo cooling in response to Atlantic Meridional Overturning Circulation decline. In either case, late Pleistocene ecological and climate records may provide useful geological analogues.

Chapter contents

6.1. Introduction

Pelagic marine environments play an important role in hosting biodiversity and influencing the global carbon cycle through the organic carbon pump. In previous chapters, I introduced new datasets related to marine productivity in the North Atlantic during the late Pleistocene, including productivity records for coccolith (Chapter 2), fish (Chapter 4), and export production (Chapter 3). In this final chapter, I provide an overview of the main results from the thesis, discuss the potential implications of these findings for future ecosystems under near-future climate change, and suggest additional work that could be undertaken to further test, extend, and refine the findings of this work. I address the overarching thesis questions that were asked in Chapter 1:

- Are there causative changes in North Atlantic primary production, export production, and fish production in response to climate on glacial-interglacial timescales?
- Do distinct plankton communities occupy the North Atlantic during glacial and interglacial intervals?
- Do changes in export productivity reflect synchronous changes in the overlying pelagic plankton and fish communities?
- Can we resolve positive trophic connections between plankton and fish using the microfossil record?

6.2. ODP Site 982

The modern subpolar Noth Atlantic is characterised by relatively high primary production (Rousseaux and Gregg, 2013; Webb, 2021; NASA Goddard Space Flight Center, Ocean Ecology Laboratory and Ocean Biology Processing Group, 2022) and mild temperatures due to the strong influence of the North Atlantic Current (NAC), which transports warm waters northwards from tropical latitudes (Krauss, 1986; Rossby, 1996). ODP Site 982 (Shipboard Scientific Party, 1996) is presently in the northern part of the North Atlantic Transitional Waters (NATW), the oceanic region defined by the influence of the NAC.

I found major increases in coccolithophore, fish, and export productivity at this site within 15 kyrs of the penultimate glacial termination (Termination II). This supports the hypothesis that the position of the NAC exerts a major control on both abiotic conditions and biological productivity in the North Atlantic during the late Pleistocene (McIntyre, Ruddiman and Jantzen, 1972; Villanueva *et al.*, 1997, 2001; Schwab *et al.*, 2012). Interglacial intervals coincided with a mild and vertically well-mixed subpolar ocean, broadly comparable to that of the Holocene. In contrast, marked temperature declines and enhanced vertical stratification characterise this region during glacial intervals, when the NAC is displaced to the south, limiting the productivity of haptophytes and supressing export production.

6.2.1. Subpolar coccolithophore production

At ODP Site 982, I found that coccolithophore production was significantly higher during interglacial intervals compared with glacial intervals. Mean NAR was over twice as high during interglacial intervals compared to glacial intervals, and individual samples from the Holocene and Marine Isotope Stage 7 (MIS7) both had an NAR over five times greater than the glacial mean. Whilst coccolithophore production increased dramatically within 5 kyr of Termination I, this is not true of the penultimate deglaciation (Termination II). Instead, sharp increases occurred more than 10 kyr after Termination II, later than increases in both export and fish production during the early LIG. High coccolithophore production during interglacial intervals likely reflects the higher relative and absolute abundances of

coccolithophores among eukaryotic phytoplankton in warm, pelagic environments in the present day (Sigman and Hain, 2012; Rousseaux and Gregg, 2013; Hagino and Young, 2015). Stronger vertical mixing during interglacial intervals due to the influence of the NAC may have also driven elevated haptophyte production by increasing the resupply of limiting nutrients to the mixed layer (Broerse *et al.*, 2000; Moore *et al.*, 2013; Hagino and Young, 2015; Guerreiro *et al.*, 2023). In contrast, the southwards migration of the NAC and NATW during glacial intervals may have created a more vertically stratified and nutrient-limited subpolar ocean (Villanueva *et al.*, 1997, 2001).

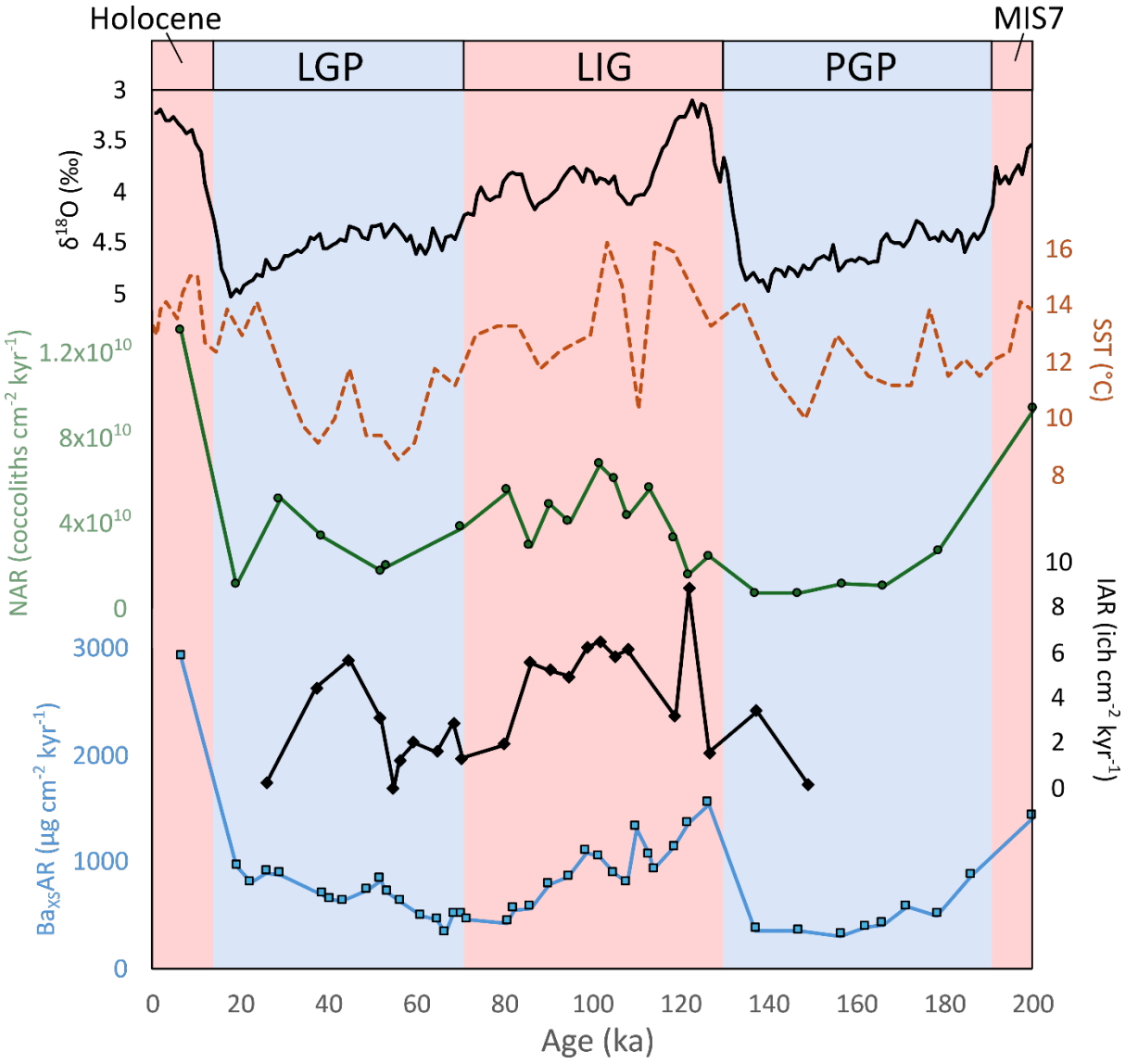

Figure 6.1 – Compilation of records for ODP Site 982, top to bottom: LR04 global $\delta^{18}O$ curve (Lisiecki and Raymo, 2005); site-specific $U^{K'}_{37}$-derived sea surface temperature (SST) reconstruction (Lawrence *et al.*, 2009; Herbert *et al.*, 2016); coccolith accumulation rate (green circles); ichthyolith accumulation rate (black diamonds); and excess barium accumulation rate (blue squares).Blue and red backgrounds indicate glacial and interglacial intervals, respectively.

6.2.2. Subpolar fish production

This study was the first to investigate glacial-interglacial changes in fish production using the pelagic ichthyolith record. Subpolar ichthyolith accumulation rates (IAR) show an overall glacial-interglacial

signal that supports the hypothesis of enhanced mesopelagic fish production during intervals of greater ocean warmth. Contrary to what might be expected from ecological first principles and modern observations (e.g. Knight and Jiang, 2009; Chassot et al., 2010; Conti and Scardi, 2010; Blanchard et al., 2012; Marshak and Link, 2021), I found that mesopelagic fish production appears to show a relatively weak relationship to coccolithophore production and primary production as reconstructed from alkenones. This suggests that temperature-induced changes to trophic transfer efficiency more strongly influence energy transfer to small fishes than absolute changes in primary production, supporting the findings of Britten and Sibert (2020) from the early Cenozoic. However, as the coccolithophore fossil record and alkenone proxy record preserves only a fraction of total primary production (Sigman and Hain, 2012; Rousseaux and Gregg, 2013), changes in the productivity of other non-fossilising autotrophs (which could itself be positively correlated to water temperature) might be influencing total fish production.

6.2.3. Subpolar export production

Export production, reconstructed using excess barium accumulation rate ($Ba_{XS}AR$), follows a similar pattern to IAR at ODP Site 982. There is a threefold and fourfold increase in $Ba_{XS}AR$ following Termination I and Termination II, respectively. Unlike NAR and IAR, $Ba_{XS}AR$ increased immediately following Termination II without a lag, suggesting a strong influence of oceanographic conditions on total organic carbon export in the subpolar North Atlantic, likely related to the influence of the NAC.

There is a moderate negative correlation (R^2=0.188) between NAR and $Ba_{XS}AR$ during the LIG, indicating the relative importance of coccolith aggregates in organic matter export was lower as total export increased in this warm climate state. In contrast, there is a moderately-significant negative relationship between NAR and $Ba_{XS}AR$ during glacial intervals, suggesting that strong coccolith production coincides with higher export under more strongly stratified ocean conditions.

Export production and fish production have weak-to-moderately negative correlations ($R^2_{glacial}$=0.182; $R^2_{interglacial}$=0.052), possibly indicating a low proportional contribution of fish faecal pellets to total organic carbon export during times of high export production, and more significant proportional contributions of faecal pellets when total export is low. This finding is consistent with estimates of the contribution of faecal pellets in modern ocean environments (Nowicki, DeVries and Siegel, 2022). However, low sample sizes in correlations for this site imply low certainty in this negative relationship.

6.3. IODP Site U1313

IODP Site U1313 is located in the mid-latitude North Atlantic and today is in the southernmost part of the NATW and close to the Azores Current and subtropical gyre boundary (Expedition 306 Scientists, 2006). Mean annual primary production here is slightly lower than at ODP Site 982, although the NAC promotes a degree of vertical mixing that prevents the site becoming permanently stratified, contrasting with the subpolar gyre (Rousseaux and Gregg, 2013; Webb, 2021; NASA Goddard Space Flight Center, Ocean Ecology Laboratory and Ocean Biology Processing Group, 2022).

The span of samples for IODP Site U1313 is less temporally extensive than ODP Site 982 due to the partial depletion of this core. This prevents characterisation of the late LGP, including the Last Glacial Maximum, and around 15 kyrs of the mid-LIG.

Notably, unlike at ODP Site 982, coccolithophore, fish, and export production show major changes in the immediate aftermath of Termination II. Instead, the interval of greatest change in the mid-latitude North Atlantic appears to have been the late LIG and early LGP. Production trends at IODP Site U1313

may be explained through a combination of enhanced vertical mixing due to the southward migration of the NAC (McIntyre, Ruddiman and Jantzen, 1972; Villanueva *et al.*, 2001) and major increases in allogenic nutrient inputs during the early LGP (Naafs *et al.*, 2012), which led to the prevalence of more eutrophic conditions during glacial intervals than are observed today.

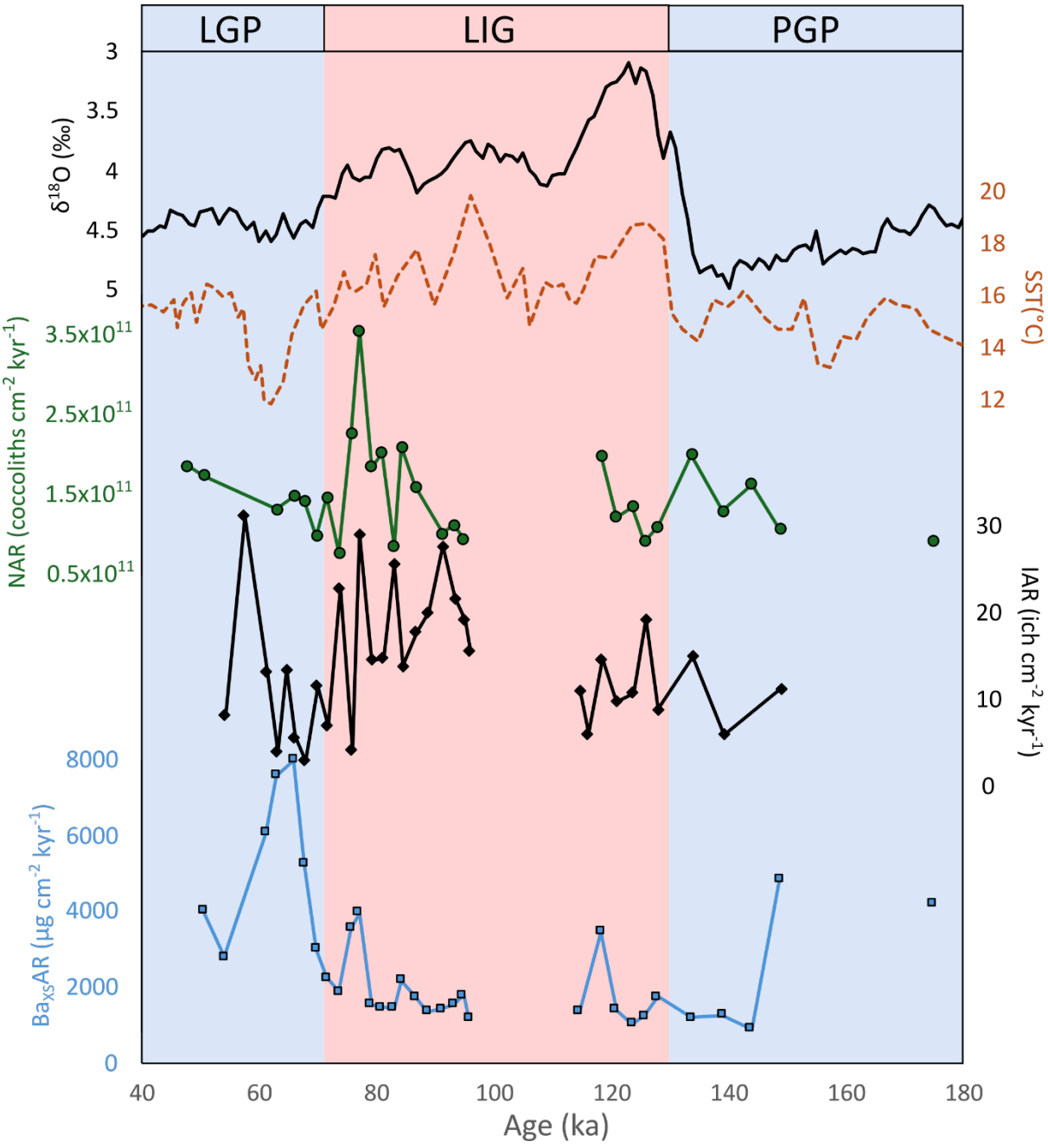

Figure 6.2 – Compilation of records for IODP Site U1313, top to bottom: LR04 global $\delta^{18}O$ curve (Lisiecki and Raymo, 2005); site-specific $U^{K'}_{37}$-derived SST reconstruction (Lawrence *et al.*, 2009; Herbert *et al.*, 2016); coccolith accumulation rate (green circles); ichthyolith accumulation rate (black diamonds); and excess barium accumulation rate (blue squares). Blue and red backgrounds indicate glacial and interglacial intervals, respectively.

6.3.1. Midlatitude coccolithophore production

At IODP Site U1313, I found no significant difference in NAR between the LIG and glacial intervals, although there was a notable increase in NAR during the late LIG. Mean NAR was around four times higher than at the subpolar site, likely due to higher temperatures. Given that the influence of the NAC likely persisted at this latitude throughout the study interval, these results suggest the warm conditions favoured by the most productive coccolithophore genera were generally present throughout the interval that was investigated. As with ODP Hole 982B, *Gephyrocapsa* spp. coccolithophore dominated the overall coccolith assemblage.

6.3.2. Midlatitude fish production

Fish production showed similar trends to that seen at the subpolar location, with significantly higher IAR during the LIG compared to the Penultimate Glacial Period (PGP) and Last Glacial Period (LGP). As with the more northerly site, the IAR trend displayed a stronger positive relationship with ocean temperature than coccolith production, supporting the hypothesis that millennial-scale mesopelagic fish production is closely tied to abiotic environmental changes. Mean IAR for all samples at this site was substantially higher than any other open ocean location where IAR has been reconstructed using comparable methods for any time in the geological past (Sibert, Hull and Norris, 2014; Sibert *et al.*, 2020). This finding suggests either that the midlatitude North Atlantic could be one of the most productive environments for mesopelagic fishes in the entire open ocean, or that the small fishes represented in the ichthyolith record tend to occupy multiple trophic steps at this location.

6.3.3. Midlatitude export production

$Ba_{XS}AR$ trends at IODP Site U1313 are opposite to those at ODP Site 982. Glacial $Ba_{XS}AR$ is significantly higher here during glacial intervals than during the LIG. Export increased dramatically following the LIG-LGP transition, and Ba_{XS} shows a strong positive relationship with aluminium concentrations (R^2=0.855), which I use as a proxy for detrital input. This result suggests that strong export at this location is driven by major increases in glacial primary production that occurred because of allogenic aeolian and/or ice-rafted nutrient inputs.

A moderate positive correlation (R^2=0.579) exists between interglacial $Ba_{XS}AR$ and NAR at IODP Site U1313, pointing towards a role for sinking coccolithophore biomass as an important contributor to total organic carbon export in the midlatitude North Atlantic when more oligotrophic conditions persist. In contrast, glacial NAR and $Ba_{XS}AR$ have no significant relationship (R^2=0.067), indicating that the importance of coccolithophore biomass to total export declines in a more eutrophic ocean.

As is the case at the subpolar location, IAR and $Ba_{XS}AR$ have a moderate negative relationship during glacial intervals (R^2=0.182) at IODP Site U1313. This result suggests a similar pattern of proportionally-low organic carbon export by fish faecal pellets during intervals of high total export production.

6.4. Implications for future anthropogenic change

The LIG was selected as an interval of interest due to the potential similarity of peak interglacial conditions (MIS5e) to low-severity, near-future climate change scenarios (Pei *et al.*, 2016; Burke *et al.*, 2018). However, the final sample resolution and diversity of climatic states (Shackleton, 1969; Tzedakis *et al.*, 2009) considered here for the LIG makes the interval less comparable to likely near-future climate states. Based on current emission projections (IPCC, 2023), it is likely that near-future climate

will fall outside of the envelope of Pleistocene climate states, potentially making older intervals such as the Pliocene and Eocene more suitable analogues over the coming centuries (Burke *et al.*, 2018).

Nonetheless, oceanographic changes occurred across the PGP–LIG transition coincident with warming. Increases in ocean temperature and enhanced vertical stratification in the mid-latitudes are both features of Pleistocene glacial terminations (Cutler *et al.*, 2003; Lisiecki and Raymo, 2005; Elderfield *et al.*, 2012) and likely consequences of future anthropogenic climate change (IPCC, 2019, 2023; Li *et al.*, 2020; Meinen *et al.*, 2020; Kuhlbrodt *et al.*, 2024). As discussed in this and prior chapters, these changes are likely to lead to a greater dominance of coccolithophores among North Atlantic phytoplankton fauna at high latitudes, and greater mesopelagic fish production across the North Atlantic basin on multi-millennial timescales. If coccolithophore dominance increases, it is likely export productivity will co-vary more strongly with coccolithophore production, but the absolute amount of organic carbon exported may decrease, particularly in the midlatitudes.

Atlantic Meridional Overturning Circulation (AMOC) stability is a major uncertainty in predicting future century-scale changes in North Atlantic environments and ecosystems because the weakening or collapse of AMOC could have a far greater impact on regional climate than global climate trends (Ditlevsen and Ditlevsen, 2023; Westen, Kliphuis and Dijkstra, 2024). The IPCC (2023) projects that AMOC weaking is 'very likely' to occur over the 21st century, though an abrupt collapse is unlikely on the same timescale. AMOC collapse would lead to significant cooling of the North Atlantic and the potential southwards displacement of the NAC (Ditlevsen and Ditlevsen, 2023; Westen, Kliphuis and Dijkstra, 2024), possibly producing regional oceanographic conditions comparable to those of Pleistocene glacial states (Nave *et al.*, 2010; Pöppelmeier *et al.*, 2021) despite a warming trend globally. In this thesis I found that regional cooling during the LIG–LGP transition coincided with significant reductions in high-latitude North Atlantic export production, and southwards shift in the export maximum, which followed the NAC. It is possible that future North Atlantic cooling could lead to similar changes. If future cooling occurs and is sustained over multi-millennium timescales, evidence from ichthyoliths indicates that mesopelagic fish productivity may also decrease, with potentially cascading impacts for organisms at higher trophic levels.

6.5. Future work

I have applied a multitude of approaches to reconstruct palaeoecology and palaeoproductivity in the late Pleistocene North Atlantic Ocean. Future work has been highlighted in relevant data chapters, but additional comments of relevance are provided below.

Geological research that utilises marine sediment is always limited by sample availability, sample size, and sedimentation rates. Although the temporal distribution of samples used in this thesis was dense compared to many deep time studies, it was still too coarse to capture some key components of the climate system. For example, Dansgaard-Oeschger cycles (Dansgaard *et al.*, 1993; Pedro *et al.*, 2022) and variations in AMOC (Guihou *et al.*, 2011; Pöppelmeier *et al.*, 2021) played an important role in defining the regional climate of the North Atlantic during the Pleistocene but occurred on sub-millennial timescales. It is not possible to capture such fine changes using the temporal density of my samples, in which a single sample spans includes more than 1000 years of sediment accumulation on average. Future work could focus on pelagic sites with high sedimentation rates to produce a record of sufficient temporal resolution to observe changes within glacial and interglacial states, which may prove more illustrative for comparisons with near-future change. This is particularly true for intervals of relatively rapid change, such as deglaciations.

The research presented in this thesis has spatial, as well as temporal, limitations. Including additional North Atlantic sediment cores in future research may be useful to test the extent to which patterns reconstructed here are local, as opposed to regional. Given the importance of the NAC to productivity conditions in the North Atlantic, it would be enlightening to test whether comparable trends are seen beyond the region of major NAC influence, such as the equatorial and South Atlantic Ocean.

The previous two suggestions have implied the inclusion of additional sample material may provide more robust conclusions. Whilst this is undoubtedly true, I would also encourage future workers to be conscious of the time it takes to process sedimentary material. The processing of samples for ichthyoliths is particularly time-consuming, as demonstrated by the cumulative thousands of hours spent processing ichthyolith samples to generate the data presented in Chapter 4. The development of further automated methods for generating geochemical and microfossil count data presents huge promise and vast time savings. However, as Chapter 2 of this thesis has highlighted, the outputs of automated methods should be treated with caution, as it may be many decades before they are reliable enough to wholly replace human workers.

The discovery of a correlation between fish production and ocean temperature in the late Pleistocene North Atlantic is a promising extension of a similar observation in the early Cenozoic (Britten and Sibert, 2020). Of the findings in this thesis, this relationship is perhaps the most novel and holds promise for future research, which could aim to measure glacial-interglacial IAR in other ocean basins to determine whether this is a global trend.

Further work could also be undertaken to test for the relationships between primary producers and fishes in deep time. In Chapter 4 I found no apparent relationship between a geochemical reconstruction of haptophyte production (Bolton *et al.*, 2011) and IAR, and in Chapter 5 I found generally weak relationships between IAR and NAR. These results suggest that primary production is less important that abiotic factors in determining mesopelagic fish production on millennial timescales. However, these two proxies provide an incomplete overview of total marine primary production. Future work should use a broader range of phytoplankton and primary production proxies to more robustly assess the relationship between trophic levels in the pelagic ocean.

This thesis provides an example of how multiple proxies can be used in a complimentary way to build a more holistic view of ecosystem and environmental change in the recent geological past. The geological record provides a means of empirically reconstructing past climatic and biotic conditions, which is of immense use in understanding both past and future conditions (Woodhouse *et al.*, 2024). The use of multiple proxies also overcomes some of the limits of the geological record, which will always be biased and incomplete; the most robust means of reconstructing past environments is likely to emerge through the combination of microfossil, geochemical, and computational approaches.

6.6. Conclusion

This thesis tested the impact of glacial-interglacial climate change on North Atlantic ecosystems and export production using new microfossil and geochemical datasets. I found that distinct changes occurred in the midlatitude and subpolar North Atlantic Ocean during the past 200 kyr. Oceanographic conditions, particularly the position of the North Atlantic Current, exerted a strong influence on both regions at different times. Ocean temperature played an important role in determining coccolithophore and fish production, and vertical stratification and allogenic nutrient inputs were important in determining the strength of export. The major findings of this thesis are that the midlatitude North Atlantic may have provided a hitherto unrecognised contribution to global organic

carbon sequestration during past glacial intervals, and that fish production appears to have been strongly associated with ocean temperature in the North Atlantic.

There is high uncertainty in predicting the status of the North Atlantic under near-future anthropogenic climate change, but this research shows that Pleistocene glacial and interglacial intervals have the potential to inform these predictions. Future work on North Atlantic ecosystems could be improved by considering the impact of sample spacing on hypothesis testing, including a greater number of site locations, and making use of newly developed automated methods.

References

Blanchard, J.L. *et al.* (2012) 'Potential consequences of climate change for primary production and fish production in large marine ecosystems', *Philosophical Transactions of the Royal Society B: Biological Sciences*, 367(1605), pp. 2979–2989. Available at: https://doi.org/10.1098/rstb.2012.0231.

Bolton, C.T. *et al.* (2011) 'Biotic and geochemical evidence for a global latitudinal shift in ocean biogeochemistry and export productivity during the late Pliocene', *Earth and Planetary Science Letters*, 308(1–2), pp. 200–210. Available at: https://doi.org/10.1016/j.epsl.2011.05.046.

Britten, G.L. and Sibert, E.C. (2020) 'Enhanced fish production during a period of extreme global warmth', *Nature Communications*, 11(1), p. 5636. Available at: https://doi.org/10.1038/s41467-020-19462-w.

Broerse, A.T.C. *et al.* (2000) 'Coccolithophore export production, species composition, and coccolith-CaCO3 fluxes in the NE Atlantic (34°N21°W and 48°N21°W)', *Deep Sea Research Part II: Topical Studies in Oceanography*, 47(9–11), pp. 1877–1905. Available at: https://doi.org/10.1016/S0967-0645(00)00010-2.

Burke, K.D. *et al.* (2018) 'Pliocene and Eocene provide best analogs for near-future climates', *Proceedings of the National Academy of Sciences of the United States of America*, 115(52), pp. 13288–13293. Available at: https://doi.org/10.1073/pnas.1809600115.

Chassot, E. *et al.* (2010) 'Global marine primary production constrains fisheries catches', *Ecology Letters*, 13(4), pp. 495–505. Available at: https://doi.org/10.1111/j.1461-0248.2010.01443.x.

Conti, L. and Scardi, M. (2010) 'Fisheries yield and primary productivity in large marine ecosystems', *Marine Ecology Progress Series*, 410, pp. 233–244. Available at: https://doi.org/10.3354/meps08630.

Cutler, K.B. *et al.* (2003) 'Rapid sea-level fall and deep-ocean temperature change since the last interglacial period', *Earth and Planetary Science Letters*, 206(3–4), pp. 253–271. Available at: https://doi.org/10.1016/S0012-821X(02)01107-X.

Dansgaard, W. *et al.* (1993) 'Evidence for general instability of past climate from a 250-kyr ice-core record', *Nature 1993 364:6434*, 364(6434), pp. 218–220. Available at: https://doi.org/10.1038/364218a0.

Ditlevsen, P. and Ditlevsen, S. (2023) 'Warning of a forthcoming collapse of the Atlantic meridional overturning circulation', *Nature Communications 2023 14:1*, 14(1), pp. 1–12. Available at: https://doi.org/10.1038/s41467-023-39810-w.

Elderfield, H. *et al.* (2012) 'Evolution of ocean temperature and ice volume through the mid-Pleistocene climate transition', *Science*, 337(6095), pp. 704–709. Available at: https://doi.org/10.1126/SCIENCE.1221294/SUPPL_FILE/ELDERFIELD_SM.PDF.

Expedition 306 Scientists (2006) 'Site U1313', in *Proceedings of the IODP, 303/306*. Integrated Ocean Drilling Program. Available at: https://doi.org/10.2204/iodp.proc.303306.112.2006.

Guerreiro, C. V. *et al.* (2023) 'Response of coccolithophore communities to oceanographic and atmospheric processes across the North- and Equatorial Atlantic', *Frontiers in Marine Science*, 10, p. 1119488. Available at: https://doi.org/10.3389/FMARS.2023.1119488/BIBTEX.

Guihou, A. *et al.* (2011) 'Enhanced Atlantic Meridional Overturning Circulation supports the Last Glacial Inception', *Quaternary Science Reviews*, 30(13–14), pp. 1576–1582. Available at: https://doi.org/10.1016/J.QUASCIREV.2011.03.017.

Hagino, K. and Young, J.R. (2015) 'Biology and paleontology of coccolithophores (Haptophytes)', *Marine Protists: Diversity and Dynamics*, pp. 311–330. Available at: https://doi.org/10.1007/978-4-431-55130-0_12/FIGURES/5.

Herbert, T.D. *et al.* (2016) 'Late Miocene global cooling and the rise of modern ecosystems', *Nature Geoscience*, 9(11), pp. 843–847. Available at: https://doi.org/10.1038/ngeo2813.

IPCC (2019) IPCC Special Report on the Ocean and Cryosphere in a Changing Climate, The Ocean and Cryosphere in a Changing Climate: Special Report of the Intergovernmental Panel on Climate Change. Cambridge University Press. Available at: https://doi.org/10.1017/9781009157964.

IPCC (2023) Climate Change 2023: Synthesis Report. Contribution of Working Groups I, II and III to the Sixth Assessment Report of the Intergovernmental Panel on Climate Change. Geneva. Available at: https://doi.org/10.59327/IPCC/AR6-9789291691647.

Knight, B.R. and Jiang, W. (2009) 'Assessing primary production constraints in New Zealand fisheries', *Fisheries Research*, 100(1), pp. 15–25. Available at: https://doi.org/10.1016/j.fishres.2009.06.001.

Krauss, W. (1986) 'The North Atlantic Current', *Journal of Geophysical Research: Oceans*, 91(C4), pp. 5061–5074. Available at: https://doi.org/10.1029/JC091IC04P05061.

Kuhlbrodt, T. *et al.* (2024) 'A Glimpse into the Future: The 2023 Ocean Temperature and Sea Ice Extremes in the Context of Longer-Term Climate Change', *Bulletin of the American Meteorological Society*, 105(3), pp. E474–E485. Available at: https://doi.org/10.1175/BAMS-D-23-0209.1.

Lawrence, K.T. *et al.* (2009) 'High-amplitude variations in North Atlantic sea surface temperature during the early Pliocene warm period', *Paleoceanography*, 24(2), p. n/a-n/a. Available at: https://doi.org/10.1029/2008PA001669.

Li, G. *et al.* (2020) 'Increasing ocean stratification over the past half-century', *Nature Climate Change 2020 10:12*, 10(12), pp. 1116–1123. Available at: https://doi.org/10.1038/s41558-020-00918-2.

Lisiecki, L.E. and Raymo, M.E. (2005) 'A Pliocene-Pleistocene stack of 57 globally distributed benthic δ 18O records', *Paleoceanography*, 20(1), pp. 1–17. Available at: https://doi.org/10.1029/2004PA001071.

Marshak, A.R. and Link, J.S. (2021) 'Primary production ultimately limits fisheries economic performance', *Scientific Reports*, 11(1), p. 12154. Available at: https://doi.org/10.1038/s41598-021-91599-0.

McIntyre, A., Ruddiman, W.F. and Jantzen, R. (1972) 'Southward penetrations of the North Atlantic polar front: faunal and floral evidence of large-scale surface water mass movements over the last 225,000 years', *Deep Sea Research and Oceanographic Abstracts*, 19(1), pp. 61–77. Available at: https://doi.org/10.1016/0011-7471(72)90073-3.

Meinen, C.S. *et al.* (2020) 'Observed Ocean Bottom Temperature Variability at Four Sites in the Northwestern Argentine Basin: Evidence of Decadal Deep/Abyssal Warming Amidst Hourly to Interannual Variability During 2009–2019', *Geophysical Research Letters*, 47(18), p. e2020GL089093. Available at: https://doi.org/10.1029/2020GL089093.

Moore, C.M. *et al.* (2013) 'Processes and patterns of oceanic nutrient limitation', *Nature Geoscience*, 6(9), pp. 701–710. Available at: https://doi.org/10.1038/ngeo1765.

Naafs, B.D.A. *et al.* (2012) 'Strengthening of North American dust sources during the late Pliocene (2.7 Ma)', *Earth and Planetary Science Letters*, 317–318, pp. 8–19. Available at: https://doi.org/10.1016/j.epsl.2011.11.026.

NASA Goddard Space Flight Center, Ocean Ecology Laboratory and Ocean Biology Processing Group (2022) *Moderate-resolution Imaging Spectroradiometer (MODIS) Chlorophyll concentration*.

Nave, S. *et al.* (2010) 'Open oceanic productivity changes at mid-latitudes during interglacials and its relation to the Atlantic Meridional Overturning Circulation', *Geophysical Research Abstracts*, 12, pp. 2010–14696.

Nowicki, M., DeVries, T. and Siegel, D.A. (2022) 'Quantifying the Carbon Export and Sequestration Pathways of the Ocean's Biological Carbon Pump', *Global Biogeochemical Cycles*, 36(3). Available at: https://doi.org/10.1029/2021GB007083.

Pedro, J.B. *et al.* (2022) 'Dansgaard-Oeschger and Heinrich event temperature anomalies in the North Atlantic set by sea ice, frontal position and thermocline structure', *Quaternary Science Reviews*, 289, p. 107599. Available at: https://doi.org/10.1016/J.QUASCIREV.2022.107599.

Pei, Q. *et al.* (2016) 'Climatic Character of Marine Isotope Stage (MIS) 5e in the Representative Regions of the World: A Review', *Advances in Earth Science*, 31(11), p. 1182. Available at: https://doi.org/10.11867/J.ISSN.1001-8166.2016.11.1182.

Pöppelmeier, F. *et al.* (2021) 'Simulated stability of the Atlantic Meridional Overturning Circulation during the Last Glacial Maximum', *Climate of the Past*, 17(2), pp. 615–632. Available at: https://doi.org/10.5194/CP-17-615-2021.

Rossby, T. (1996) 'The North Atlantic Current and surrounding waters: At the crossroads', *Reviews of Geophysics*, 34(4), pp. 463–481. Available at: https://doi.org/10.1029/96RG02214.

Rousseaux, C. and Gregg, W. (2013) 'Interannual Variation in Phytoplankton Primary Production at A Global Scale', *Remote Sensing*, 6(1), pp. 1–19. Available at: https://doi.org/10.3390/rs6010001.

Schwab, C. *et al.* (2012) 'Coccolithophore paleoproductivity and ecology response to deglacial and Holocene changes in the Azores Current System', *Paleoceanography*, 27(3). Available at: https://doi.org/10.1029/2012PA002281.

Shackleton, N.J. (1969) 'The last interglacial in the marine and terrestrial records', *Proceedings of the Royal Society of London. Series B. Biological Sciences*, 174(1034), pp. 135–154. Available at: https://doi.org/10.1098/rspb.1969.0085.

Shipboard Scientific Party (1996) 'Site 982', in *Proceedings of the Ocean Drilling Program, 162 Initial Reports*. Ocean Drilling Program, pp. 91–138. Available at: https://doi.org/10.2973/odp.proc.ir.162.104.1996.

Sibert, E.C. *et al.* (2020) 'No state change in pelagic fish production and biodiversity during the Eocene–Oligocene transition', *Nature Geoscience*, 13(3), pp. 238–242. Available at: https://doi.org/10.1038/s41561-020-0540-2.

Sibert, E.C., Hull, P.M. and Norris, R.D. (2014) 'Resilience of Pacific pelagic fish across the Cretaceous/Palaeogene mass extinction', *Nature Geoscience*, 7(9), pp. 667–670. Available at: https://doi.org/10.1038/ngeo2227.

Sigman, D.M. and Hain, M.P. (2012) 'The Biological Productivity of the Ocean', *Nature Education*, 3(6), pp. 1–16.

Tzedakis, P.C. *et al.* (2009) 'Interglacial diversity', *Nature Geoscience*, 2(11), pp. 751–755. Available at: https://doi.org/10.1038/ngeo660.

Villanueva, J. *et al.* (1997) 'A biomarker approach to the organic matter deposited in the North Atlantic during the last climatic cycle', *Geochimica et Cosmochimica Acta*, 61(21), pp. 4633–4646. Available at: https://doi.org/10.1016/S0016-7037(97)83123-7.

Villanueva, J. *et al.* (2001) 'A latitudinal productivity band in the Central North Atlantic over the last 270 kyr: An alkelone perspective', *Paleoceanography*, 16(6), pp. 617–626. Available at: https://doi.org/10.1029/2000PA000543.

Webb, P. (2021) 'Patterns of Primary Production', in *Introduction to Oceanography*. Roger Williams University. Available at: https://rwu.pressbooks.pub/webboceanography/chapter/7-4-patterns-of-primary-production/.

Westen, R.M. van, Kliphuis, M. and Dijkstra, H.A. (2024) 'Physics-based early warning signal shows that AMOC is on tipping course', *Science Advances*, 10(6), p. 1189. Available at: https://doi.org/10.1126/SCIADV.ADK1189.

Woodhouse, A. *et al.* (2024) 'The Micropaleoecology Framework: Evaluating Biotic Responses to Global Change Through Paleoproxy, Microfossil, and Ecological Data Integration', *Ecology and Evolution*, 14(11), p. e70470. Available at: https://doi.org/10.1002/ece3.70470.

Appendix: Sample information and generated datasets

This appendix contains tables providing detailed sample information, including: full sample ID, depth information, reconstructed ages, sample density, and sedimentation rate for all samples from ODP Site 982 and IODP Site U1313.

Additionally, for both cores, it includes raw data and accumulation rates for all newly generated datasets described in this thesis.

Contents

Sample number	Exp	Site	Hole	Core	Core Type	Section	Top Interval (cm)	Bottom Interval (cm)	Volume (cc)	Metres below sea floor (mbsf)	Metres composite depth (mcd)	Age (kyr)	Sample density (g cm^{-3})	Sed rate (cm kyr^{-1})
2	162	982	B	1	H	1	43	45	20	0.43	0.43	6.5	1.50	5.32
3	162	982	B	1	H	1	87	89	20	0.87	0.87	19.2	1.50	2.27
4	162	982	B	1	H	1	94	96	20	0.94	0.94	22.3	1.50	2.27
5	162	982	B	1	H	1	102	104	20	1.02	1.02	25.8	1.50	2.19
6	162	982	B	1	H	1	109	111	20	1.09	1.09	29.1	1.50	2.14
7	162	982	B	1	H	1	116	118	20	1.16	1.16	32.4	1.50	2.08
8	162	982	B	1	H	1	120	122	20	1.2	1.2	34.3	1.50	2.03
9	162	982	B	1	H	1	123	125	20	1.23	1.23	35.8	1.50	2.03
10	162	982	B	1	H	1	126	128	20	1.26	1.26	37.3	1.50	2.03
11	162	982	B	1	H	1	129	131	20	1.29	1.29	38.7	1.50	2.08
12	162	982	B	1	H	1	132	134	20	1.32	1.32	40.2	1.50	2.08
13	162	982	B	1	H	1	135	137	20	1.35	1.35	41.6	1.50	2.03
14	162	982	B	1	H	1	138	140	20	1.38	1.38	43.1	1.50	2.03
15	162	982	B	1	H	1	141	143	20	1.41	1.41	44.6	1.50	2.03
16	162	982	B	1	H	1	144	146	20	1.44	1.44	46.0	1.50	2.08
17	162	982	B	1	H	1	147	149	20	1.47	1.47	47.5	1.50	2.08
18	162	982	B	1	H	2	0	2	20	1.5	1.5	48.9	1.50	2.08
19	162	982	B	1	H	2	3	5	20	1.53	1.53	50.4	1.50	2.08
20	162	982	B	1	H	2	6	8	20	1.56	1.56	51.9	1.50	2.08
21	162	982	B	1	H	2	9	11	20	1.59	1.59	53.3	1.50	2.03
22	162	982	B	1	H	2	12	14	20	1.62	1.62	54.8	1.50	2.03
23	162	982	B	1	H	2	15	17	20	1.65	1.65	56.2	1.50	1.95
24	162	982	B	1	H	2	18	20	20	1.68	1.68	57.8	1.50	1.95
25	162	982	B	1	H	2	21	23	20	1.71	1.71	59.3	1.50	1.95
26	162	982	B	1	H	2	24	26	20	1.74	1.74	61.0	1.50	1.68
27	162	982	B	1	H	2	27	29	20	1.77	1.77	62.8	1.50	1.68
28	162	982	B	1	H	2	30	32	20	1.8	1.8	64.6	1.50	1.63
29	162	982	B	1	H	2	33	35	20	1.83	1.83	66.5	1.50	1.57
30	162	982	B	1	H	2	36	38	20	1.86	1.86	68.4	1.50	1.57

	31	162	982	B	1	H	2	39	41	20	1.89	1.89	70.3	1.50	1.53
	32	162	982	B	1	H	2	41	43	20	1.91	1.91	71.6	1.50	1.53
Q1		162	982	B	1	H	2	53.5	55.5	20	2.035	2.035	79.8	1.50	1.56
	33	162	982	B	1	H	2	55	57	20	2.05	2.05	80.7	1.50	1.56
Q2		162	982	B	1	H	2	57	59	20	2.07	2.07	82.0	1.50	1.56
	34	162	982	B	1	H	2	63	65	20	2.13	2.13	85.9	1.50	1.54
	35	162	982	B	1	H	2	70	72	20	2.2	2.2	90.2	1.50	1.77
N1		162	982	B	1	H	2	77	79	20	2.28	2.28	94.5	1.50	1.96
N2		162	982	B	1	H	2	85	87	20	2.36	2.36	98.5	1.50	2.07
N3		162	982	B	1	H	2	91	93	20	2.42	2.42	101.5	1.50	2.04
N4		162	982	B	1	H	2	98	100	20	2.49	2.49	104.8	1.50	2.07
N5		162	982	B	1	H	2	104	106	20	2.55	2.55	107.8	1.50	2.05
Q3		162	982	B	1	H	2	109	111	20	2.59	2.59	109.8	1.51	2.03
	36	162	982	B	1	H	2	115	117	20	2.65	2.65	112.8	1.52	1.92
Q4		162	982	B	1	H	2	117	119	20	2.67	2.67	113.9	1.52	1.92
N6		162	982	B	1	H	2	125	127	20	2.76	2.76	118.5	1.53	1.92
N7		162	982	B	1	H	2	131	133	20	2.82	2.82	121.6	1.54	1.89
N8		162	982	B	1	H	2	139	141	20	2.9	2.9	126.4	1.55	1.58
N9		162	982	B	1	H	3	1	3	20	3.02	3.02	137.0	1.57	1.03
	37	162	982	B	1	H	3	12	14	20	3.12	3.12	146.8	1.59	1.02
Q6		162	982	B	1	H	3	14	16	20	3.14	3.14	148.8	1.59	1.02
N10		162	982	B	1	H	3	21	23	20	3.22	3.22	156.5	1.60	1.03
Q7		162	982	B	1	H	3	28	30	20	3.28	3.28	162.2	1.61	1.08
N11		162	982	B	1	H	3	32	34	20	3.33	3.33	166.0	1.61	1.42
Q8		162	982	B	1	H	3	41	43	20	3.41	3.41	171.4	1.63	1.66
	38	162	982	B	1	H	3	53	55	20	3.53	3.53	178.4	1.64	1.84
Q9		162	982	B	1	H	3	68	70	20	3.68	3.68	186.2	1.66	2.08
	39	162	982	B	1	H	3	101	103	20	4.01	4.01	200.0	1.67	2.94

Sample number	Age (kyr)	Sample density (g cm^{-3})	Sed rate (cm kyr^{-1})	Total nannoliths	NAR (nannoliths cm^{-2} kyr^{-1})	Al (ppm)	Ba (ppm)	Ba_{XS} (ppm)	$Ba_{XS}AR$ (µg cm^{-2} kyr^{-1})	AlAR (µg cm^{-2} kyr^{-1})	Total ichthyoliths	Ichthyolith abundance (ich g^{-1})	IAR (ich cm^{-2} kyr^{-1})
2	6.5	1.497	5.32	1.64E+10	1.30E+11	16880	413	367	2922	134412			
3	19.2	1.497	2.27	3.35E+09	1.14E+10	52793	426	283	964	179560			
4	22.3	1.496	2.27			44579	357	236	803	151617			
5	25.8	1.496	2.19			45580	396	273	895	149574	1	0.07	0.23
6	29.1	1.496	2.14	1.61E+10	5.16E+10	34847	368	274	879	111736			
7	32.4	1.496	2.08										
8	34.3	1.496	2.03										
9	35.8	1.496	2.03										
10	37.3	1.496	2.03								28	1.47	4.45
11	38.7	1.496	2.08	1.09E+10	3.39E+10	32832	310	221	690	102335			
12	40.2	1.496	2.08			30270	289	207	646	94350			
13	41.6	1.496	2.03										
14	43.1	1.496	2.03			23539	273	209	634	71382			
15	44.6	1.496	2.03								35	1.88	5.71
16	46.0	1.496	2.08										
17	47.5	1.496	2.08										
18	48.9	1.496	2.08			28904	313	235	731	89832			
19	50.4	1.496	2.08										
20	51.9	1.496	2.08	5.75E+09	1.79E+10	50031	402	267	829	155485	13	1.00	3.11
21	53.3	1.496	2.03	6.68E+09	2.03E+10	38507	339	235	714	117075			
22	54.8	1.496	2.03								0	0.00	0.00
23	56.2	1.496	1.95			49762	351	217	632	145000	8	0.42	1.23
24	57.8	1.496	1.95										
25	59.3	1.496	1.95								13	0.70	2.03
26	61.0	1.496	1.68			26910	267	194	488	67533			
27	62.8	1.496	1.68										
28	64.6	1.496	1.63			20379	242	186	453	49531	11	0.66	1.61
29	66.5	1.496	1.57			24889	208	141	332	58530			
30	68.4	1.496	1.57			18489	266	216	509	43479	22	1.24	2.91
31	70.3	1.496	1.53	1.68E+10	3.85E+10	22870	283	221	507	52460	11	0.59	1.34

	32	71.6	1.496	1.53			9227	224	199	457	21165			
Q1		79.8	1.495	1.56								12	0.83	1.94
	33	80.7	1.495	1.56	2.39E+10	5.58E+10	13336	221	185	431	31160			
Q2		82.0	1.495	1.56			8335	258	236	551	19475			
	34	85.9	1.495	1.54	1.28E+10	2.94E+10	13437	284	248	570	30945	40	2.42	5.57
	35	90.2	1.495	1.77	1.85E+10	4.91E+10	11319	329	298	791	30008	40	1.98	5.25
N1		94.5	1.495	1.96	1.40E+10	4.10E+10	10320	320	292	857	30296	27	1.68	4.94
N2		98.5	1.495	2.07			8761	377	354	1092	27065	28	2.02	6.24
N3		101.5	1.495	2.04	2.22E+10	6.78E+10	8291	365	343	1047	25331	27	2.14	6.53
N4		104.8	1.496	2.07	1.97E+10	6.09E+10	10454	318	289	895	32320	28	1.90	5.86
N5		107.8	1.505	2.05	1.41E+10	4.35E+10	15811	303	260	802	48759	28	2.00	6.16
Q3		109.8	1.510	2.03			10282	455	427	1312	31568			
	36	112.8	1.519	1.92	1.93E+10	5.63E+10	10681	394	365	1065	31201			
Q4		113.9	1.522	1.92			13334	354	318	929	39022			
N6		118.5	1.534	1.92	1.13E+10	3.35E+10	24243	451	385	1137	71539	13	1.08	3.18
N7		121.6	1.543	1.89	5.62E+09	1.64E+10	30507	548	466	1360	89145	43	3.04	8.87
N8		126.4	1.554	1.58	1.02E+10	2.50E+10	40007	735	627	1540	98175	12	0.64	1.58
N9		137.0	1.571	1.03	4.74E+09	7.65E+09	34635	318	225	362	55828	29	2.13	3.44
	37	146.8	1.585	1.02	4.57E+09	7.42E+09	41386	328	216	351	67216			
Q6		148.8	1.588	1.02								1	0.08	0.13
N10		156.5	1.599	1.03	7.12E+09	1.18E+10	42019	301	187	309	69324			
Q7		162.2	1.608	1.08			54137	371	224	389	93789			
N11		166.0	1.615	1.42	4.74E+09	1.09E+10	42388	294	180	413	97407			
Q8		171.4	1.626	1.66			44144	334	215	579	118839			
	38	178.4	1.643	1.84	9.07E+09	2.74E+10	35140	261	166	502	106124			
Q9		186.2	1.659	2.08			39791	360	253	873	137547			
	39	200.0	1.674	2.94	1.91E+10	9.42E+10	19896	342	288	1419	97966			

Sample number	Exp	Site	Hole	Core	Core Type	Section	Top Interval (cm)	Bottom Interval (cm)	Volume (cc)	Metres below sea floor (mbsf)	Metres composite depth (mcd)	Age (kyr)	Density (g cm^{-2} kyr^{-1})	Sed rate (cm kyr^{-1})
1	306	1313	A	1	H	2	111	113	20	2.63	2.61	47.9	1.43	9.09
2	306	1313	A	1	H	2	133	135	20	2.85	2.83	50.7	1.44	5.56
3	306	1313	A	1	H	3	5	7	20	3.07	3.05	54.3	1.44	6.90
4	306	1313	A	1	H	3	27	29	20	3.29	3.27	57.5	1.45	6.90
5	306	1313	A	1	H	3	49	51	20	3.51	3.49	61.3	1.46	5.41
6	306	1313	A	1	H	3	59	61	20	3.60	3.59	63.1	1.46	5.56
7	306	1313	A	1	H	3	67	69	20	3.68	3.67	64.7	1.47	6.90
8	306	1313	A	1	H	3	76	78	20	3.77	3.76	66.0	1.47	6.48
9	306	1313	A	1	H	3	85	87	20	3.86	3.85	67.8	1.47	4.35
10	306	1313	A	1	H	3	94	96	20	3.95	3.94	69.9	1.47	4.40
11	306	1313	A	1	H	3	102	104	20	4.03	4.02	71.7	1.48	4.40
12	306	1313	A	1	H	3	111	113	20	4.12	4.11	73.8	1.48	4.35
13	306	1313	A	1	H	3	120	122	18	4.21	4.2	75.8	1.48	7.66
14	306	1313	A	1	H	3	129	131	20	4.30	4.29	77.2	1.49	10.87
15	306	1313	A	1	H	3	138	140	20	4.39	4.38	79.2	1.49	4.38
16	306	1313	A	1	H	3	146	148	20	4.47	4.46	81.1	1.49	4.40
17	306	1313	A	1	H	4	5	7	20	4.56	4.55	83.1	1.48	4.35
18	306	1313	A	1	H	4	14	16	20	4.65	4.64	84.5	1.48	4.37
19	306	1313	A	1	H	4	23	25	20	4.74	4.73	86.8	1.47	4.35
20	306	1313	A	1	H	4	31	33	20	4.82	4.81	88.8	1.47	4.44
21	306	1313	A	1	H	4	40	42	20	4.91	4.9	91.3	1.46	4.35
22	306	1313	A	1	H	4	48	50	20	5.00	4.98	93.4	1.46	4.40
23	306	1313	A	1	H	5	5	7	20	5.09	5.05	95.0	1.46	5.48
P1	306	1313	A	1	H	5	9	10	20	5.13	5.09	95.9	1.46	3.64
P2	306	1313	A	2	H	1	0	2	20	5.21	5.81	114.8	1.42	3.77
24	306	1313	A	2	H	1	5	7	20	5.26	5.86	116.1	1.42	3.77
25	306	1313	A	2	H	1	14	16	20	5.35	5.95	118.5	1.41	3.77
26	306	1313	A	2	H	1	23	25	20	5.44	6.04	120.9	1.41	3.46
27	306	1313	A	2	H	1	33	35	20	5.53	6.14	123.8	1.40	3.74

28	306	1313	A	2	H	1	41	43	20	5.61	6.22	125.9	1.40	3.74
29	306	1313	A	2	H	1	49	51	20	5.70	6.3	128.1	1.39	3.77
30	306	1313	A	2	H	1	70	72	20	5.92	6.51	133.9	1.38	3.70
31	306	1313	A	2	H	1	92	94	20	6.14	6.73	139.2	1.37	4.65
32	306	1313	A	2	H	1	114	116	20	6.36	6.95	144.1	1.36	4.69
33	306	1313	A	2	H	1	136	138	20	6.58	7.17	149.0	1.36	4.65
34	306	1313	A	2	H	2	118	120	20	7.89	8.49	175.1	1.40	4.00

Sample number	Age (ka)	Density (g cm^{-3})	Sed rate (cm kyr^{-1})	Total nannoliths	NAR (nannoliths cm^{-2} kyr^{-1})	Al (ppm)	Ba (ppm)	$Ba_{xs}AR$ (µg cm^{-2} kyr^{-1})	AlAR (µg cm^{-2} kyr^{-1})	Total ichthyoliths	Abundance (ich g^{-1})	IAR (ich cm^{-2} kyr^{-1})
1	47.9	1.43	9.09	1.43E+10	1.86E+11							
2	50.7	1.44	5.56	1.75E+10	1.74E+11	23686	569	4027	189041			
3	54.3	1.44	6.90			17091	329	2818	170219	12	0.83	8.26
4	57.5	1.45	6.90							41	3.11	31.14
5	61.3	1.46	5.41			34346	862	6069	270882	28	1.67	13.14
6	63.1	1.46	5.56	1.62E+10	1.32E+11	31726	1018	7577	257768	7	0.48	3.90
7	64.7	1.47	6.90							17	1.33	13.40
8	66.0	1.47	6.48	1.56E+10	1.48E+11	28791	916	7977	273865	7	0.60	5.69
9	67.8	1.47	4.35	2.24E+10	1.43E+11	26750	896	5270	171119	7	0.45	2.90
10	69.9	1.47	4.40	1.52E+10	9.87E+10	19929	519	3018	129152	24	1.79	11.57
11	71.7	1.48	4.40	2.26E+10	1.47E+11	17629	395	2254	114470	15	1.07	6.96
12	73.8	1.48	4.35	1.21E+10	7.77E+10	15658	336	1893	100767	48	3.55	22.86
13	75.8	1.48	7.66	2E+10	2.27E+11	15754	357	3566	178920	4	0.37	4.19
14	77.2	1.49	10.87	2.2E+10	3.56E+11	8860	269	3962	143138	26	1.80	29.03
15	79.2	1.49	4.38	2.84E+10	1.85E+11	7413	256	1542	48353	28	2.23	14.53
16	81.1	1.49	4.40	3.1E+10	2.03E+11	8789	249	1474	57449	23	2.25	14.74
17	83.1	1.48	4.35	1.32E+10	8.49E+10	9333	253	1468	60155	66	3.98	25.66
18	84.5	1.48	4.37	3.26E+10	2.10E+11	16426	383	2190	106131	36	2.14	13.83
19	86.8	1.47	4.35	2.5E+10	1.60E+11	9141	299	1755	58561	43	2.77	17.77
20	88.8	1.47	4.44			6500	226	1360	42453	49	3.06	19.99
21	91.3	1.46	4.35	1.59E+10	1.02E+11	6334	241	1429	40344	76	4.34	27.61
22	93.4	1.46	4.40	1.75E+10	1.13E+11	8760	266	1554	56257	45	3.37	21.63
23	95.0	1.46	5.48	1.19E+10	9.54E+10	7035	244	1799	56182	66	2.40	19.17
P1	95.9	1.46	3.64			6882	242	1183	36420	29	2.94	15.57
P2	114.8	1.42	3.77			8706	283	1388	46625	21	2.07	11.07
24	116.1	1.42	3.77							16	1.12	5.99
25	118.5	1.41	3.77	3.73E+10	1.99E+11	25377	720	3474	135235	38	2.74	14.61
26	120.9	1.41	3.46	2.51E+10	1.22E+11	10357	317	1409	50418	28	2.00	9.75
27	123.8	1.40	3.74	2.58E+10	1.35E+11	11072	229	1045	58061	31	2.04	10.71
28	125.9	1.40	3.74	1.76E+10	9.19E+10	7911	260	1247	41368	57	3.67	19.20

29	128.1	1.39	3.77	2.1E+10	1.10E+11	11469	365	1760	60356	28	1.68	8.82
30	133.9	1.38	3.70	3.91E+10	2.01E+11	8306	259	1213	42581	32	2.92	14.97
31	139.2	1.37	4.65	2.03E+10	1.30E+11	7930	223	1288	50643	10	0.92	5.90
32	144.1	1.36	4.69	2.56E+10	1.63E+11	10346	170	910	66054			
33	149.0	1.36	4.65	1.69E+10	1.07E+11	20645	821	4855	130931	22	1.78	11.27
34	175.1	1.40	4.00	1.63E+10	9.15E+10	24043	813	4194	134741			